

# **UNIVERSITÀ DEGLI STUDI DI NAPOLI “FEDERICO II”**

**Dottorato di ricerca in Scienze della Terra  
XXIV ciclo**



## **Dolomitization in basinal limestones of the Lagonegro Units: from early diagenesis to tectonically-driven fluid flow**

*Tutor*

**Prof. Alessandro Iannace**

*Dottoranda*

**Tatyana Gabellone**

*Coordinatore*

**Prof. ssa Maria Boni**

*In ogni cosa ho voglia di arrivare  
sino alla sostanza.*

*Nel lavoro, cercando la mia strada,  
nel tumulto del cuore.*

*Sino all'essenza dei giorni passati,  
sino alla loro ragione,  
sino ai motivi, sino alle radici,  
sino al midollo.*

*Eternamente aggrappandomi al filo  
dei destini, degli avvenimenti,  
sentire, amare, vivere, pensare,  
effettuare scoperte*

...

*Boris Pasternak*

# Ringraziamenti

Questa tesi di dottorato è il frutto di tanto impegno e sacrificio, e senza il prezioso aiuto di alcune persone non avrei potuto portare avanti questa ricerca e giungere a questo importante traguardo. Pertanto vorrei ringraziare tutti coloro i quali hanno contribuito alla realizzazione di questa tesi, sperando di non dimenticare nessuno...

Inizio col ringraziare il mio tutor, il Prof. Alessandro Iannace, per avermi dato l'opportunità di svolgere questo progetto di ricerca e per avermi sempre spronata a essere più intraprendente e a svolgere autonomamente il mio lavoro. Lo ringrazio anche per avermi dato l'opportunità di svolgere un periodo del mio dottorato in Francia, presso l'IFP Energies nouvelles.

Ringrazio il Dott. Mariano Parente che mi ha seguita durante la tesi di laurea specialistica e che mi ha avvicinata al "mondo dei carbonati". È anche grazie a lui se oggi sono arrivata fin qui.

Grazie al Prof. Stefano Mazzoli, per le continue discussioni e per avermi fornito molti chiarimenti sulla geologia dell'Appennino meridionale.

Un enorme grazie va a colei che può considerarsi la mia co-tutor, la Dott.ssa Marta Gasparrini, che mi ha seguita durante il mio stage presso l'IFP Energies nouvelles. Grazie Marta per la tua disponibilità, per le risposte ai miei dubbi e per i tuoi preziosi consigli.

Ringrazio il mio *referee*, il Dott. Fabio Lapponi, per avermi dato degli utili suggerimenti per migliorare questa tesi.

Un ringraziamento molto sentito va alla Dott.ssa Laura Galluccio, alla quale sono "accomunata"...grazie per avermi trasmesso molte delle tue conoscenze, pratiche e teoriche, aiutandomi soprattutto all'inizio del mio dottorato. Grazie anche per non avermi fatto mancare mai in tuo supporto morale.

Ringrazio Eni S.p.A. per avermi concesso di consultare i log stratigrafici dei pozzi della Val d'Agri e per avermi fornito i cutting dei pozzi Acerno e Monte Gargaruso. In particolare ringrazio il Dott. Alfredo Pugliese, che si è interessato dell'organizzazione della mia visita in Eni a Milano. Ringrazio anche Shell Italia E&P per avermi fornito i campioni del pozzo Monte Foi.

Grazie a tutti coloro che mi hanno dato "un passaggio" in auto in Basilicata: Dario Morante, Pasquale Milano, Francesco Dati (Ciccio) e mia madre. Grazie Ciccio anche per l'aiuto che mi hai dato in campagna per la raccolta dei dati strutturali, ma soprattutto grazie per la tua amicizia ed il tuo sostegno morale nei momenti più difficili.

Ringrazio il mio collega, amico, nonché "coabitante" (cit.) Alberto, col quale ho condiviso molti momenti di questo dottorato. Grazie per aver rallegrato con il tuo umorismo geologico le giornate trascorse in dipartimento...

Ringrazio il Dott. Sergio Bravi, per avermi aiutata nella realizzazione delle sezioni sottili, il Dott. Lucio Tufano, per l'aiuto fornitomi nella ricerca di molte pubblicazioni ed

il Dott. Vincenzo Monetti, per aver messo a mia disposizione il suo laboratorio in diverse occasioni.

Ringrazio la Dott.ssa Chiara Invernizzi e la Dott.ssa Paola Ronchi per la loro disponibilità e per avermi fornito delle informazioni utili ai fini della mia ricerca.

Grazie ad Andrea per l'aiuto nel trasporto dei miei campioni col motorino.

Ringrazio Stefania e lo zio Luca per avermi ospitata durante i miei soggiorni “lavorativi” milanesi.

Ringrazio il mio allenatore Gianpaolo e tutta la sua famiglia per il loro appoggio e sostegno morale. Qui a Napoli siete stati per me una seconda famiglia. Grazie Gianp anche per aver avuto la pazienza di allenare una “mezza atleta” come me.

Ringrazio gli amici del “ma te !?”, gli amici di Alezio e Sara che in questi anni mi sono stati sempre vicini anche se da lontano...

Infine ringrazio i miei genitori e mio fratello per il loro amore e per avermi sempre appoggiata in ogni mia scelta. Questa tesi è dedicata a voi.

## **Acknowledgements**

I am grateful to the IFP Energies nouvelles for giving me the possibility to work in their laboratories. I would like to thank as well Dr. Youri Hamon for helping me to solve a problem with the cathodoluminescence.

I thank Dr. Ulrike Schulte and Dr. Dieter Buhl who performed the geochemical analyses.

At last but not least, thanks to all of my “French” friends who made more beautiful my stay in Rueil Malmaison.



# Table of contents

<b>Table of contents .....</b>	<b>1</b>
<b>Abstract.....</b>	<b>4</b>
<b>Riassunto.....</b>	<b>6</b>
<b>Chapter 1: Introduction .....</b>	<b>8</b>
<b>Chapter 2: The <i>Calcari con selce</i> Formation in the frame of the Southern Apennines.....</b>	<b>10</b>
2.1 Geological Structure of the Southern Apennines.....	10
2.2 Thermal history of the fold and thrust belt .....	12
2.3 The evolution of the Lagonegro Basin.....	12
2.4 The <i>Calcari con selce</i> Formation and dolomites distribution.....	14
<b>Chapter 3: Early versus late dolomitization models.....</b>	<b>19</b>
3.1 The “dolomite problem” .....	19
3.2 Dolomitization models .....	19
<b>Chapter 4: Methods .....</b>	<b>23</b>
4.1 Field work and wells analysis .....	23
4.2 Peels, cutting and thin sections preparation .....	23
4.3 Petrographic analyses.....	24
4.3.1 Transmitted light microscopy .....	24
4.3.2 Cathodoluminescence (CL) microscopy .....	24
4.4 Geochemical methods .....	24
4.4.1 Oxygen and Carbon stable isotope analyses .....	24
4.4.2 Major to trace element analyses (ICP-AES) .....	26
4.4.3 Sr isotope analyses .....	26
4.5 Fluid Inclusions (FIs) study .....	27
4.5.1 Microthermometry: principles and parameters .....	27
4.5.2 Microthermometry procedure .....	28
4.5.3 Thermodynamic calculations and computer programs .....	28

<b>Chapter 5: Field observations .....</b>	<b>29</b>
5.1 Distribution of dolomite bodies .....	29
5.2 Molise and northern area outcrops: features of dolomites .....	31
5.3 Southern area outcrops: features of precursor limestones .....	32
5.4 Southern area outcrops: features of dolomites .....	35
<b>Chapter 6: Distribution of dolomites in subsurface.....</b>	<b>40</b>
6.1 The <i>Calcari con Selce</i> Formation in the Val d'Agri exploration and production wells .....	40
6.2 Stratigraphic logs of the studied wells .....	40
<b>Chapter 7: Petrography.....</b>	<b>44</b>
7.1 Features of the precursor limestone .....	44
7.2 Dolomites of the northern area.....	47
7.3 Dolomites of the southern area .....	50
7.4 Dolomites of wells cuttings.....	53
<b>Chapter 8: Geochemistry .....</b>	<b>56</b>
8.1 Oxygen and Carbon stable isotope analyses .....	56
8.2 ICP-AES analyses .....	59
8.2.1 Strontium (Sr) .....	59
8.2.2 Iron (Fe) and Manganese (Mn) .....	60
8.2.3 Barium (Ba).....	63
8.3 Sr isotope analyses .....	63
<b>Chapter 9: Fluid inclusions (FIs) study.....</b>	<b>66</b>
9.1 Samples location .....	66
9.2 Fluid inclusions petrography .....	66
9.3 Behaviour of FIs during microthermometry .....	69
9.4 Microthermometry results.....	71
9.5 Bulk density and composition of FIs .....	79
9.6 P-T conditions during FIs trapping .....	80
9.7 Preliminary conclusions from FIs study .....	82
<b>Chapter 10: Discussion .....</b>	<b>84</b>

---

10.1 The diagenetic history of undolomitized limestones .....	84
10.2 Comparison between Campagna-San Fele and Pignola-Val d'Agri dolomites...	87
10.3 A possible scenario for the early dolomitization event.....	90
10.4 Late burial dolomitization event .....	92
10.4.1 Timing of dolomitization .....	92
10.4.2 Origin of zebra structures.....	95
10.4.3 Origin of fluids.....	96
<b>Conclusions and perspectives.....</b>	<b>101</b>
<b>References .....</b>	<b>103</b>
<b>Appendix .....</b>	<b>116</b>
Appendix 1: Structural data .....	116
Appendix 2: Results of geochemical analyses .....	124
Appendix 3: Results of fluid inclusions microthermometry .....	129

## Abstract

The Triassic pelagic carbonates of the Lagonegro Basin Units from the Southern Apennines fold and thrust belt (Italy) are often replaced by dolomites, which in some cases show fabric and petrographic characteristics typical of late burial saddle dolomites displaying zebra-like structures (Iannace *et al.*, in press).

The aim of this thesis was to carry out a systematic regional study on Lagonegro dolomites, both on outcrops and on subsurface samples (cuttings from oil wells), in order to define dolomites extent, timing relative to Southern Apennines tectonic history, and fluids origin, by means of a combination of field work, and petrographic and geochemical investigations.

The Lagonegro Basin succession, together with the Apennine Platform successions, is now imbricated in a pile of nappes of the Southern Apennines chain. This latter is a NE-directed fold and thrust belt, formed by progressive collision between Afro-Adriatic and Eurasian plates during the Neogene (Mazzoli and Helman, 1994, and references therein), with the Apulian promontory representing the orogenic foreland. The classical restorations of the pre-orogenic (Triassic to Paleogene) palaeogeography of the Southern Apennines show that the African (Apulian) passive margin was characterized by the Meso-Cenozoic pelagic Lagonegro Basin, located between two coeval carbonate platforms, Apennine and Apulian platforms (Pescatore and Tramutoli, 1980; Mostardini and Merlini, 1986).

The evolution of the Lagonegro Basin was punctuated by two massive dolomitization events, which generated two distinct dolomite types displaying different petrographic and geochemical features. A fine crystalline and fabric preservative dolomite crops out in the northern area (Molise, Campagna and San Fele-Mount Pierno), whereas a coarse crystalline and fabric destructive dolomite, showing zebra-like and hydrofracturing structures is present in the southern area (from Pignola to the high Val d'Agri).

Geochemical data (enrichment in  $^{18}\text{O}$  in respect with typical Upper Triassic seawater values, high Sr and low Mn and Fe content, Sr isotopes consistent with Upper Triassic seawater) allow to interpret dolomites of the northern area as the result of an early replacement caused by cold, marine and oxidizing fluid, in a shallow burial. It is proposed that dolomitizing fluids were expelled through a reflux from the Norian Apenninic carbonate platform toward the proximal Lagonegro Basin, or alternatively they were put into motion through a Kohout convection of seawater, heated thanks to a geothermal anomaly.

Dolomites located in the southern area, display a depletion in  $^{18}\text{O}$  compared to Upper Triassic seawater values and show lower Sr, higher Mn and Fe contents, and higher Sr isotopes ratios in respect with early dolomites of the northern area. It is suggested that the southern area was affected, during Neogene time, by a late burial dolomitization, which was the result of a large scale “squeegee” fluid flow during Southern Apennines fold and thrust belt formation. The geochemistry of saddle dolomite samples indicates an origin by warm fluids (105-125 °C). Integration with available thermal data (Corrado *et*

*al.*, 2005; Mazzoli *et al.*, 2008) into the regional deformation history, by assuming a fluid in thermal equilibrium with the host rocks, suggests that the fluid flow took place after maximum burial, in early stages of exhumation, between 5 and 4 Ma and under 3-4 km of burial.

The dolomitizing fluids of southern area dolomites had salinities in the range of slightly modified to normal marine seawater (1.9-6.4 eq. wt % NaCl with a mean of 3.7) and oxygen isotopic composition typical of saline formation waters. Two possible sources for such fluids can be envisaged. They could be formation waters, diluted with fresh waters delivered during the smectite-illite transformation at depth, squeezed out from the surrounding Triassic and Cretaceous fine-clastic formations or Miocene marine pore-waters expelled from the *mélange* zone that separates the allochthonous wedge from the buried Apulian platform.

The fluid flow event was a major phenomenon affecting the fold and thrust belt and it could be expected that the dolomite bodies which are reported in the Apulian subsurface (Murgia *et al.*, 2004) might have the same origin of Lagonegro dolomites from the southern area. As the carbonates of the Apulia platform host major oil fields of continental Europe, the fluid flow that took place along with Southern Apennines belt formation could be of economic significance, providing secondary porosity development.

## Riassunto

I carbonati pelagici triassici, appartenenti alle Unità Lagonegresi della catena sud-appenninica, sono spesso sostituiti da dolomie, le quali in alcuni casi mostrano fabric e caratteristiche petrografiche tipiche di dolomie tardive da seppellimento, presentando strutture di tipo “zebra” (Iannace *et al.*, in press).

Lo scopo di questa tesi è stato quello di effettuare uno studio regionale sulle dolomie della successione lagonegrese, sia su campioni di superficie che di sottosuolo (cutting di pozzi petroliferi), al fine di determinare l'estensione della dolomitizzazione, il suo *timing* in relazione alla storia tettonica dell'Appennino meridionale, e l'origine dei fluidi dolomitizzanti, attraverso l'integrazione di lavoro di campo ed analisi petrografiche e geochemiche.

La successione del Bacino di Lagonegro, insieme alle successioni di Piattaforma Appenninica, è attualmente imbricata in una pila di falde che costituiscono la catena dell'Appennino meridionale. Quest'ultima è una catena a pieghe e falde, vergente a NE, formatasi attraverso la progressiva collisione tra la placca Afro-Adriatica e quella Euroasiatica durante il Neogene (Mazzoli and Helman, 1994, e riferimenti all'interno), con il promontorio Apulo che costituisce l'avanpaese orogenico. Le classiche ricostruzioni paleogeografiche pre-orogeniche (dal Triassico al Paleogene) dell'Appennino meridionale mostrano che il margine passivo Africano era caratterizzato dal bacino pelagico di Lagonegro (Meso-Cenozoico), ubicato tra due piattaforme carbonatiche coeve (Piattaforma Appenninica ed Apula).

L'evoluzione del Bacino di Lagonegro è stata segnata da due eventi di dolomitizzazione massiva, che hanno generato due differenti tipi di dolomia, i quali presentano diverse caratteristiche petrografiche e geochemiche. Nell'area più settentrionale di affioramento delle Unità Lagonegresi (Molise, Campagna e San Fele-Monte Pierno) è presente una dolomia finemente cristallina e che in molti casi preserva il fabric originario, mentre nell'area meridionale (da Pignola fino all'alta Val d'Agri) si incontra una dolomia più grossolana e che spesso oblitera il fabric originario, presentando strutture di tipo “zebra” e strutture da idrofratturazione.

I dati geochemici (arricchimento in  $^{18}\text{O}$  rispetto ai tipici valori dell'acqua marina del Triassico Superiore, alto contenuto in Sr, basso contenuto in Mn e Fe, e rapporti isotopici dello Sr coerenti con i valori stimati per l'acqua marina del Triassico Superiore) consentono di interpretare le dolomie dell'area settentrionale come il risultato di una sostituzione precoce causata da fluidi marini, freddi ed ossidanti, in un ambiente di seppellimento poco profondo. Si ritiene che questi fluidi siano stati espulsi attraverso un “reflux” dalla piattaforma carbonatica appenninica del Norico verso le facies più prossimali del Bacino di Lagonegro, o che, in alternativa, siano acque marine mobilizzate attraverso una convezione di tipo Kohout.

Le dolomie ubicate nell'area meridionale presentano valori di  $\delta^{18}\text{O}$  più bassi rispetto a quelli stimati per l'acqua marina del Triassico Superiore, e mostrano concentrazioni più basse di Sr e più alte di Mn e Fe, e rapporti isotopici dello Sr più alti rispetto alle

dolomie precoci dell'area settentrionale. Si ritiene che l'area meridionale del Bacino Lagonegrese sia stata interessata, durante il Neogene, da una dolomitizzazione tardiva da seppellimento, risultante da un'ampia espulsione di fluidi dalla catena sud-appenninica durante la messa in posto di quest'ultima. I risultati delle analisi delle inclusioni fluide indicano per la dolomia un'origine da fluidi caldi (105-125 °C). Il confronto con i dati termici disponibili (Corrado *et al.*, 2005; Mazzoli *et al.*, 2008) nella storia di deformazione regionale, assumendo fluidi in equilibrio termico con la roccia incassante, suggerisce che l'espulsione dei fluidi è avvenuta dopo il massimo seppellimento, nelle prime fasi dell'esumazione della catena, tra 5 e 4 Ma e sotto 3-4 km di seppellimento.

I fluidi delle dolomie dell'area meridionale presentano salinità nel range di acque marine da normali a leggermente modificate (1.9-6.4 eq. wt % NaCl con una media di 3.7), ed una composizione isotopica dell'ossigeno con valori tipici di acque di formazione saline. Due sono le possibili sorgenti di questi fluidi. Essi potrebbero essere acque di formazione, diluite con acqua dolce rilasciata durante la trasformazione smectite-illite in profondità, espulse dalle circostanti formazioni silicoclastiche del Triassico e del Cretaceo, oppure potrebbero essere acque marine mioceniche stivate nei pori ed espulse dai depositi del *mélange*, il quale è un orizzonte che separa il cuneo alloctono dalla Piattaforma Apula sepolta.

L'espulsione dei fluidi è stata un importante fenomeno che ha interessato la catena sud-appenninica, e si può supporre che i corpi dolomitizzati individuati nel sottosuolo apulo (Murgia *et al.*, 2004), il quale oggi contiene i maggiori campi petroliferi dell'Europa continentale, abbiano la stessa origine delle dolomie presenti dell'area meridionale del Bacino Lagonegrese.

# Chapter 1: Introduction

Shallow-water carbonates can be affected by dolomitization in different moments of the evolution of a sedimentary basin, from early, surface-related to deep burial diagenesis and even after exhumation (epigenetic). On the contrary, deep-water slope and basinal carbonates commonly are not dolomitized. Nevertheless, small quantities of dolomite, whose formation is related to bacterial sulfate reduction and methanogenesis, were found in deep-sea pelagic sediments in the form of layers and nodules (Kelts and McKenzie, 1982, and references therein). The occurrence of massive dolomite in basinal sequences is rarely reported (Cervato, 1990; Mresah, 1998; Fu *et al.*, 2006) and, in addition, it is enigmatic, since neither modern nor ancient analogues have been satisfactory explained (Mresah, 1998).

In the Triassic pelagic *Calcari con selce* (Cherty Limestones) Formation of the Lagonegro succession (Southern Apennines fold and thrust belt, Italy) the presence of massive bodies of dolomite is known since the second half of the last century (Scandone, 1967). These dolomites constitute another uncommon example of widespread dolomitization in a basinal succession, thus representing an interesting case study to improve knowledge on dolomitization processes affecting this type of successions.

Iannace *et al.* (in press) recently reported the occurrence of a zebra-like, saddle dolomite in three different outcrops of the Lagonegro Basin, proposing for it a burial origin, related to Neogene tectonics of the Southern Apennines chain. Observations and data produced by these authors constitute a starting point for this research, whose objective was to carry out a systematic regional study on Lagonegro dolomites distribution, both on outcrops and on subsurface samples. The aims of this work were:

- (i) to evaluate the extension of the dolomitization phenomenon in the Lagonegro Units;
- (ii) to characterize the chemical-physical diagenetic environment, i.e. to characterize the dolomitizing fluids and their probable sources;
- (iii) to provide new constraints to the understanding of the relationships between fluid flow and the structural and burial history of the tectonic belt.

The methodology of study comprised:

- (i) field survey and qualitative mapping of carbonates of the *Calcari con selce* Formation;
- (ii) examination of subsurface data from Val d'Agri exploration wells;
- (iii) detailed sampling and diagenetic studies on surface and subsurface samples, performed with the conventional techniques used in sedimentary petrography.

Oliver (1986) first recognized the key roles in hydrocarbons migration and transport of minerals of the tectonically expelled fluids during fold and thrust belts development. Since then, many other studies dealt the relationships between structural deformation and fluid flow in fold and thrust belts and their foreland (Bradbury and Woodwell, 1987; Ghisetti *et al.*, 2001; Swennen *et al.*, 2003, 2004; Roure *et al.*, 2005; Dewever, 2008). A



good reconstruction of the fluid flow history in these complex areas is essential to understand the formation of ore deposits (Heijlen *et al.*, 2001; 2003) and hydrocarbon migration (Swennen *et al.*, 2004).

The dolomites from the Lagonegro successions do not host hydrocarbons and are not associated with base-metal mineralization. Nevertheless, understanding their origin and emplacement mechanism is important in interpreting similar dolomites economically more significant. Moreover it could be argued that dolomite bodies known in subsurface in the foreland of the Southern Apennine fold and thrust belt (Murgia *et al.*, 2004; see Fig.1), might be related to the same fluid flux that originated the Lagonegro Basin dolomites. As this foreland consists of shallow-water carbonates of the Apulia platform which now host major oil fields of continental Europe, the fluid flow that took place along with Southern Apennines belt formation could be of economic significance, providing secondary porosity development.

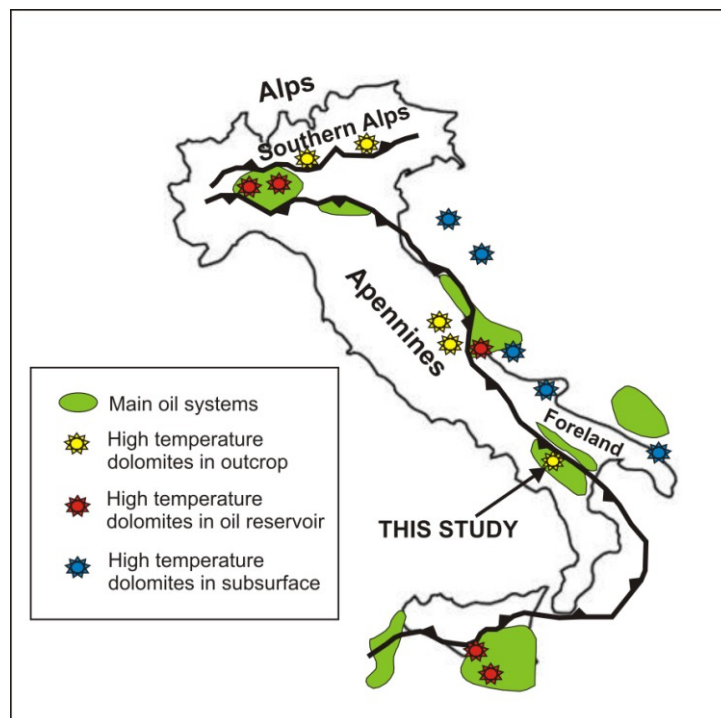


Figure 1: Documented occurrence of high temperature dolomites in the Italian peninsula, both in subsurface reservoir and outcrop cases (redrawn after Bertello *et al.*, 2010 and Ronchi *et al.*, 2012).

The present thesis has been organized as follow:

- (i) The geological and structural frame of the studied succession is presented in Chapter 2;
- (ii) A brief overview of the main dolomitization models is summarized in Chapter 3;
- (iii) The different methodologies used in this work are shown in Chapter 4;
- (iv) Chapters 5, 6, 7, 8 and 9 display the results of field work and petrographic, geochemical and microthermometric analyses, performed both on surface and subsurface samples;
- (v) Finally, the discussion of the obtained results and the dolomitization models envisaged for the Lagonegro Basin dolomites are presented in Chapter 10.

## Chapter 2: The *Calcari con selce* Formation in the frame of the Southern Apennines

### 2.1 Geological Structure of the Southern Apennines

The Southern Apennines fold and thrust belt (Fig.2) consists of a stack of several tectonic units made up of Mesozoic-Paleogene successions and their flysch-like Neogene cover, tectonically superposed onto the buried part of the Apulian Platform shallow-water carbonates (Mostardini and Merlini, 1986; Casero *et al.*, 1988; Cello and Mazzoli, 1998). This complex fold and thrust belt mainly formed as a result of Neogene deformation of the former Adriatic passive margin during Europe-Africa plate collision (Mazzoli and Helman, 1994, and references therein). From top to bottom, the belt consists of ocean-derived Units, shallow-water carbonates of the Apennine Platform Units and pelagic and hemipelagic basinal sediments of the Lagonegro Units.

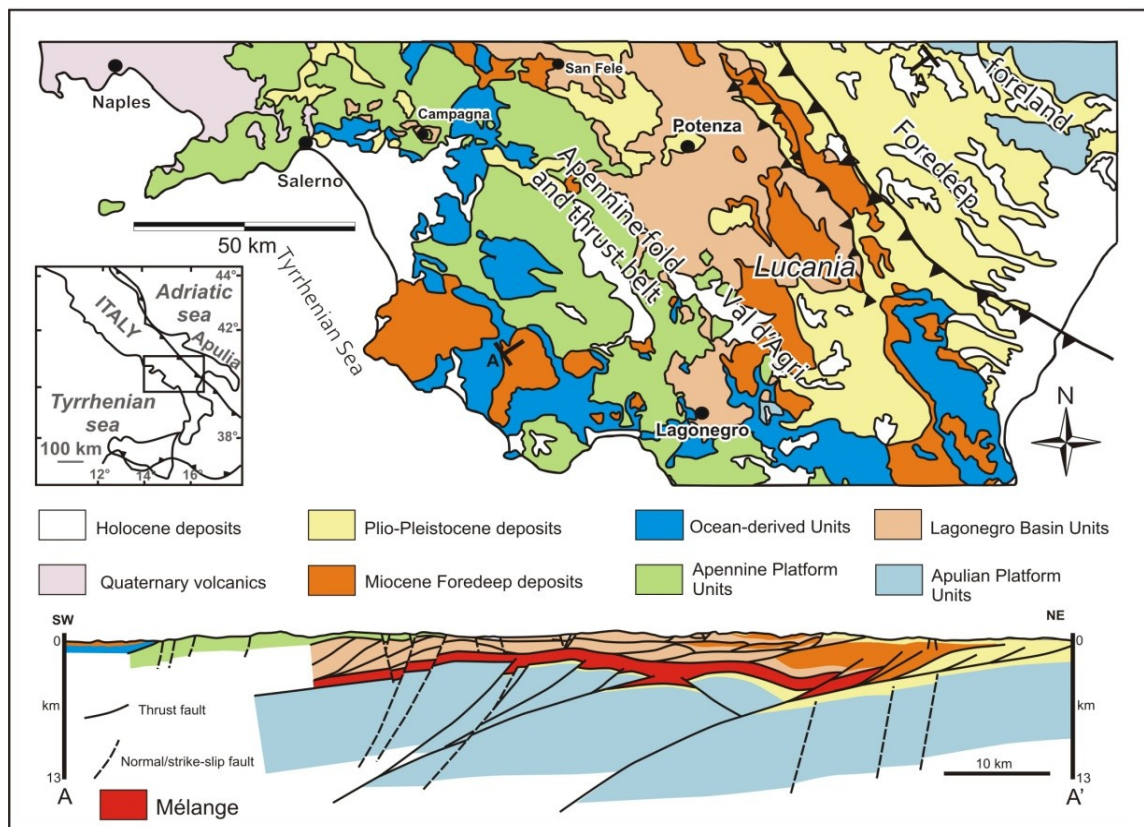


Figure 2: Simplified geological scheme and cross section of Southern Apennines (modified after Ciarcia *et al.*, 2009).

The deformation history of the Lagonegro Units was first outlined by Scandone (1972) who recognised at a regional scale the presence of two superimposed nappes, which were named Lagonegro Unit II and Lagonegro Unit I. The former is the upper nappe and present more proximal depositional characteristics, whereas the latter is the lower nappe, showing more distal sedimentary features. Doubts about this matching between thrust

units and sedimentary facies were raised by Carbone *et al.* (1991) and Mazzoli *et al.* (2001). These latter authors performed a more detailed structural study and proposed a different structural evolution and showed that, from Triassic to Cretaceous times, the Southern Apennines were in a passive margin phase (Fig.3A). Shortening started during the Miocene, with a first phase of buckling and minor thrusting that caused the “closure” of the Lagonegro Basin (Fig.3B). In Pliocene times, a second phase of thrusting led to the regional duplication of the Lagonegro Units (Fig.3C). This was followed by the emplacement of the allochthonous wedge above the westernmost portion of the Apulian Platform, a process that formed the structural traps which presently host the major oil fields of southern Italy (Shiner *et al.*, 2004). Gravitational readjustments dominated within the allochthonous wedge, triggering denudation and tectonic exhumation (assisted by erosion; Mazzoli *et al.*, 2008). Active shortening was taken up by the underlying Apulian crust, producing basement-involved inversion at depth.

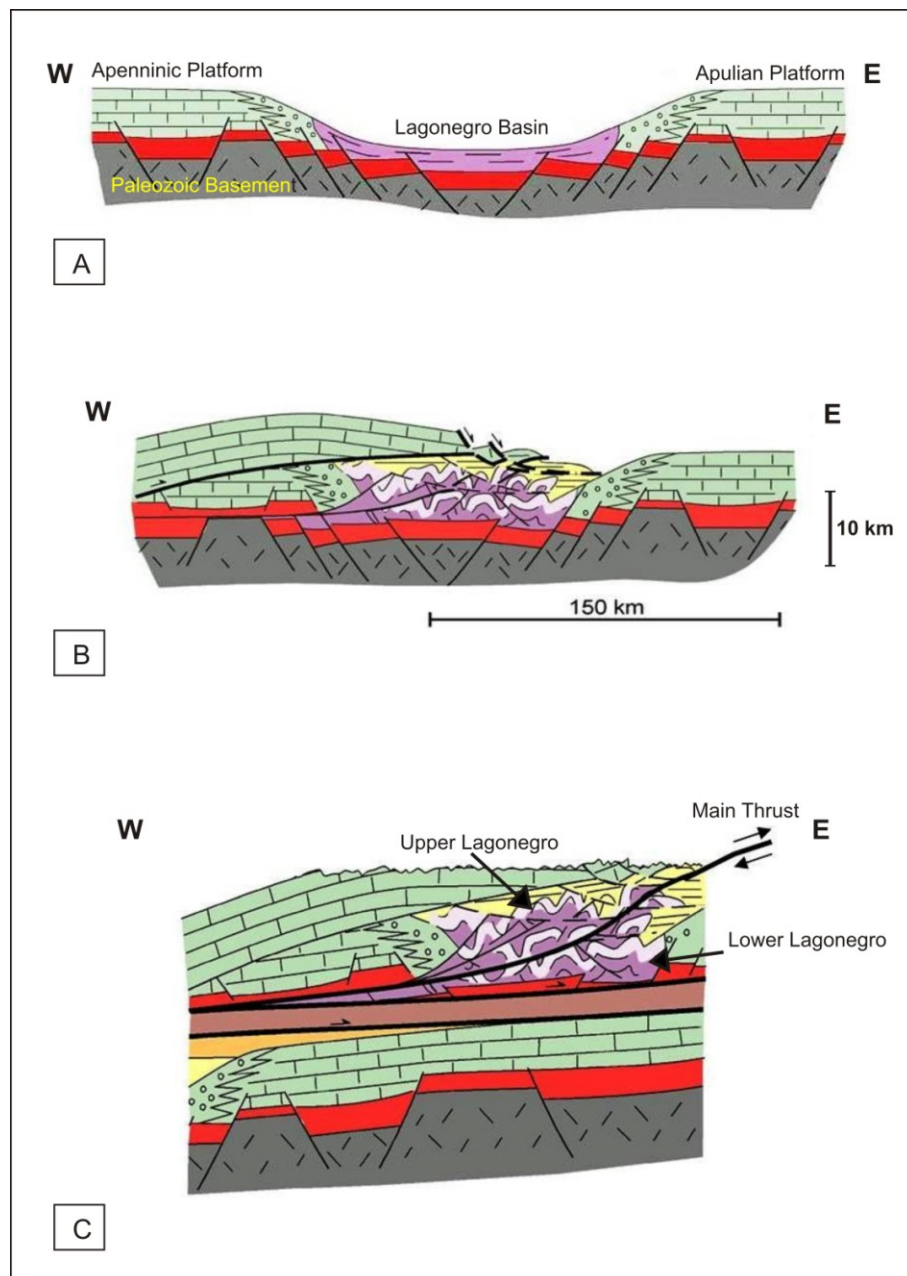


Figure 3 (previous page): Summary structural model for the evolution of the Southern Apennines from the Triassic to the Plio-Pleistocene (modified after Shiner *et al.*, 2004). Three different phases of structural evolution are illustrated: A) Mesozoic-Paleogene passive margin phase. B) Miocene buckling and first thrusting phase in the Lagonegro Basin. C) Pliocene second phase of thrusting that led to the doubling of the Lagonegro Units.

The detachment between the allochthonous wedge and the buried Apulian shallow-water carbonates is marked by a *mélange* zone up to several hundred meters thick (Fig.2). It consists mainly of intensely deformed and overpressured deep-water mudstones and siltstones of Miocene to Lower Pliocene age, including blocks of material derived from the overlying allochthon (Mazzoli *et al.*, 2001; Butler *et al.*, 2004; Shiner *et al.*, 2004).

Around early-middle Pleistocene boundary a major geodynamic change occurred and a new tectonic regime was established in the Apennine chain and adjacent foothills (Cinque *et al.*, 1993). The structures related to this new regime, characterized by a NE-SW oriented maximum extension, consist of extensional and transcurrent faults that postdate and dissect the thrust belt (Cello *et al.*, 1982; Butler *et al.*, 2004).

## 2.2 Thermal history of the fold and thrust belt

The burial history of the Southern Apennines is constrained by recent studies based on thermal and thermochronological data, which combine the analysis of organic and inorganic indicators (i.e. vitrinite reflectance and clay minerals), apatite fission tracks and fluid inclusions microthermometry on syntectonic vein cements (Aldega *et al.*, 2003, 2005; Corrado *et al.*, 2005; Mazzoli *et al.*, 2008). These studies pointed out that the Apenninic platform domain underwent a tectonic burial never exceeding 2 km, whereas the Lagonegro domain locally experienced burial depth in excess of 5 km.

In the Lagonegro Units, differences in the amount of tectonic burial and erosion/exhumation ages were detected along the strike of the chain. The former are associated with lateral variations of thrust sheet thickness (Aldega *et al.*, 2005). To the north (in the area from Potenza to the high Val d'Agri, see Fig.2), rocks of the Lagonegro Units reached a maximum burial of 3.8 km and a temperature peak in the range of 130-160 °C, in the Miocene during the first thrusting phase. The second phase of thrusting coincided with the beginning of exhumation. The latter is well constrained by apatite fission track data that provide cooling ages clustering around 5.5 Ma (Mazzoli *et al.*, 2008). To the south (Lagonegro area, Fig.2) maximum reconstructed burial is in excess of 5 km and peak temperatures are above 180 °C, while exhumation is substantially younger, apatite fission track cooling ages clustering in the last 2.5 Ma (Corrado *et al.*, 2002; Mazzoli *et al.*, 2008).

## 2.3 The evolution of the Lagonegro Basin

The classical restorations of the pre-orogenic (Triassic to Paleogene) palaeogeography of the Southern Apennines show that the African (Apulian) passive margin was characterized by carbonate platforms alternating deep-sea basins (D'Argenio *et al.*, 1975; Sgroso, 1988). More simple models suggest the presence of a unique Meso-Cenozoic pelagic basin, known as Lagonegro Basin, between two coeval carbonate



platforms, Apenninic and Apulian Platforms (Pescatore and Tramutoli, 1980; Mostardini and Merlini, 1986; see Fig.4), in accordance with a previous model proposed by Ogniben (1969). Despite there is a general agreement on the external provenance of the Lagonegro Basin in respect with the Apenninic Platform, some authors (Marsella *et al.*, 1995) alternatively proposed an internal provenance of the Lagonegro Units.

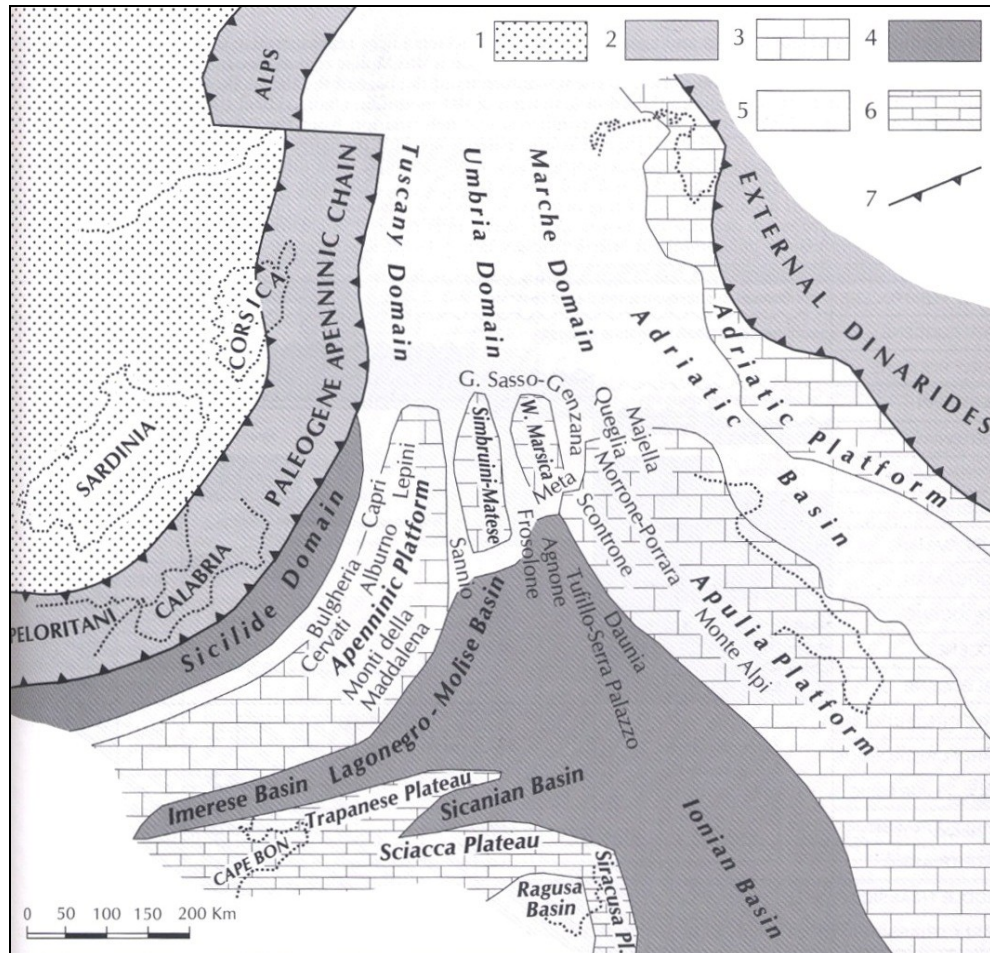


Figure 4: Palinspastic restoration of the Central Mediterranean region in the late Oligocene showing the distribution of the Central and Southern Apennine platforms and basins before their incorporation in the mountain chain (from Patacca and Scandone, 2004). 1) European foreland. 2) Paleogene mountain chains. 3) Shallow-water carbonate platforms. 4) Deeper-water basins. 5) Basinal areas with isolated structural highs. 6) Wide pelagic plateau. 7) Fronts of the orogenic belts.

The Lagonegro Basin is considered a branch of the Mesozoic western Tethys Ocean (Finetti, 1982; Sengor *et al.*, 1984; Ciarapica and Passeri, 1998, 2002; Stampfli *et al.*, 1998, 2003). Northward, the Lagonegro Basin appeared divided in two branches (Lagonegro branch and Molise branch) separated by another carbonate platform (i.e. the Simbruini-Matese Platform; Patacca and Scandone, 2003).

The Lagonegro hemipelagic succession (Fig.5) starts with the *Monte Facito* Formation, given by Lower-Middle Triassic shelfal, fine-grained siliciclastics containing carbonate buildups with dasycladacean algae and sponges (Scandone, 1967; Ciarapica *et al.*, 1990). The thickness of this Formation is about 200 m in the Lagonegro Unit II, whereas it was never encountered in the Lagonegro Unit I. The overlying *Calcari con selce*

Formation, Upper Triassic in age, consists mainly of micritic limestones, often dolomitized, containing thin-shelled bivalves and radiolarians, with beds and chert nodules. Locally, they consist of calcarenites, calcirudites and marls. The thickness of the *Calcari con selce* Formation is variable; in outcrops it is about 500 m in the Lagonegro Unit I and about 200 m in the Lagonegro Unit II. This Formation gradually passes towards to the overlaying *Scisti Silicei* Formation, consisting of Jurassic shales, radiolarites and resedimented interbeds of silicified carbonates. The thickness of the *Scisti Silicei* Formation is variable and reaches 90 m in the Lagonegro Unit I and 250 m in the Lagonegro Unit II. On the top, the *Flysch Galestrino* (Lower Cretaceous) and the *Flysch Rosso* (Upper Cretaceous-Oligocene) formations complete the Lagonegro succession. The former is made up of turbiditic siliceous marls and shales, while the latter consist of calcareous-clastic sediments interbedded with reddish marls and shales. The term “flysch” is inherited from old literature, since these two formations actually represents pre-orogenic sediments. True siliciclastic, turbidite deposits of the compressional stage are represented by the overlying Miocene sandstones and shales.

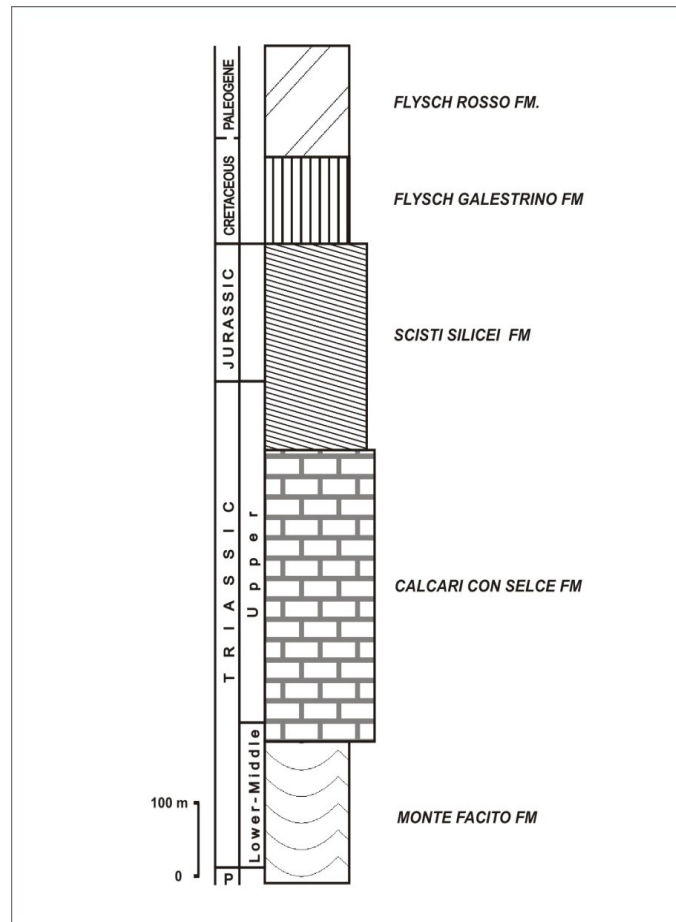


Figure 5: Simplified stratigraphic column of the Lagonegro succession.

## 2.4 The *Calcari con selce* Formation and dolomites distribution

According to Scandone (1967) the *Calcari con selce* Formation, despite its name (*calcari con selce* = cherty limestone), is actually represented by dolomites in many outcrops from the northern area of the Lagonegro Basin (from San Fele to the Val

d'Agri, see Fig.2). Dolomites mostly occur in the hanging-wall to the major thrust that duplicates the Lagonegro Units (Marsico Nuovo Thrust; Fig.6A); therefore, according to Scandone (1967), dolomites are present only in the Lagonegro Unit II. No dolomite occurrences are reported in the Lagonegro Basin cropping out further to the south (Lagonegro area; Fig.2), where only the Lagonegro Unit I crops out. However, according to the structural interpretation proposed by Bonardi *et al.* (1988) and Mazzoli *et al.* (2001), the dolomites outcropping close to Pignola and Abriola (Fig.6B) rest in the footwall to the Marsico Nuovo Thrust. Therefore, according to the latter authors, dolomitized cherty limestones occur not only in the hanging-wall, but also in the footwall to the Marsico Nuovo Thrust. As previously mentioned in paragraph 2.1, the subdivision in tectonic units by Scandone (1972) was influenced by the different sedimentary features observed, thus implying a match between thrust sheets and sedimentary facies. Field observations carried out in this research, integrated with stratigraphical information from Monte Gargaruso well, allow to consider the structural interpretation of Bonardi *et al.* (1988) and Mazzoli *et al.* (2001) as the more correct.

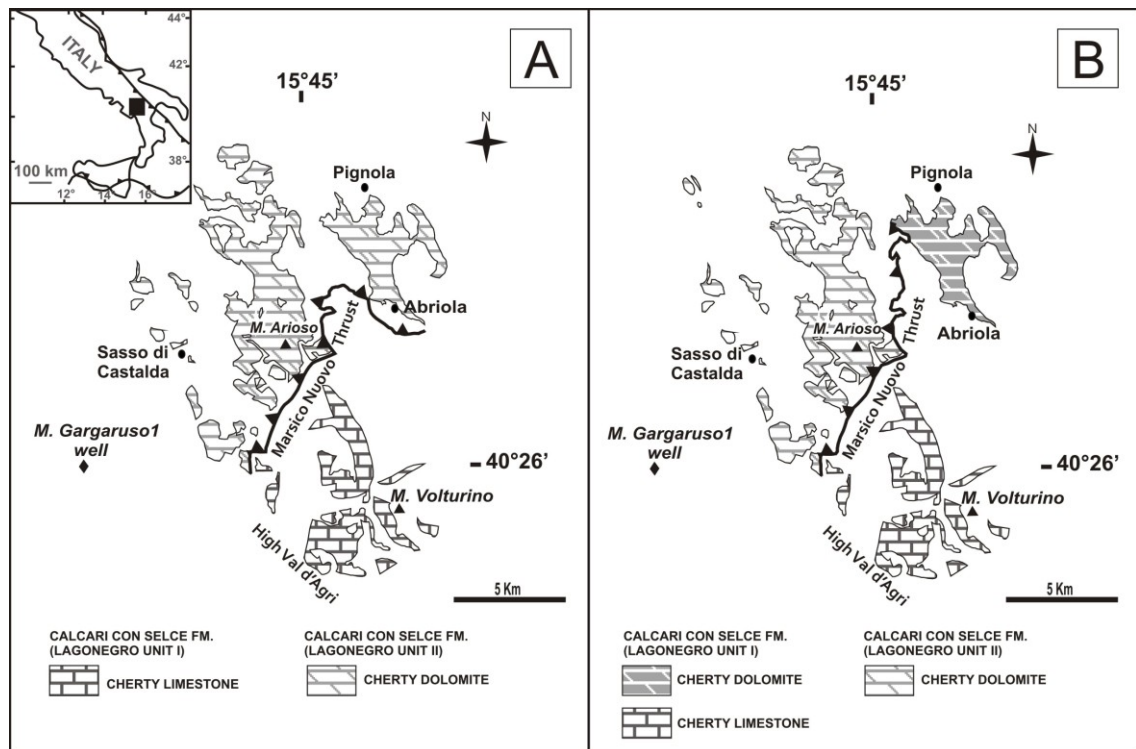


Figure 6: Distribution of the *Calcari con selce* Formation in the Pignola-high Val d'Agri area: comparison between two different structural interpretations. A) According to Scandone (1967) the Pignola-Abriola succession is in the hanging-wall to the Marsico Nuovo Thrust, thus belonging to the Lagonegro Unit II. B) According to Bonardi *et al.* (1988) and Mazzoli *et al.* (2001) the same succession is in the footwall to the Marsico Nuovo Thrust, thus belonging to the Lagonegro Unit I.

Scandone (1967) recognized the presence of four different facies both in the *Calcari con selce* and in the *Scisti Silicei* formations. These facies actually represent four different succession types, depending on the proximity to the Apenninic Platform margin. They are oriented N-S, with the more proximal successions occurring to the north (Fig.7). The main difference is that in proximal and in intermediate successions (respectively San



Fele and Pignola facies), the limestones of the *Calcarei con selce* Formation are often dolomitized, whereas in more distal successions (Armizzone and Lagonegro-Sasso di Castalda facies) they are not affected by dolomitization. As dolomitization is not only a syndepositional process, but it can occur as well very late after deposition, and even after exhumation (see paragraph 3.2 for references), the presence of dolomites in a succession does not constitute a good proof for the proximity of the succession. Nevertheless, Scandone (1967) recognized other elements supporting the proximity of the northernmost facies, such as the presence of intraformational dolomitic breccias with angular fragments of chert in the *Calcarei con Selce* Formation, and the presence of numerous levels of graded calcirudites and calcarenites in the *Scisti Silicei* Formation.

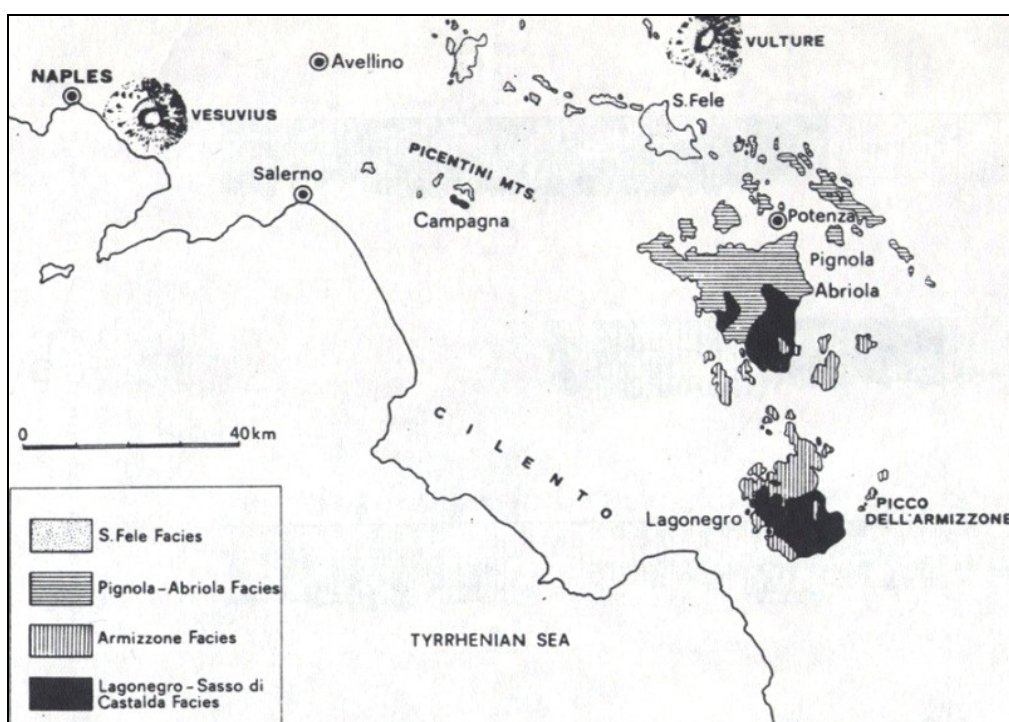


Figure 7: Facies distribution of the Lagonegro succession in Southern Apennines according to Scandone (1975). From San Fele to Lagonegro the facies became progressively more distal.

The *Calcarei con selce* outcropping to the south consist only of well-bedded cherty calcilutites with shale interlayers. In the *Scisti Silicei* of intermediate successions, the graded breccias are still present but they become progressively less frequent, until they completely disappear in distal successions. The absence of breccias and resedimented levels in the successions of the south indicate that these latter are far from the source area (i.e. the platform margin). Moreover, the thickness of the *Scisti Silicei* is greater in northern outcrops and lesser in those of the south, thus indicating that towards to the south the sedimentation rate was very low, which is typical of deep environment.

The same facies trend, displaying increasingly distal features moving from north to south, based on the abundance of platform-derived carbonate turbidites and on the thickness of the *Scisti Silicei* Formation, was identified by Bertinelli (2003). The facies arrangement of this author differs from that of Scandone (1967) only for the number of the facies, which in the former case are three instead of four.



Miconnet (1988) also recognized important lateral variations of the Lagonegro Basin facies, arranged along a currently N-S oriented axis, showing sedimentological features from proximal to distal. These lateral variations of the facies are similar to those found in deep-sea fans. The features of proximal successions (i.e. those outcropping to the north) recognized by Miconnet (1988) in the *Calcarei con selce* Formation are: thick beds (3-4 meters), irregular stratification, numerous nodular or lentiform beds, numerous coarse sediments, rare shales and pelites, bad grading, abrupt stratification surfaces and numerous figures of currents. The presence of dolomites to the north is presented as an element indicating proximality as well. Another element of proximality is the higher sedimentation rate in the *Scisti Silicei* Formation in northern successions. On the contrary, the facies of the *Calcarei con Selce* Formation outcropping to the south display distal features, such as: thinner beds (10-50 cm), plane and parallel stratification with presence of bed-parallel and convolute laminations, particles always fines, and abundant shales and pelites, good grading and absence of dolomites.

Passeri *et al.* (2005) observed the same N-S orientation of the stratigraphic successions proposed by the previously mentioned authors, without adding any new elements supporting this paleogeographic interpretation. These authors also suggested the existence of a basin opened southwards and bordered by wide carbonate platform systems in the northern side, and proposed a relationship between dolomitization and proximality, as dolomitization is most common in northern areas and in Molise, where the outcropping successions show characteristics of major proximality. The late diagenetic dolomitization of the proximal facies was referred to the migration of high Mg solutions squeezed out by the sulphate of the underlying *Burano Anhydrites* Formation during its compaction.

Marsella (1988) proposed a different interpretation of the facies arrangement. For this author the facies display a proximal to distal trend from west to east (Fig.8). These facies are currently organized in parallel outcrop zones having an apenninic orientation, with the Maddalena Mountains representing the slope area that linked the Apenninic Platform to the Lagonegro Basin. However, the study of Marsella is incomplete, as he analyzed only the northern outcrops of the Lagonegro succession, from San Fele to the high Val d'Agri, ignoring the distal characteristics exhibited by the successions in southern outcrops (i.e. near Lagonegro village).

Pescatore *et al.* (1999) identified the most distal facies in the present-day central zone of the Lagonegro Basin, whereas the western and the eastern sectors represent the proximal facies. In fact they recognized that in the westernmost areas, the successions are characterized by frequent occurrence of coarse to fine calciclastic deposits settled by dense gravity flows coming from a carbonate platform margin as well as by slumps and greater thicknesses of the single formations. The geometry of the sedimentary bodies, the paleocurrent directions, and the grain size distribution of the redeposited limestones allowed these authors to state that the carbonate input came from the western sectors. In the eastern sector, the facies are similar to those observed in the western sector, but in this case the input came from the eastern sectors.

The bibliographical review on the Lagonegro Basin palaeogeography reported in this paragraph indicates that there are two main interpretations: the successions (or “facies”), from proximal to distal, are currently arranged N-S or alternatively W-E. Both interpretations could be considered as a simplification of a more complex palaeogeography.

Combining together all the stratigraphic elements reported by the different authors, it could be envisaged that the closure of the Lagonegro Basin was towards north, and the successions closer to the platform margin (i.e. to the source area for coarse turbiditic sediments) are now located in a north-northwest area, while distal successions are placed further to the south, in areas close to Mount Volturino and to Lagonegro village.

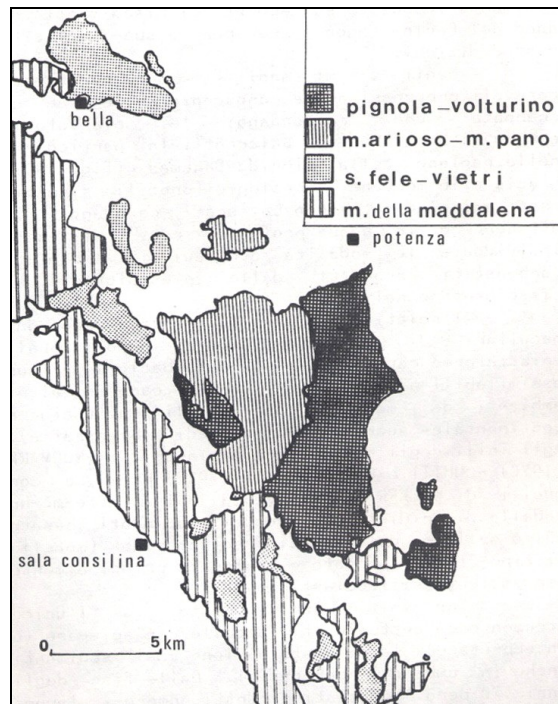


Figure 8: Facies distribution of the Lagonegro succession in Southern Apennines according to Marsella (1988). The facies are oriented West-East and the Maddalena mountains represent the slope area connecting the Apenninic Platform to the Lagonegro Basin.

## Chapter 3: Early versus late dolomitization models

### 3.1 The “dolomite problem”

Dolomites in Quaternary sediments have a limited thickness (one to few meters) and are few tens of kilometers wide (Warren, 2000). They form in few and restricted areas of Earth's surface, such as the lakes of the Coorong Gulf in southern Australia (Alderman and Skinner, 1957; Warren, 1990), the sabkha environments of the Persian Gulf (McKenzie, 1981; Warren, 1991), the islets of Florida and Netherlands Antilles (Deffeyes *et al.*, 1965; Major *et al.*, 1992), the tidal plains of Bahamas (Lasemi *et al.*, 1989; Mitchell and Horton, 1995), and the coastal system of Lagoa Vermelha in Brasil (Vasconcelos and Mckenzie, 1997). Huge volumes of dolomites, whose successions are hundreds meters thick, were instead found in sedimentary rocks of the geological record. Modern analogous cannot explain the formation of these ancient dolomites (Zenger, 1972).

Since more than 200 years, studies on dolomites represent an open challenge, as chemical and hydrological conditions that lead to dolomites formation are still poorly understood. The fundamental “dolomite problem” is that stoichiometric dolomite has never been inorganically synthesized in laboratory at typical depositional environments conditions. Therefore, geochemical parameters, needful to calculate dolomitizing fluids composition, should be extrapolated from high temperature experiments (Machel, 2004). Another unresolved problem is the understanding of why dolomites abundance decreases from Paleozoic to Present time.

### 3.2 Dolomitization models

The large amount of studies on “dolomite problem” produced in the last thirty years, have shown how the dolomitization cannot be related to a unique phenomenon, but to a series of mechanisms synthesized in different dolomitization models (Fig.9). Dolomitization can act very soon after deposition, by means of surface-related processes, generally producing small amount of dolomites, or it can take place later, in intermediate to deep burial (over 1 km of depth) settings, where massive dolomite bodies are commonly formed. The essential requirements for dolomitization are a source of Mg and a transport mechanism able to carry the Mg to the site of dolomitization. Mass balance calculation indicates that hundreds of pore volumes of fluids must be exchanged in order to complete the dolomitization reaction (Land, 1980). Dolomitization models substantially represent hydrological models that try to predict an efficient mechanism for pumping Mg-rich fluids into carbonate formations. These models can be divided into six categories: evaporative, seepage-reflux, meteoric-marine mixing, seawater models, microbial/organogenic, and burial models.

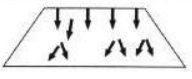

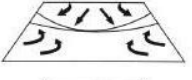

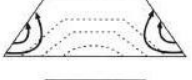

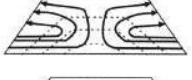
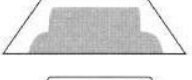
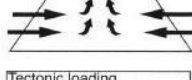
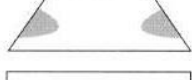

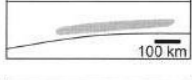
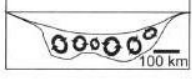



Dolomitization Model	Source of Mg <sup>2+</sup>	Delivery Mechanism	Hydrological Model	Predicted Dolomite Patterns
A. Reflux Dolomitization	seawater	storm recharge, evaporative pumping density-driven flow		
B. Mixing Zone (Dorag) Dolomitization	seawater	tidal pumping		
C1. Seawater Dolomitization	normal seawater	slope convection (K <sub>v</sub> > K <sub>h</sub> )		
C2. Seawater Dolomitization	normal seawater	slope convection (K <sub>h</sub> > K <sub>v</sub> )		
D1. Burial Dolomitization (local scale)	basinal shales	compaction-driven flow		
D2. Burial Dolomitization (regional scale)	various subsurface fluids	tectonic expulsion topography-driven flow		
D3. Burial Dolomitization (regional scale)	various subsurface fluids	thermo-density convection		
D4. Burial Dolomitization (local and regional scales)	various subsurface fluids	tectonic reactivation of faults (seismic pumping)		

Figure 9: Dolomitization models, illustrated as groundwater flow system and predicted dolomitization pattern (Amthor *et al.*, 1993, modified by Machel, 2004).

Fluids involved in the evaporative and in the seepage-reflux models are hypersaline brines. The **evaporative** model envisages direct precipitation of penecontemporaneous dolomites in evaporitic environments like sabkhas (McKenzie, 1981) and in coastal evaporitic lakes (Von der Borch and Lock, 1979). The **seepage-reflux** model predicts the generation of dolomitizing fluids through evaporation of lagoon water or tidal flat pore waters and then the percolation and descent of these concentrated seawater into the underlying carbonates (Adams and Rhodes, 1960; Fisher and Rodda, 1969). The downward fluid motion would be driven by the density contrast between the heavy, concentrated seawater and the lighter groundwater.

The **meteoric-marine** mixing model requires hyposalines solutions, which originate from the mixing of seawater and freshwater (Hanshaw *et al.*, 1971). In diluted solutions, the high Mg/Ca ratio of seawater is retained, but some of the kinetic obstacles due to the high ionic strength of seawater are removed (Folk and Land, 1975), thus favoring dolomite precipitation. This model has been invoked to explain ancient dolomite sequences not associated with evaporites, but the model has received much criticism, as extensively dolomitization has not been unambiguously proven in any freshwater-seawater mixing zone, in recent or in ancient carbonates (Land, 1985; Machel and Mountjoy, 1986, 1987; Hardie, 1987).

**Seawater** dolomitization models refer to a group of models whose common denominator is seawater as the principle dolomitizing fluid, and that differ in hydrology and/or depth and timing of dolomitization (Machel, 2004). All dolomites in this group are post-depositional, and the diagenetic settings range in depth from shallow to intermediate burial. Different mechanisms were invoked to put into motion marine

fluids, and various hydrologic systems were proposed: seawater thermal convection or Kohout model (Sanford *et al.*, 1998), ocean current pumping (Saller, 1984), reflux of slightly concentrated seawater (Simms, 1984), and tidal pumping along shorelines (Carballo *et al.*, 1987).

The **microbial/organogenic** model (Kelts and McKenzie, 1982; Mazzullo, 2000) considers bacterial sulphate reduction and/or methanogenesis as mechanisms promoting dolomitization. This model accounts for small amounts of syndepositionally or early post-depositionally dolomite, and its main requirements are seawater and organic-rich materials.

**Burial** models explain dolomitization processes, acting after lithification in intermediate to deep burial settings, and forming massive dolomite successions. In these settings the kinetic requirements for dolomite formation are more easily satisfied than at surface. The increasing temperature with depth reduces the proportion of hydrated  $\text{Mg}^{2+}$  ions, thus increasing the dolomitization rates. All burial models differ mainly in the nature of the drives and directions of fluid flow (Morrow, 1982, 1998). Four main types of fluid flow take place in subsurface diagenetic settings: (1) compaction flow, (2) thermal convection, (3) topography driven flow, and (4) tectonically-driven flow. In addition, hydrothermal or hydrofrigid fluids may be injected into any burial setting where fractures open up. According to the **compaction flow** (Illing, 1959), seawater, or its subsurface derivatives buried along with the sediments, are pumped through the rocks as result of compaction dewatering. This model never became popular, as the limited amounts of compaction water cannot account for large masses of dolomite (Morrow, 1982).

**Thermal convection** is driven by spatial variations in temperature that result in changes in pore-water density and thus effective hydraulic head. Variations in temperature may be due to elevated heat flux in the vicinity of igneous intrusions (Wilson *et al.*, 1990), the lateral contrast between warm platform waters and cold ocean waters (Kohout *et al.*, 1977), or lithology controlled variations in thermal conductivity (Phillips, 1991; Jones *et al.*, 2004).

The **topography driven flow** (Garven and Freeze, 1984; Garven, 1985) may take place in uplifted thrust belts exposed to meteoric recharge. The elevated topography of the thrust belt provides the hydrodynamic potential for gravity-driven meteoric fluids, concentrated by water-rock interaction, to circulate rapidly into the foreland basin, in front of the thrust belt, across distances of several hundreds of kilometers.

The **tectonically-driven flow** (Oliver, 1986) is triggered by tectonic loading and compression during the development of orogenic thrust belts and causes the expulsion of metamorphic and/or basinal fluids towards the basin margins. This model has often been invoked (Qing and Mountjoy 1992, 1994; Amthor *et al.* 1993; Drivet and Mountjoy, 1997), even though fluxes of the tectonically-induced flow appear to be low (Machel *et al.*, 2000).

**Hydrothermal** dolomitization is not a model in its own right because hydrothermal conditions may occur in a variety of situations in all types of diagenetic settings from near surface to deep burial, especially where fractures transgress more than one burial-

diagenetic zone. Hydrothermal dolomite is formed by fluids having temperatures 5-10 °C higher than the surrounding host rock (Michel and Lonnee, 2002) that flow upwards through active faults and fractures (Taylor and Sibley, 1986; Hurley and Budros, 1990). The hydrothermally dolomitized rock bodies usually are limited to plumes in the vicinity of faults and fractures, but the process may be also effective on a basinal scale, eventually combined with other hydrological models, i.e. free convection.

## Chapter 4: Methods

### 4.1 Field work and wells analysis

Field survey was performed in order to qualitatively evaluate the extension of the dolomitization phenomenon in the outcropping areas of the Lagonegro Basin successions. In these areas, the spatial distribution of dolomite bodies was qualitatively mapped in order to evaluate the volumes of the dolomitized rocks related to the undolomitized ones.

A total of 125 rock specimens of both dolomites and precursor limestones from the *Calcari con selce* Formation were collected for standard petrographic and geochemical analyses in different study areas. The northern area comprises the Mount Marrone (Molise region), the tectonic window of Campagna (Campania region) and the San Fele-Mount Pierno outcrops (Lucania). The southern area includes outcrops that go from Pignola village to high Val d'Agri area (Lucania; see Fig.10 and 11).

Three outcrops (Pignola, Madonna del Sasso and Sasso di Castalda; Fig.11) were selected for the structural analysis of veins systems. Orientation (dip direction and angle of dip) of bedding and cleavage planes was measured in the field in dolomitized and undolomitized bodies. Calcite and dolomite veins systems present in the studied rock bodies were analyzed as well. Orientation of more than 300 veins was measured, in order to reconstruct the main stress fields. Relative timing of the different veins generations, and relative timing respect to burial and tectonic stylolites were investigated.

The distribution of dolomitized bodies in the Lagonegro Units was investigated as well in subsurface. Over 30 stratigraphic logs of wells penetrating the Lagonegro successions, mostly located in the Val d'Agri oil fields, were examined in order to verify if the *Calcari con selce* Formation is affected or not by dolomitization. Fifty cutting specimens were collected from Acerno 1, Monte Gargaruso 1 and Monte Foi 1 wells, and destined to petrographic and geochemical analyses.

### 4.2 Peels, cutting and thin sections preparation

Twenty polished slabs of both limestones and dolomites were used for acetate peels preparation. The polished surface of 10 slabs was etched in dilute (about 1%) HCl for a few seconds, and was then washed and thoroughly dried. Ten other slabs were instead stained with Alizarin-red S. This solution was prepared following the procedure of Dickson (1966). After treatment with the staining solution for about 30-60 seconds the calcite assumes a red colour, while the dolomite remains uncoloured. Acetone was applied to all the etched (with HCl as well as with Alizarina-red S) surfaces, and the frosted side of the acetone peel was then rolled out on them. The acetate peel was removed from the slabs after half an hour.

From polished slabs of the surface collected specimens, 112 thin sections of both dolomite and precursor limestone were prepared. Half of the slabs were previously

impregnated with a low-viscosity resin (Epothin®) coloured with a blue additive (EpoBlue®). The coloring allowed to highlight the pore spaces.

For each well cutting (50 specimens), small (few millimeters) fragments of dolomite rocks were picked and incorporated with a glue. Thin sections of the incorporated samples were prepared.

Over 30 thin sections were finally stained with Alizarin red-S in order to discriminate the calcite and the dolomite phases.

### 4.3 Petrographic analyses

#### *4.3.1 Transmitted light microscopy*

Petrographic observations were performed observing all the thin sections under transmitted light using a Leica DM-EP microscope. The classification of dolomite textures proposed by Sibley and Gregg (1987) and later by Warren (2000) was used to describe the studied dolomites. The crystal size is reported as diameter in  $\mu\text{m}$ .

Petrographic observations of macroscopic features (crosscutting relationships of veins and stylolites) were carried out on acetate peels under transmitted light using a Leica Wild M420 microscope.

#### *4.3.2 Cathodoluminescence (CL) microscopy*

Cathodoluminescence (CL) microscopy was carried out on most of the prepared thin sections. It is a technique based on luminescence characteristics of minerals submitted to a high voltage electron beam. Luminescing conditions occur in impure crystalline substances, where ions in the crystal structure act either as luminescent centre, activating the luminescence, or as inhibitors of luminescence. The luminescence in carbonates ranges from yellow-orange to black (non luminescent) colours and reflects the presence of major to trace elements.  $\text{Mn}^{2+}$  is known to be the most effective activator of luminescence for calcites and dolomites, whereas  $\text{Fe}^{2+}$  is regarded to be a quencher of luminescence (Long and Agrell, 1965; Sommer, 1972; Ebers and Kopp, 1979; Pierson, 1981). Minor activators are REEs like  $\text{Sm}^{3+}$ ,  $\text{Eu}^{2+}$  and  $\text{Eu}^{3+}$ , whereas  $\text{Co}^{2+}$ ,  $\text{Ni}^{2+}$  and  $\text{Fe}^{3+}$  have a quencher function. CL often allows to recognize crystal zoning, by illuminating different mineralogical phases, which often remain undistinguishable under normal light petrographic examination.

A CCL 8200 mk3 was used for cold CL analyses. Part of the thin sections was analyzed for cold CL using a Technosyn 8200 Mark II (OPEA, France) at IFP Energies nouvelles (Paris, France). A beam voltage ranging from 10 and 20 kV and a current comprise between 150 and 200  $\mu\text{A}$  were used.

### 4.4 Geochemical methods

#### *4.4.1 Oxygen and Carbon stable isotope analyses*

Stable isotopes analyses in diagenetic studies are based on fractionation, which is the distributional difference of isotopes of the same element during a reaction from one



phase to another phase (such as mineral precipitation or recrystallization). Variations in isotopic ratios are small but they can be precisely measured.

Oxygen and carbon stable isotopes are the most widely applied geochemical methods in dolomite research, as they often allow to infer the diagenetic environment responsible for dolomitization. The O and C isotope composition of a sample is expressed relative to a standard of known isotopic composition, by means of the  $\delta^{18}\text{O}$  and  $\delta^{13}\text{C}$  notations. These are calculated as:

$$\delta^{18}\text{O} = [ (^{18}\text{O}/^{16}\text{O})_{\text{sample}} - (^{18}\text{O}/^{16}\text{O})_{\text{standard}} / (^{18}\text{O}/^{16}\text{O})_{\text{standard}} ] \cdot 10^3 \text{ ‰}$$

and

$$\delta^{13}\text{C} = [ (^{13}\text{C}/^{12}\text{C})_{\text{sample}} - (^{13}\text{C}/^{12}\text{C})_{\text{standard}} / (^{13}\text{C}/^{12}\text{C})_{\text{standard}} ] \cdot 10^3 \text{ ‰}$$

The  $\delta^{18}\text{O}$  values of carbonates allow to determine, as a first approximation, the  $\delta^{18}\text{O}$  value and/or the temperature of the fluid present during crystallization, and possibly allow to discriminate between meteoric, marine and/or evaporitic waters. The  $\delta^{13}\text{C}$  values are closely related to the  $\delta^{13}\text{C}$  of the bicarbonate dissolved in the fluid from which the mineral precipitated. Alteration of the primary  $\delta^{13}\text{C}$  not always occurs during diagenesis, and it depends on the amount of C present in the diagenetic fluids. The  $\delta^{13}\text{C}$  of the carbonates can be used for instance to identify, whether meteoric water (carrying soil  $\text{CO}_2$ ) was involved, or whether  $\text{CO}_2$  from organic matter maturation was available during diagenesis.

O and C stable isotopes analyses were performed at the Isotopen-labor of the Institut für Geologie, Mineralogie und Geophysik of the Ruhr-University (Bochum, Germany). A few milligrams of dolomite sample were drilled out with a dentist drill. About 0.5 mg of powder were put in an oven for 2 hours at 70°C. The isotopic value was measured through a Mass Spectrometer Finnigan Delta S. The oxygen isotopic composition of dolomite was corrected using the fractionation factors given by Rosenbaum and Sheppard (1986). The precision ( $1\sigma$ ), monitored by replicate analyses of international standard and one laboratory standard, is  $\pm 0.09\text{‰}$  for the carbon and  $\pm 0.13\text{‰}$  for the oxygen. All of the  $\delta^{18}\text{O}$  and  $\delta^{13}\text{C}$  values for carbonates are reported in conventional per mil (‰) relative to the V-PDB international standard (Vienna Pee Dee Belemnite, South Carolina USA). The O isotope composition of fluids is expressed relative to the SMOW (Standard Mean Oceanic Water) international standard. This represents the average O isotope composition of present day seawater (0‰). The conversion of the  $\delta^{18}\text{O}$  values from the PDB to the SMOW scale is expressed by an equation calculated by Anderson and Arthur (1983):

$$\delta^{18}\text{O}_{\text{SMOW}} = 1.03 \delta^{18}\text{O}_{\text{PDB}} + 30.86$$

#### 4.4.2 Major to trace element analyses (ICP-AES)

ICP-AES (Inductively Coupled Plasma - Atomic Emission Spectrometry) measurements were performed to determine major (Ca and Mg) and trace elements (Sr, Mn, Fe and Ba) concentration of the studied dolomites.

During precipitation, carbonate cements incorporate various trace and minor elements proportionally to their concentration in the fluid. The element's incorporation is dominantly by substitution for  $\text{Ca}^{+2}$ , rather than interstitially between lattice planes, at site defects, as adsorbed cations, or within inclusions (Veizer, 1983; Banner, 1995).

When a compatible trace element substitutes for a host element in the lattice, the incorporation of the trace element into the solid from the mother liquid can be described by the Homogeneous Distribution Equation (McIntyre, 1963). This is expressed as:

$$({}^m\text{X}_\text{T}/{}^m\text{X}_\text{H})_{\text{solid}} = k \cdot ({}^m\text{X}_\text{T}/{}^m\text{X}_\text{H})_{\text{liquid}}$$

where  $m$  is the molar concentration,  $\text{X}_\text{T}$  is the trace element,  $\text{X}_\text{H}$  is the host element and  $k$  is the distribution coefficient. The distribution coefficient  $k$  can be used to predict the element partitioning. For  $k > 1$ , the guest ion will be partitioned preferentially into the solid. For  $k < 1$ , the ratio of the guest to host ions in the solid is less than the same ratio in the fluid. For  $k = 1$  no partitioning occurs, and the guest to host ratio will be the same in the solid and in the fluid. However, the distribution coefficients of the elements are relatively crude estimates and can be dramatically affected by temperature, major element composition of the solid phase (stoichiometry and degree of ordering), the rate of precipitation of the cement (Mucci and Morse, 1983; Given and Wilkinson, 1985; Banner, 1995) and non-equilibrium precipitation. Furthermore, experimental values for dolomite are difficult to obtain, since dolomite cannot be precipitated directly in the laboratory at realistic diagenetic temperatures. Therefore, the minor and trace element content of dolomites could help only to distinguish between different dolomite types, and to obtain general information on the nature of the dolomitizing fluids. (Brand and Veizer, 1980; Land 1980; Kretz, 1982; Veizer, 1983; Machel, 1988).

Analyses were performed at the Institut für Geographie of the Ruhr-University (Bochum, Germany). Approximately 1 mg of powder was dissolved in 1 ml of HCl 1 Mol, diluted in 4 ml of  $\text{H}_2\text{O}$  and analyzed with an atomic spectrometer (ICP-AES). The accuracy of measurements is  $< \pm 2\%$  of the measured concentration. The data are expressed in ppm for the minor and trace elements, and in wt % for the major elements.

#### 4.4.3 Sr isotope analyses

Strontium has four naturally occurring stable isotopes:  $^{88}\text{Sr}$  (82.53%),  $^{87}\text{Sr}$  (7.04%),  $^{86}\text{Sr}$  (9.87%), and  $^{84}\text{Sr}$  (0.56%).  $^{88}\text{Sr}$ ,  $^{86}\text{Sr}$  and  $^{84}\text{Sr}$  are not part of any decay series, while  $^{87}\text{Sr}$  is generated by the decay of  $^{87}\text{Rb}$ . Dolomite excludes rubidium from its structure and incorporates strontium as a substitute for calcium. As no significant fractionation occurs during precipitation, the  $^{87}\text{Sr}/^{86}\text{Sr}$  of dolomite is the same as the one in the fluids from which it precipitated (or subsequently re-equilibrated). The  $^{87}\text{Sr}/^{86}\text{Sr}$  of the fluids from

which the dolomite formed is in turn related to the minerals that provided strontium through water-rock interaction.

The Sr isotope analyses were performed at the Isotopen-labor of the Institute für Geologie, Mineralogie und Geophysik of the Ruhr-University (Bochum-Germany). The measurements were carried out on 1 mg of powder in a 2.5 M HCL. The separation between the two components was done by the standard procedure of ionic exchange. The Sr isotope ratio was determined by means of a Thermal-ionization Finnigan Mat 262 Mass Spectrometer. The Sr ratio values were then normalized to a ratio value of  $^{87}\text{Sr}/^{86}\text{Sr} = 0.1194$ . The precision was better than 0.000004.

## 4.5 Fluid Inclusions (FIs) study

### 4.5.1 Microthermometry: principles and parameters

Fluid inclusions (FIs) are small drops of fluid (liquid and/or gas) entrapped as imperfections in a crystal that grows in presence of a fluid phase. FIs analysis may provide information about temperatures, pressures and composition of the sealed fluids, which are useful for the reconstruction of the ancient diagenetic environments. On the basis of the timing of their formation, FIs could be classified, in *primary*, *secondary* and *pseudosecondary* (Goldstein and Reynolds, 1994).

A group of fluid inclusions that were trapped at the same time is called Fluid Inclusion Assemblage (FIA). A FIA represent a “fluid event” in the history of the system, as all the inclusions of the FIA are supposed to be trapped approximately at the same temperature and pressure, and contain a fluid of approximately the same composition (Samson *et al.*, 2003).

Microthermometry analysis of FIs is based on phase changes that occurred when an inclusion is heated and cooled. The parameters that could be observed and measured in two-phase liquid-vapor inclusions are explained hereunder:

- The homogenization temperature ( $T_h$ ) is the temperature at which the vapour and liquid homogenize (the inclusion become monophasic).  $T_h$  represents the minimum trapping temperature of the fluid within the host rock, and it gives an indication of the bulk fluid density.  $T_h$  is measured during heating runs.
- The temperature of gas nucleation ( $T_{ng}$ ) and the temperature of ice nucleation ( $T_{ni}$ ) are measured during cooling runs. The former is the temperature at which a bubble of gas nucleates after homogenization, and the second one is the temperature at which ice-like phases (ice and salt hydrates) nucleate.
- The apparent eutectic temperature ( $T_{eap}$ ) and the final melting temperature ( $T_{mi}$ ) are observed when the inclusion is heated again, after freezing.  $T_{eap}$  represents the temperature at which the first liquid is seen, and  $T_{mi}$  represents the temperature at which the ice-like phases completely melt. These two parameters give information on fluid salinity and composition.

#### 4.5.2 Microthermometry procedure

Ten double polished thick sections (100-120  $\mu\text{m}$ ) of dolomite were prepared by the Petrolab of Latina (Italy) and used for the FIs analysis. One thick section (120  $\mu\text{m}$ ) of limestone containing a calcite nodule pre-dating the dolomites was investigated as well.

A detailed FI petrography on thick sections allowed to distinguish different FIAs according to shape, phase proportions and spatial distribution of the FIs within the crystals, in order to group the FIs in different petrographic types.

A Linkam MDS 600stage mounted on a Nikon LV100 Eclipse was used for the microthermometry measures. Here size, shape, liquid/gas ratio of the FIs were petrographically established. A video camera Pixlink MegaPixel FireWire was mounted onto the microscope and connected to a computer screen in order to facilitate FIs observation. The Linksys 32 (Version 2.0.2) software enabled all the operations for FI petrography and microthermometry. Calibrations were performed using synthetic fluid inclusions at  $-56.6\text{ }^{\circ}\text{C}$  ( $\text{CO}_2$ ),  $0.1$  and  $374\text{ }^{\circ}\text{C}$  ( $\text{H}_2\text{O}$ ),  $-20.9\text{ }^{\circ}\text{C}$  ( $\text{NaCl-H}_2\text{O}$ ).

Each thick section was cut in very small chips. The chips were placed in the stage chamber, which includes a sample port controlled by X-Y manipulator, where they were heated by thermal conduction and cooled by a flux of  $\text{N}_2$  through the stage, in order to accomplish high and low temperature measurements respectively. Microthermometry was accomplished on the two-phase FIs. The accuracy of the data is about  $\pm 1\text{ }^{\circ}\text{C}$  for heating runs and about  $\pm 0.1\text{ }^{\circ}\text{C}$  for cooling runs.

The volumetric proportion of the liquid phase relative to the total volume, referred as degree of fill (F), was calculated for large FIs at room temperature from screen images by measuring areas. According to Bakker and Diamond (2006), with  $F > 0.9$  the area fraction is nearly equal to volume fraction,  $\pm 4\%$  of the measured fraction.

Salinities were calculated from final ice melting temperatures using the equation of Bodnar (1993) in terms of the  $\text{H}_2\text{O-NaCl}$  system, and are reported as equivalent weight percent NaCl (eq. wt % NaCl).

#### 4.5.3 Thermodynamic calculations and computer programs

Composition and density of fluid inclusions were calculated using the computer package FLUIDS (Bakker, 2003; Bakker, 2009), which include the programs BULK and LONER32.

The program BULK was used to determine bulk fluid properties of individual FIs. The final melting temperature (mean value) and the homogenization temperature (minimum, maximum and mode values) were entered in the program. The output data were the density (g/cc), the molar volume (cc/mol) and the amount of substance fractions of FIs at  $20^{\circ}\text{C}$ , calculated using a purely empirical thermodynamic model and the equation of state for aqueous systems of Krumgalz *et al.* (1996).

The program LONER32 was used to calculate the isochore slope for each sample. The input data were the mean value of the salinity and the homogenization temperature (minimum, maximum and mode values) of the FIs. The program used the model of Bodnar and Vityk (1994) to give the corresponding pressure values for each homogenization temperature. The isochores were constructed in P-T diagrams.

## Chapter 5: Field observations

### 5.1 Distribution of dolomite bodies

Field survey has confirmed that dolomites replacing the cherty limestones of the *Calcari con selce* Formation are widespread. The northernmost occurrence of basinal dolomites is constituted by the Mount Marrone outcrops (Molise region; see Fig.10), whose succession is ascribed to the Molise Basin. This latter, in the Mesozoic era, constituted a branch, extending towards the north, of the Lagonegro Basin. The limestones of the *Calcari con selce* Formation appear almost completely dolomitized in the outcrops located in the northern area. This area comprises the tectonic window of Campagna and the San Fele-Mount Pierno outcrops (Fig.10).

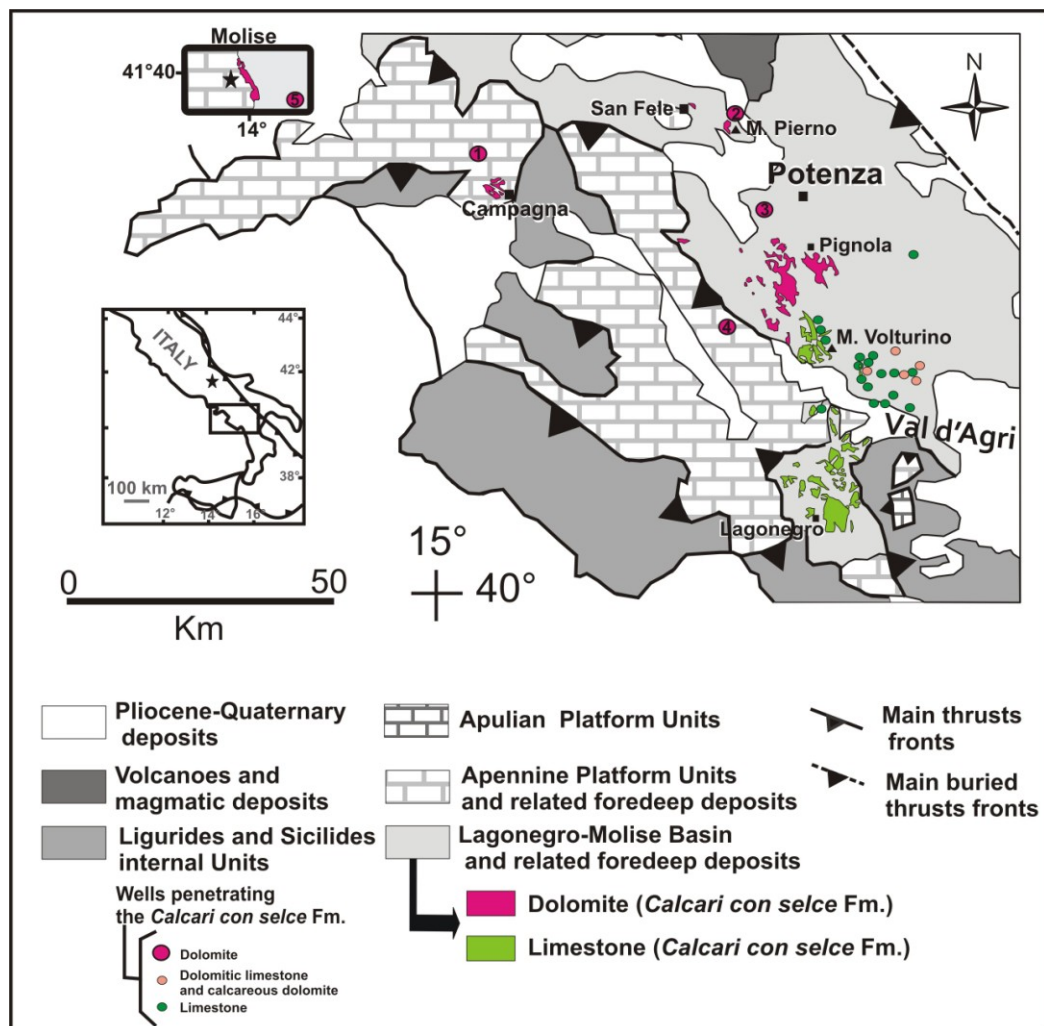


Figure 10: Geologic map of Southern Apennines (modified after Butler *et al.*, 2004). Fuchsia polygons indicate the distribution of dolomitized limestones of the *Calcari con selce* Formation, while green polygons indicate the distribution of undolomitized limestones of the same Formation. Fuchsia dots represent the location of the wells in which the cherty limestones of the *Calcari con selce* Formation are almost completely dolomitized (1-Acerno; 2-San Fele, 3-Monte Foi, 4-Monte Gargaruso, 5-Frosolone). Pink dots represent the location of the wells in which the cherty limestones are only partially dolomitized. Green dots correspond to wells in which the cherty limestones are not dolomitized.

In the southern area, which goes from Pignola to the high Val d'Agri area (Fig.10 and 11), dolomites distribution is not uniform, as many outcrops of undolomitized precursor limestones were also found. Further to the south, in the areas close to Mount Volturino and to Lagonegro village (Fig.10), the *Calcarei con selce* Formation never shows the presence of dolomites. Therefore, these areas were not investigated in detail.

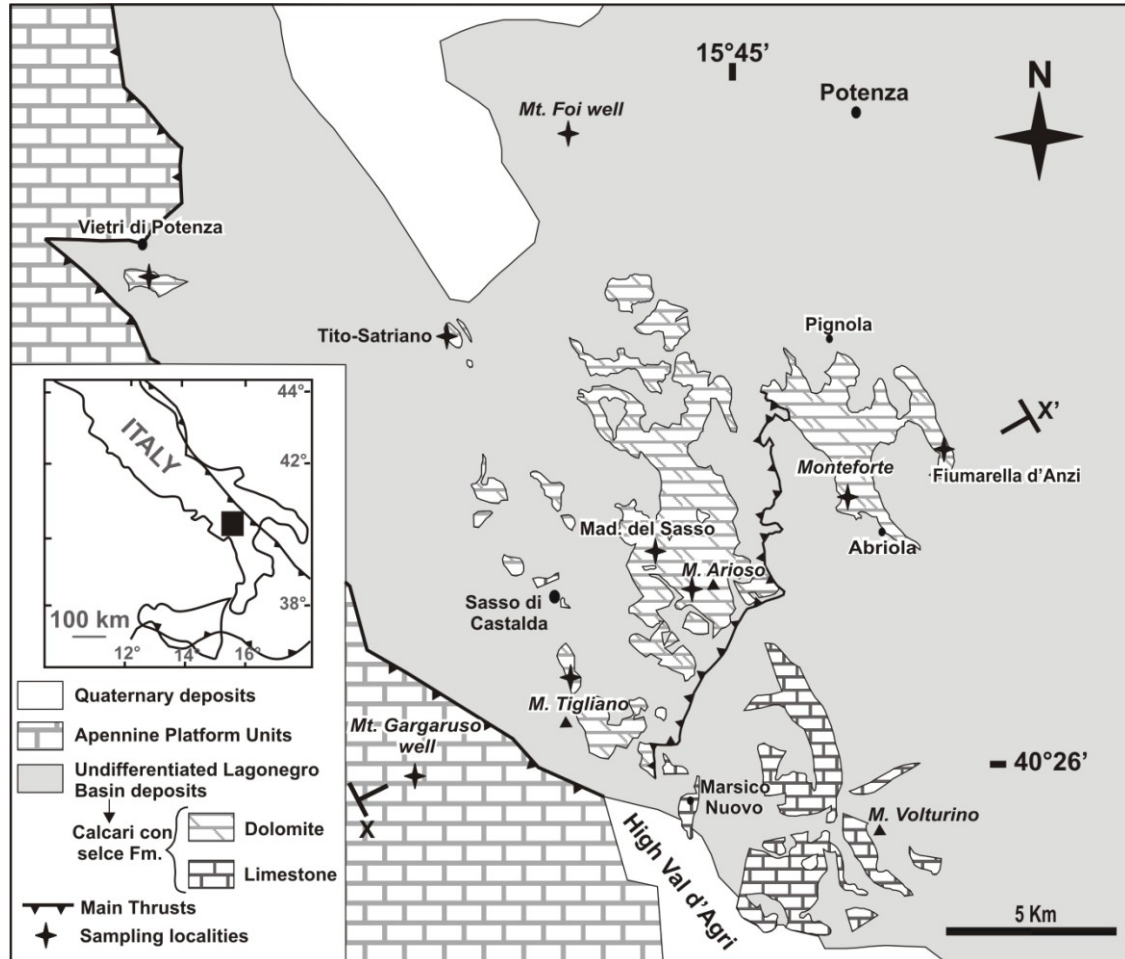


Figure 11: Distribution of the *Calcarei con selce* Formation in the southern area (Pignola-high Val d'Agri). Dolomitized cherty limestones of the *Calcarei con selce* Formation are both in the hanging-wall and in the footwall of the main thrust that doubles the Lagonegro Units. X-X' section is represented in Figure 46.

According to the structural model of Bonardi *et al.* (1988) and Mazzoli *et al.* (2001), dolomitized cherty limestones are both in the hanging-wall and in the footwall of the main thrust that doubles the Lagonegro Units (Fig.11).

Macroscopic and petrographic characteristics of the studied dolomites pointed out that the northern area (Mount Marrone, Campagna and San Fele-Mount Pierno) and the southern area (from Pignola to the high Val d'Agri) underwent different dolomitization processes. Therefore, in the following paragraphs, dolomites description of northern and southern area will be presented separately. Moreover, the description of precursor limestones features was carried out only for the outcrops of the southern area, where many dolomitization fronts were observed.



## 5.2 Molise and northern area outcrops: features of dolomites

Dolomites outcropping in the northern area, including those of Mount Marrone, are generally fine crystalline and fabric retentive.

The dolomitized succession of the Mount Marrone (Molise) consists of thinly bedded medium to coarse-grained dolomites, containing nodules and beds of chert. These dolomites are overlayed by massive banks (some meters thick) of grey dolomites (Fig.12). The massive banks are often interlayed with thin-bedded nodular dolomites containing chert nodules.

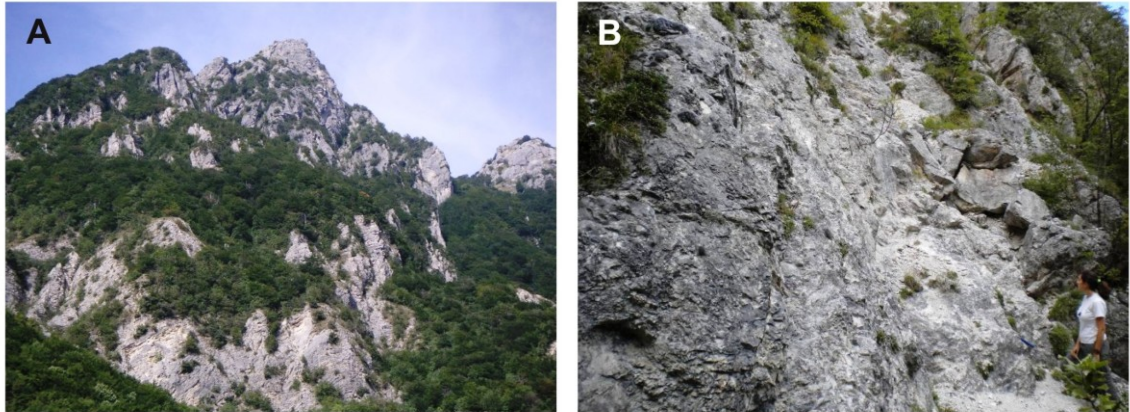


Figure 12: Dolomites outcropping at Mount Marrone (Molise). A) Mountain view. B) Outcrop of massive dolomites.

In the tectonic window of Campagna, dolomite bodies consist of dark grey and yellowish to beige well-bedded dolomite (Fig.13A). The beds thickness is in the range of 5-15 cm. Chert lenses and chert nodules are abundant. These dolomites are characterized by the presence of bed-parallel laminations and cross-laminations (Fig.13B). Locally clastic rich beds are interbedded with the dolomites (Fig.13C). Veinlets of milky white saddle dolomite are common (Fig.13B).

In Mount Pierno (Fig.13D) and in the San Fele village outcrops the dolomitized limestones of the *Calcari con selce* Formation consist of light grey medium to coarse crystalline dolomite containing chert nodules. Both massive and bedded (30-40 cm thick) dolomites are present (Fig.13E-F). The massive dolomites are characterized by dolomite cemented vugs. The passage to the overlain *Scisti Silicei* Formation is marked by the presence of partially dolomitized graded calcarenites and calcirudites beds. Dolomitization fronts were never observed in any outcrops of the northern area.

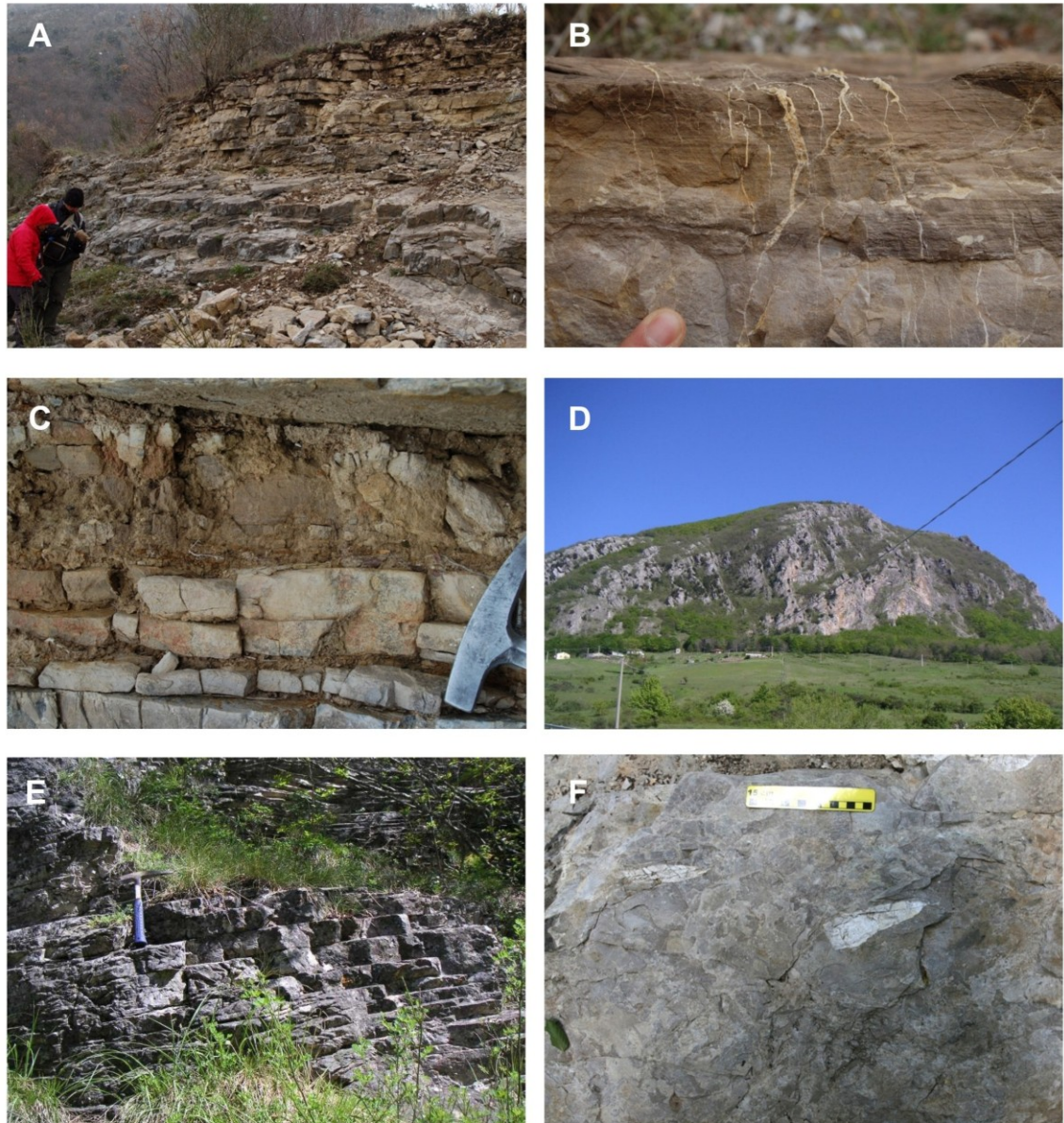


Figure 13: Dolomites outcropping in the northern area. A) Well-bedded dolomites (Campagna). B) Dolomite with laminations cross-cut by veinlets of saddle dolomite (Campagna). C) Alternation of dolomite layers and clastic layers (Campagna). D) Panoramic view of Mount Pierno. E) Well-bedded dolomites (Mount Pierno). F) Massive block of dolomite containing chert nodules (Mount Pierno); scale bar is 15 cm.

### 5.3 Southern area outcrops: features of precursor limestones

The undolomitized limestones of the *Calcari con Selce* Formation in the study areas consist of dark grey, well bedded (5 to 20 cm) mudstone to wackestone containing cm-sized chert nodules, chert beds and thin marly interlayers (Fig.14A). In few instances, these limestones host calcite nodules, 1 to 8 cm in diameter (Fig.14B).

Bedding parallel stylolites (BPS), due to rock compaction during burial, occur in the limestones (Fig.14A) and they are present as well in the dolomitized rocks, showing the same orientation. BPS locally correspond with bedding planes.



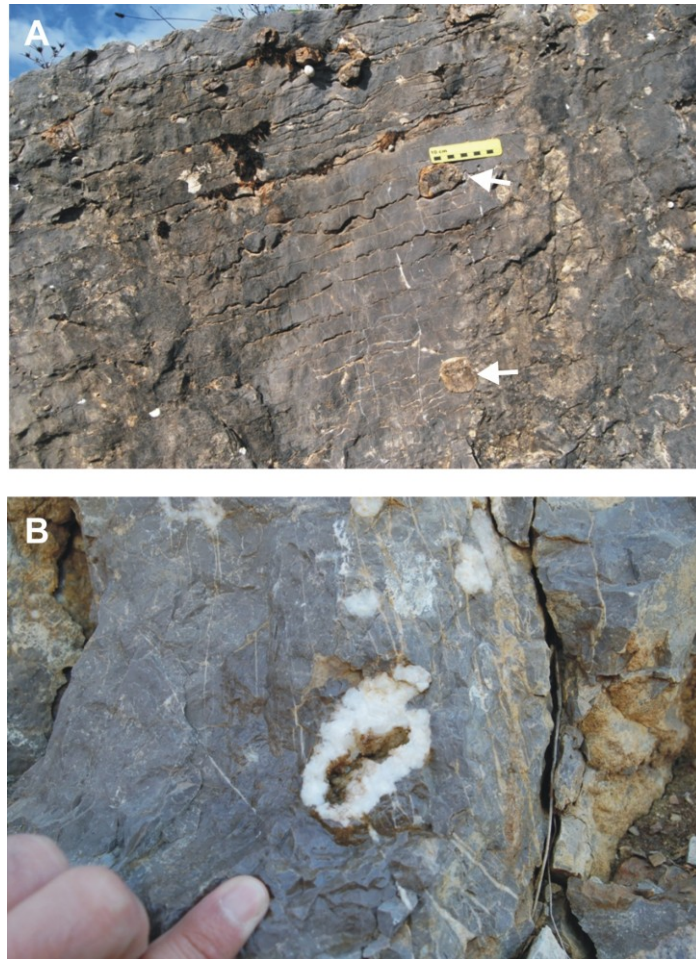


Figure 14: Host limestones of the *Calcari con selce* Formation. A) The limestone contains chert nodules (white arrows). Bedding parallel stylolites are well developed. Scale bar is 10 cm. B) Calcite nodule.

Tectonic stylolites (TS) are well developed both in limestones and dolomites. These stylolites constitute a spaced pressure solution cleavage, which crosscut the BPS. This cleavage, oriented NNE-SSW, according to Mazzoli *et al.* (2001), developed during the first compression phase of the Southern Apennines. TS predate dolomitization, as they preserved the same geometric pattern developed in the limestones, in the dolomitized portions of the succession (Fig.15). As limestones and dolomites present a very different mechanical behaviour, if the cleavage had developed after dolomitization, its spacing would have been different in the two lithologies.

Multiple generations of calcite veins, few mm thick and variously oriented, occur in the precursor limestones (Fig.16A), but they were never observed within dolomitized bodies. An exception is represented by thin calcite veins occurring in the dolomites, only close to the boundaries with the limestones, and mostly recognizable from acetate peels or thin sections observation (Fig.16B). These veins start in the limestone and continue in the dolomites for few cm; they sometimes break off and continue as open fractures.

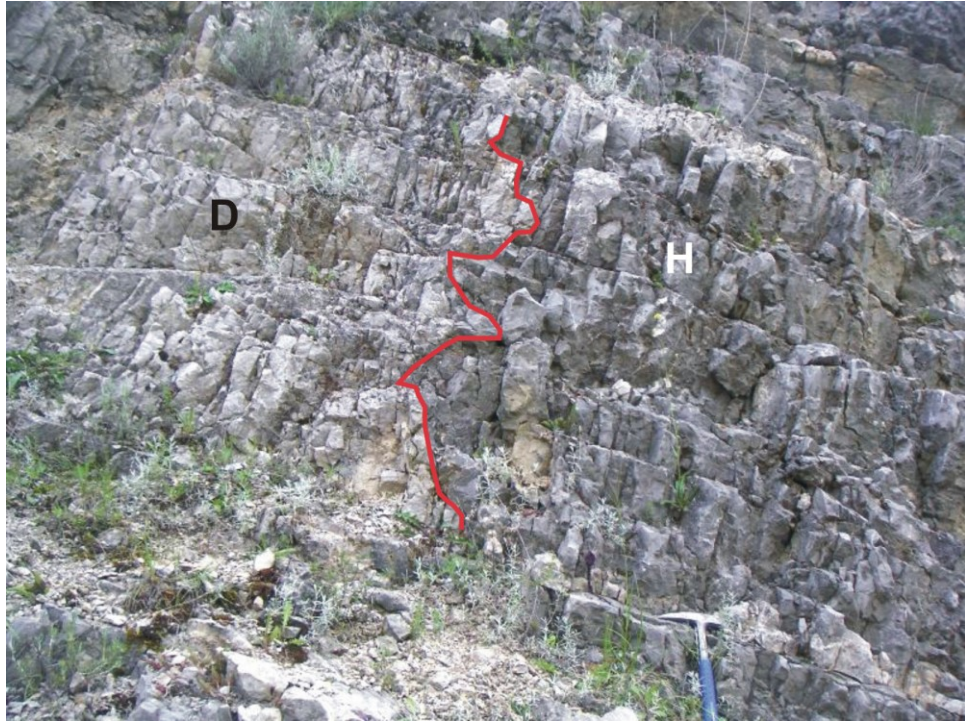


Figure 15: Dolomitization front (red line) crosscutting the stratification. A pressure solution cleavage is well developed both in host limestones (H) and dolomites (D) and displays the same geometric pattern in both the lithologies.

A set of dolomite veins, oriented NNW-SSE, is also present in the limestones that are close (few meters) to some dolomitization fronts. These veins reopened and refilled an older set of calcite veins. Both calcite and dolomite veins crosscut BPS, whereas dolomite veins are crosscut at least by one of these calcite veins generations, translucent in hand sample. This latter is oriented NNE-SSW, and seems to be controlled by cleavage planes.

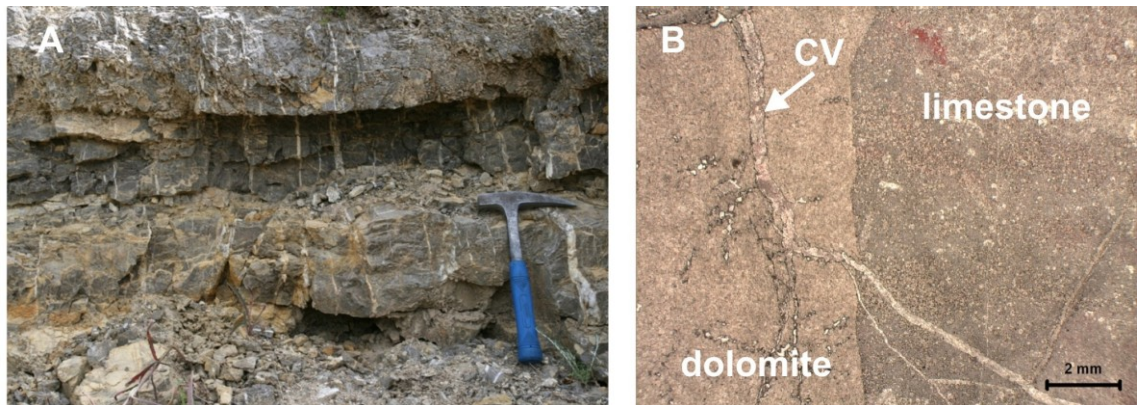


Figure 16: Veins systems in the precursor limestone. A) Calcite veins mostly sub-vertical in respect with the bedding. B) Image of a peel displaying a dolomitization front. A calcite vein (CV) crosses the boundary limestone-dolomite. Diffused dolomite crystals are scattered in the limestone matrix.

Orientation (strike direction) of bedding, cleavage and veins systems, measured both in limestones and dolomites, is graphically represented in the rose diagrams of Fig.17. All the measurements are reported in Appendix 1.



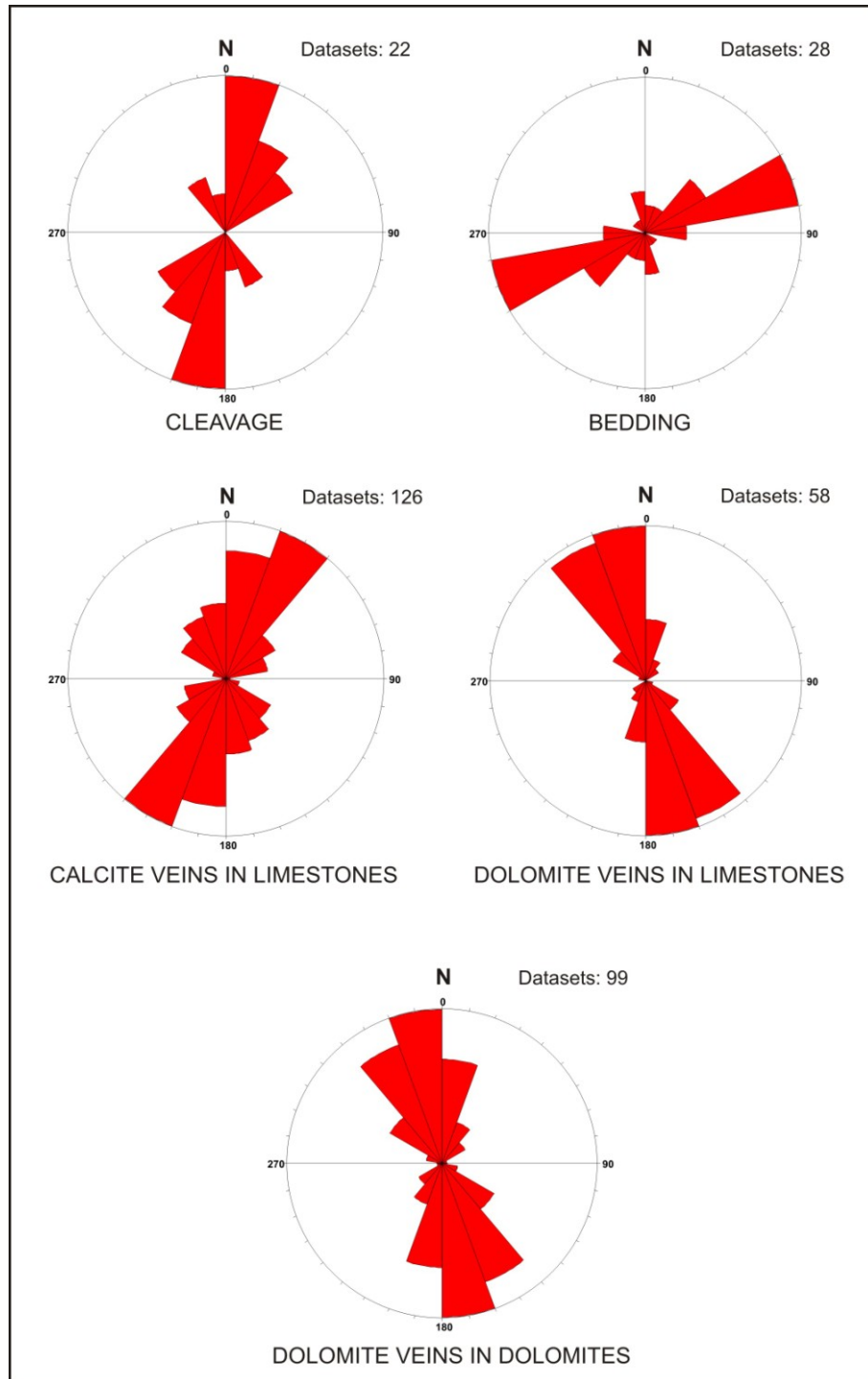


Figure 17: Rose diagrams of cleavage, bedding and veins orientations in limestones and dolomites of the *Calcari con selce* Formation. Cleavage and bedding planes orientations were measured both in limestones and dolomites.

#### 5.4 Southern area outcrops: features of dolomites

Dolomites outcropping in the southern area, from Pignola to high Val d'Agri, are mostly coarse crystalline and fabric destructive. They display a different style of dolomitization respect to the dolomites of the northern area, previously described.

In many outcrops, the dolomites constitute irregular bodies, and undolomitized limestone tongues are sometimes recognized within the dolomitized portions.

Dolomitization fronts are common. They are usually sharp and crosscutting respect to the bedding planes (Fig.18); rarely they are concordant with the stratification. Locally, the limestone-dolomite boundary is characterized by the presence of diffused dolomite crystals within the limestones, scattering in a space of few centimetres (Fig.16B), and by dolomites veinlets starting in the dolomites and continuing in the limestones.

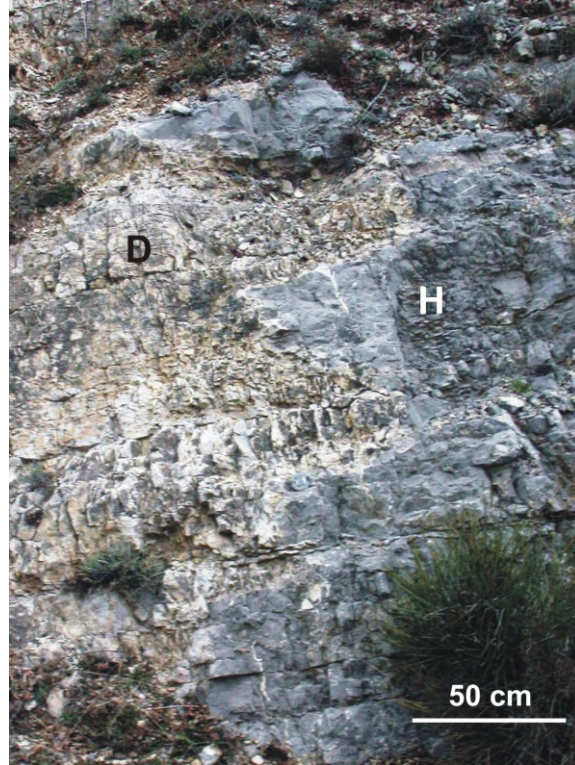


Figure 18: Contact between host limestone (H) and dolomite (D). The boundary between the two lithologies is sharp and cut through the bedding planes.

The macroscopic features observed in the precursor limestones, as chert nodules, chert beds and marly interlayers are still visible in the dolomites. Conversely the calcite nodules hosted in the limestones, were never observed in the dolomites.

Dolomites occur in well-bedded successions. They are characterized by the presence of zebra-like structures, which consist of alternating bands of light grey replacive dolomite and white sparry void-filling dolomite (Fig.19A-F). They are frequently bedding parallel and the boundary between the grey and the white bands sometimes correspond with a bedding parallel stylolite, which predates the dolomites formation (Fig.19B).

The zebra are widespread and occur in many outcrops but they are not ubiquitous and seem to be confined in some layers, comprised between layers composed of replacive grey dolomite only. In some instances, chert beds seem to have acted as a seal and to have exerted a control in focussing the fluids (Fig.19C). Generally, in thicker bedded dolomite the grey replacive dolomite is dominant and the zebra-structures tend to be absent, whereas in thinner beds bedding parallel stylolites are better developed and zebra-structures tend to be more abundant. In the latter case, the proportion between the grey dolomite and milky white dolomite is about 1:1, i.e. the white, void-filling dolomite is very abundant (Fig.19D).



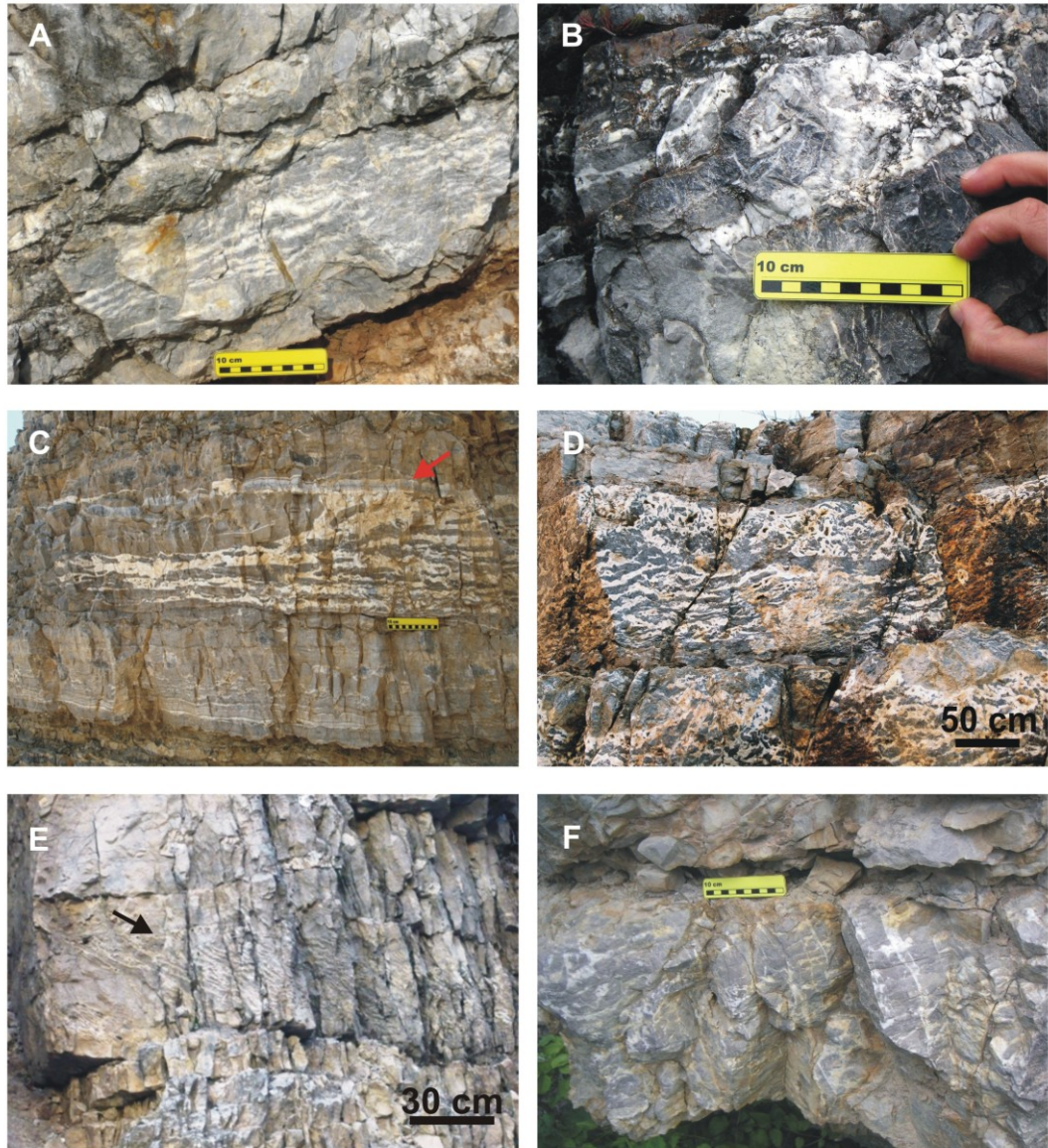


Figure 19: Dolomites outcropping in the southern area. A) Zebra structures parallel to the bedding. B) Grey replacive dolomite and white sparry dolomite cements. In this case the boundary grey-white dolomite corresponds with a bedding-parallel stylolite. C) Zebra structures which are confined by a chert layer (red arrow) in the upper part. D) Zebra structures. The white dolomite is very abundant and the proportion between the grey dolomite and the milky white dolomite is about 1:1. E) Zebra structures obliquely oriented (black arrow) with respect to the bedding. Cleavage planes are sub-vertical. F) Zebra structures crosscut by subvertical white sparry dolomite veins.

Locally, bands of void-filling dolomite are oriented obliquely with respect to the main, bed-parallel zebra (Fig.19E). This *en echelon* vein array geometry is consistent with a simple shear component of the deformation controlling vein development (Mazzoli and Di Bucci, 2003; Mazzoli *et al.*, 2004, and references therein), a feature that has been frequently described in other zebra-dolomites (Wallace *et al.*, 1994; Nielsen *et al.*, 1998; Vandeginste *et al.*, 2005; Diehl *et al.*, 2010). Bedding-parallel simple shear may be related with flexural slip/flow folding, or be associated with the gliding of rock panels during thrusting.

Frequently, the zebra fabric is crosscut by white sparry dolomite veins, sub-vertical respect to the bedding and oriented NNW-SSE (Fig.19F). Dolomite-filled veins, with the same orientations are also present in the unreplaced limestone, close to the boundaries with the dolomite bodies (see previous paragraph and Fig.17).

Brecciated dolomites were also observed in many outcrops. They consist of cm- to dm-large clasts of grey replacive dolomites engulfed by white dolomite cements (Fig.20A-B). The clasts display a sharp boundary and are generally broadly rectangular in shape, although smoothed to curved surfaces were also observed. Evidence of dissolution was locally observed at the borders of the grey dolomite clasts. Angular chert clasts were also immersed in the white sparry dolomite cement. This brecciated fabric suggests that it formed by hydraulic fracturing under the action of overpressured fluids (Fontboté and Gorzawski, 1990).

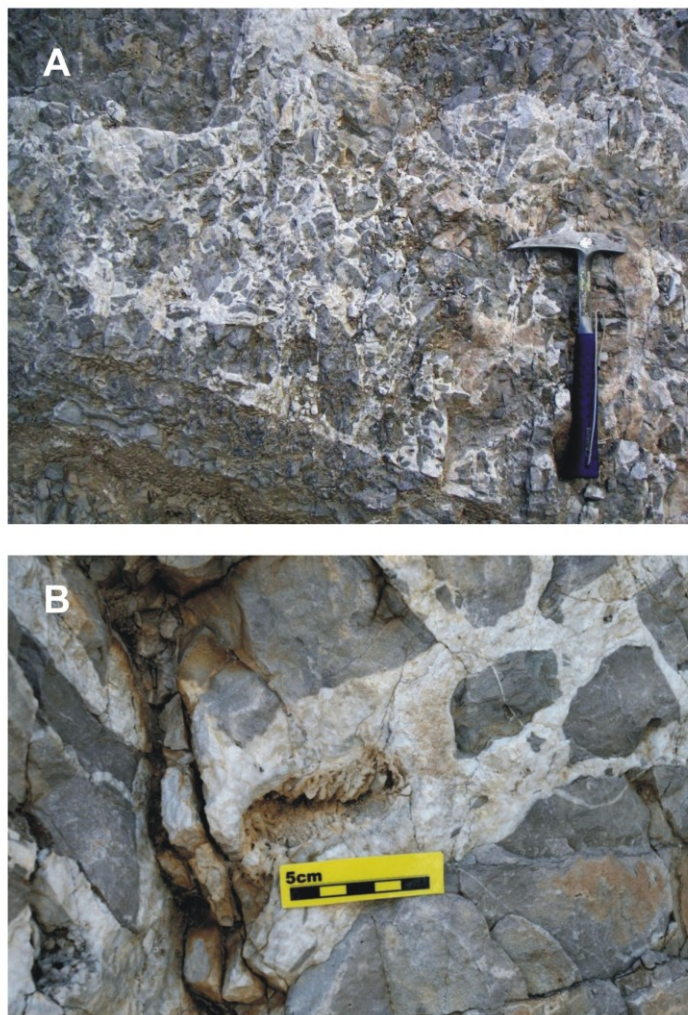


Figure 20: Dolomites outcropping in the southern area. A) Brecciated fabric. B) Dolomitic breccia consisting of clasts of grey replacive dolomite engulfed by white dolomite cements.

Despite dolomites outcropping in the southern area are almost completely fabric destructive, some sedimentary features of the precursor limestone were rarely preserved in the dolomite, such as plane-parallel and convolute laminations and ghosts of radiolarians and thin-shelled bivalves. In some instance, primary sedimentary breccias,





Figure 21: Normal faults dissecting the well-bedded dolomites.

now dolomitized, are still recognizable. The clasts and the matrix of these breccias are both replaced by grey dolomite, but some of the clasts consist of angular chert. The studied dolomite bodies were affected by post-dolomitization extensional tectonics, since steep, normal faults cut through the different dolomite types and display no geometrical relationship with the dolomitization fronts (Fig.21).

## Chapter 6: Distribution of dolomites in subsurface

### 6.1 The *Calcari con Selce* Formation in the Val d'Agri exploration and production wells

The largest oil and gas accumulations of Italy are located in the Val d'Agri oil fields in the Southern Apennines (Bertello *et al.*, 2010). Exploration and production wells were drilled in this area in order to reach the reservoir rocks, represented by the Cretaceous to Miocene limestones and dolomites of the Apulian Platform. The Lagonegro Basin successions, which tectonically overlain the Apulian Platform successions, are often encountered in the boreholes.

Over 30 stratigraphic logs of wells penetrating the Lagonegro successions were examined in order to verify if the *Calcari con selce* Formation is affected or not by dolomitization and to roughly evaluate the dolomites distribution in subsurface. Stratigraphic logs of many exploration wells of Italy are available on the web (<http://unmig.sviluppoeconomico.gov.it/videpi/default.htm>). Confidential data from production wells were consulted as well, thanks to Eni S.p.a. permission. The location of all surveyed well logs is reported in Figure 10.

Four of the observed logs (Acerno 1, Monte Gargaruso 1, Monte Foi 1, San Fele 1) show the presence of Triassic cherty dolomites belonging to the *Calcari con selce* Formation. Two of these wells are located in the northern area (Acerno 1 and San Fele 1), while the other two (Monte Gargaruso 1 and Monte Foi 1) are in the southern area. Two other wells (Tempa la Manara and Monte Enoc 1) contain minor dolomites, dolomitized limestone and calcareous dolomites, whereas the Costa Molina wells (Costa Molina, Costa Molina 2 and Costa Molina 3DirA) hold only dolomitized limestones (these wells are represented by the pink dots in Fig.10). In all the other examined wells no dolomites occurrence is documented. All these wells are located in the southernmost area.

Cherty dolomites of presumed Triassic age were described also in the Frosolone 2 well (Pieri, 1966), located in the Molise region. Bertinelli *et al.* (2002) identified a resemblance between the dolomites of Frosolone 2 well and the dolomites outcropping in the Mainarde range at Mount Marrone. These dolomites were interpreted by these authors as belonging to the pelagic succession of the Molise Basin; therefore dolomites of Frosolone 2 well represent the northernmost occurrence in subsurface of the Lagonegro-Molise Basin succession.

### 6.2 Stratigraphic logs of the studied wells

The Acerno 1 well (Fig.22) is located in correspondence of the north-western margin of the Campagna tectonic window. In the first 1235 meters, the borehole encountered the Lagonegro deposits, at depth comprised between 295-472 m, sandwiched between two carbonate units (Alburno Cervati and Monte Croce Units). The Lagonegro deposits here,



belonging to the Lagonegro Unit II, consist of dolomites and dolomitic limestones belonging to the *Calcari con selce* Formation (Patacca, 2007). The Lagonegro deposits, middle Triassic-Lower Cretaceous in age, were encountered also from 1235 m to 4286 m, organized into four thrust sheets separated by tectonic contacts at 1992, 3409 and 3975 meters. In this thick pile of Lagonegro deposits, dolomites of the *Calcari con selce* Formation are present at depths between 3409 and 3975 m.

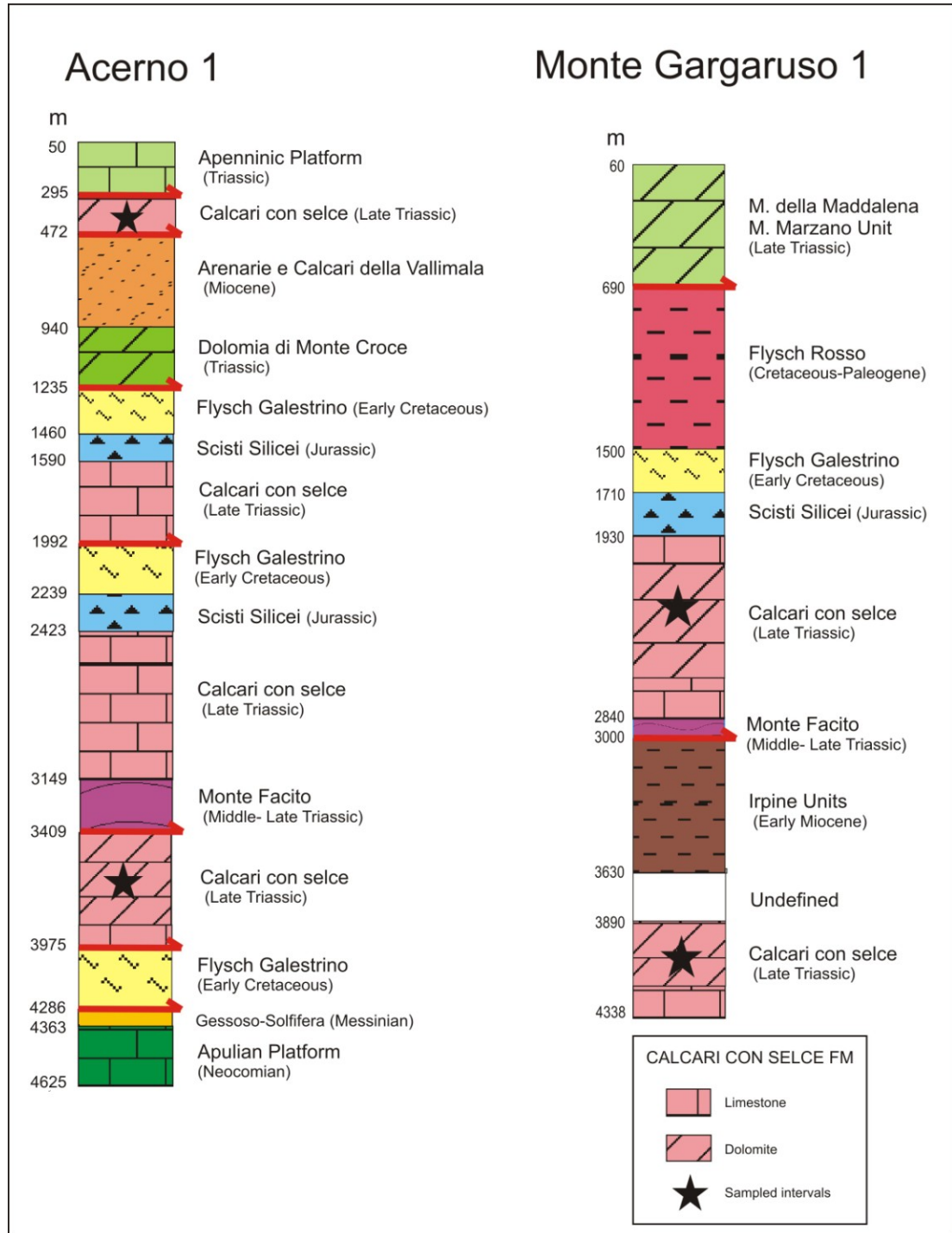


Figure 22: Stratigraphic logs of Acerno 1 and Monte Gargaruso 1 wells.

The Monte Gargaruso 1 well (Fig.22) is located on the Maddalena Mountains. The lithostratigraphic succession penetrated by the borehole is constituted by overthrust allochthonous terms. Two tectonic contacts are present in the crossed succession: the first one is the thrust that put the Triassic carbonate Platform Units on the Lagonegro Units (Lower Triassic–Lower Cretaceous); the second one is the thrust that double the Lagonegro Units. The dolomitized limestones of the *Calcari con selce* Formation are present both in the Lagonegro Unit I and in the Lagonegro Unit II, respectively in the hanging-wall and in the footwall of the thrust, at depths comprised between 2090-2640 m and 3890-4200 m.

The Monte Foi 1 well (Fig.23) is located about 30 km far from the outer (north-eastern) margin of the mountain chain. It penetrated a thick antiformal stack structure constituted by imbricates belonging to the Lagonegro Unit II, consisting of basinal deposits in age from Lower-Middle Triassic to the Lower Cretaceous (Patacca, 2007). The *Calcari con selce* Formation, constituted mainly by dolomites, was encountered four times in the borehole at depths comprised between 319-802 m, 860-1298 m, 2298-2840 m and 3035-3610 m.

The San Fele 1 well (Fig.23) was drilled near the Mount Pierno, close to the village of San Fele. It encountered a pile of imbricates, more than 5000 m thick, composed of Mesozoic basinal deposits referable to the Lagonegro Unit II. This structure, whose thickness is at least four times greater than the involved stratigraphic sequence (1500-1600 m thick from the *Monte Facito* to the *Flysch Galestrino* formations), constitutes the same antiformal stack encountered in the Monte Foi 1 well (Patacca, 2007). Therefore, the *Calcari con selce* Formation was encountered four times in the borehole at depths comprised between 586-908 m, 1967-2207 m, 3705-4252 m and 4830-5120 m. The first two intervals consist of calcareous dolomites, whereas the last two intervals contain mostly dolomitic limestones.

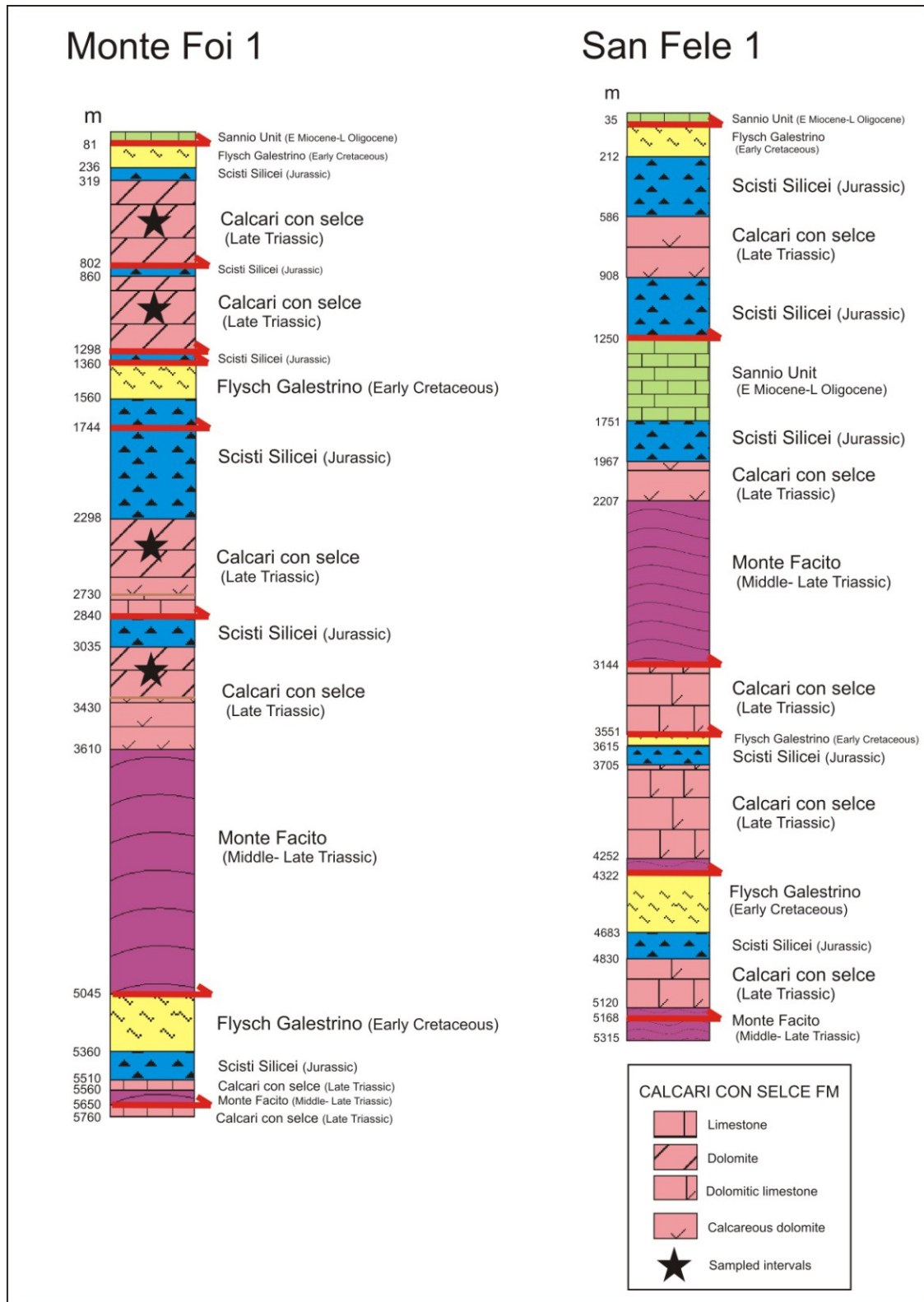


Figure 23: Stratigraphic logs of Monte Foi 1 and San Fele 1 wells.

## Chapter 7: Petrography

### 7.1 Features of the precursor limestone

Typical microfacies of the limestones of the *Calcarei con selce* Formation are mainly mudstones and wackestones with thin-shelled bivalves and calcified radiolarians (Fig.24A). These mud-wackestones are commonly recrystallized and show a uniform dull orange to dull red CL (Fig.24B). Locally they contain calcite nodules with blocky crystals that present an unzoned bright orange CL. The boundary between the limestone and the calcite nodules is frequently characterized by the presence of euhedral rhombs of dolomite (planar-E texture), 50 to 250  $\mu\text{m}$  in diameter, showing a bright red CL, replacing the limestone micrite (Fig.24C-D).

In the limestones close to the dolomitization fronts, dolomite cement occasionally precipitated along the bedding parallel stylolites (Fig.24E-F).

Many generations of veins were recognized. Thin (mostly 10-20  $\mu\text{m}$  of thickness) calcite veins (Cal1), not recognizable in hand samples, are often crosscut by the BPS, indicating a pre or a syn-burial origin (Fig.24E). In CL they vary from dull luminescent, indistinguishable from the matrix, to non-luminescent.

Thick (up to 3 mm) calcite veins (Cal2), consisting of blocky calcite, showing the same dull orange colour of the matrix in CL, postdate the BPS (Fig.25A-B).

Veins filled with saddle dolomite, up to 6 mm in thickness, bright red luminescent in CL, were encountered in the limestones that are close to the dolomitization fronts. These veins, in some cases, reopened and refilled Cal2 veins and they always crosscut the BPS (Fig.25C-D-E). Their orientation is NNW-SSE.

The dolomite veins, in turn are crosscut by 2-3 mm thick calcite veins (Cal3), sometimes translucent in hand samples, containing blocky crystals (Fig.24F, 25F, 26A). These veins, oriented NNE-SSW, are set on cleavage planes; indeed, in some instance, the veins are lined by tectonic stylolites (sub-perpendicular to bedding; Fig.26C). Cal3 veins in CL are not luminescent (Fig.26B).



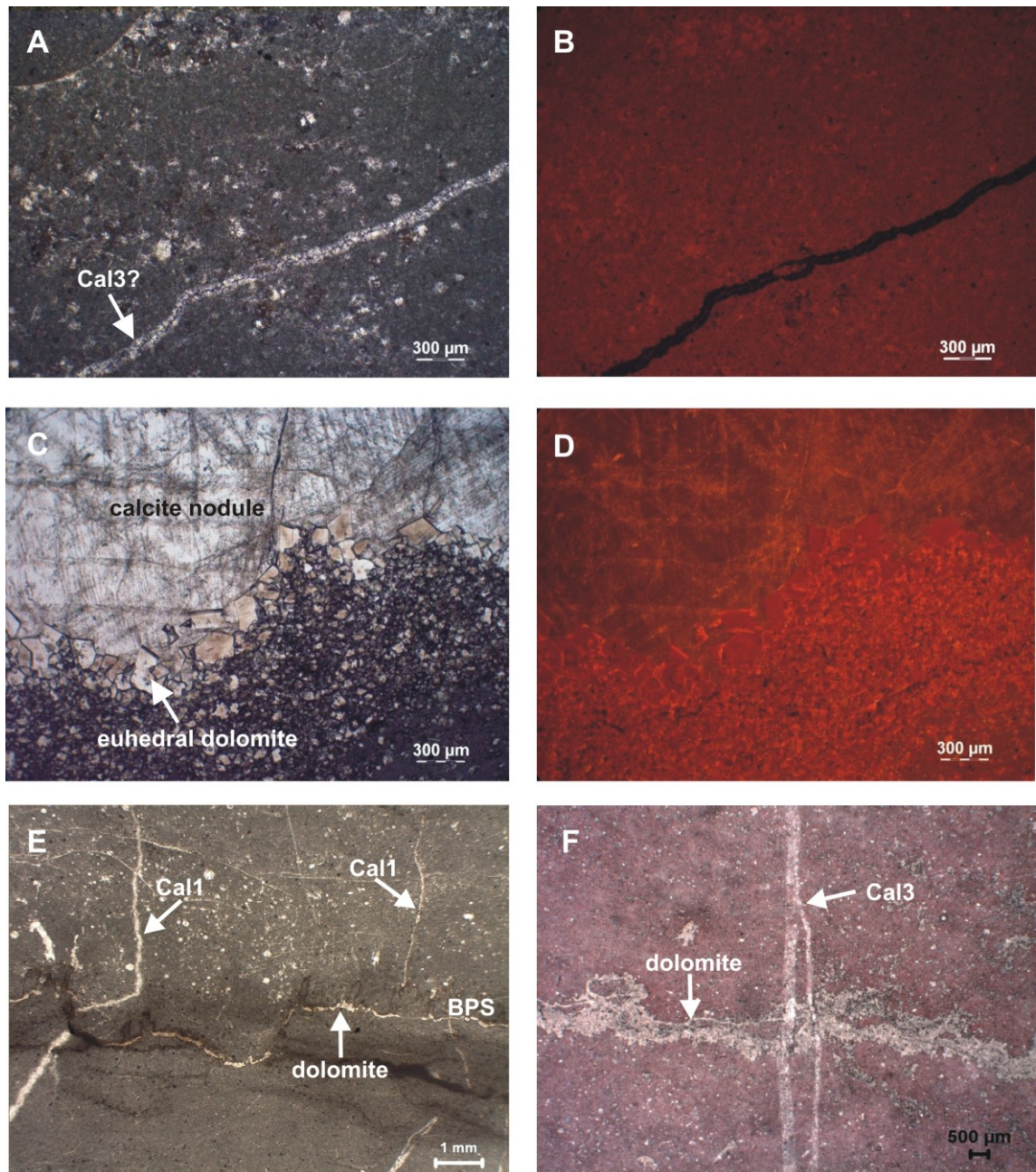


Figure 24: Photomicrographs of the precursor limestone. A) Wackestone with thin-shelled bivalves and calcified radiolarians, crosscut by a calcite vein (maybe Cal3). Plane-polarised light. B) CL image of A. The wackestone shows a dull orange luminescence, whereas the calcite vein is non luminescent. C) Calcite nodule bordered by euhedral rhombs of dolomite. Plane-polarised light. D) CL image of C. The calcite nodule is bright orange, whereas the euhedral dolomite shows bright red luminescence. E) Acetate peel: Cal1 veins crosscut by a bedding parallel stylolite. Dolomite cement precipitated along the stylolite. F) Stained acetate peel: mudstone (pink colour) partially dolomitised. Dolomite (uncoloured) is crosscut by a calcite vein (Cal3).



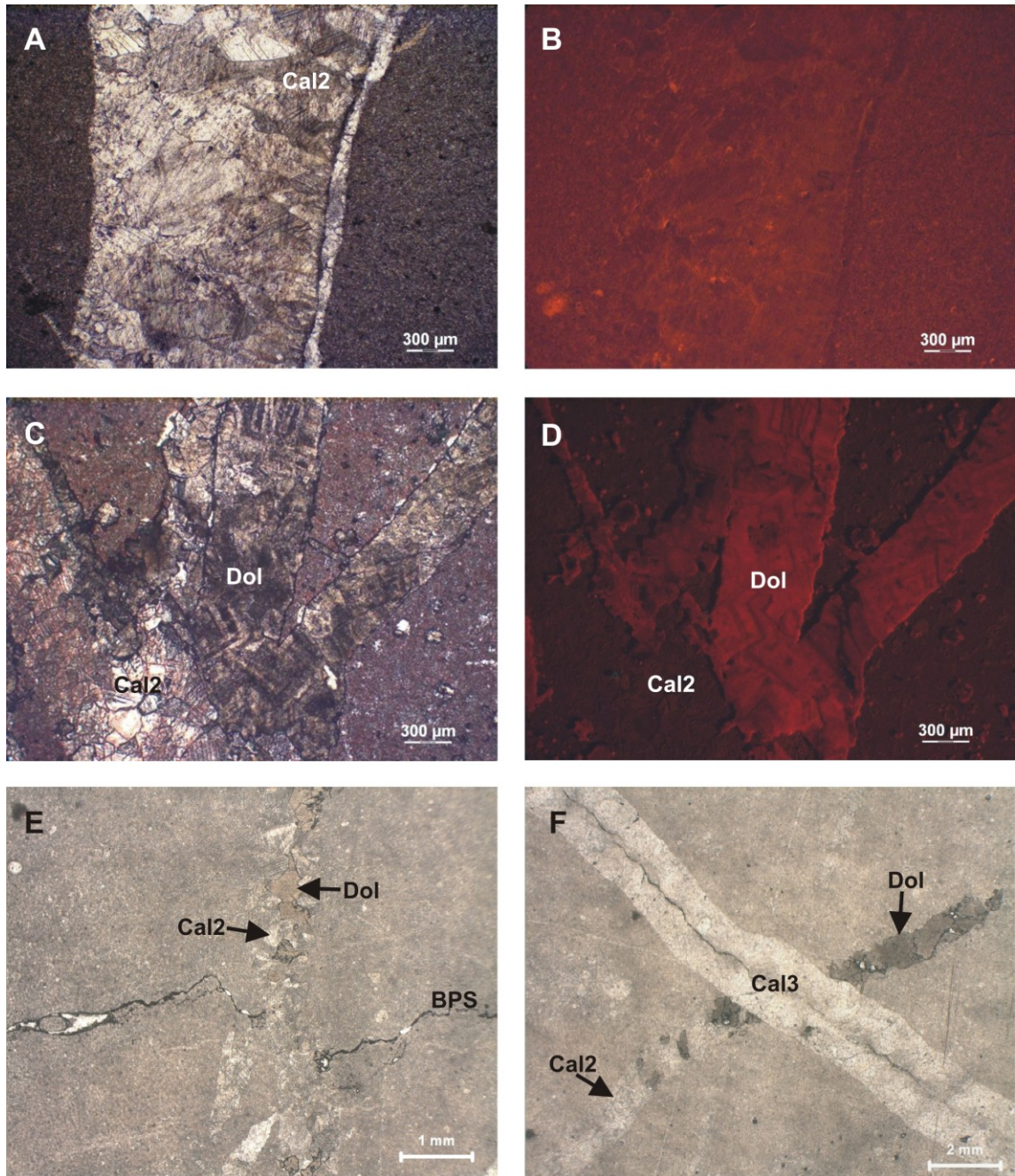


Figure 25: Photomicrographs of the precursor limestone. A) Mudstone crosscut by a Cal2 vein. Plane-polarised light. B) CL image of A. The vein displays a dull orange colour undistinguishable from this of the mudstone. C) Stained thin section: mudstone (pink colour) crossed by a dolomite vein (uncoloured) grown on an older calcite vein (Cal2, pink colour). Plane-polarised light. D) CL image of C. Cal2 displays the same dull red colour of the mudstone, whereas the dolomite vein is bright red. E) Acetate peel: Cal2 vein crosscutting a bedding parallel stylolite (BPS). Dolomite cement reopened the Cal2 vein. F) Acetate peel: Cal2 vein reopened by dolomite cement, both crosscut by Cal3 vein.

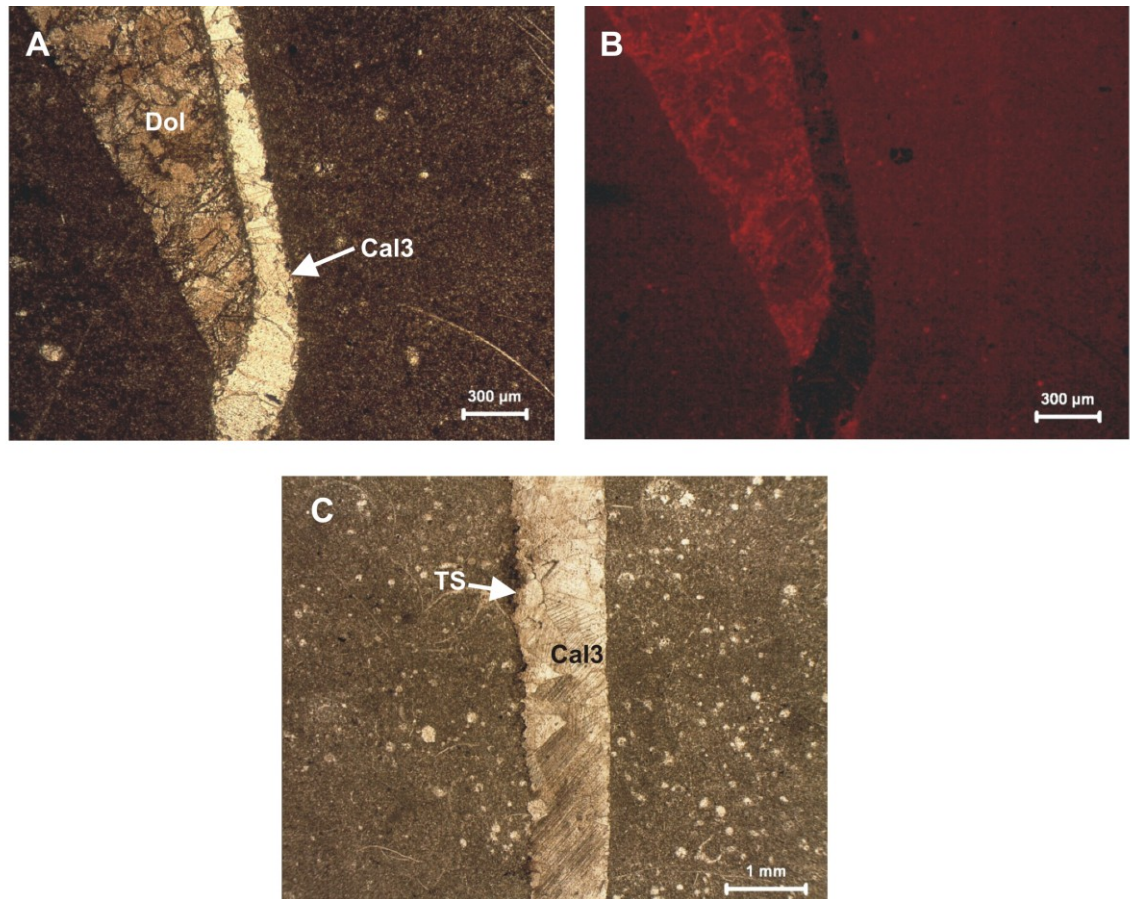


Figure 26: Photomicrographs of the precursor limestone. A) Dolomite vein crosscut by Cal3 vein. Plane-polarised light. B) CL image of A. The dolomite vein displays a bright red colour, while Cal3 is non luminescent. C) Cal3 vein lined by a tectonic stylolite (TS). Plane-polarised light.

## 7.2 Dolomites of the northern area

Petrographic analysis pointed out that the dolomite type outcropping in all the northern outcrops has a relatively homogeneous crystal size distribution varying mostly from 40 to 100  $\mu\text{m}$ . The mosaics are principally unimodal, non-planar, with anhedral crystals showing a cloudy centre and straight extinction.

In particular, dolomites of the Mount Marrone present a mosaic of anhedral dolomite crystals of 40-80  $\mu\text{m}$  (Fig.27A). In CL they vary from dull red luminescent to non luminescent (Fig.27B). Dolomite-cemented irregular vugs are present. They contain subeuhedral crystals of 200-400  $\mu\text{m}$  with straight to slightly undulose extinction, showing zoning bands that alternate dull red and black colour under CL (Fig.27C-D). These crystals are sometimes immersed in a fine-dolomite, dull red luminescent, matrix. Quartz veinlets (40  $\mu\text{m}$ ), postdating the dolomitization, were also encountered. Any primary sedimentary structure was observed in thin section.

The dolomites of Campagna and Mount Pierno often retain features of the primary fabric, such as thin laminations, ghosts of fossils and brecciated facies (Fig.27E-F). These dolomites present a non-planar texture with anhedral crystals having a mean size of 50-100  $\mu\text{m}$  and showing a dull red luminescence in CL (Fig.28A-B-C-D). In some



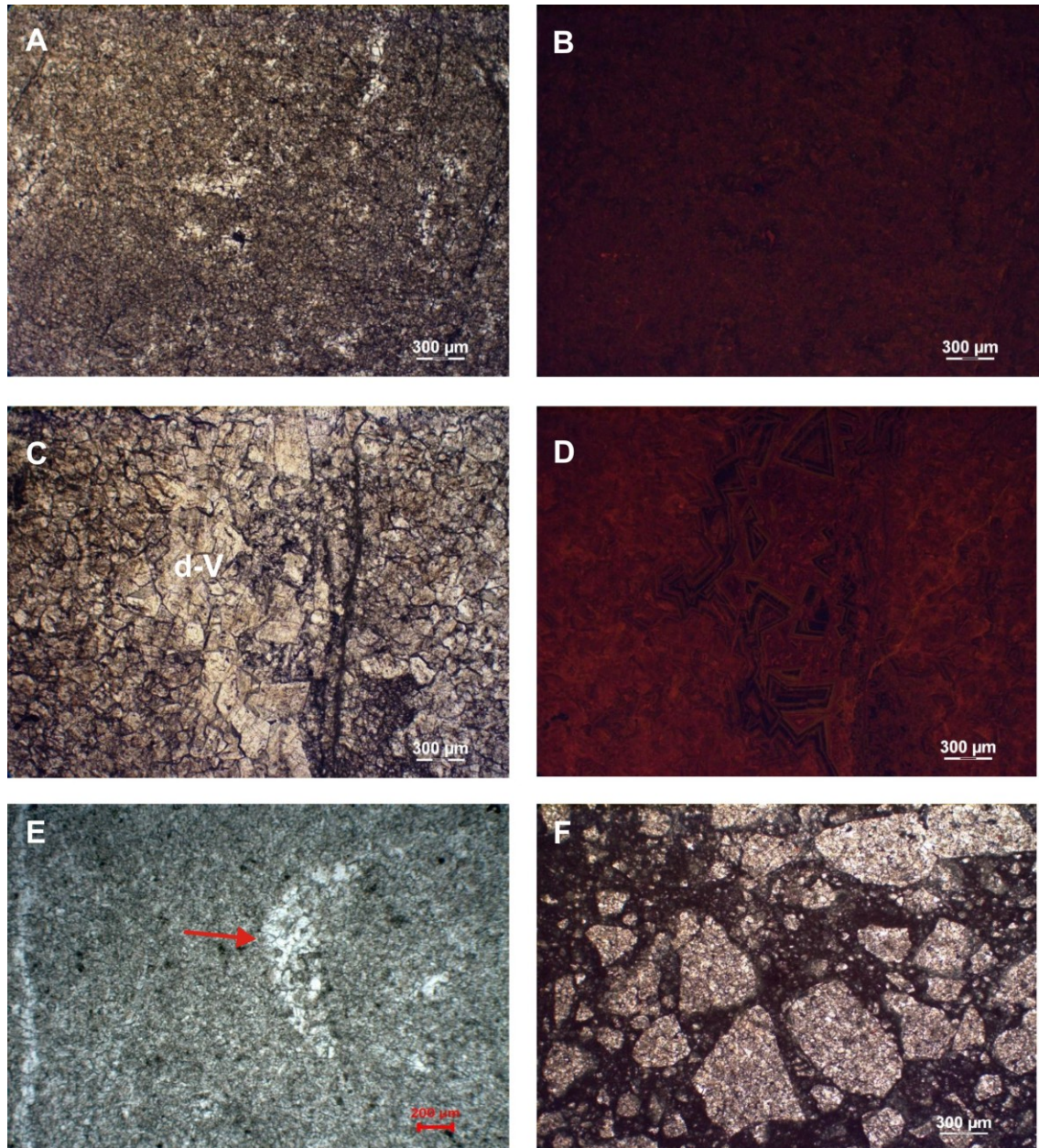


Figure 27: Photomicrographs of dolomites from northern area. A) Non-planar mosaic of dolomite crystals of 40-80  $\mu\text{m}$  (Mt. Marrone). Plane-polarised light. B) CL image of A. The mosaic is non luminescent. C) Dolomite-cemented irregular vug (d-V; Mt. Marrone). Plane-polarised light. D) CL image of C. The dolomite cement shows zoning bands that alternate dull red and black colour. E) Ghost of a fossil (red arrow; Mt. Pierno). Plane-polarised light. F) Sedimentary breccia (Mt. Pierno). The matrix is calcareous, while the clasts are dolomitized. Plane-polarised light.

cases, mosaic with finer (20-30  $\mu\text{m}$ ) crystals were also observed. Dolomite veins, 80-100  $\mu\text{m}$  thick and non luminescent in CL, were sometimes observed (Fig.28C-D). Other dolomite veins, 80  $\mu\text{m}$  in thickness, showing a bright red luminescence, are less common (Fig.28E-F). Quartz veins (100  $\mu\text{m}$  up to 2 mm thick) were also observed (Fig.28E). Vugs cemented by saddle dolomite crystals with a size of 300-400  $\mu\text{m}$ , showing under CL a dull red colour with zonation, are frequent (Fig.29A-B). The chert nodules hosted in the dolomites contain euhedral rhombs of dolomite (50-100  $\mu\text{m}$ ), and in some cases the nodules are almost completely replaced by dolomite (Fig.29C-D).



At San Fele, the dolomites are coarser. They show a planar-S mosaic with subeuhedral crystals of 100-200  $\mu\text{m}$ , having a dull red luminescence in CL (Fig.29E-F). These dolomites contain dolomite-cemented vugs displaying saddle crystals.

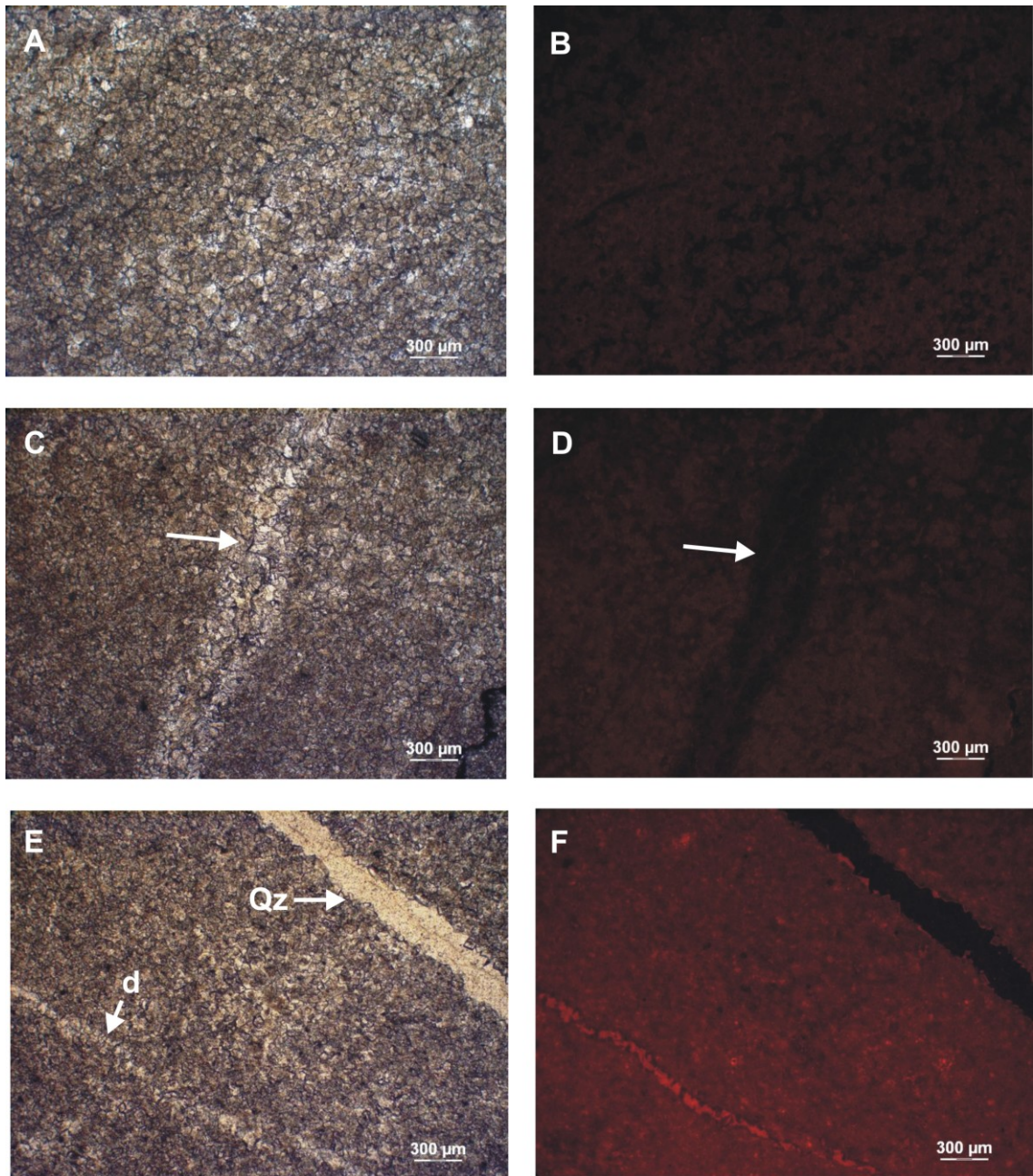


Figure 28: Photomicrographs of dolomites from northern area. A) Non-planar mosaic with crystals of 50-100  $\mu\text{m}$  (Campagna). Plane-polarised light. B) CL image of A. The mosaic is non luminescent. C) Mosaic similar to this of picture A, displaying a dolomite vein (white arrow; Campagna). Plane-polarised light. D) CL image of C. The dolomite vein is non luminescent. E) Non-planar mosaic with crystals of 50-100  $\mu\text{m}$  (Mt. Pierno). The mosaic holds a dolomite vein (d) and a quartz vein (Qz). Plane-polarised light. F) CL image of E. The mosaic shows a dull red luminescence, while the dolomite vein is bright red.



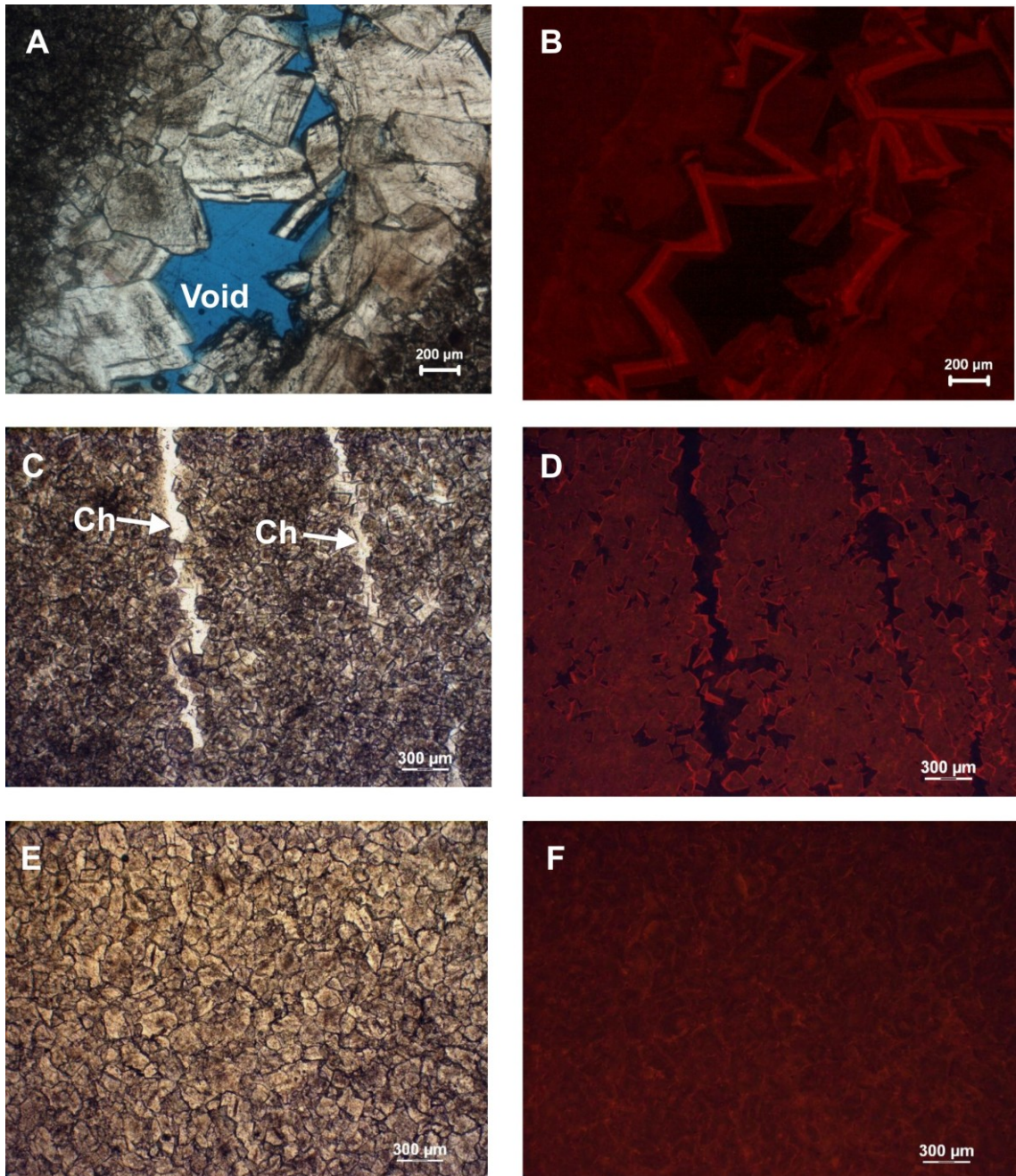


Figure 29: Photomicrographs of dolomites from northern area. A) Vug partially cemented by saddle dolomite crystals with a size of 300-400  $\mu\text{m}$  (Mt. Pierno). Plane-polarised light. B) CL image of A. The crystals present growth zone showing different luminescence colours (from dull red to non luminescent). C) Chert (Ch) nodule almost completely replaced by subeuhedral dolomite crystals of 50-100  $\mu\text{m}$  (Mt. Pierno). Plane-polarised light. D) CL image of C. The dolomite crystals display a dull red luminescence. E) Planar-S mosaic with crystals of 100-200  $\mu\text{m}$  (San Fele). Plane-polarised light. F) CL image of E. The mosaic shows a dull red luminescence.

### 7.3 Dolomites of the southern area

Petrographic observations allowed to distinguish three main dolomite phases occurring in the dolomite bodies outcropping in the southern area. They were respectively called Dol1, Dol2 and Dol3.

Dol1 corresponds to the grey dolomite recognized in the field, which is the volumetrically most abundant dolomite type. It consists of a polymodal planar-S to non-



planar mosaic of anhedral and subeuhedral cloudy crystals showing two main size populations (40-80  $\mu\text{m}$  and 150-200  $\mu\text{m}$ ) and straight extinction (Fig.30A). In CL, these crystals show a dull red, uniform and unzoned luminescence (Fig.30B).

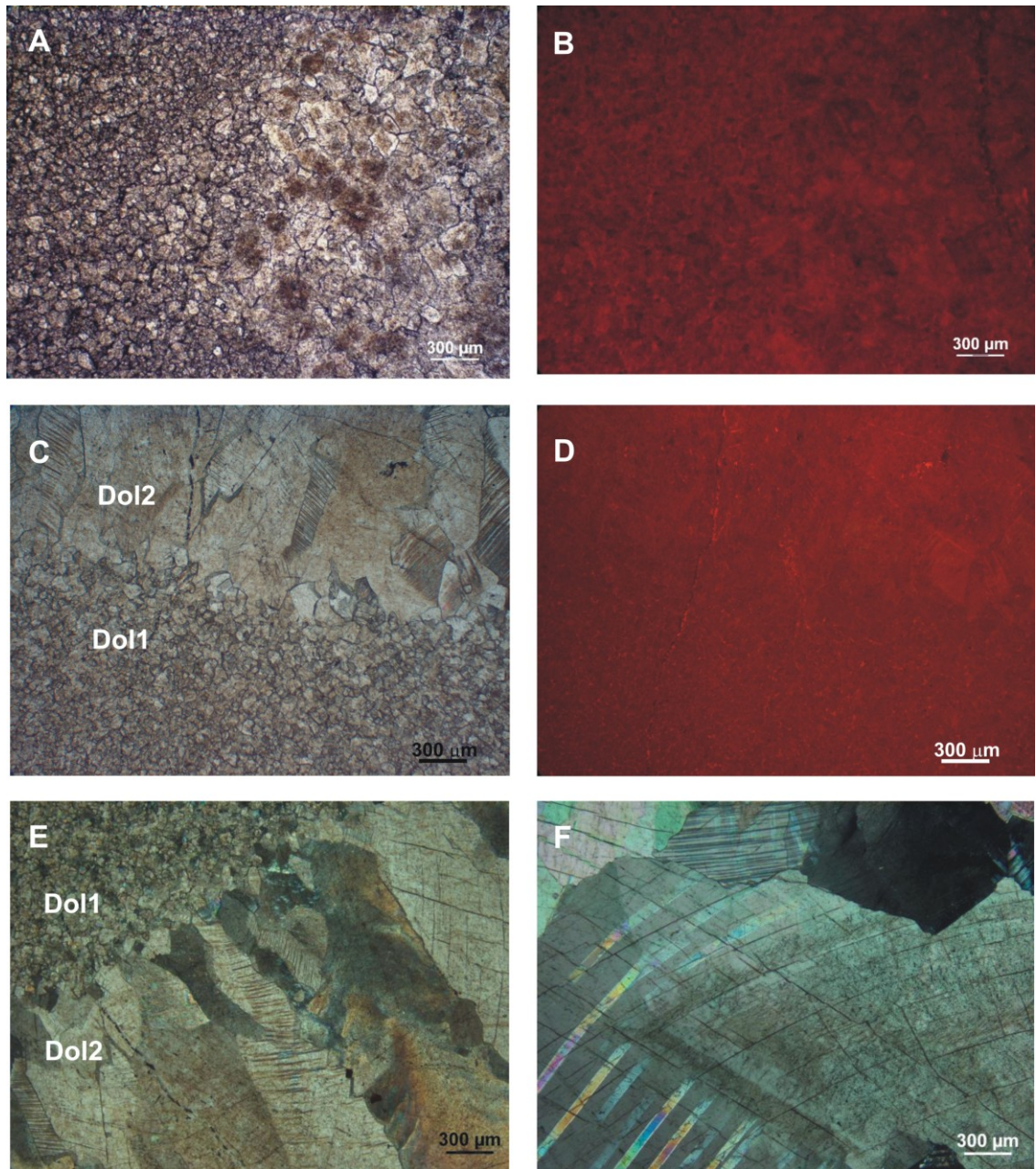


Figure 30: Photomicrographs of dolomites from southern area. A) Dol1 showing two main size populations: fine (40-80  $\mu\text{m}$ ) crystals are on the left of the picture, while coarser crystals (150-200  $\mu\text{m}$ ) are on the right. Plane-polarised light. B) CL image of A. The crystals display a dull red and unzoned luminescence. C) Dol1 and Dol2 showing non transitional contact. Plane-polarised light. D) CL image of C showing Dol1 and Dol2 with undistinguishable dull red and uniform luminescence. E) Abrupt transition from Dol1 to Dol2. Dol2 crystals are elongated towards the cavity centre and twinned. Cross-polarised light. F) Particular of a Dol2 crystal displaying curved crystal twins and curved cleavage. Cross-polarised light.

Dol2 corresponds to most of the white dolomite recognized in the field, which is less abundant respect to Dol1, but present in all the outcrops. The transition between Dol1 and Dol2 is not gradual, as they present a sudden increase in the crystal size (Fig.30C-



E). Dol2 shows a non-planar texture with saddle crystals having diameter ranging from 800  $\mu\text{m}$  up to several mm, commonly elongated towards the cavities centre, i.e. along the growth direction (Fig.30E). They present sweeping extinction and crystal faces, cleavage planes and twins, all curved. The Dol2 crystals are uniformly cloudy indicating the presence of inclusions homogeneously distributed within the crystals and have a dull red and uniform CL undistinguishable from the one of Dol1 (Fig.30D). The last generation of Dol2 crystals, that point to the cavities, display a non-planar-C texture and scimitar-like shape (Fig.30F). It may exhibit a more or less developed zoning due to alternation of zones of different FIs content (Fig.31A-B). Typically, the last growth zone of the Dol2 crystals shows a dull orange CL (Fig.31D).

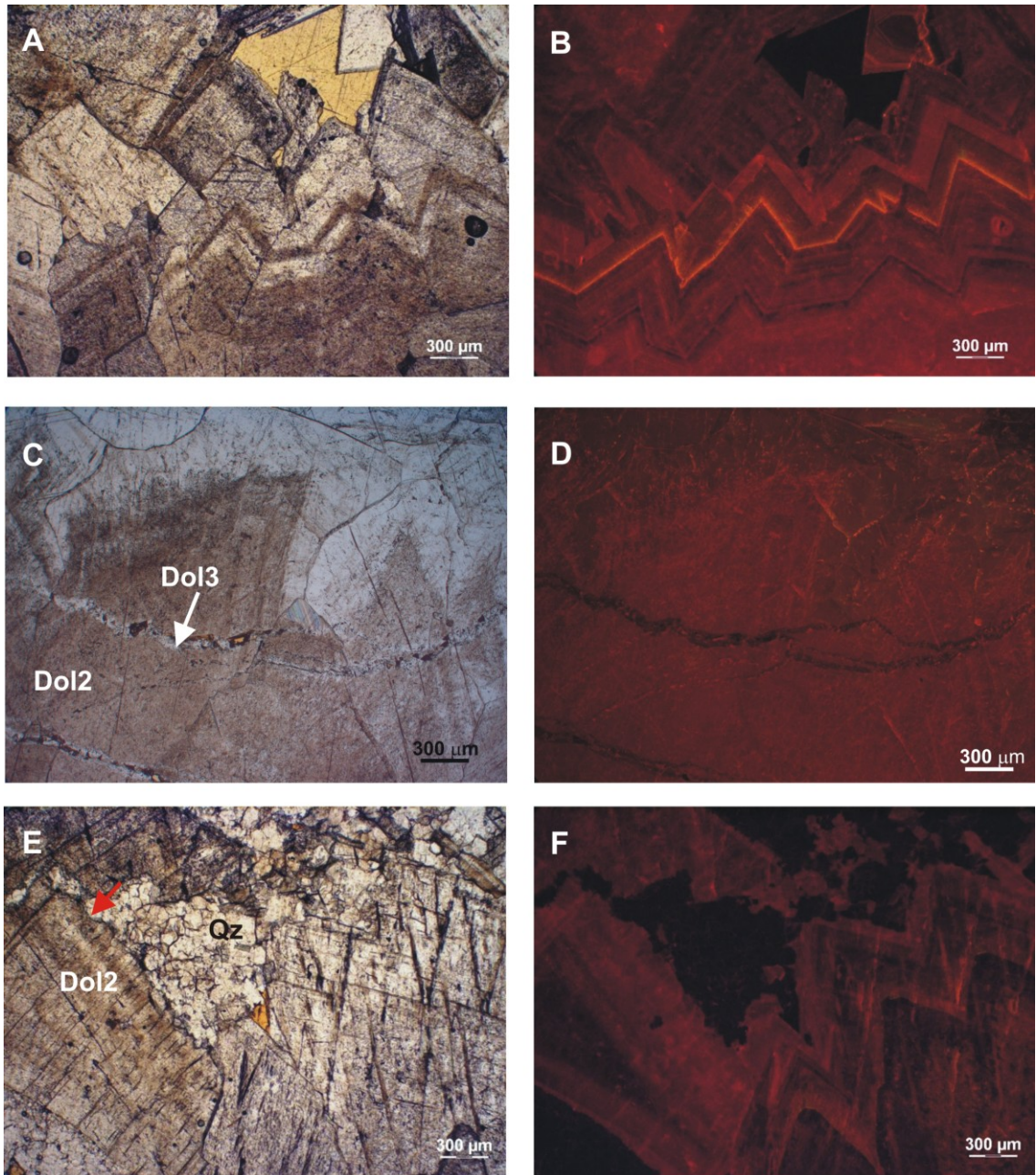


Figure 31(previous page): Photomicrographs of dolomites from southern area. A) Dol2 crystals that point to a cavity and exhibit a zoning due to alternation of zones of different FIs content. Plane-polarised light. B) CL image of A. The crystals display growth bands having different luminescence. C) Dol2 given by curved crystals, uniformly cloudy. Dol3 is present in the vein that cross-cut Dol2 crystals. Plane-polarised light. D) CL image of C. The last growth zone of the Dol2 shows a dull orange CL, whereas Dol3 is non-luminescent. E) Dol2 crystals and a quartz-filled cavity. The borders of the Dol2 crystals show evidence of dissolution (red arrow). Plane-polarised light. F) CL image of E.

Dol2 commonly lines vuggy pores and fractures, but it is locally followed by Dol3, translucent in hand sample, mainly consisting of non-planar-C crystals, up to several mm in diameter, that growth in crystallographic continuity with Dol2, and shows a dark red up to non-luminescent colour without zonations under CL. In other cases Dol3 constitutes the matrix of a micro-breccia, whose clasts are made up of angular fragments of Dol2 (100-400  $\mu\text{m}$  in diameter). More commonly, Dol3 crystals fill thin fractures which cut through Dol1 and Dol2; in this case no crystallographic continuity is observed (Fig.31C-D).

A late phase of quartz cement was recognised as well, but only in few samples. This quartz is polycrystalline and fills the cavity centre which is left open after the precipitation of Dol2. Dolomite crystals at the boundary with the quartz cement display evidence of dissolution (Fig.31E-F). This quartz phase could be the result of the recrystallisation during dolomitization of the original chert contained in the precursor limestones.

Dolomites of the southern area present mostly pervasive coarse-grained textures that destroy any original depositional fabric. Nevertheless in few samples, primary features, such as sedimentary breccias textures, thin laminations and ghosts of fossils, were retained.

#### 7.4 Dolomites of wells cuttings

Dolomite type observed in the cuttings of Acerno 1 well present different mosaics: a non-planar one with anhedral crystals of 20-30  $\mu\text{m}$  of diameter (Fig.32A), and a planar-S one with coarser subeuhedral crystals (100-200  $\mu\text{m}$ ) often cloudy in the core (Fig.32C), both displaying from dull red to black luminescence in CL (Fig.32B-D). Dolomite cements showing non-planar textures with crystal > 800  $\mu\text{m}$  having sweeping extinction (Fig.32E) and dull red luminescence in CL, were observed, mostly in the upper dolomitized interval of the Acerno 1 well (between 295 and 472 m of depth). These crystals often display the presence of twins. Dolomite veins (200  $\mu\text{m}$  thick), non luminescent in CL were also observed (Fig.32F). In few samples, brecciated facies, completely dolomitized were recognised.

Dolomites of Monte Gargaruso 1 and Monte Foi 1 well cuttings display similar textural features. They consist of non-planar to planar-S mosaics showing different crystal sizes, mostly comprised between 40-80  $\mu\text{m}$  and 100-200  $\mu\text{m}$  (Fig.33A). In CL they present a dull red uniform luminescence (Fig.33B). Cements of saddle dolomite are very common in both wells, and show sweeping extinction, curved cleavage planes, curved twins and a dull red colour indistinguishable from the matrix dolomite colour in CL (Fig.33C-D-E).



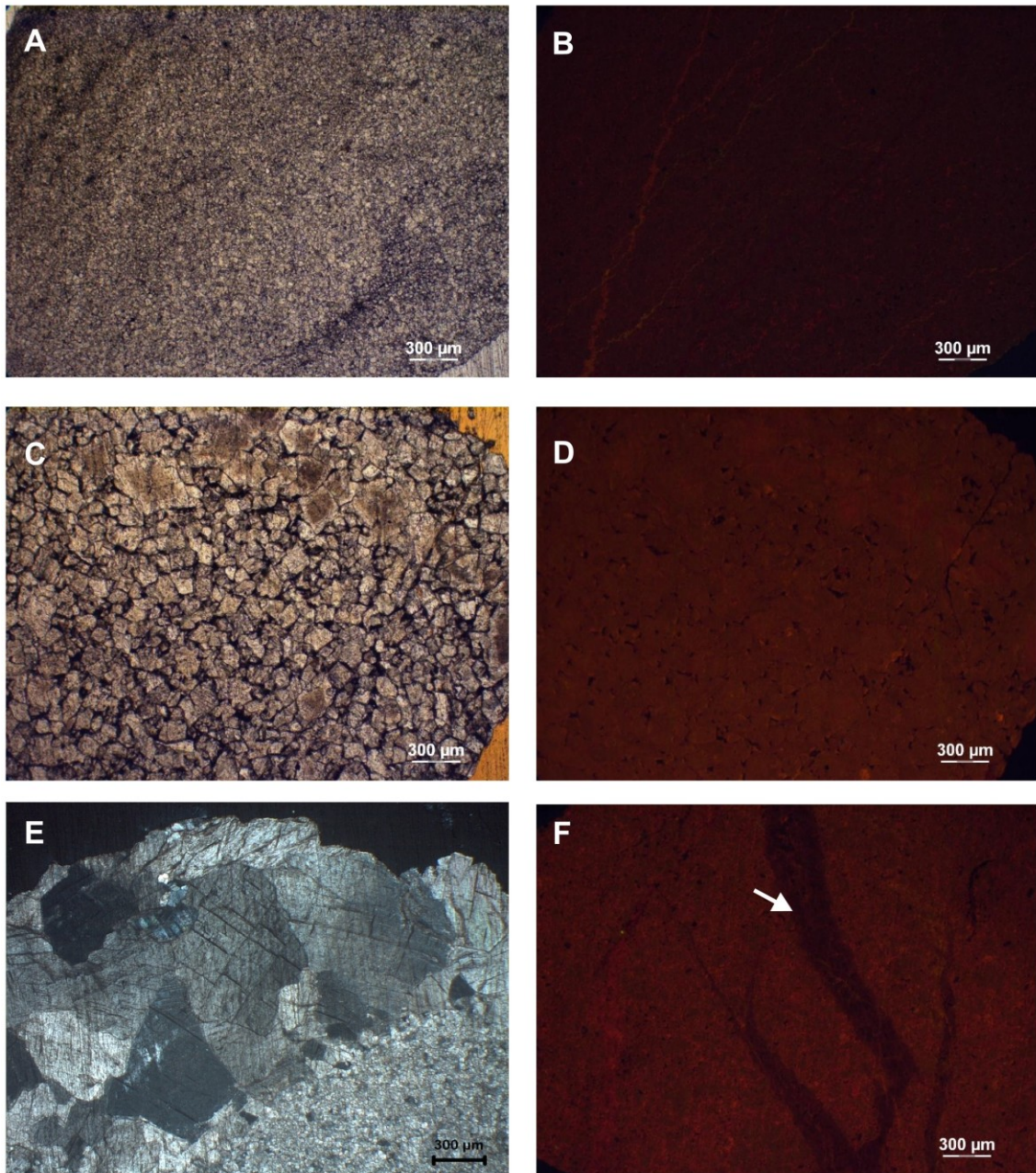


Figure 32: Photomicrographs of Acerno well dolomites. A) Mosaic of very fine dolomite crystals (20-30  $\mu\text{m}$ ). Plane-polarised light. B) CL image of A. The mosaic is non luminescent. C) Planar-S mosaic with crystals of mostly 100-200  $\mu\text{m}$ . Plane-polarised light. D) CL image of C. The mosaic displays a dull red luminescence. E) Dolomite cement showing non-planar texture and sweeping extinction. Cross-polarised light. F) CL image of a non luminescent dolomite vein (white arrow). The matrix displays a dull red luminescence.

These cements are sometimes non luminescent, whereas they more often display zonation of dull red bands and darker bands (Fig.33D). Quartz veins, 150-400  $\mu\text{m}$  thick, consisting of subeuhedral crystals with mean size of 150-300  $\mu\text{m}$ , were observed, especially in the Monte Gargaruso 1 cuttings (Fig.33F). Many fragments of chert were observed. They contain scattered euhedral dolomite crystals (ranging between 60 and 80  $\mu\text{m}$  in diameter), and dolomite veins, both presenting a dull red luminescence in CL.



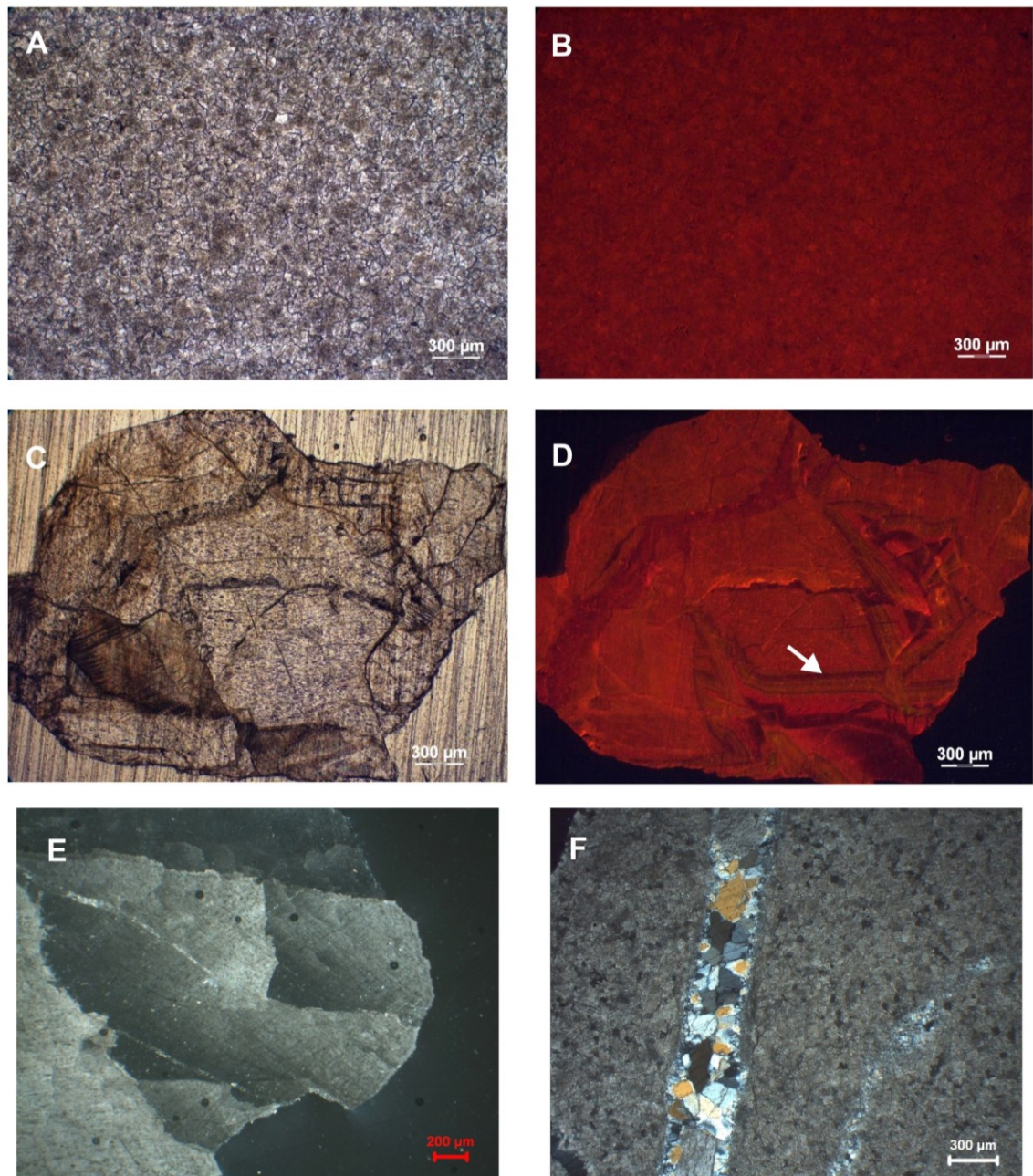


Figure 33: Photomicrographs of Mt. Gargaruso and Mt. Foï wells dolomites. A) Non-planar mosaic having crystals of 100-200  $\mu\text{m}$ . Plane-polarised light. B) CL image of A. The mosaic presents a uniform red luminescence. C) Fragment of saddle dolomite cement. Plane-polarised light. D) CL image of C displaying a red luminescence. The edges of the crystals show alternating bands with different luminescence colour (white arrow). E) Saddle crystals showing sweeping extinction. Cross-polarised light. F) Quartz vein. Cross-polarised light.



## Chapter 8: Geochemistry

### 8.1 Oxygen and Carbon stable isotope analyses

O and C stable isotopes were measured on a total of 84 dolomite specimens sampled in different areas. Twenty-one specimens are from the northern area (Molise, Campagna and Mt. Pierno-San Fele areas), 34 from the southern area (Pignola and high Val d'Agri areas), 8 from Acerno well, 8 from Monte Gargaruso well and 13 from Monte Foi well. In the samples of the southern area, a separation between the replacive dolomite type (Dol1) and the void filling dolomite type (Dol2+Dol3) was possible.

The results are reported in Appendix 2. The statistic parameters of  $\delta^{18}\text{O}$  and  $\delta^{13}\text{C}$  from the different areas and wells are summarized in Table 1.

Dolomites location	$\delta^{18}\text{O}_{\text{PDB}}$ [‰]	$\delta^{13}\text{C}_{\text{PDB}}$ [‰]
<b>Northern area</b> (21)	min. -2.5	2.6
	mean -0.4	3.1
	max. 1.0	3.6
	std. dev. 1.0	0.3
<b>Southern area Dol1</b> (34)	min. -9.5	2.2
	mean -5.4	2.5
	max. -2.9	2.9
	std. dev. 1.7	0.2
<b>Southern area Dol2 + Dol3</b> (18)	min. -11.8	2.2
	mean -6.5	2.4
	max. -4.5	2.6
	std. dev. 1.7	0.1
<b>Acerno well</b> (8)	min. -1.0	2.4
	mean -0.2	3.0
	max. 0.6	3.9
	std. dev. 0.6	0.5
<b>Mt. Gargaruso well</b> (8)	min. -7.0	2.2
	mean -4.7	2.6
	max. -2.8	2.7
	std. dev. 1.4	0.2
<b>Mt. Foi well</b> (13)	min. -7.0	1.7
	mean -5.1	2.5
	max. -3.2	2.8
	std. dev. 1.2	0.3

Table 1: O and C isotope geochemistry. The statistic parameters of  $\delta^{18}\text{O}$  and  $\delta^{13}\text{C}$  (‰ PDB) are reported for samples coming from the different study areas and wells. For the samples of southern area, statistic parameters related to the two different dolomite types (Dol1 and Dol2+Dol3) are reported separately. In parenthesis there is the number of measured samples. Min. = minimum value, mean = mean value, max. = maximum value, std. dev. = standard deviation.

Surface and subsurface data, plotted together in the same  $\delta^{18}\text{O}$  vs.  $\delta^{13}\text{C}$  cross-plot, display the presence of two distinct clusters of values, showing different trends (Fig.34). The first cluster includes dolomites from the outcrops of the northern area and dolomites

from Acerno well. They present  $\delta^{18}\text{O}$  values ranging from -2.5 and 1.0 ‰ with an overall mean of -0.4 ‰, and  $\delta^{13}\text{C}$  values comprised between 2.3 and 3.9 ‰ with a mean of 3.1 ‰. About half of these  $\delta^{18}\text{O}$  values fall in the Upper Triassic seawater isotopic range (Veizer *et al.*, 1999; Korte *et al.*, 2005), whereas the other half values are slightly enriched in  $^{18}\text{O}$  respect to the same seawater values.  $\delta^{13}\text{C}$  values are instead all consistent with Upper Triassic seawater values.

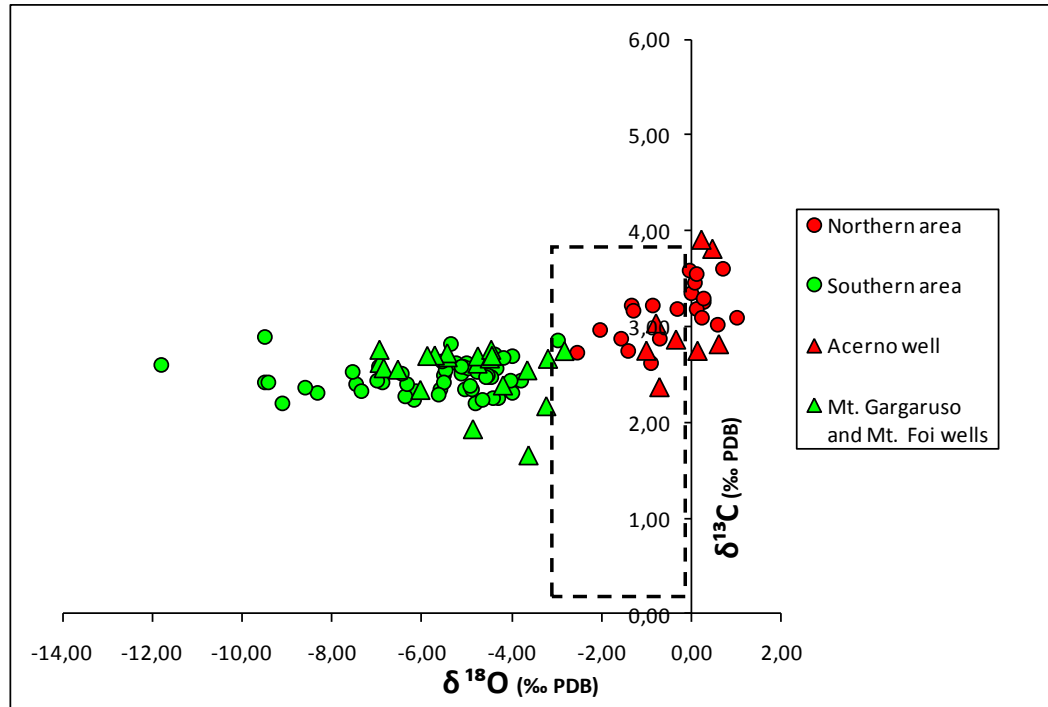


Figure 34: Covariation plot between  $\delta^{18}\text{O}$  and  $\delta^{13}\text{C}$  of the studied dolomites. The isotope composition of Upper Triassic seawater (Veizer *et al.*, 1999; Korte *et al.*, 2005) is reported in the dashed frame.

The second cluster consists of dolomites from the southern area and dolomites from the two wells Monte Gargaruso and Monte Foi. All these dolomites show a large spread of  $\delta^{18}\text{O}$  values, that range from -11.8 and -2.8 ‰, with most of the values falling between -8 and -3.5 ‰. The  $\delta^{18}\text{O}$  mean value is -5.6 ‰.  $\delta^{13}\text{C}$  shows less dispersed values, that range from 1.7 to 2.9 ‰ and have a mean of 2.5 ‰. These  $\delta^{13}\text{C}$  values are consistent with Upper Triassic seawater values, while  $\delta^{18}\text{O}$  values are quite depleted.

Replacive and void-filling dolomites from the same sample do not show significant differences in carbon isotopes ratios (Fig.35), while they present slightly differences in oxygen isotopes ratios. Generally, the void-filling dolomite type is lighter in  $\delta^{18}\text{O}$  respect to the corresponding replacive dolomite type (Fig.36). This is not true only for three samples.

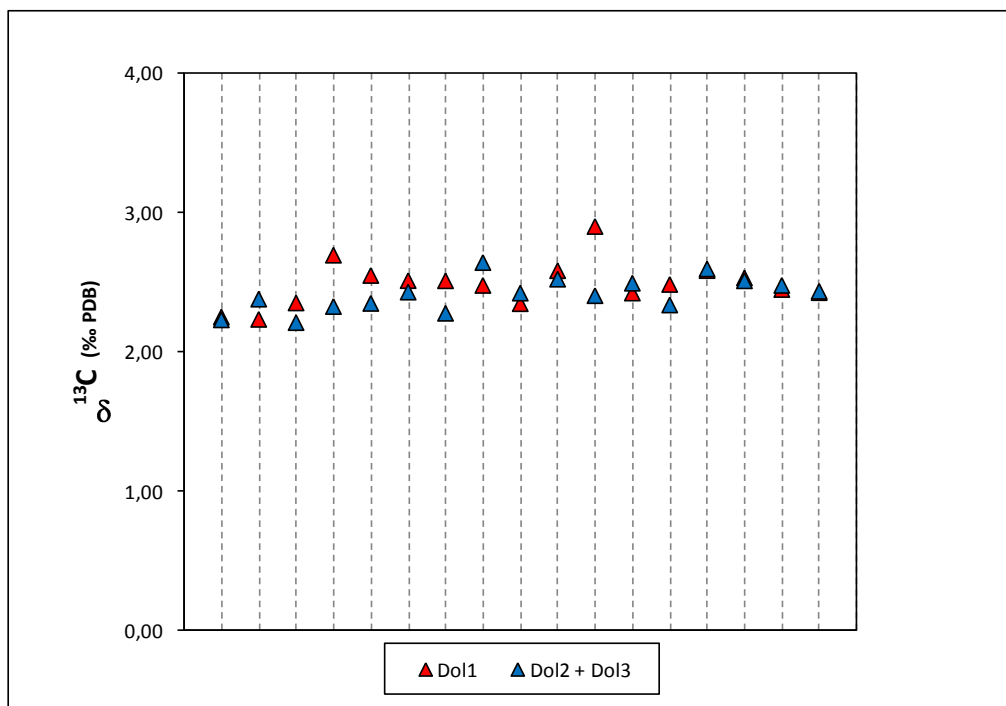


Figure 35: The trend of C isotope composition in single sampled sites of the southern area.  $\delta^{13}\text{C}$  values of the two different dolomite types from the same rock sample are plotted on the same vertical dashed line.

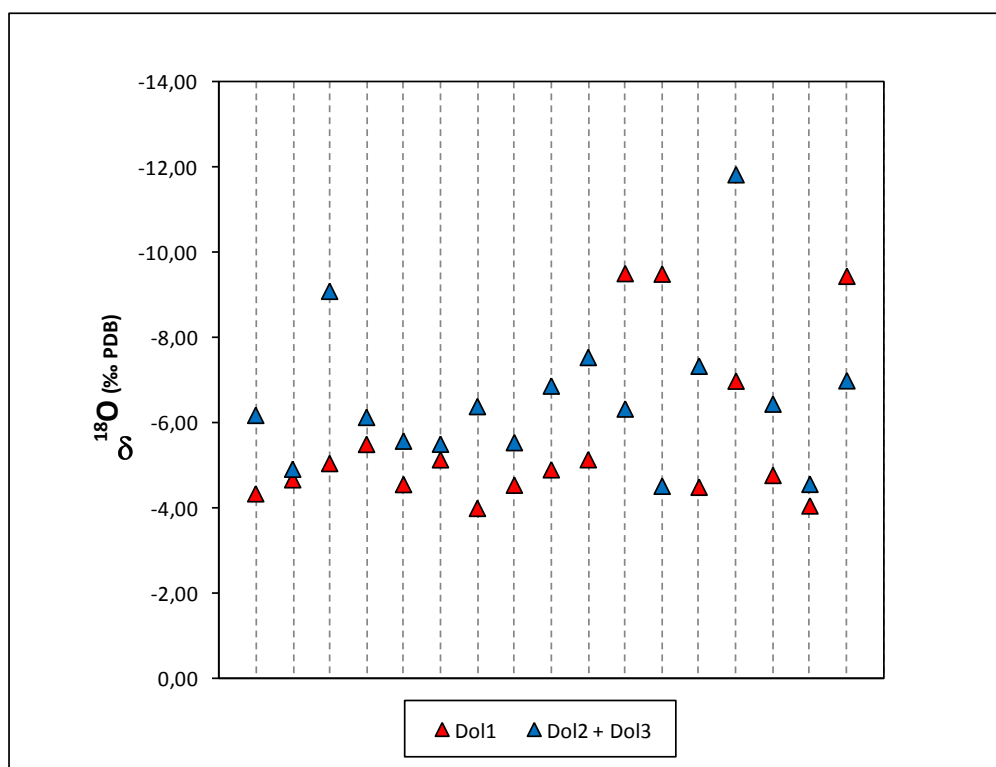


Figure 36: The trend of O isotope composition in single sampled sites of the southern area.  $\delta^{18}\text{O}$  values of the two different dolomite types from the same rock sample are plotted on the same vertical dashed line.

## 8.2 ICP-AES analyses

A total of 52 dolomite specimens were analysed for major (Ca and Mg) and trace elements (Sr, Mn, Fe and Ba) content. Ca, Mg, Sr, Mn and Fe concentrations were obtained for 12 specimens from the northern area (Molise, Campagna, San Fele areas), 20 specimens from the southern area (Pignola and high Val d'Agri areas), and for 7, 2 and 11 cuttings specimens, respectively from Acerno, Monte Gargaruso and Monte Foi wells. Distinction in elements content between the replacive (Dol1) and the void-filling (Dol2+3) dolomite types was performed for the samples from the southern area. All the results are listed in Appendix 2. The statistic parameters of the concentration of all measured elements in the different areas and wells are reported in Table 2.

Dolomites location		Ca (%)	Mg (%)	Sr (ppm)	Fe (ppm)	Mn (ppm)	Ba (ppm) *
<b>Northern area (12)</b>	min.	20,89	10,78	69	59	26	0,48
	mean	22,41	11,71	99	533	118	1,80
	max.	23,64	12,80	205	2949	234	3,84
	std. dev.	0,94	0,66	37	799	65	1,44
<b>Southern area Dol1 (20)</b>	min.	20,32	10,34	33	34	143	0,45
	mean	20,96	12,09	51	579	231	1,00
	max.	21,64	12,64	99	1739	334	2,20
	std. dev.	0,30	0,65	16	475	52	0,53
<b>Southern area Dol2 + Dol3 (14)</b>	min.	20,88	11,66	41	136	153	0,05
	mean	21,50	12,31	75	696	225	0,76
	max.	22,49	12,75	136	2286	292	3,04
	std. dev.	0,43	0,37	27	545	41	0,84
<b>Acerno well (7)</b>	min.	18,93	10,78	63	193	31	22
	mean	20,81	12,04	97	670	71	136
	max.	21,48	12,50	171	2463	161	252
	std. dev.	0,85	0,58	36	805	48	85
<b>Mt. Gargaruso well (2)</b>	min.	19,84	11,05	60	135	178	46
	mean	20,44	11,63	63	623	210	48
	max.	21,05	12,20	66	1110	241	50
	std. dev.	0,86	0,81	4	689	45	3
<b>Mt. Foi well (11)</b>	min.	10,15	4,92	31	86	157	0,97
	mean	18,63	9,97	57	1268	251	4,53
	max.	22,26	12,33	97	5129	554	11,40
	std. dev.	3,98	2,83	23	1631	111	3,18

Table 2: Geochemistry of elements from ICP-AES analysis. The statistic parameters of the concentrations of Ca, Mg, Sr, Fe, Mn and Ba are reported for samples coming from the different study areas and wells. For the samples of southern area, statistic parameters related to the two different dolomite types (Dol1 and Dol2+Dol3) are reported separately. In parenthesis there is the number of measured samples. \*Samples measured for Ba concentration are 4, 14 and 10 respectively for the northern area, the Dol1 of the southern area and the Dol2+Dol3 of the southern area. min. = minimum value, mean = mean value, max. = maximum value, std. dev. = standard deviation.

### 8.2.1 Strontium (Sr)

Sr displays a low concentration (< 205 ppm) in all samples. It varies between 69 and 205 ppm in northern area samples, displaying a mean of 99 ppm. The Acerno well cuttings present a very similar Sr concentration (range of 63-171 ppm and mean of 97 ppm). Samples from southern area and from Monte Gargaruso and Monte Foi wells present slightly lower Sr content respect to the samples from northern area and Acerno well. Sr content of southern area samples is comprised between 33 and 136 ppm and shows a

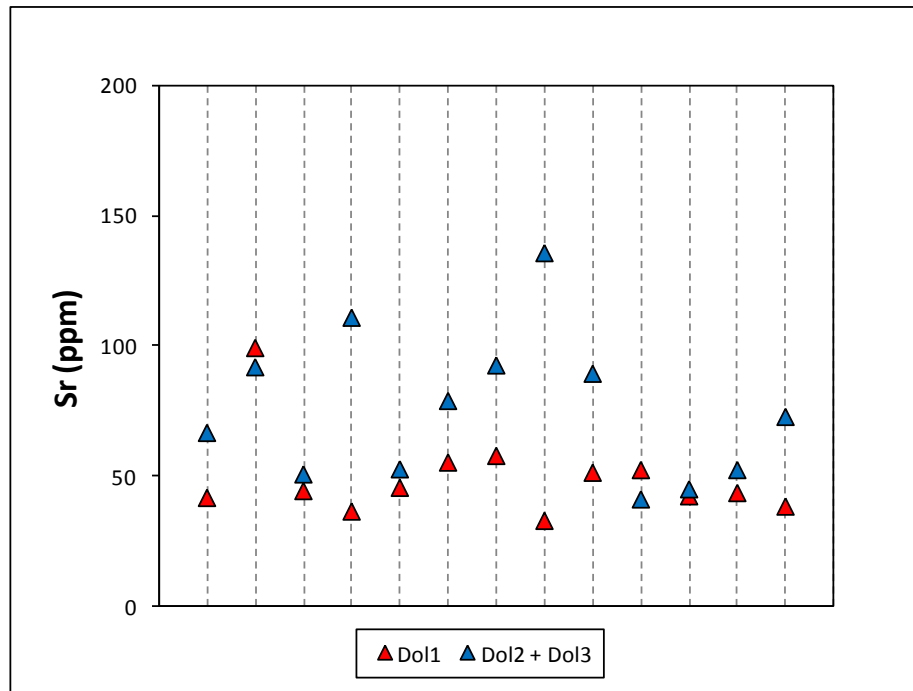


Figure 37: The trend of Sr concentrations in single sampled sites of the southern area. Sr contents of the two different dolomite types from the same rock sample are plotted on the same vertical dashed line.

mean of 61 ppm. Sr contents of replacive and void-filling dolomite types from the same rock sample were compared (Fig.37). Generally the void-filling dolomite is slightly enriched in Sr respect to the replacive dolomite. Only two samples do not follow this rule. Monte Gargaruso and Monte Foi wells cuttings display Sr concentration ranging respectively between 60 and 63, and between 31 and 97 ppm. The mean values are respectively 63 and 57 ppm.

### 8.2.2 Iron (Fe) and Manganese (Mn)

Mn concentration of dolomites from the northern area and the Acerno well is quite low and varies respectively between 26 and 234 ppm and between 31 and 161 ppm. Mean values are respectively 118 and 71 ppm. Mn shows higher concentrations, ranging mostly from 143 and 334 ppm, in dolomites from the southern area and the other two wells. Mean values for southern area, Monte Gargaruso well and Monte Foi well samples are in that order 229, 210 and 251 ppm.

Mn content does not differ significantly from replacive and void-filling dolomite types of the same sample (Fig.38).

Fe content does not vary so much in the different localities and present values slightly scattered. Most of the values range from 34 to 1110 ppm. Northern area dolomites show a mean of 533 ppm, while dolomites from southern area present a mean of 627 ppm. In the latters, Fe concentration of replacive and void-filling dolomites of the same rock sample were evaluated. Void-filling dolomites are commonly enriched in Fe, but four exceptions to this rule are reported (Fig.39). Cuttings of Acerno well and Monte Gargaruso well display Fe content mean values correspondingly of 670 and 623 ppm.

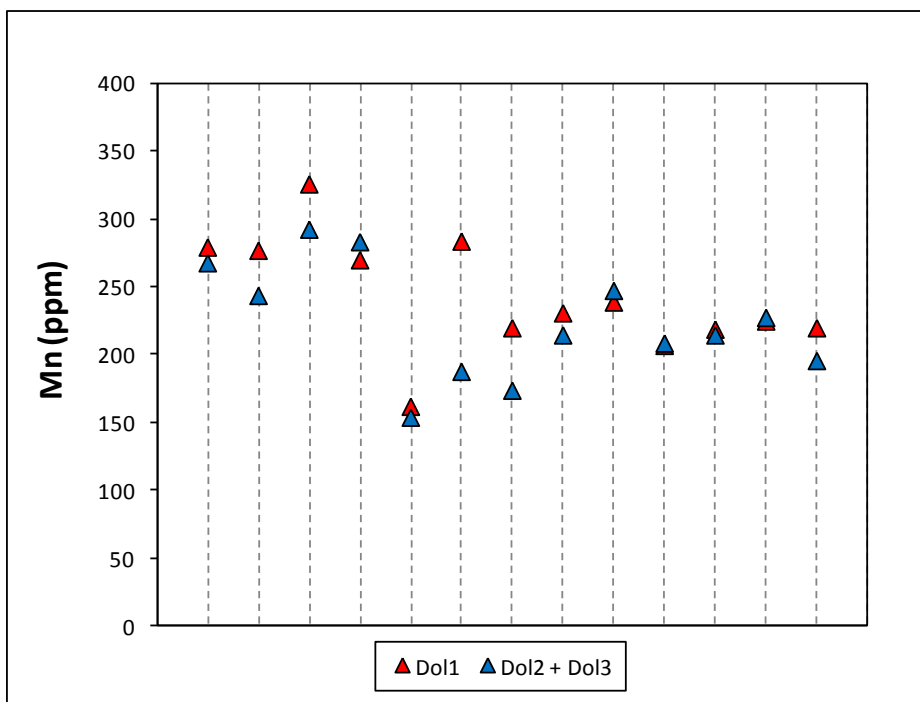


Figure 38: The trend of Mn concentrations in single sampled sites of the southern area. Mn contents of the two different dolomite types from the same rock sample are plotted on the same vertical dashed line.

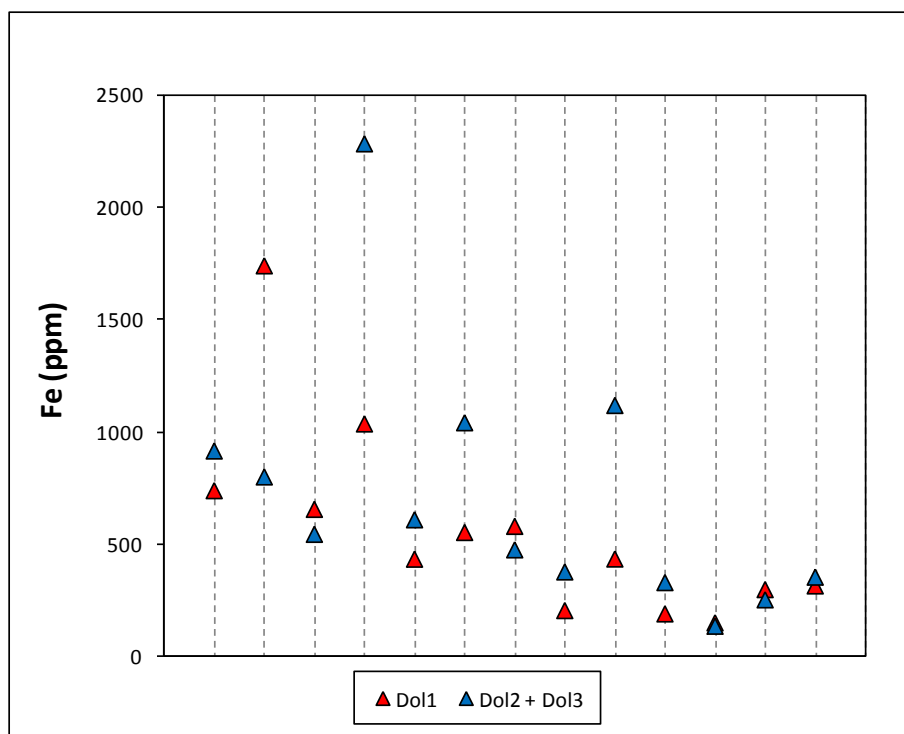


Figure 39: The trend of Fe concentrations in single sampled sites of the southern area. Fe contents of the two different dolomite types from the same rock sample are plotted on the same vertical dashed line.

Only samples from Monte Foi well display a slightly higher Fe concentration, ranging from 86 to 5129 ppm, with a mean of 1268 ppm.

In the two cross-plot Mn vs. Sr and Fe vs. Sr (Fig.40-41), the presence of two different clouds of values is evident. Dolomites from the northern area, including those from Acerno well, display lower Mn and higher Sr values respect to dolomites from the southern area, including those from Monte Gargaruso and Monte Foi wells.

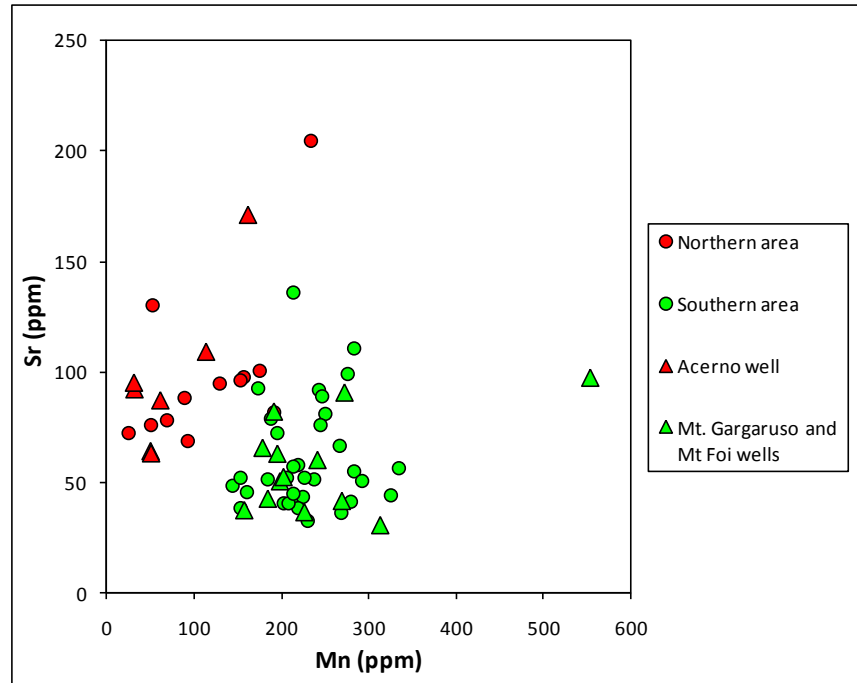


Figure 40: Covariation plot between Mn and Sr concentrations in the studied dolomites.

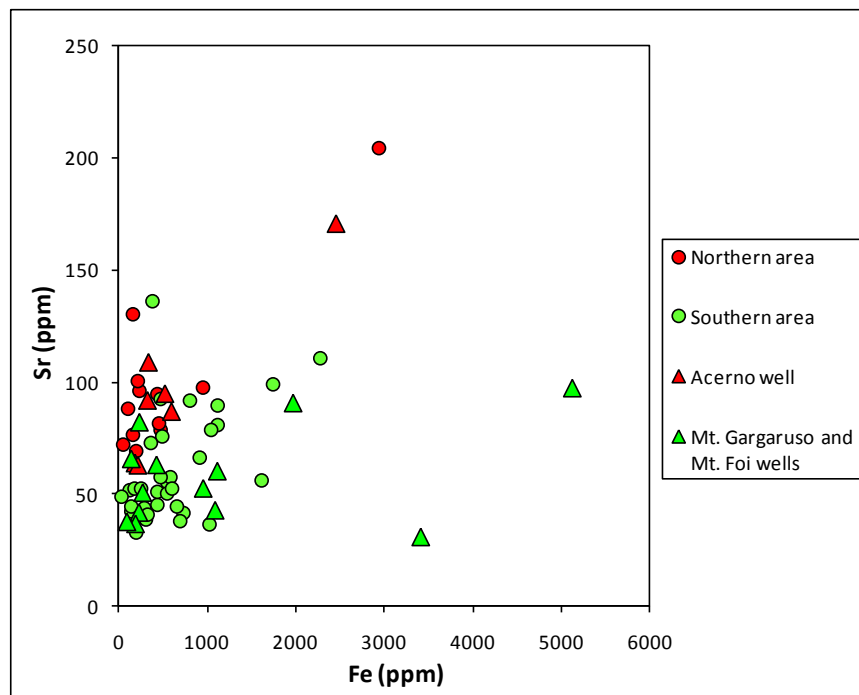


Figure 41: Covariation plot between Fe and Sr concentrations in the studied dolomites.



### 8.2.3 Barium (Ba)

Ba concentration was measured on 4 samples from the northern area, 14 samples from the southern area, and on 7, 2 and 11 cuttings specimens, respectively from Acerno, Monte Gargaruso and Monte Foi wells. Ba displays very low concentration in samples from both northern and southern areas. The ranges are respectively 0.48-3.84 ppm and 0.05-3.04 ppm, while mean values are respectively 1.80 and 0.9 ppm. Monte Foi well cuttings present low Ba concentration as well (range of 0.97-11.4 ppm and mean of 4.53 ppm). Monte Gargaruso and Acerno wells cuttings, instead, display higher concentration of Ba, which ranges respectively between 46 and 50 ppm, and between 22 and 252 ppm. Mean values for samples of these two wells are in that order 48 and 136 ppm. In southern area samples, the comparison between replacive dolomite and void-filling dolomite of the same rock sample pointed out that the void-filling type is depleted in Ba respect to the replacive type (Fig.42). Only one sample constitutes an exception to this rule.

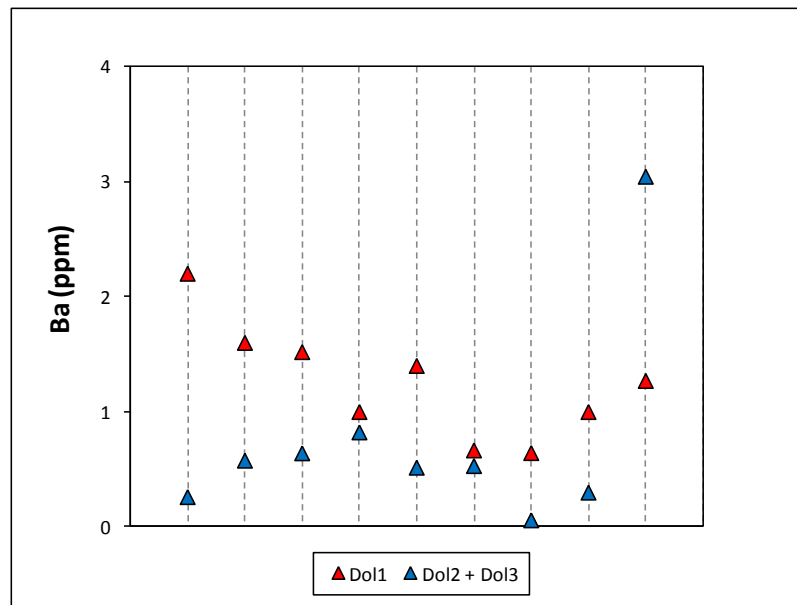


Figure 42: The trend of Ba concentrations in single sampled sites of the southern area. Ba contents of the two different dolomite types from the same rock sample are plotted on the same vertical dashed line.

### 8.3 Sr isotope analyses

Sr isotope ratios were measured on 6 dolomite specimens: two of them are from the northern area, two from the southern area (from the replacive type, i.e. Dol1) and the others two from Monte Gargaruso well. All the results are reported in Appendix 2, while the statistic parameters of  $^{87}\text{Sr}/^{86}\text{Sr}$  ratios in the different localities are summarized in Table 3.

Dolomites from the northern area have  $^{87}\text{Sr}/^{86}\text{Sr}$  ratios comprised between 0.707661 and 0.708038, with mean at 0.707849. Dolomites from the southern area present  $^{87}\text{Sr}/^{86}\text{Sr}$  ratios between 0.707908 and 0.708595, with mean at 0.708251.  $^{87}\text{Sr}/^{86}\text{Sr}$  ratios for dolomites from Monte Gargaruso well range between 0.707831 and 0.708274, and have a mean of 0.708052.

Dolomites location		$^{87}\text{Sr}/^{86}\text{Sr}$
<b>Northern area</b> (2)	min.	0,707661
	mean	0,707849
	max.	0,708038
	std. dev.	0,000267
<b>Southern area Dol1</b> (2)	min.	0,707908
	mean	0,708251
	max.	0,708595
	std. dev.	0,000486
<b>Mt. Gargaruso well</b> (2)	min.	0,707831
	mean	0,708052
	max.	0,708274
	std. dev.	0,000313

Table 3: Sr isotopes geochemistry. The statistic parameters of  $^{87}\text{Sr}/^{86}\text{Sr}$  ratios are reported for samples coming from the two different study areas and from Mt. Gargaruso well. Statistic parameters of southern area samples refer to the replacement dolomite type (Dol1). In parenthesis there is the number of measured samples. Min. = minimum value, mean = mean value, max. = maximum value, std. dev. = standard deviation.

Dolomites from the two areas and from the well do not show any evident grouping in the cross-plots Sr content vs.  $^{87}\text{Sr}/^{86}\text{Sr}$  ratios (Fig.43) and  $\delta^{13}\text{C}$  vs.  $^{87}\text{Sr}/^{86}\text{Sr}$  ratios (Fig.44). In the cross-plot  $\delta^{18}\text{O}$  vs.  $^{87}\text{Sr}/^{86}\text{Sr}$  ratios (Fig.45) dolomites from the northern area display  $^{87}\text{Sr}/^{86}\text{Sr}$  values all consistent with those estimated for the Upper Triassic seawater (McArthur and Howarth, 2004), while dolomites from the southern area and from Monte Gargaruso well present slightly enriched Sr isotopes ratios in respect with the same seawater values.

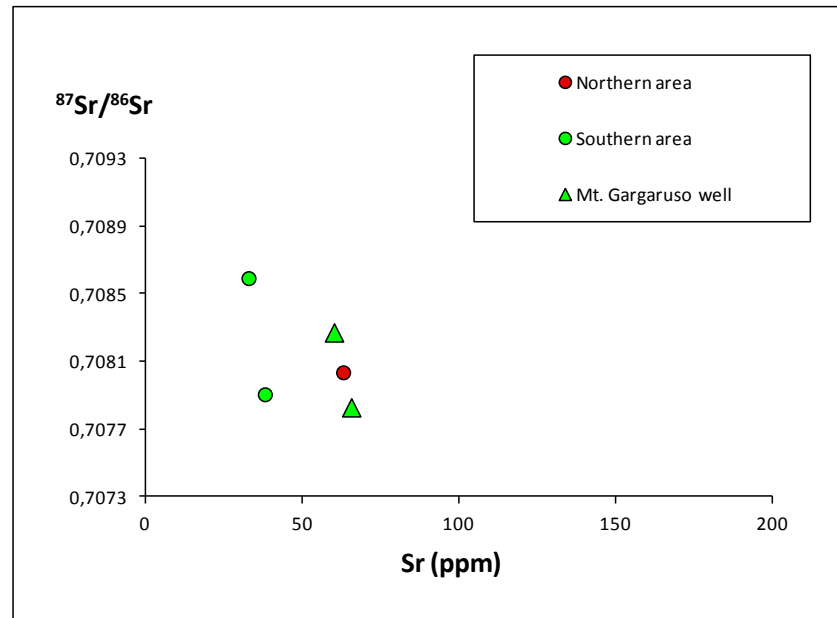


Figure 43: Covariation plot between Sr content and  $^{87}\text{Sr}/^{86}\text{Sr}$  ratios for the studied dolomites.

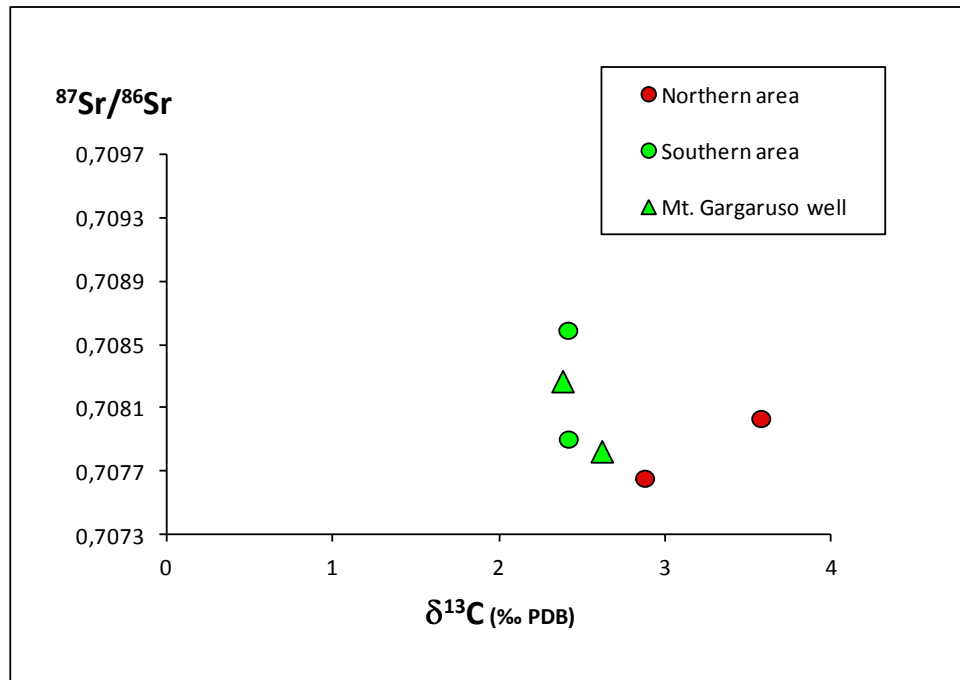


Figure 44: Covariation plot between  $\delta^{13}\text{C}$  and  $^{87}\text{Sr}/^{86}\text{Sr}$  ratios for the studied dolomites.

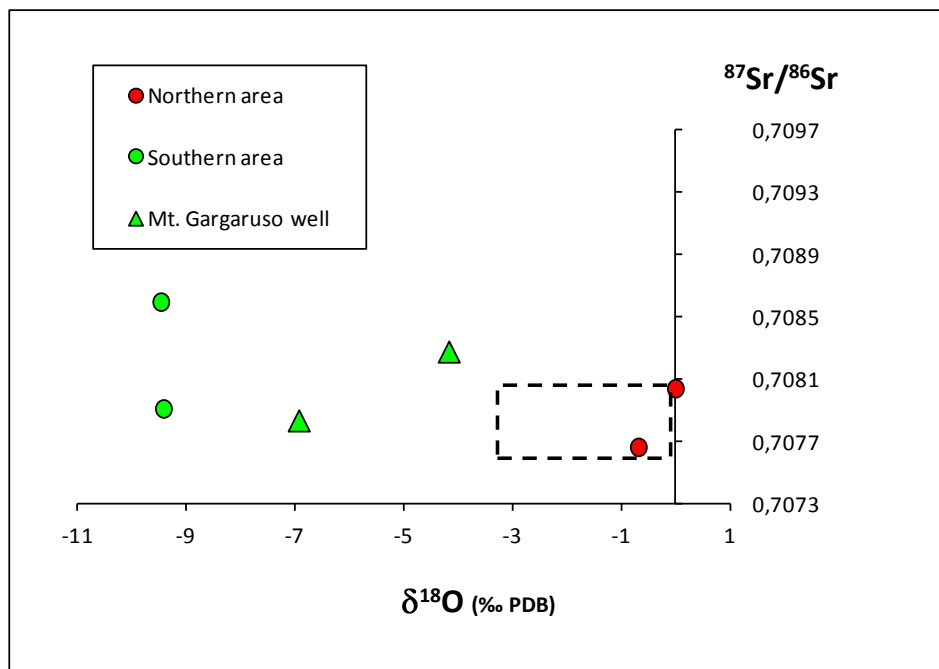


Figure 45: Covariation plot between  $\delta^{18}\text{O}$  and  $^{87}\text{Sr}/^{86}\text{Sr}$  ratios for the studied dolomites. The isotope composition of Upper Triassic seawater (Veizer *et al.*, 1999; McArthur and Howarth, 2004) is reported in the dashed frame.

## Chapter 9: Fluid inclusions (FIs) study

### 9.1 Samples location

FIs microthermometry was performed on 11 samples belonging to the *Calcari con selce* Formation.

Eight dolomite samples were collected along a W-SW to E-NE transect that goes from Monte Gargaruso well to Fiumarella d'Anzi river (Fig.11 and 46). Three of these samples come from the Monte Gargaruso well (cuttings). The location of the other samples along the transect is: Mount Tigliano, Madonna del Sasso, Mount Arioso, Monteforte and Fiumarella d'Anzi.

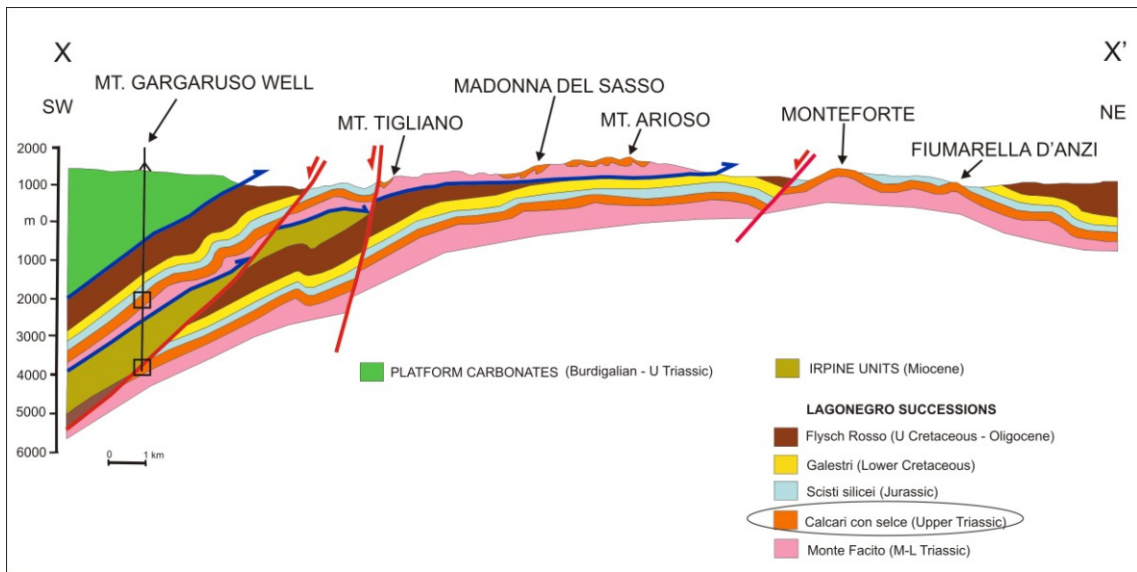


Figure 46: Geologic section of X-X' trace in Figure 11 displaying the location of the sampling localities of specimens for fluid inclusions analysis. Along this transect the cherty limestones of the *Calcari con selce* Formation are almost completely replaced by dolomites.

Two other dolomite samples were collected in the outcrops of Vietri di Potenza and Tito-Satriano, which are located in a north-northwest area compared to the above mentioned transect (Fig.11).

One limestone sample containing a calcite nodule predating the dolomites was investigated as well. It was sampled at Pignola (in an outcrop located near Monteforte) close to a dolomitization front; it represents a limestone preserved from the dolomitization process.

### 9.2 Fluid inclusions petrography

The studied ***limestone sample*** is a mudstone containing radiolarian and very thin bivalves. It is cross-cut by calcite veins (up to 150  $\mu\text{m}$  in thickness) that stop at the contact with a calcite nodule. The latter consists of blocky crystals. The transition from limestone to calcite filling the nodules consists of euhedral rhombs of dolomite (planar-E

texture), 50 to 250  $\mu\text{m}$  in diameter, which replace the limestone micrite (Fig.24C). The blocky cement of the calcite nodule holds both small ( $< 2\mu\text{m}$ ) monophasic and biphasic liquid-rich inclusions with length that does not exceed 10  $\mu\text{m}$ . The shape of biphasic inclusions varies from crystallographically controlled to irregular. Crystallographically controlled FIs are those FIs whose shape is controlled by crystallographic directions, such as cleavage planes and crystal borders. They generally display one or more sides running parallel to such crystallographic directions. The degree of fill (F) of the studied FIs in the blocky calcite is comprised between 0.91 and 0.95.

The studied **dolomite samples** consist of the major matrix replacement dolomite phase (Dol1), and the less abundant void-filling dolomite phase (Dol2). The void-filling Dol3 phase was never observed in any of the studied samples for FIs microthermometry. Dol1 crystals contain abundant FIs, but their small size ( $< 2\mu\text{m}$ ) and the cloudiness of crystals made unable any further characterization. Dol2 crystals are uniformly cloudy indicating the presence of inclusions homogeneously distributed within the crystals. The last generation of Dol2 is constituted by non-planar-C scimitar-like shape crystals showing a zonation, related to the alternation of growth zones with different FIs content (Fig.31A). Dol2 holds both small ( $< 2\mu\text{m}$ ) monophasic and biphasic liquid-rich inclusions. The latter have a size of mostly 5-10  $\mu\text{m}$  of length (see Table 4 for details on FIs sizes). Their shape varies mainly from irregular to crystallographically controlled (Fig.47A),

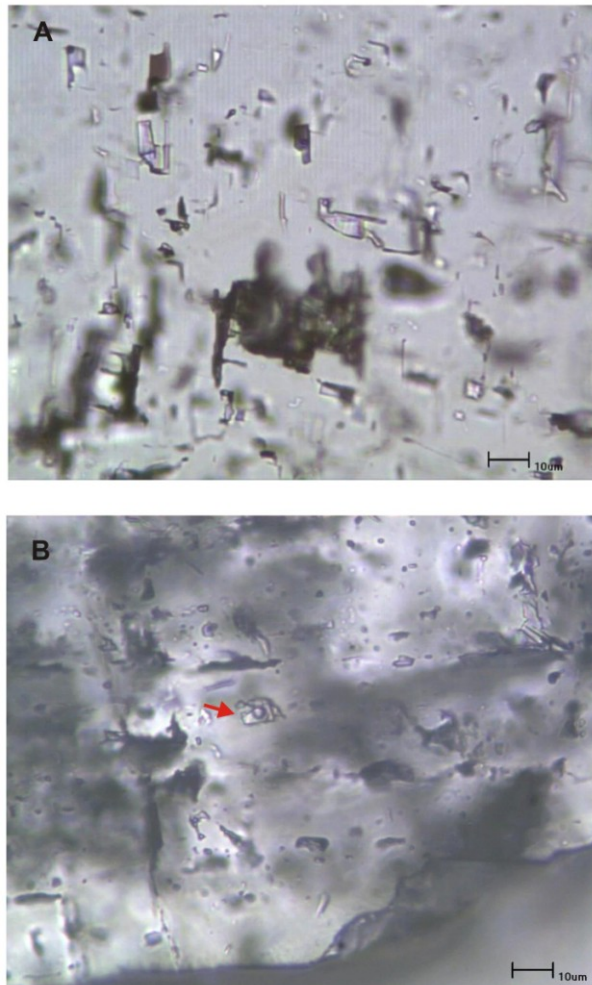




Figure 47 (previous page): Examples of the studied fluid inclusions at room temperature. A) FIA consisting of crystallographically controlled inclusions. B) Rectangular FI displaying a low liquid-vapor ratio (large bubble, red arrow), indicating that the inclusion lost some liquid (leakage) or underwent volume expansion (thermal re-equilibration).

rectangular (Fig.47B) and elongated.  $F$  is between 0.83 and 0.98. Different types of FIs were recognized in Dol2 according to their occurrence within the host crystals (Fig.48 and 49):

- Type 1: FIs occurring in crystal core
- Type 2: FIs along growth zones
- Type 3: FIs along crystal edge (generally FI poor)
- Type 4: FIs occurring in patchy concentrations (not related to any particular petrographic position)
- Type 5: FIs isolated
- Type 6: FIs aligned along trails which do not propagate through the crystals

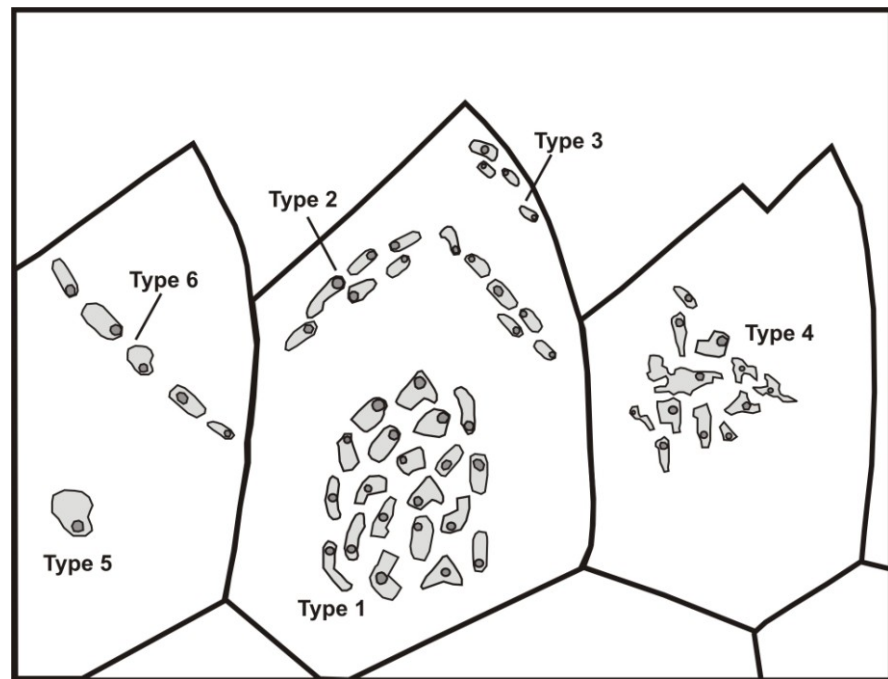


Figure 48: Sketch illustrating the occurrence of the different types of FIs in the studied dolomites.

Although a later dolomite recrystallization with FIs redistribution cannot be excluded, type 1, 2 and 3 share the typical features of primary FIs. Indeed, their distribution in the crystals is controlled by growth zonations and their shape is often crystallographically controlled, i.e. one or more sides of the FIs are parallel to crystal borders or cleavage planes. Inclusions of type 4 and 5 have an indeterminate origin, whereas type 6 FIs are pseudosecondary. Type 5 and 6 are quite rare, while type 4 is present only in one sample.

All of the observed FIs in both calcite and dolomite samples types can be characterised in a  $H_2O$ -salt system, as they do not show any fluorescence under UV light.

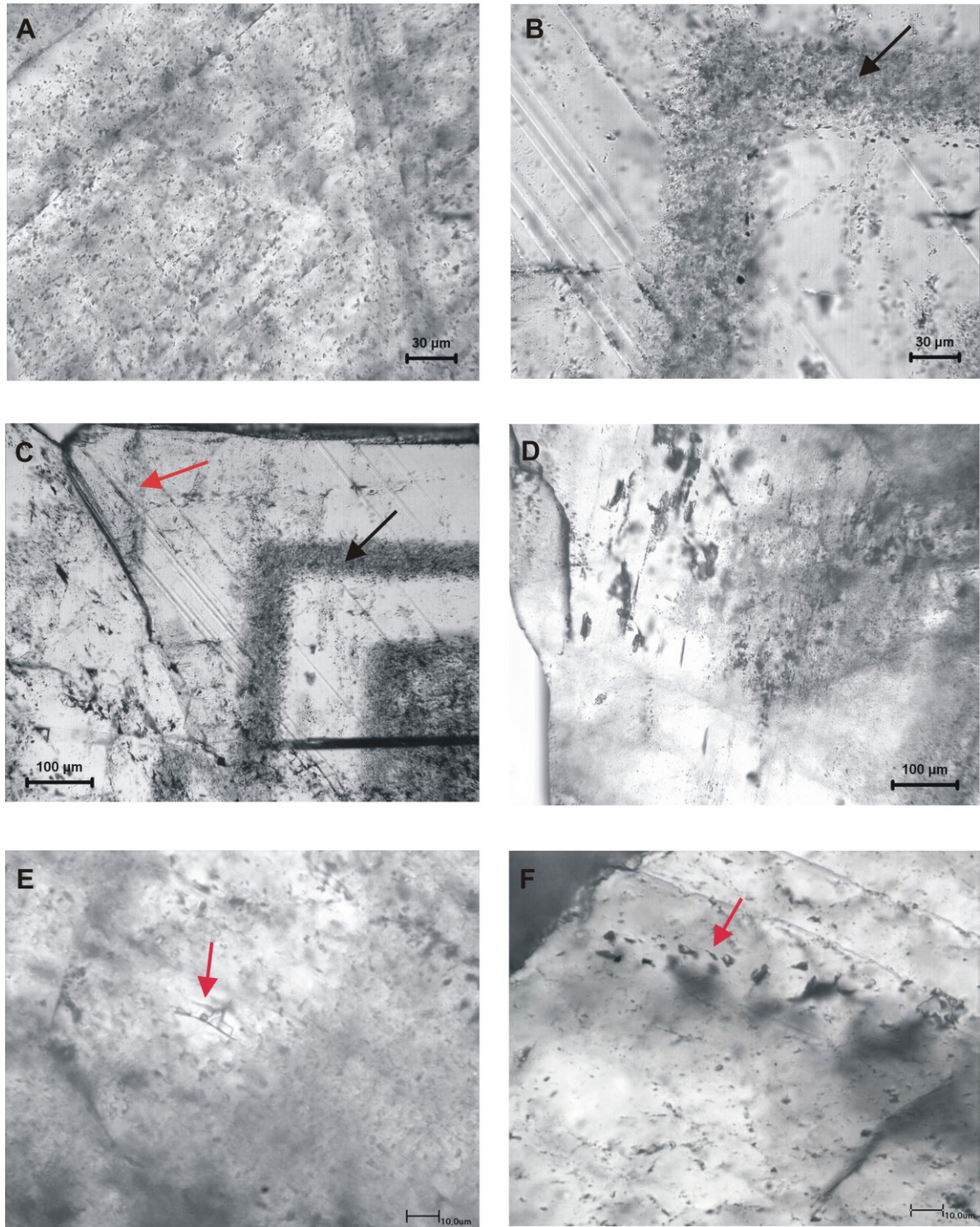


Figure 49: Petrographic pictures representing the different types of FIs in the studied dolomites. A) FIs occurring in a crystal core (type 1). B) FIs along a growth zone (black arrow; type 2). C) FIs along a growth zone (black arrow; type 2) and along a crystal edge (red arrow; type 3). D) FIs occurring in patchy concentration (type 4). E) Isolated FI (red arrow; type 5). F) FIs aligned along a pseudo-secondary trail (red arrow; type 6).

### 9.3 Behaviour of FIs during microthermometry

Microthermometry was performed on aqueous biphasic FIs of the calcite from the limestone sample and on aqueous biphasic FIs of Dol2 from the 10 dolomite samples.

**Calcite sample** - Homogenization ( $T_h$ ) occurred in the liquid field. The ice-like phases nucleated between -35 and -50 °C during the first cooling run. Approximately half of the inclusions had a metastable behaviour with the ice melting abruptly at temperatures higher than the real ones. Some of them were apparently monophasic FIs at room temperature and nucleated the gas bubble only after complete freezing and subsequent reheating. No  $T_{eapp}$  was observed for any inclusions. The measured homogenization temperatures cover a large range of values; the higher values (>105°C) represent the consequence of a probably thermal re-equilibration that affected the sample, although repeated  $T_h$  measurements did not show increasing values. Despite the thermal re-equilibration, the microthermometric results were graphically presented considering only the lower values (more representative of the true temperatures) for the interpretation of the data.

**Dolomite samples** - FIs type 4, 5 and 6 present consistent values of  $T_h$  and  $T_{m_i}$  with respect to primary FIs (type 1, 2, 3), therefore no separation between the microthermometric results of the primary, pseudosecondary and indeterminate FIs was made. Homogenization ( $T_h$ ) occurred in the liquid phase. Most FIs renucleated the vapour bubble during cooling after homogenisation at temperatures between 30 and 90 °C, but some of them did not nucleate anymore the bubble and appeared monophasic at room temperature. The nucleation of the gas bubble for these inclusions was obtained after FIs freezing and subsequent reheating. This metastable behaviour of the  $T_{n_g}$  at room temperature allows to exclude a low-temperature (< 50°C) origin for the observed monophasic all-liquid FIs in Dol2. The nucleation of ice-like phases occurred mainly between - 41 and - 46 °C during the first cooling run. Most of the FIs displayed a metastable behaviour of the  $T_{m_i}$ . In these FIs the ice melted suddenly at temperatures above those derived from thermodynamic criteria. Due to the small size of the FIs and their metastable behavior, it was not possible to determine the  $T_{eapp}$ .

The FIs of the 3 samples coming from the Monte Gargaruso well and the FIs of the sample from Monteforte outcrop probably underwent overheating with consequent thermal re-equilibration and/or leakage. Indeed, most of these inclusions homogenized at temperatures higher than 200 °C, value that is more than 90°C higher compared to the overall mode of the other samples (see paragraph 9.4), representing the same fluid event (according to geochemical similarities). Some of these overheated FIs had low liquid-vapor ratio (larger bubbles; Fig.47B) compared to the FIs of the other samples, indicating that the inclusions lost some liquid (leakage) or underwent volume expansion (thermal re-equilibration). The microthermometric results of these re-equilibrated samples are graphically represented in Fig.50.

Both calcite and dolomite FIs displayed a very common metastable behaviour of the final melting of ice. These melting temperatures, which may occur well above 0 °C, have no meaning in terms of fluid salinity (Goldstein and Reynolds, 1994). Real salinities could be calculated from the few FIs which displayed stable ice melting. The latter were most commonly observed in FIs with lower liquid/vapour ratio (larger bubbles), which consequently correspond to higher temperatures. This is the reason why in the  $T_h$ -salinity or  $T_h$ - $T_{m_i}$  cross plots reported in Fig.52 and Fig.56 and 57 the cloud

of dots indicate higher mean Th compared to those derived from the Th frequency distribution histograms of Fig.51A, 53 and 54.

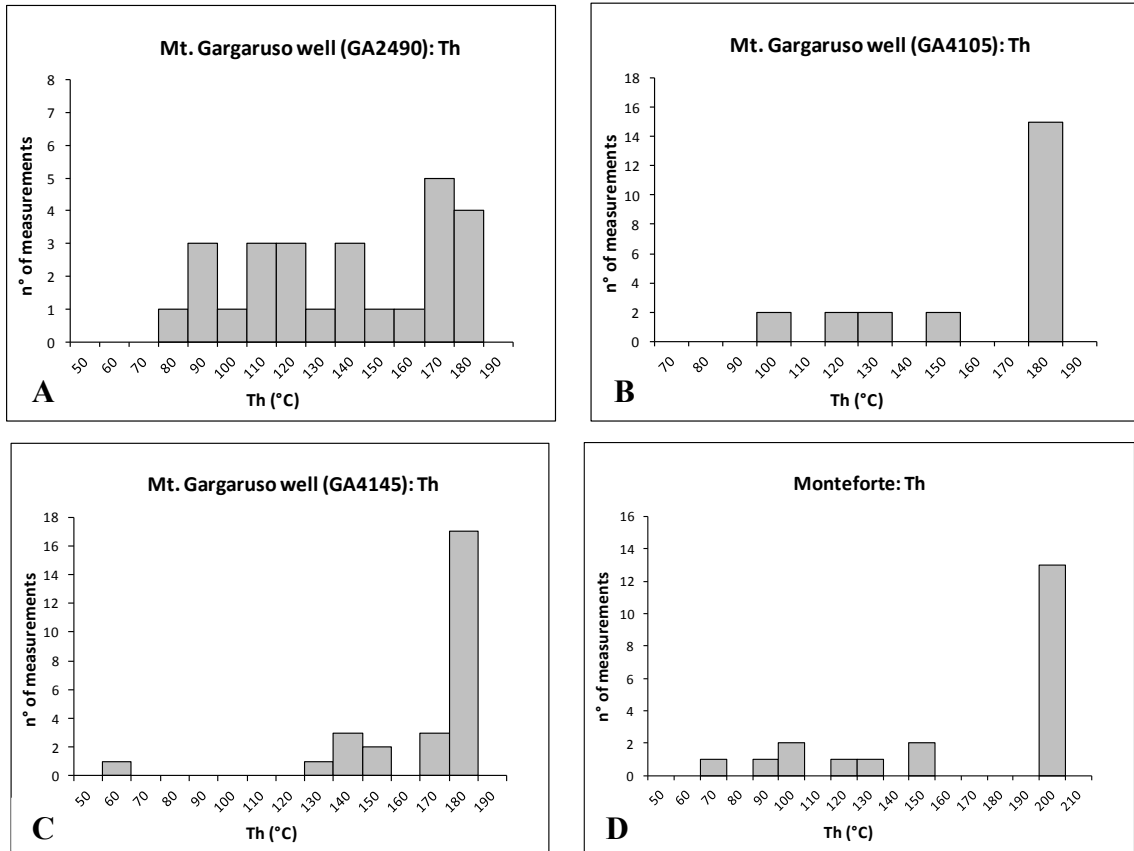


Figure 50: Histograms showing the frequency distribution of homogenization temperatures (Th) values of different FIs types from dolomite samples of Mount Gargaruso well (A, B and C), and from Monteforte outcrop (D). All these samples underwent thermal re-equilibration, represented by the tail of Th values towards high temperatures. Values in the intervals 180-190 °C and 200-210 °C are minimum values of Th, as the corresponding FIs homogenized at higher temperatures (not reported for graphical reasons).

## 9.4 Microthermometry results

**Calcite sample** - The main results of microthermometry of calcite FIs are summarized in Table 4. Microthermometry was accomplished on a total of 49 FIs recording a range of Th between 69 and 161 °C. Such a large spread of Th values can be observed in the histogram of Fig.51A. This data distribution can be interpreted as due to thermal re-equilibration of FIs by later high temperature events. Therefore, by considering the lower set of values only, a normal distribution can be drawn with the thermally re-equilibrated FIs represented by the tail towards higher temperatures. Low temperatures measurements were performed on 14 FIs recording  $T_{m_i}$  between -1.3 and -6 °C, with a mode of -3 °C (Fig.51B) and a mean of -3.6 °C. These values correspond to a range of salinity of 2.2 - 9.2 eq. wt % NaCl with mode and mean respectively of 5 and 5.8 eq. wt % NaCl (Fig. 52A).

Sample	Locality	Type	Shape	Size (µm)	F	Th (C°)		Tm <sub>ice</sub> (C°)	
						mode	range	mode	range
<b>TG40</b>	Fiumarella d'Anzi	2-3-4	Crystallographically controlled - Rectangular	< 10	0,92/0,93	95 (47)	75/117	-	-1,8/-2,6
<b>TG58</b>	Monteforte	2-5	Crystallographically controlled - Irregular	5 - 10	0,91/0,96	-	-	-	-
<b>TG61</b>	Madonna del Sasso	1-2-3	Rectangular- Elongated	< 10	0,87/0,97	85 (45)	67/104,5	-	-1,1/-1,3
<b>TG81</b>	Vietri di Potenza	1-2-3	Crystallographically controlled - Rectangular	< 5	0,83/0,91	115 (31)	87/121	-	-1,9/-2,7
<b>TG84</b>	Tito - Satriano	1-3	Crystallographically controlled - Elongated	< 10	0,91/0,92	115 (32)	87/129	-2,9 (6)	-1,2/-2,9
<b>TG89</b>	Mount Arioso	1-2-3	Crystallographically controlled - Elongated	up to 15	0,91/0,97	95 (32)	86/115	-	-1,5/-3,2
<b>TG104</b>	Mount Tigliano	2-3	Crystallographically controlled - Irregular	up to 15	0,91/0,98	105 (47)	71/118	-1,1 (6)	-1,1/-3,2
<b>GA2490</b>	Mt. Gargaruso well	1-3-6	Crystallographically controlled - Rectangular	< 5	-	-	-	-	-2,2/-4,0
<b>GA4105</b>	Mt. Gargaruso well	1-2-3-6	Elongated - Triangular	< 10	0,95	-	-	-	-
<b>GA4145</b>	Mt. Gargaruso well	1-2-3-6	Crystallographically controlled - Rectangular	5 - 10	0,9	-	-	-	-1,7/-3,7
<b>826 (CALCITE)</b>	Pignola	-	Crystallographically controlled - Irregular	< 10	0,91/0,95	85 (49)	69/105	-3 (14)	-1,3/-6,0

Table 4: Petrographic features of two-phase (Liquid + Vapour) FIs at room temperature from ten dolomite samples and one calcite sample (826) from different localities. The size is given as length in µm. F stands for degree of fill. FIs types are distinguished according to their occurrence within the host crystals (see the text for numbers explanation). The table also summarizes the main results of microthermometry. The mode and range values of Th and Tm<sub>i</sub> are reported. In parenthesis, the number of Th and Tm<sub>i</sub> measurements, accomplished for each sample, is reported. Monophase all-liquid FIs present in both dolomite and calcite samples are not reported in this table as they are interpreted to be two-phase FIs with vapour bubble metastably absent at room temperature.

The bivariate plot of Th and Tm<sub>i</sub> (Fig. 52B) shows a positive correlation between the two variables, indicating that some inclusions underwent leakage and refilling (Goldstein and Reynolds, 1994). As explained in paragraph 9.3 these plots are tricky as



they would suggest much higher Th mean values compared to what established in Fig. 51A, but they allow to visualize the salinity variation as a function of temperature (either real or resulted by overheating). It is interesting to note that the higher salinities are recorded in the lower temperature FIs and vice versa. A possible interpretation is that the FIs from the calcite sample are representative of two slightly different fluid populations. Anyway, this hypothesis cannot be validated because of lack of secondary FIs recording the late high temperature events.

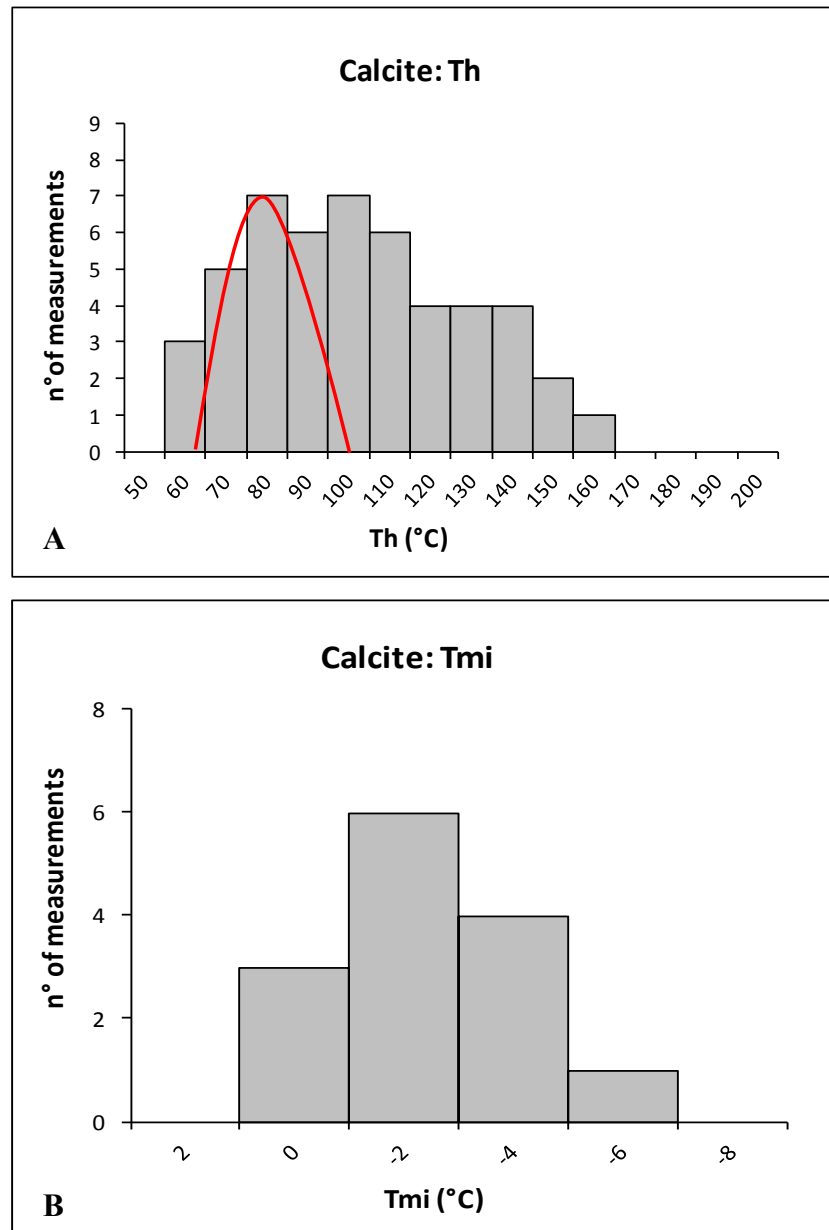


Figure 51: Microthermometry results for FIs of the calcite sample. A) Homogenization temperature (Th) frequency distribution. The gaussian includes the set of lower Th values having a mode at 85°C. The tail towards higher temperatures represents the thermally re-equilibrated FIs. B) Ice melting temperature (T<sub>mi</sub>) frequency distribution.

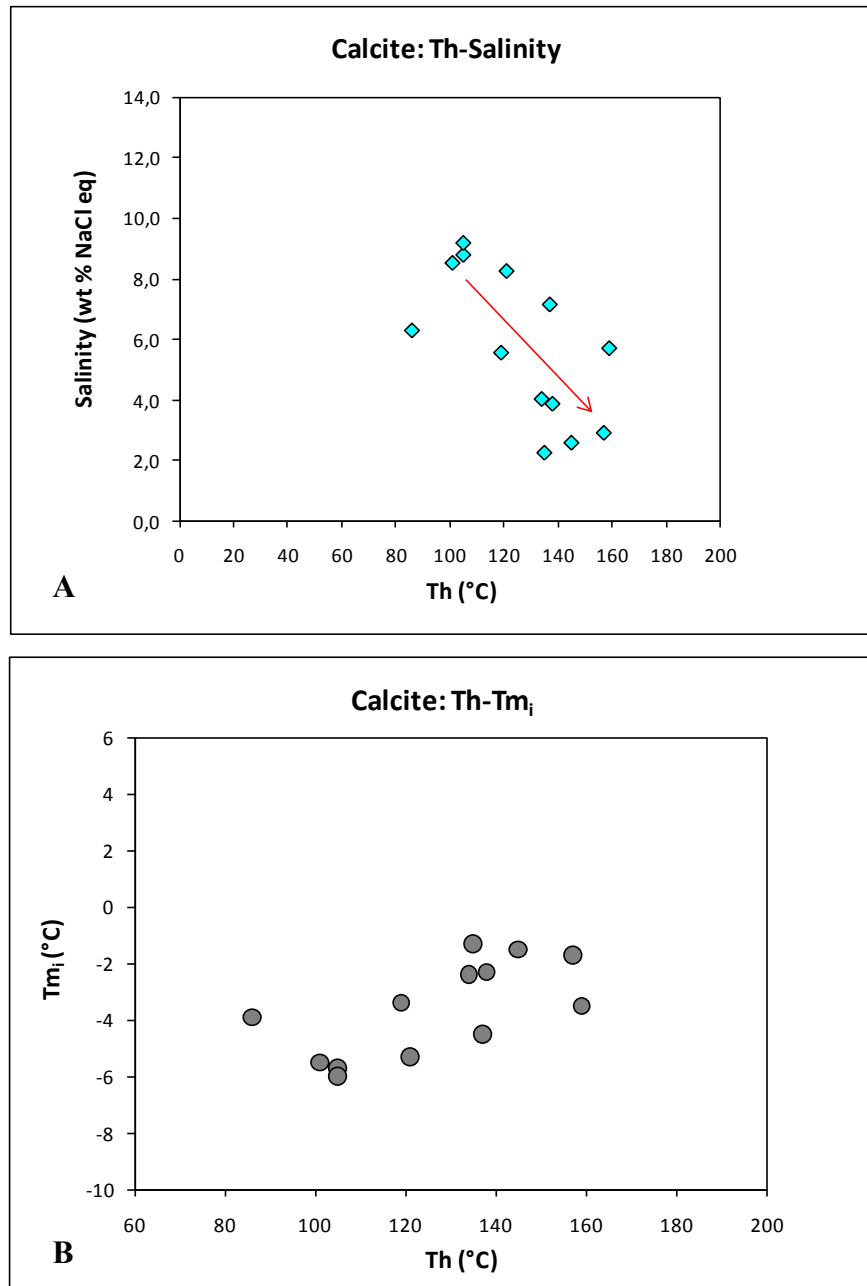


Figure 52: Microthermometry results for FIs of the calcite sample. A) Th-salinity cross-plot. The red arrow indicates the trend towards lower salinities in the FIs which have recorded overheating. B) Th-Tm<sub>i</sub> cross-plot.

**Dolomite samples** - The main results of microthermometry of FIs in dolomites are summarized in Table 4. FIs having anomalous Th values (i.e. too low or too high relative to the normal distribution of data) were not considered for the data interpretation, but they were graphically reported (Fig.53 and 54). All the samples present a small portion of FIs that underwent thermal re-equilibration. These FIs are graphically represented in the Th frequency histogram by a tail towards higher temperatures (>120-130°C).

#### Mount Tigliano

Th was measured on a total of 47 FIs (types 2 and 3), recording values between 71 and 118 °C (overall mode 105 °C; Fig.53A). Homogenization temperature of type 2 FIs

shows a bimodal distribution, with mode of 95°C and 105°C, whereas type 3 FIs have a normal distribution of Th, with a mode of 105°C. Tm<sub>i</sub> was measured only on 6 FIs with a mode of -1.1 °C and a range between -1.1 and -3.2 °C, which corresponds to a salinity between 1.9 and 5.3 eq. wt % NaCl.

**Madonna del Sasso**

Th was measured on 45 FIs of types 1, 2 and 3, giving a range of 67-104.5 °C and an overall mode of 85 °C (Fig.53B). Considering separately FIs of the three different types, they do not present a clear mode of Th. Low temperatures measurements were performed only on 3 FIs, giving a Tm<sub>i</sub> between -1.1 and - 1.3 °C, which correspond to a salinity between 1.9 and 2.2 eq. wt % NaCl.

**Mount Arioso**

Microthermometry was accomplished on 32 FIs of types 1, 2 and 3. Type 1 FIs present a Th mode of 95°C; type 2 FIs do not show a clear Th mode; type 3 FIs have a Th mode of 85°C. The overall range and the overall mode of Th values are respectively 86-115 °C and 95°C (Fig.53C). Only 2 values of Tm<sub>i</sub> were obtained, -1.5 and -3.2 °C, corresponding to a salinity of 2.6 and 5.3 eq. wt % NaCl respectively.

**Fiumarella d'Anzi**

Th was measured on 47 FIs belonging to types 2, 3 and 4. Th values present a normal distribution in the frequency diagram, showing a range between 75 and 117°C and an overall mode of 95°C (Fig.54A). Type 2 and type 3 FIs do not show a clear mode, whereas type 4 FIs present a mode of 105 °C. Tm<sub>i</sub> could be measured only on 2 FIs with values of -1.8 and -2.6, corresponding to 3.1 and 4.3 eq. wt % NaCl of salinity.

**Vietri di Potenza**

Th measurements were performed on a total of 31 FIs of types 1, 2 and 3, not distinguished in the diagram of Fig.54B. Th ranges between 87 and 121 °C with a mode of 115 °C. Only 4 low temperatures measurements could be accomplished and gave a range of Tm<sub>i</sub> between -1.9 and -2.7 °C, that correspond to a range of salinity between 3.2 and 4.3 eq. wt % NaCl.

**Tito-Satriano**

Th was measured on a total of 32 FIs of types 1 and 3, recording values between 87 and 129 °C with an overall mode of 115 °C. The data present a gaussian distribution in the frequency diagram (Fig.54C). Type 1 FIs do not show a clear mode, whereas type 3 FIs present a mode of 115°C. Tm<sub>i</sub> was measured on 6 FIs showing a mode of -2.9 °C and a range between -1.2 and -2.9 °C which corresponds to a range of salinity of 2.1- 4.8 eq. wt % NaCl.

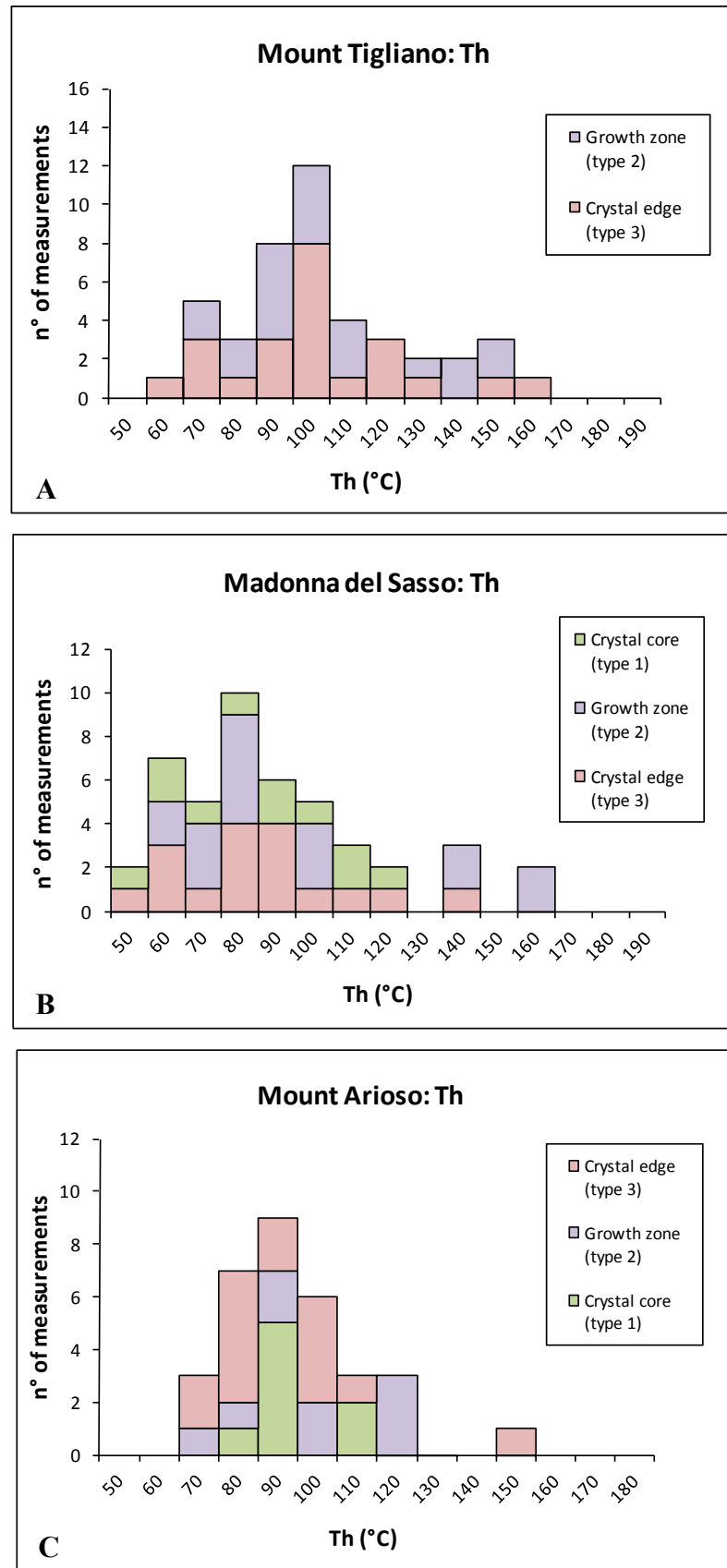


Figure 53: Histograms showing the frequency distribution of homogenization temperatures (Th) values of different FIs types from dolomite samples of different localities. A) Mount Tigliano. B) Madonna del Sasso. C) Mount Arioso.

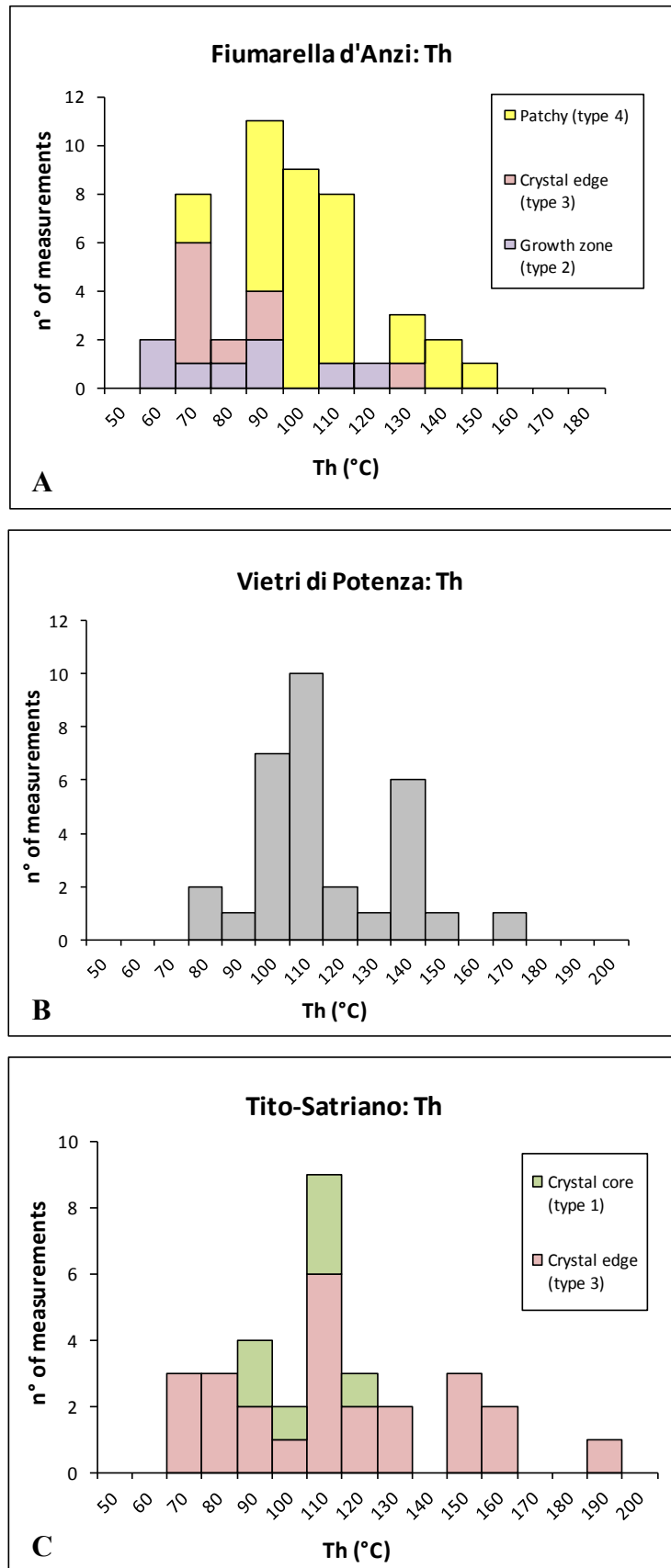


Figure 54: Histograms showing the frequency distribution of homogenization temperatures (Th) values of different FIs types from dolomite samples of different localities. A) Fiumarella d'Anzi. B) Vietri di Potenza. C) Tito-Satriano.



Because of the high number of FIs with a metastable behavior, only few  $T_{m_i}$  values could be measured for each sample. Nevertheless these  $T_{m_i}$  values are quite homogeneous in all samples (including the samples that underwent thermal re-equilibration) and present an overall range between -1.1 and -4 °C, with a broad mode of -2.5 °C and a mean of -2.2 °C. (Fig.55) These values correspond to a range of salinity between 1.9 and 6.4 eq. wt % NaCl, with a mode of 4.3 and a mean of 3.7 eq. wt % NaCl (Fig.56).

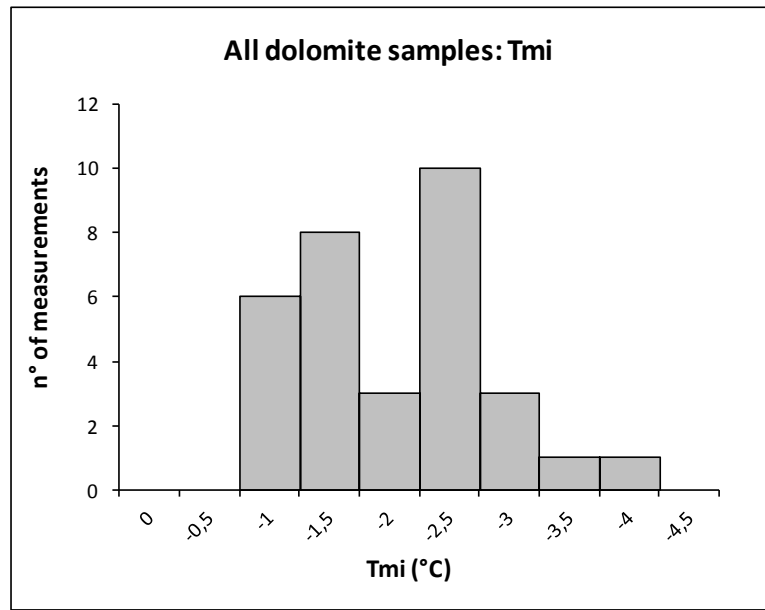


Figure 55: Histogram showing the frequency distribution of ice melting temperatures ( $T_{m_i}$ ) values for FIs of all dolomite samples.

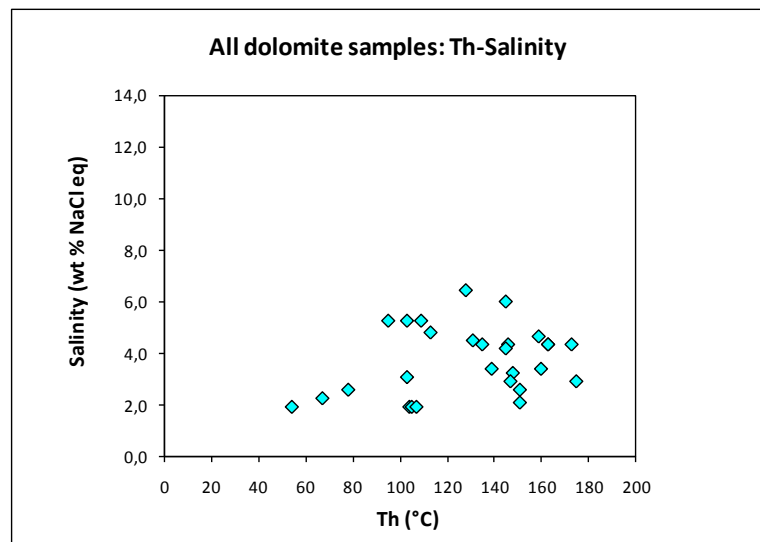


Figure 56: Bivariate plot showing the covariance between homogenization temperature ( $T_h$ ) and salinity data for FIs of all dolomite samples. Salinity is expressed in eq. wt % NaCl.

The  $T_h$ - $T_{m_i}$  covariance diagram (Fig.57) shows an increase of  $T_h$  values, as  $T_{m_i}$  values remain constant (i.e. only one population of fluids). This trend indicates that the

inclusions underwent stretching of their walls (Goldstein and Reynolds, 1994). As explained in paragraph 9.3 these cross-plots are tricky, as they would suggest much higher Th mean values compared to what established in Fig.53 and 54. This is just due to the fact that stable melting was observed in FIs with larger vapour bubble, which are those most possibly affected by re-equilibration.

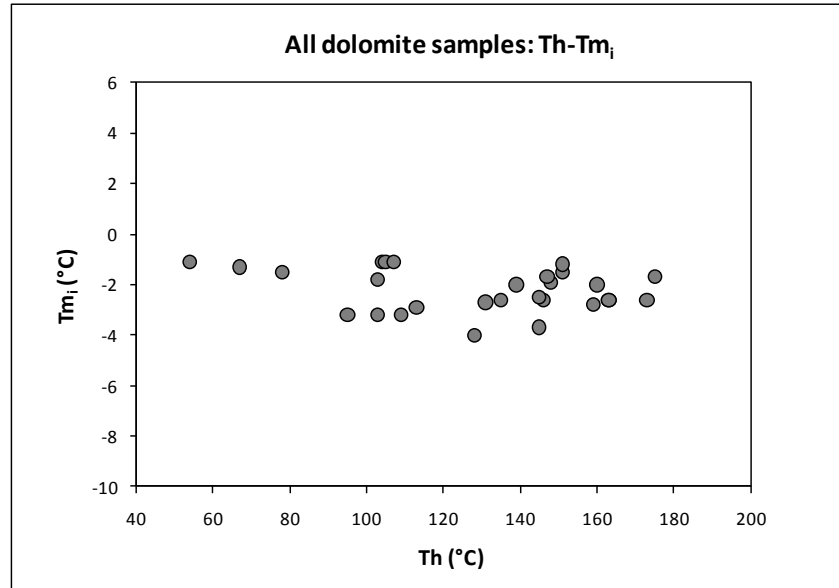


Figure 57: Covariance between Th and  $Tm_i$  of FIs from all dolomite samples.

## 9.5 Bulk density and composition of FIs

Bulk density and composition of all studied FIs were calculated as described in paragraph 4.5.3. The molar volume of these FIs ranges between 18.50 and 19.26  $\text{cm}^3/\text{mol}$  (i.e. density between 0.988 and 0.963  $\text{g}/\text{cm}^3$ ). Maximum, minimum and mode values of FIs molar volume and density for each sample are reported in Table 5. The mole fractions of the different species present (i.e.  $\text{H}_2\text{O}$ ,  $\text{Na}^+$  and  $\text{Cl}^-$ ) are reported for FIs of each sample in Table 6.

Sample	Locality	Max		Min		Mode	
		Vm (cc/mol)	D (g/cc)	Vm (cc/mol)	D (g/cc)	Vm (cc/mol)	D (g/cc)
TG40	Fiumarella d'Anzi	19,092896	0,968403	18,647279	0,991545	18,839777	0,981413
TG61	Madonna del Sasso	18,881742	0,967996	18,504299	0,987741	18,668988	0,979028
TG81	Vietri di Potenza	19,154175	0,967483	18,771970	0,987181	19,078574	0,971317
TG84	Tito-Satriano	19,265488	0,962971	18,778407	0,987949	19,083891	0,972134
TG89	Mount Arioso	19,078574	0,971317	18,762284	0,987691	18,852399	0,982970
TG104	Mount Tigliano	19,095183	0,966089	18,598487	0,991890	18,937000	0,974159
826 (CALCITE)	Pignola	19,027533	0,986816	18,716137	1,003235	18,824920	0,997437

Table 5: Molar volume (cc/mol) and density (g/cc) of the studied FIs. The calculated minimum (Min), maximum (Max) and mode values are reported for each sample.

Sample	Locality	Max			Min			Mode		
		Bulk composition			Bulk composition			Bulk composition		
		xH <sub>2</sub> O	xNa <sup>+</sup>	xCl <sup>-</sup>	xH <sub>2</sub> O	xNa <sup>+</sup>	xCl <sup>-</sup>	xH <sub>2</sub> O	xNa <sup>+</sup>	xCl <sup>-</sup>
TG40	Fiumarella d'Anzi	0,976818	0,011591	0,011591	0,976818	0,011591	0,011591	0,976818	0,011591	0,011591
TG61	Madonna del Sasso	0,98712	0,00644	0,00644	0,98712	0,00644	0,00644	0,98712	0,00644	0,00644
TG81	Vietri di Potenza	0,974804	0,012598	0,012598	0,974804	0,012598	0,012598	0,974804	0,012598	0,012598
TG84	Tito-Satriano	0,973803	0,013098	0,013098	0,973803	0,013098	0,013098	0,973803	0,013098	0,013098
TG89	Mount Arioso	0,974804	0,012598	0,012598	0,974804	0,012598	0,012598	0,974804	0,012598	0,012598
TG104	Mount Tigliano	0,978847	0,010577	0,010577	0,978847	0,010577	0,010577	0,978847	0,010577	0,010577
826 (CALCITE)	Pignola	0,963047	0,018477	0,018477	0,963047	0,018477	0,018477	0,963047	0,018477	0,018477

Table 6: Mole fractions of the different species present (i.e. H<sub>2</sub>O, Na<sup>+</sup> and Cl<sup>-</sup>) in the studied FIs. The calculated minimum (Min), maximum (Max) and mode values are reported for each sample.

## 9.6 P-T conditions during FIs trapping

Homogenization temperatures of FIs obtained with microthermometry represent the minimum temperatures at which FIs were entrapped. A “pressure correction” should be applied, in order to get the real trapping temperatures. For this calculation, composition of the inclusions and pressure at the time of entrapment must be known. The latter must be determined with independent methods. Considering the maximum burial of 3.8 km, and peak temperatures of 130-160 °C experienced by the studied succession (Corrado *et al.* 2005, Mazzoli *et al.* 2008), prevailing hydrostatic pressure conditions during dolomitization can be assumed. According to a hydrostatic pressure gradient of 10.1 MPa/km (obtained by considering a seawater density of 1.03 g/cm<sup>3</sup>) the peak burial depth would have corresponded to a maximum pressure of 38.38 MPa.

Trapping temperatures for the different FIs were calculated by means of isochores constructed for the Th mode values in P-T diagrams.

The 4 dolomite samples coming from Mount Tigliano, Madonna del Sasso, Mount Arioso and Fiumarella d'Anzi, all located along the studied transect, were grouped together (Group 1) giving an overall Th mode of 95±10 °C. The two samples from Vietri di Potenza and Tito-Satriano, coming from a north-western area compared to the transect samples, were assembled in another group (Group 2) having Th mode of 115°C.

The overall mean salinity (3.7 eq. wt % NaCl) was used for slope isochores calculations for both the two groups of samples, as no significant salinity differences were found between the FIs of the two groups.

The “pressure correction” for the calcite sample was calculated considering Th mode, minimum and maximum values (85, 69 and 105 °C, respectively) and the mean salinity of 5.8 eq. wt % NaCl.

In the P-T diagrams the maximum trapping temperatures of FIs are given by the intersections between the constructed isochores and the maximum pressure line (Fig.58). The true values of dolomitization temperature (by assuming thermal equilibrium between the fluid and the rocks) must be between the maximum and the homogenisation conditions.

The calculated maximum trapping temperatures for all the dolomite samples belonging to the two considered groups are equal to Th+18-20 °C. Therefore, maximum trapping temperatures for FIs from dolomite samples of Group 1 are comprised between 105 and 125 °C, whereas FIs from dolomites belonging to the Group 2 were possibly trapped at temperatures between 107 and 149 °C.

The calcite sample presents maximum trapping temperature of Th+17-18 °C, therefore the calcite precipitated at maximum temperatures comprised between 87 and 123 °C.

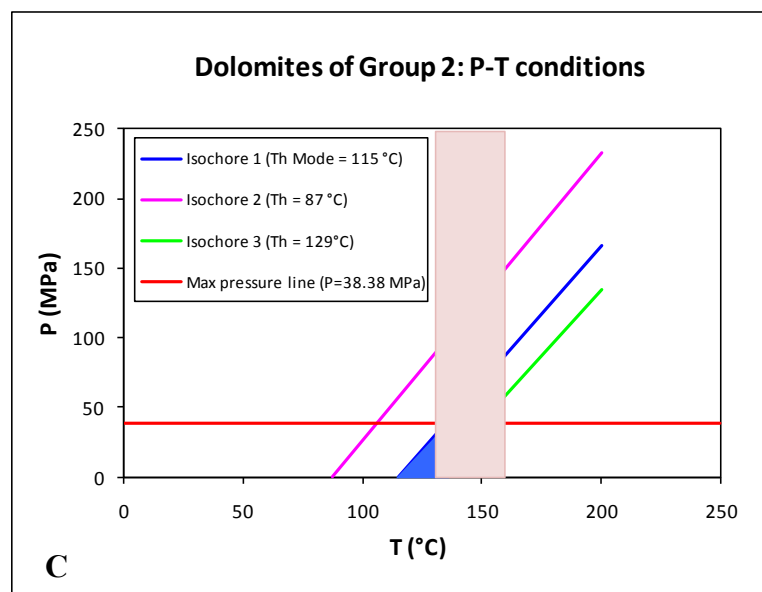
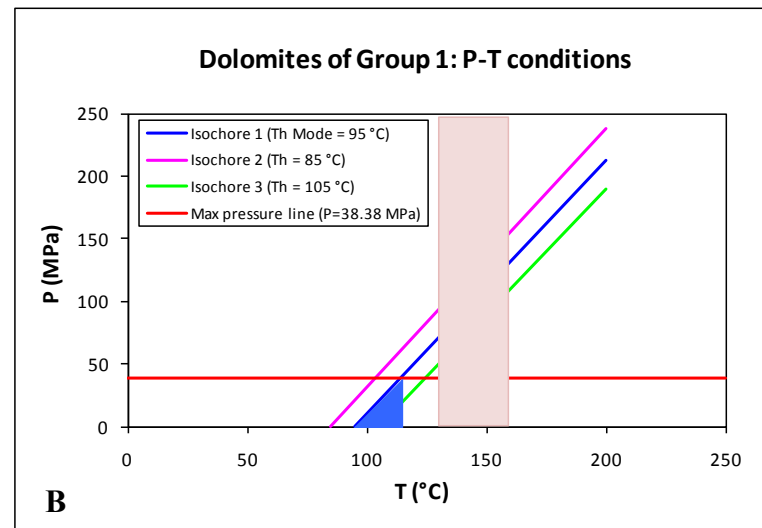
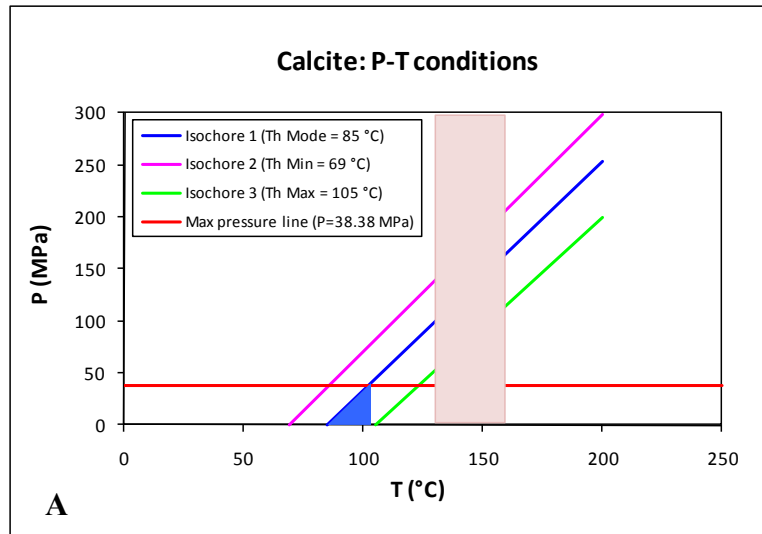




Figure 58 (previous page): P-T plots illustrating the maximum pressure line and its intersection point with isochores constructed from the Th mode values of the studied FIs (blue line). Isochores from minimum and maximum Th values are represented as well (pink and green lines, respectively). The blue triangle includes the temperature range for FIs trapping after maximum pressure correction on measured Th values. The pinkish square defines the field of temperature (130-160 °C) which characterised the peak burial conditions of the first compressional phase. A) FIs of the calcite sample. B) FIs of dolomites of Group 1. C) FIs of dolomites of Group 2.

### 9.7 Preliminary conclusions from FIs study

The analysed calcite nodule precipitated from warm (Th mode = 85 °C) and saline fluids (from normal seawater up to three times more saline than seawater). The large range of Th values and the spreading of these values towards higher temperatures suggest that the sample underwent thermal re-equilibration and leakage. These phenomena were probably the results of a natural overheating of the sample due to later thermal events (see paragraph 10.1 for a more complete discussion).

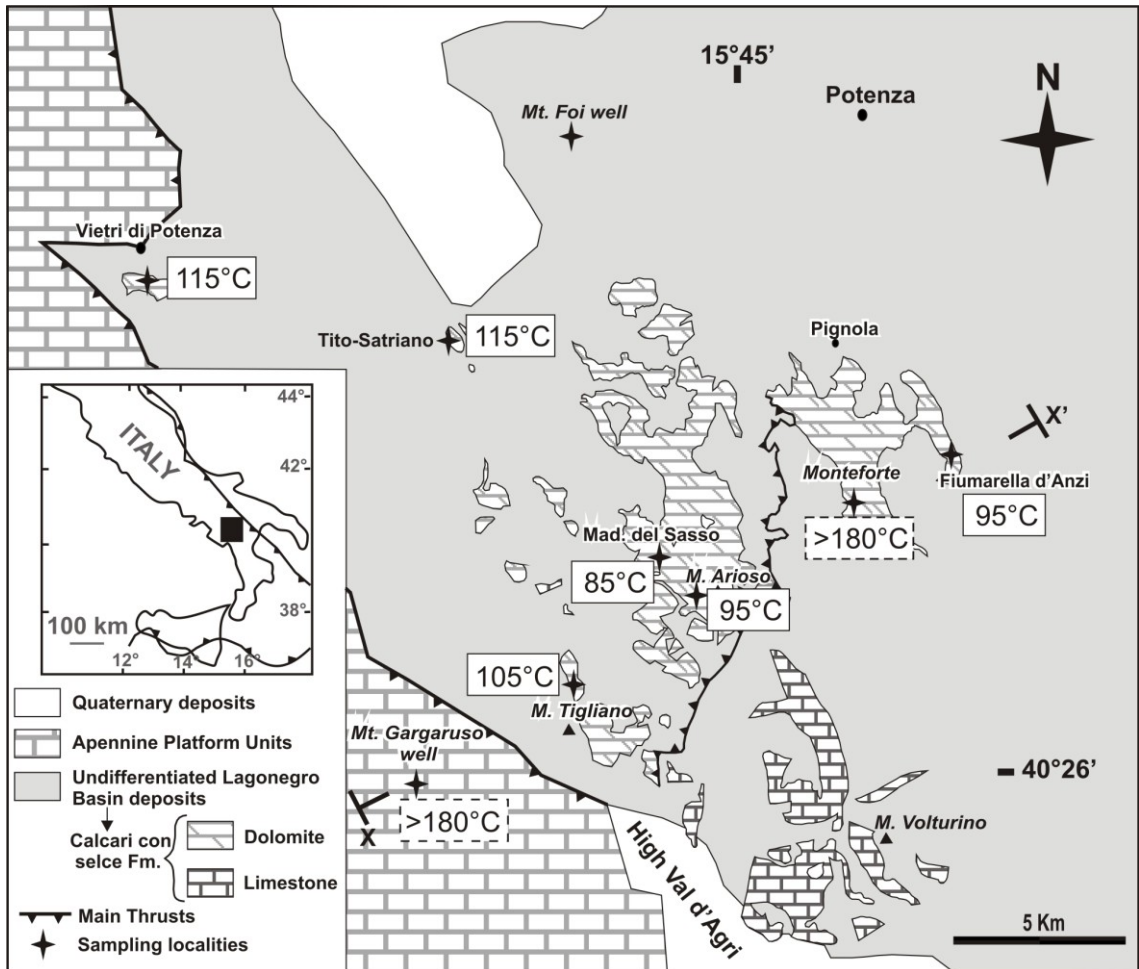


Figure 59: Geographical distribution of the measured homogenization temperatures in dolomite samples. Temperatures displayed in dashed frames represent the thermally re-equilibrated samples.

Also 4 dolomite samples contain FIs that showed a behaviour suggesting thermal re-equilibration: the 3 samples from Monte Gargaruso well and the sample from Monteforte. Fluid inclusions from cutting samples probably underwent overheating

during drawing operations from the well. Thermal re-equilibration underwent by the FIs of Monteforte sample could be due to the presence of a fault close to this sampling locality. These FIs probably underwent a mechanical stress and leakage or thermal re-equilibration caused by late hot fluids circulating through the fault plane, although any later paragenetic phase testifying these late fluids was found in the sample.

The main purpose of this microthermometric study was to verify temperature differences along the transect which goes from Monte Gargaruso well to Fiumarella d'Anzi (Fig.59). Samples located along the transect, do not show any temperature trend from W-SW to E-NE (Fig.59). They present an overall Th mode of  $95 \pm 10$  °C. These high temperatures indicate a burial origin. Most Th values are in the range of 70-120 °C. This relatively large range of values could suggest thermal re-equilibration of some FIs. Nevertheless, the frequency distribution of Th data is symmetric in each samples and Th measured in FIs of the same assemblage are consistent. Th variations are more possibly due to FIs distribution in the crystals (e.g. core versus external part, different growth zones; Goldstein and Reynolds, 1994). Actually, FIs of crystal edge (type 3), in some sample, present Th values lower than FIs of growth zone (type 2) and crystal core (type 1), indicating the progressive cooling of the fluid as the dolomite cement is precipitating.

Samples located in the north-west area (i.e. Vietri di Potenza and Tito-Satriano; Fig.59) present slightly (about 20°C) higher Th values (Th mode = 115 °C) respect to the samples of the transect (south area). The possible causes for the temperature differences from north to south will be discussed in paragraph 10.4.1.

The dolomitizing fluids do not present significant salinities differences along the transect or from north to south. They had salinities in the range of slightly modified to normal marine seawater (1.9-6.4 eq. wt % NaCl with a mean of 3.7).

## Chapter 10: Discussion

### 10.1 The diagenetic history of undolomitized limestones

The diagenetic history of undolomitized limestones was not the main focus of this study, nevertheless some considerations can be carried out on the basis of petrographic observations of the precursor limestones and fluid inclusions analysis performed on a pre-dolomite calcite nodule.

The limestones of the *Calcarei con selce* Formation display a uniform dull orange to dull red CL, and present  $\delta^{18}\text{O}$  values slightly more negative compared to the coeval seawater (Iannace *et al.*, in press; Fig.60). These values are probably the result of slight  $^{18}\text{O}$  depletion in the carbonates as a consequence of the temperatures experienced during burial, and are indicative of a recrystallization. On the contrary,  $\delta^{13}\text{C}$  and  $^{87}\text{Sr}/^{86}\text{Sr}$  values (Fig.60 and 61) overlap those of the Upper Triassic seawater (Veizer *et al.*, 1999; McArthur and Howarth, 2004), indicating that they are rock-buffered.

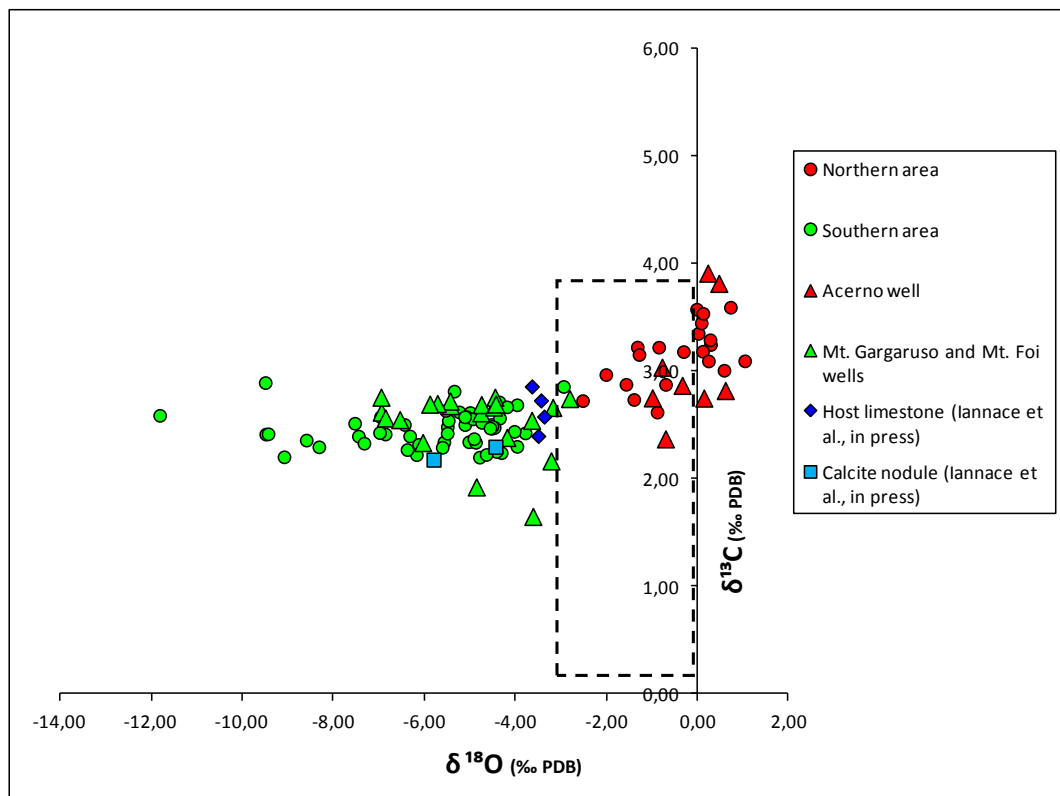


Figure 60: Covariation plot between  $\delta^{18}\text{O}$  and  $\delta^{13}\text{C}$  of the studied dolomites. Host limestone and calcite nodule values (from Iannace *et al.*, in press) are reported as well. The isotope composition of Upper Triassic seawater (Veizer *et al.*, 1999; Korte *et al.*, 2005) is reported in the dashed frame.

Only in few instances, the precursor limestones host calcite nodules, which represent a diagenetic phase predating an early phase of dolomite. In fact euhedral rhombs of dolomite grew along the nodules border. Calcite nodules seem also to predate the studied

dolomites, because they are absent in the fully dolomitized outcrops, where pseudomorphs of dolomite nodules were instead observed.

The blocky calcite which occurs in the nodules display  $\delta^{18}\text{O}$  values within the burial range (Choquette and James, 1990; Fig.60), and Sr isotope ratios in line with Triassic seawater stored as limestones pore water (Fig.61).

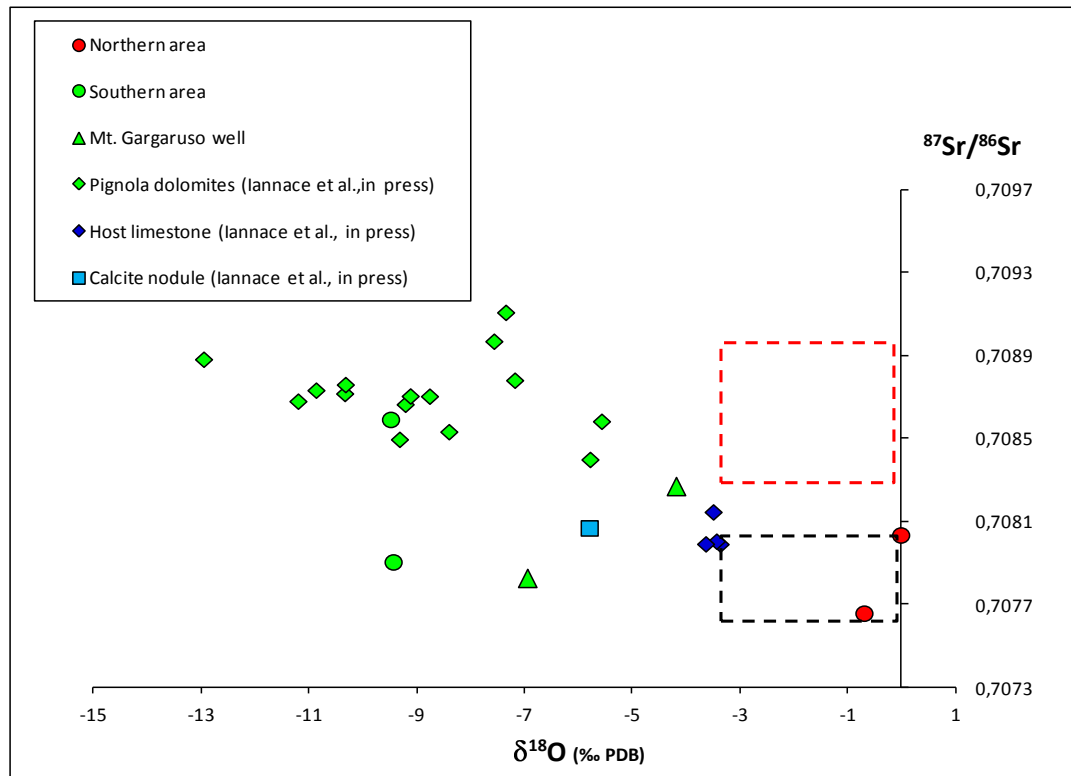


Figure 61: Covariation plot between  $\delta^{18}\text{O}$  and  $^{87}\text{Sr}/^{86}\text{Sr}$  ratios for the studied dolomites. Further data from Iannace *et al.* (in press) are reported as well. The isotope composition of Upper Triassic seawater (Veizer *et al.*, 1999; McArthur and Howarth, 2004) is reported in the black dashed frame, while Miocene seawater composition (McArthur and Howarth, 2004) is reported in the red dashed frame.

Fluid inclusions indicate that this calcite precipitated from warm (Th mode = 85 °C) and saline fluids (from normal seawater up to three times more saline than seawater). The large range of the obtained Th values and the spreading of these values toward high temperatures suggest that the sample underwent thermal re-equilibration and leakage. These phenomena were probably the result of a natural overheating of the sample due to later thermal events. Peak burial conditions recorded for the Lagonegro Units during the Southern Apennines deformation in Miocene time (Corrado *et al.*, 2005; Mazzoli *et al.*, 2008) indicate a maximum temperature range of 130-160 °C. The obtained temperature for the studied calcite nodule is quite low in respect with these peak burial temperatures. Therefore, this calcite is interpreted to be formed during first stages of burial, before the first compressional phase also responsible of the peak burial conditions and to be re-equilibrated during later stages of deeper burial, because of higher temperatures. Another cause of the calcite thermal re-equilibration could be the advent of later higher temperature fluids (Th mode = 95-115 °C), i.e. the fluids that have dolomitized the precursor *Calcarei con selce* limestones.



This latter interpretation is supported by the covariance observed in the Th-Tm<sub>i</sub> cross-plots (Fig.52B) and the salinity values of calcite FIs falling into two rough populations (Fig.52A). The first population of FIs (higher salinity and lower temperature) could represent the original fluids responsible for the blocky calcite precipitation, possibly basinal brines up to three times more saline than normal seawater (intraformational fluids). The second population of FIs (lower salinity like for the dolomite FIs and higher temperature) could be represented by inclusions overheated during deeper burial and partially refilled by the lower salinity fluids responsible for dolomitization (extraformational fluids of more superficial origin).

In general, combining microthermometry and stable isotopic data, it is possible to characterize the isotopic composition of the fluids. Based on this assumption, the mode value of Th for the calcite (85°C) was plotted together with  $\delta^{18}\text{O}$  value for the same cement (Fig.62). The  $\delta^{18}\text{O}$  of the fluid in equilibrium with the calcite in the nodule was calculated using the fractionation equation of Friedman and O'Neil (1977). After applying the pressure correction for peak burial conditions (see the arrow in Fig.62), the obtained  $\delta^{18}\text{O}_{\text{SMOW}}$  value become higher of about 2 per mil because shifting the dot upward of 18 °C. The result indicates that the fluid responsible for the calcite precipitation had  $\delta^{18}\text{O}$  values between 6 and 8 per mil SMOW, a composition which is consistent with saline formation waters.

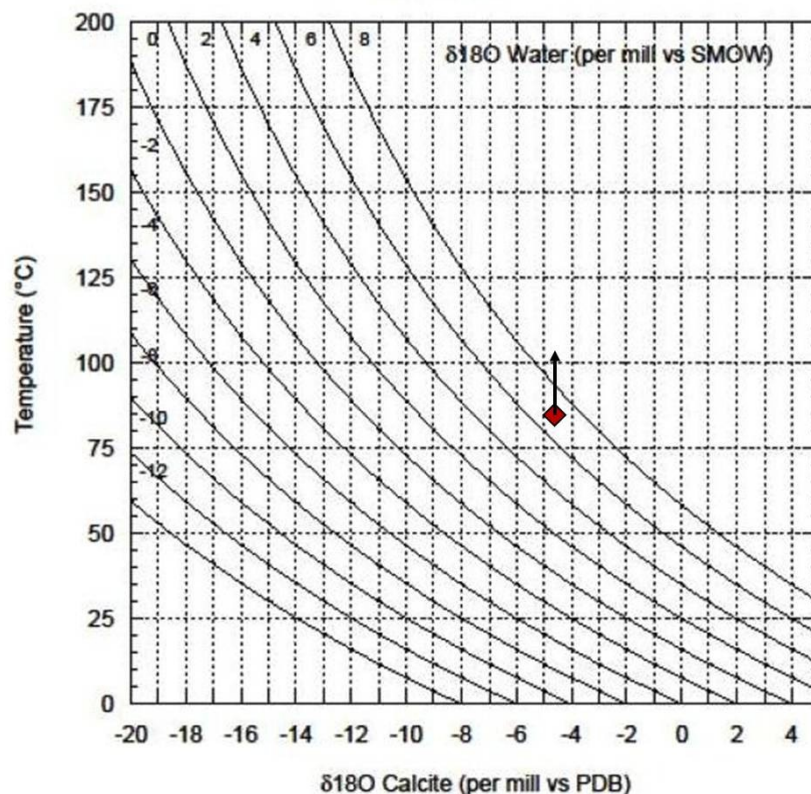


Figure 62: Plot of precipitation temperature versus  $\delta^{18}\text{O}$  value of the calcite nodule. The  $\delta^{18}\text{O}$  composition of the fluid in equilibrium with calcite as function of the temperature was calculated using the fractionation equation of Friedman and O'Neil (1977). The  $\delta^{18}\text{O}$  value of the calcite sample (Iannace *et al.*, in press) was plotted against the mode value of Th. Arrow above the dot indicates the maximum possible pressure correction.

While the origin of the calcite cement that fills the nodules is quite clear, the nature of the vugs remains unclear. Similar calcite-filled vugs were observed by Nader *et al.* (2004) in the Jurassic dolostones of the *Kesrouane* Formation (Lebanon) and were interpreted as pseudomorphs of nodular evaporite moulds. Many other cases of calcite pseudomorphs after evaporite are documented (e.g. Swennen *et al.*, 1981; Kendall, 2001; Bodzioch, 2003). Other similar calcite nodules were identified by Coniglio *et al.* (1994) in the Ordovician carbonates from the Michigan Basin (Ontario, Canada) and were described as vugs developed in leached corals or stromatoporoid heads.

None of these origins (evaporite or macrofossils moulds) can be envisaged for the calcite nodules of the *Calcari con selce*, as this latter formed in a deep-sea environment, which is incompatible with evaporites and/or corals presence. It could be a speculation that the studied calcite nodules are the result of a replacement of the chert nodules. Walker (1962) showed evidences that the replacement of carbonate minerals by chert, is a reversible process, and therefore, chert nodules can be replaced by later carbonate minerals. Such reversal process may occur in response to variations in pH where interstitial water is highly alkaline (above pH 9) or in response to variations in temperature where sediments have been deeply buried.

Many calcite-filled veins generations were recognized in the precursor limestone. At least one of these veins systems clearly postdates the burial stylolites and predates the dolomites formation, as these calcite veins were reopened and refilled with dolomite cement. The calcite veins predating dolomitization could be formed during the first phase of deformation (buckling and thrusting) of the Southern Apennines.

## 10.2 Comparison between Campagna-San Fele and Pignola-Val d'Agri dolomites

Field survey and examination of stratigraphic logs of wells penetrating the Lagonegro succession have confirmed that dolomites replacing Triassic cherty limestones (*Calcari con selce* Formation) of the Lagonegro succession are widespread. However, petrographic characteristics and geochemical data pointed out that the successions of northern area (Mount Marrone, Campagna and San Fele-Mount Pierno) and southern area (from Pignola to high Val d'Agri) underwent different dolomitization processes. The features of the two different dolomites are summarized in Table 7.

Dolomites of the northern area, including those from Acerno well cuttings, are mostly fine grained, displaying non-planar textures and unimodal crystals size. These dolomites have a replacive origin; this is indicated by the preservation of many sedimentary features of the precursor limestones. Unimodal size distribution generally results from a single nucleation event on homogeneously distributed nucleation sites with uniform growth rate (Sibley and Gregg, 1987). Non-planar dolomite crystals typically form above the critical roughening temperature (50–60 °C), although they may also develop below this temperature at high supersaturation conditions (Gregg and Sibley 1984; Sibley and Gregg, 1987).

Dolomitization under early diagenetic conditions and from low temperature fluids could be deduced for dolomites of the northern area from the results of oxygen stable isotopes

	CAMPAGNA-SAN FELE DOLOMITES (NORTHERN AREA)	PIGNOLA-HIGH VAL D'AGRI DOLOMITES (SOUTHERN AREA)
<b>Macroscopic features</b>	Fine crystalline and fabric retentive	Coarse crystalline Zebra and hydrofracturing structures
<b>Petrography</b>	Replacive, fine, non-planar, unimodal mosaic	Replacive, fine, non-planar, polymodal mosaic + void filling saddle crystals
<b>Cathodoluminescence</b>	From dull red to non luminescent	Dull red
<b><math>\delta^{18}\text{O}</math></b>	Slightly higher respect to Upper Triassic seawater values	Lower respect to Upper Triassic seawater values
<b><math>\delta^{13}\text{C}</math></b>	Consistent with Upper Triassic seawater	Consistent with Upper Triassic seawater
<b><math>^{87}\text{Sr}/^{86}\text{Sr}</math></b>	Consistent with Upper Triassic seawater	Enriched respect to Upper Triassic seawater
<b>Sr content</b>	Higher (mean= 98 ppm)	Lower (mean= 62 ppm)
<b>Mn content</b>	Lower (mean= 95 ppm)	Higher (mean= 229 ppm)
<b>Fe content</b>	Lower (mean= 602 ppm)	Higher (mean= 792 ppm)

Table 7: Synthesis of the main petrographic and geochemical features of dolomites from northern and southern Lagonegro areas.

analysis.  $\delta^{18}\text{O}$  values of these dolomites are slightly (+1 ‰) enriched in respect with Upper Triassic seawater values (Veizer *et al.*, 1999; Korte *et al.*, 2005). As  $\delta^{18}\text{O}$  of dolomites directly precipitating from seawater at room temperature generally presents an increase of about +3‰ PDB respect to coeval seawater values (Land, 1980, 1985; Vasconcelos *et al.*, 2005), the obtained oxygen signatures are quite well in line with Upper Triassic marine signatures.

$\delta^{13}\text{C}$  values mostly reflect the initial composition of the precursor carbonate, as carbon in pore fluids is contained as dissolved carbonate and it is buffered by host rock. The  $\delta^{13}\text{C}$  signature of dolomites from northern area is very uniform and varies between +2 and +4 ‰, values that are all consistent with Upper Triassic seawater values. Also Sr isotopes ratios of these dolomites are in line with Upper Triassic seawater (McArthur and Howarth, 2004).

Dolomites of northern area are dull red to non luminescent in CL, and moreover they are characterized by low Fe and Mn contents. Both features are typical of oxidizing fluids, which are often responsible for early, near surface, dolomitization, whereas burial dolomitization present a typical higher Fe and Mn content because of reducing nature of subsurface fluids (Land, 1980; Machel *et al.*, 1991).

Generally, early diagenetic dolomites have higher Sr content than later diagenetic coarsely crystalline dolomites (Land, 1980; Morrow, 1982; Tucker and Wright, 1990). Typical marine Sr content is about 500-600 ppm (Tucker and Wright, 1990). However, in relatively closed systems, where water-rock interaction is limited, the mineralogy of the precursor is an important factor controlling the trace elements signature (Brand and Veizer, 1980). While marine aragonite, with its very high Sr content (8000 to 10000

ppm), will produce after replacement dolomites with Sr content of 500-600 ppm, marine high- and low-Mg calcites ( $\text{Sr} \approx 1000\text{--}2000$  ppm) should form dolomites with lower Sr concentration (Warren, 2000). Dolomites with Sr values higher than 500-600 ppm are instead thought to be associated with hypersaline waters (Butler and Burns 1969, Behrens and Land 1972). The studied dolomites of northern area, present Sr concentration of 60-200 ppm, which is in agreement with an early replacement of a marine calcite precursor.

Dolomites outcropping in the southern area, from Pignola to high Val d'Agri, display very different macroscopic, petrographic and geochemical characteristics in comparison with dolomites of the northern area. Dolomites from cuttings from Monte Gargaruso and Monte Foi wells show very similar petrographic and geochemical features in respect with southern area dolomites from outcrops. All these dolomites consist of one major grey replacive type and a less abundant white void-filling type, which often form zebra-like structures. The replacive nature of the grey dolomite can be deduced by the halos of dolomite crystals scattered within the limestone mud at the limestone-dolomite boundaries. In addition, some sedimentary features of the precursor limestone were rarely preserved in the dolomites, clearly demonstrating that the dolomite replaced the limestone.

The sharp boundaries between limestones and dolomites, mostly crosscutting the stratification, suggest a late origin for the dolomites. These dolomites present typical features of burial dolomites such as abundant void-filling saddle dolomite crystals and non-planar texture of the replacive type (Radke and Mathis, 1980; Gregg and Sibley, 1984; Taylor and Sibley, 1986). This latter often display two main populations sizes. A polymodal distribution of the crystal size could be due to dolomite recrystallization, or alternatively it could reflect textural differences in the precursor limestone (Machel, 2004). In this case, the first hypothesis is favoured, as the precursor limestones are quite homogeneous mudstones and wackestones. Moreover, recrystallization is suggested as well by the large spreading of  $\delta^{18}\text{O}$  values (Nielsen *et al.*, 1994). These values are quite depleted relative to coeval seawater hypothetical values (i.e. Upper Triassic; Veizer *et al.*, 1999; Korte *et al.*, 2005), displaying an isotopic trend typical of burial dolomites (Morse and Mackenzie, 1990; Tucker and Wright, 1990). In most samples the void-filling dolomite type is slightly more depleted in  $^{18}\text{O}$  respect to the corresponding replacive dolomite type. This fact may reflect changing isotopic composition of the dolomitizing fluids over time, high water/rock ratio, and/or higher temperature for the void-filling dolomite. Anyway, these two dolomites were probably produced by the circulation of the same fluid, as they display the same uniform cathodoluminescence colour.  $\delta^{13}\text{C}$  values are less dispersed and reflect the values of the host limestone because they are buffered by the host rock carbon content. Sr isotopes data indicate a slightly more radiogenic nature of dolomites from the southern area compared to their precursor limestones and to dolomites from the northern area (Fig.61).

A late origin for the dolomites from southern area is suggested also by their trace elements content. Sr concentration is very low, both in the replacive and in the void filling types. A similar low Sr concentration (a few tens of ppm) was reported by many



authors for other late burial dolomites (Mattes and Mountjoy, 1980; Barnaby and Read, 1992; Montañez, 1994). Fe and Mn content is instead higher in respect with that of early dolomites from northern area. Since most subsurface fluids are reducing, late burial dolomites are generally characterized by high Fe and Mn content (Land, 1980; Barnaby and Read, 1992; Morrow, 1982).

Finally, a burial origin is supported by the calculated trapping temperatures for the void-filling dolomites, which are comprised between 115 and 135 °C. In fact, by a depth of few kilometres temperatures are in excess of 60-70°C.

### 10.3 A possible scenario for the early dolomitization event

Petrographic and geochemical data allow to interpret the Upper Triassic basinal dolomites of the Lagonegro succession, outcropping in Molise, Campagna and Mount Pierno-San Fele (northern area), as the result of an early replacement caused by cold, marine and oxidizing fluids, in a shallow burial. That means that it is necessary to look for a Norian setting leading to a surface-related dolomitization of the basinal limestones.

Here it is suggested that there is a linkage between the dolomitization of the Apenninic platform margin and that of the more proximal Lagonegro basinal facies. As discussed in paragraph 2.4, the paleogeography of the Lagonegro Basin was probably more complex than that envisaged by various authors (Scandone, 1967; Marsella, 1988; Miconnet, 1988; Pescatore *et al.*, 1999; Bertinelli, 2003; Passeri *et al.*, 2005), and it is still matter of discussion. Regardless of this complication, most models indicate that the closure of the basin was towards the north, and therefore proximal facies are located to the north.

In the Norian, the presence of an early massive dolomitization in the alpine and peri-mediterranean carbonate platforms is well known (Iannace and Frisia, 1994 and references therein). These dolomites are classically referred to as *Hauptdolomit*, *Main Dolomite* or *Dolomia Principale*. The Triassic was a favourable time for dolomitization with high Mg/Ca ratios in seawater and the development of very wide carbonate platform systems (Mackenzie and Morse, 1992; Sun, 1994). Iannace and Frisia (1994) attributed the Norian large-scale dolomitization event to specific palaeoceanographic, tectonic and climatic conditions in the Tethyan region, such as warm and arid climate, and restricted oceanographic circulation, which promoted hypersalinity and stratified conditions, respectively. Balog *et al.* (1999) also recognized a strong climate control on dolomitization in the Hungarian Late Triassic platform.

In these peritidal domains and under such an arid climate, penecontemporaneous dolomites were formed most likely through the density-driven circulation of hypersaline brines (Frisia, 1994; Iannace and Frisia, 1994; Haas and Demény, 2002). Mastandrea *et al.* (2006) suggested a microbial primary origin for the peritidal dolomite facies of the *Dolomia Principale* of Northern Calabria (Southern Italy). In a recent review, Mckenzie and Vasconcelos (2009) also proposed a microbial dolomitization model to explain the massive dolomite of the Norian *Dolomia Principale*, and observed that the environmental factors proposed by Iannace and Frisia (1994) are also conducive to the microbial growth.

For the dolomites of the northern Lagonegro area, a microbial mediation can be excluded, because dolomites associated with organic diagenetic processes have extremely depleted  $\delta^{13}\text{C}$  composition (Vasconcelos *et al.*, 2005). The isotope data are instead in good agreement with signatures from recent dolomites interpreted to be of marine or evaporitic origin (Warren, 2000 and references therein). In addition, the oxygen and carbon isotope signatures are comparable to those of other Norian dolomites (Frisia, 1994; Ogorelec *et al.*, 1999; Haas and Demény, 2002).

As previously mentioned, dolomitization occurring in the northern area is imagined to be related to the proximity of the facies to the platform margin. Fluids responsible for the widespread dolomitization of platform carbonates, remained as pore-waters in platform dolomites, could have been expelled from the platform toward the basin, because of the increasing sedimentary loading, thus triggering dolomitization of the more proximal basinal facies in a shallow burial (Fig.63). A similar model, providing the reflux of Mg-brines from the platform toward the proximal basin was already proposed by Passeri *et al.* (2005) for the Lagonegro dolomites. These authors invoked the presence of high Mg solutions derived from evaporites compaction. Anyway, no evidences of evaporites are documented in the study area and, in addition, evaporite related fluids should have generated much higher concentration of Sr in the dolomites (Warren, 2000). Therefore, the dolomitizing fluids are more probably marine or marine derived fluids. A reflux of slightly concentrated seawater through a carbonate platform, resulting in a subsurface dolomitization, was first suggested by Simms (1984). Since then, other authors explained many widespread ancient platform dolomites as the result of dolomitization by near-normal seawater or connate pore fluids: Whitaker *et al.*, (1994) proposed a seawater thermal convection combined with reflux of slightly evaporated seawater; Vahrenkamp and Swart (1994) suggested seawater circulation in the mixing-zone in response to partial platform exposure.

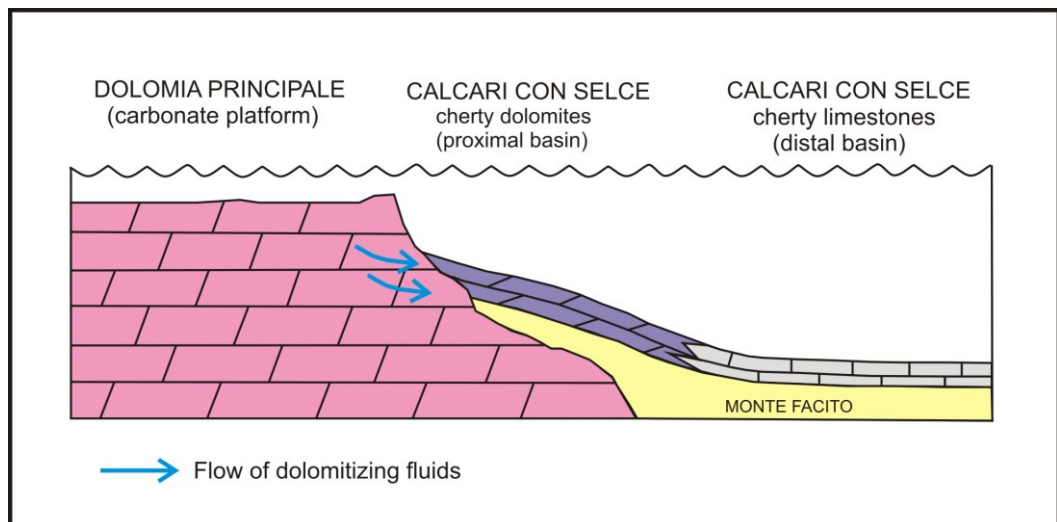


Figure 63: Proposed reflux model for the dolomites of the *Calcare con selce* Formation outcropping in the northern area.

Two other cases of massive dolomitization affecting Upper Triassic proximal successions of deep-water basins in the mediterranean area are known. One case is the

“Baca Dolomite” which represents bedded or massive dolomites with chert, deposited in the Slovenian Basin during the Norian and the Rhaetian (Buser 1986; Gale, 2010). The other case is given by the so called “dolomite breccias” of the *Fanusi* Formation, deposited in the Imerese basinal succession during the Late Triassic–Early Jurassic (Catalano and D’Argenio, 1982). These latter dolomites were interpreted to be formed in a slope setting by marine-derived pore fluids moved through Kohout convection (Deweever, 2008). This model predicts that a geothermal heating warmed up the seawater and created a flow half-cell into the slope where dolomitization took place. A higher thermal activity has been invoked to explain the geothermal heating of dolomitizing fluids of the *Fanusi* Formation. This anomalous thermal activity can be expected in the Central Mediterranean during the Triassic and Jurassic, due to the break-up of Pangea and the opening of numerous rift systems in the area.

If this geothermal eating was effective in the Mediterranean area during the Triassic, a similar Kohout convection model cannot be ruled out for the studied early dolomites of the Lagonegro Basin. Dolomitization could have been caused by a cold seawater influx into the sediments along the proximal basin. These waters were heated and put into motion by a thermal convection mechanism.

## 10.4 Late burial dolomitization event

### *10.4.1 Timing of dolomitization*

The field, petrographic and geochemical characteristics of the investigated dolomite bodies from the southern area (from Pignola to high Val d’Agri) allow to interpret them as burial, epigenetic and high temperature dolomites. These dolomites constitute an example of dolomitization occurring within a fold and thrust belt, in the external part of a collisional orogen. Other cases of high temperature zebra-dolomites formed in the external units of fold and thrust belts have been described in the last years by several authors (Qing and Mountjoy, 1994; Boni *et al.*, 2000; Swennen *et al.*, 2003; Vandeginste *et al.*, 2005; Gasparrini *et al.* 2006).

It is assumed that the Lagonegro dolomitizing fluids were in thermal equilibrium with the host rock, therefore the studied dolomites were considered as geothermal (*sensu* Machel and Lonnee, 2002). In fact, in the studied areas, no evidence for a hydrothermal origin can be found, such as relationships of the dolomite bodies with deep-seated normal faults. On the contrary, normal faults cut through the different dolomite types (replacement and void-filling), thus indicating that extensional tectonics postdate the dolomitization.

The studied dolomites postdate the development of a pressure-solution cleavage that, according to Mazzoli *et al.* (2001), developed during the first compression phase. In fact, this cleavage preserved the same geometric pattern developed in the limestones, in the dolomitized portions of the succession (Fig.15).

The timing of dolomitization may be constrained by referring to available thermometric data from the Southern Apennines (Aldega *et al.*, 2003, 2005; Corrado *et al.*, 2002, 2005; Mazzoli *et al.*, 2008). Reconstructed burial curve for the Lagonegro succession (Aldega *et al.*, 2003) indicates that during the Mesozoic the succession was buried at

lower depth than 2 km. A first phase of buckling and associated reverse faulting took place in the Miocene (Mazzoli *et al.*, 2001; Shiner *et al.* 2004) at an approximate depth, in the high Val d'Agri area, of 3.8 km and peak temperatures of 130-160 °C. A second phase of thrusting coincided with the beginning of exhumation and NNE-directed shortening and led to the tectonic doubling of the Lagonegro Units. This phase is dated 5.5 to 2.5 Ma (Mazzoli *et al.*, 2008).

According to the calculated maximum trapping temperatures (see paragraph 9.6 and Fig.58) of dolomites sampled along a SW-NE transect in the high Val d'Agri area, even by taking into account the maximum possible trapping conditions (overall  $T_{\max}$  of  $115 \pm 10$  °C), the dolomitizing fluid had temperatures lower than those of the peak burial (130-160 °C; Corrado *et al.*, 2005) suffered by the Lagonegro Units in the area crossed by the studied section. An entrapment of dolomitizing fluid before the thermal peak can be excluded, as no significant thermal re-equilibration was observed in the studied samples, excluding the cuttings samples, whose thermal re-equilibration was caused by overheating during drawing operations from the well, and the Monteforte sample which was sampled near a fault (thermally re-equilibrated by late hot fluids circulating through the fault plain). Moreover, as previously mentioned, the dolomites are clearly post-cleavage, and therefore post-thermal peak.

The calculated trapping temperatures for the studied dolomites better fit to the second phase of deformation, which is associated with exhumation and cooling of the Lagonegro Units during the Plio-Pleistocene. Apatite fission track data (Corrado *et al.*, 2005; Mazzoli *et al.*, 2008) indicates that the studied succession, between 5 and 4 Ma, crossed the isotherm of 100-110°C, under 3-4 km of burial.

Thrust faults probably constituted the conduit for extraformational fluids migration. The expulsion of large volumes of fluids during compressional deformation is often referred to as “squeegee” fluid flow (Oliver, 1986). Some authors stated that fluxes of the tectonically-induced flow appear to be low (Machel and Cavell, 1999; Machel *et al.*, 2000), and unlikely can explain the origin of extensive open space dolomite cement because of their limited supply of solute (Morrow, 1998). Nevertheless, the tectonically-driven flow model has often been invoked to explain the occurrence of high temperature dolomites in different fold and thrust belts and in their foreland (Qing and Mountjoy 1992, 1994; Montañez, 1994; Drivet and Mountjoy 1997; Swennen *et al.*, 2003b; Vandeginste *et al.*, 2005; Ronchi *et al.*, 2010, 2012).

Within the Pignola-Val d'Agri area, dolomites located north-west (Vietri di Potenza and Tito-Satriano) respect to those of the transect (high Val d'Agri) present slightly (about 20 °C) higher Th values (Th mode = 115 °C). No thermometric data for the former sampling localities (i.e. Vietri di Potenza and Tito-Satriano) are present in literature, therefore the maximum burial suffered by the successions in the north-west area is not available. The “pressure correction” for these samples was performed assuming that the north-west area reached the same maximum burial of 3.8 km of the transect area (south), but it is possible that the north-west area reached higher depths, that justify the temperature difference from Vietri di Potenza to the high Val d'Agri. Two different hypotheses could be envisaged to explain the higher burial in the north-west area:



- (i) The timing of dolomitization was different in north and south areas, and the two areas were buried at different depths during dolomitization (Fig.64A). After maximum burial, the exhumation rate was the same in the two areas. Dolomitization occurred first in the north area (at a slightly deeper burial) and later in the southern area (at higher exhumation).
- (ii) The timing of dolomitization was the same in northern and southern areas (Fig.64B), but the burial during dolomitization was higher in the northern area, because of a major tectonic loading. It is known that the areas of Vietri di Potenza and Tito-Satriano are closer to the thrust that put the Apenninic Platform Units onto the Lagonegro Units.

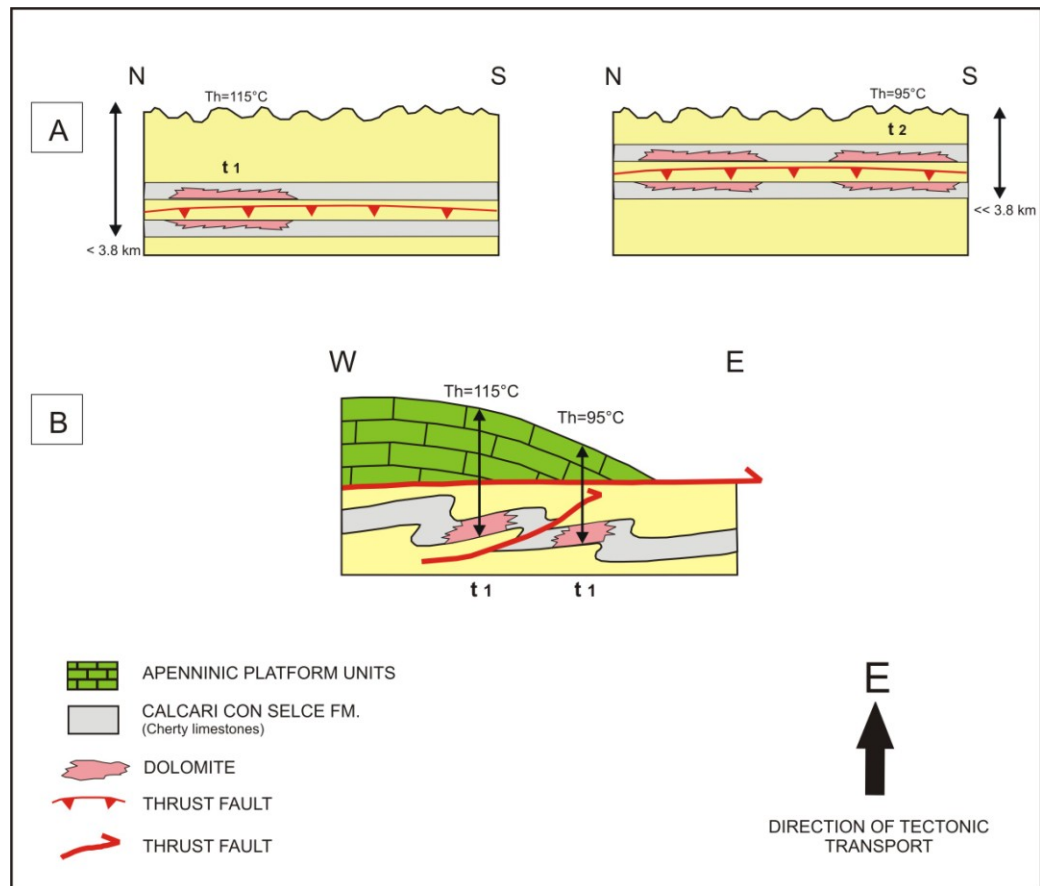


Figure 64: Schematic models illustrating two different explanations for the higher temperatures recorded in dolomites from the north-west area in respect with those of southern area. A) After maximum burial (3.8 km), exhumation was the same in the two areas. Dolomitization occurred first (t1) in the N, when the Lagonegro succession was at deeper depth. Exhumation continued and then dolomitization (t2) affected the succession of southern area, which was at minor depth. B) Dolomitization was contemporaneous (t1) in the N and in the S. During dolomitization the N-NW area was found at higher depth, which was due to the presence of a major tectonic loading.

The first hypothesis is the less probable, as it is known that the thrusts motion was contemporaneous in the whole Lagonegro area, and therefore, dolomitization by tectonically-expelled fluids probably occurred at the same time in northern and southern areas.

In the limestones close to dolomitization fronts, many dolomite veins were observed, and they are crosscut at least by one calcite veins system. The origin of this latter could be related to the extensional tectonic regime that was established in the Apennine chain during early-middle Pleistocene. Anyway, to better constrain the origin of the calcite veins postdating the dolomitization, detailed petrographic and geochemical studies on these veins are necessary.

#### 10.4.2 Origin of zebra structures

Zebra textures in dolomite bodies were recognized by many authors as rhythmic alternations (mm- or cm-scale) of dark fine-grained replacement dolomite and white void-filling coarse dolomite, which both makes up “abba” sequences, thick up to some tens of cm. These structures occur in various environments and they are often associated with ore deposits. There is no agreement about zebra fabric origin and interpretations vary from syngedimentary (Fontboté and Amstutz, 1983) to early diagenetic (Beales and Hardy, 1980; Martín *et al.* 1987), and to epigenetic (Bogacz *et al.*, 1973; Arne and Kissin 1989; Tompkins *et al.*, 1994; Boni *et al.* 2000). Fundamental requirement for zebra formation is the occurrence of voids in the dolomitic host rock, within which the white dolomite cement precipitates. Voids can be due to pre-existing fractures or can be formed or enlarged by dissolution phenomena. Fluids pressure must be equal or higher than the lithostatic pressure, so that the cavities are not be closed by the sedimentary loading.

Different theories on the rhythmicity of the bands exist. Some authors proposed a sedimentary facies control (e.g. fine layering, microbial or evaporite laminae) on the zebra fabric development (Beales and Hardie, 1980; Martín *et al.* 1987; Tompkins *et al.*, 1994). Others authors excluded an inherited rhythmicity and recognized the control by external factors, e.g. tectonic structures, such as cleavage, microcracks and fissures (Wallace *et al.*, 1994; Nielsen *et al.*, 1998; Boni *et al.*, 2000; Vandeginste *et al.*, 2005; Gasparrini *et al.*, 2006). A third theory envisages self-organization processes (Fontboté, 1993; Merino *et al.*, 2006).

The zebra structures observed in the studied dolomites of the *Calcari con selce* Formation developed mostly parallel to the bedding. Pre-existing bedding parallel stylolites and bedding planes clearly acted as preferential pathways for dolomitizing fluids. Nevertheless, the precursor limestone lacks former depositional rhythmicity at the zebra scale, and additionally, zebra structures obliquely oriented in respect with the stratification were observed as well in few cases, thus excluding a complete control by the sedimentary facies. As already proposed by other authors (Wallace *et al.*, 1994; Gasparrini *et al.*, 2006; Lopez-Horgue *et al.*, 2010), it could be argued that the observed zebra structures formed along pre-existing fissure planes, which represent a “weakened” part of the rock through which fluids could more easily circulate.

Extension and related fracturing of limestone beds in an overpressured regime probably generated the zebra structures. Particularly, the brecciated fabrics suggest that they formed by hydraulic fracturing under the action of overpressured fluids. The fluids ingress must have broken the precursor rock into pieces, where dolomite replacement

caused the grey dolomite and cementation the white dolomite. Thus, even though some evidences of dissolution are present, it is believed that most of the space for the precipitation of the white void-filling phase was created by extension.

The origin of the white, void-filling dolomite bands in an overpressured rock has been suggested by many authors (Boni *et al.*, 2000; Vandeginste *et al.*, 2005; Gasparrini *et al.*, 2006; Diehl *et al.*, 2010).

The position of the *Calcari con selce* Formation, calcareous and intensely fractured, sandwiched between the fine-clastic *Monte Facito* Formation (below) and the siliceous and fine-clastic Jurassic to Lower Cretaceous formations (*Scisti Silicei* and *Flysch Galestrino*, above), is particularly favourable for focussing fluid flow and engendering overpressure during tectonic shortening. Noteworthy is that overpressures have been actually encountered during well operation in the *mélange* zone which separates the Lagonegro Units and the tectonically underlying Apulian Platform reservoir carbonates (Mazzoli *et al.*, 2001; Shiner *et al.*, 2004).

#### 10.4.3 Origin of fluids

The dolomitizing fluids of late, burial dolomites of the Lagonegro succession, present salinities in the range of slightly modified to normal marine seawater (range of 1.9-6.4 eq. wt % NaCl with a mean of 3.7) and are slightly more radiogenic than Upper Triassic seawater. These salinities are quite low in respect with those of others similar high temperature dolomites formed by means of fluid flow triggered by tectonic loading (Qing and Mountjoy, 1994; Montañez, 1994; Hitzman *et al.*, 1998).

Most late, void-filling, saddle dolomites from many different localities of the Earth, are reported to be precipitated from brines with salinities two to nine times that of modern seawater (Davies and Smith, 2006 and references therein). Brines in sedimentary basins are genetically related to evaporites in three ways: 1) dissolution of evaporite minerals (generally halite), 2) interstitial fluids in evaporites which are expelled from their source rock during compaction, 3) incongruent alteration of hydrous evaporite minerals (carnalite; Carpenter, 1978). Other mechanisms generating saline groundwater are infiltration of subaerially evaporated seawater or non-marine fluids, and water-rock interactions in sediments (Hardie, 1990).

The salinity for the Lagonegro dolomites could be the result of slightly modified seawater or of saline formation waters diluted with fresh water.

A similar case of syntectonic dolomitization by low salinity fluids it is known in the Southern Alps, and it was explained by Ronchi *et al.* (2010) by a mixing of meteoric waters with deep basinal brines. These authors assumed that meteoric recharge would be in agreement with the high relief of the Alpine belt during collision, that probably caused increasing rainfall and provided the hydraulic head which allowed a deeply penetration of surface waters.

In the Lagonegro Units, the possibility of a massive input of meteoric waters from the already emergent chain may be excluded, because of its inconsistency with geochemical data. The oxygen isotope composition of the fluids responsible for dolomitization in the Lagonegro succession was determined by combining the results of geochemistry and

microthermometry (Fig.65). The  $\delta^{18}\text{O}$  values of single dolomite cements were plotted against the mode values of Th for the same cement. It results that the fluids responsible for the void-filling dolomite (Dol2) precipitation had  $\delta^{18}\text{O}$  values between 2 and 7 per mil SMOW. These values may be increased of about 2 per mil by shifting the dots upward of 18-20 °C if considering the maximum possible temperatures obtained after pressure correction for peak burial conditions (see arrows in Fig.65). This oxygen isotope composition inferred for the dolomitizing fluids is comprised between values characteristic of seawater and those of saline formation waters, while meteoric waters typically display negative oxygen isotope values.

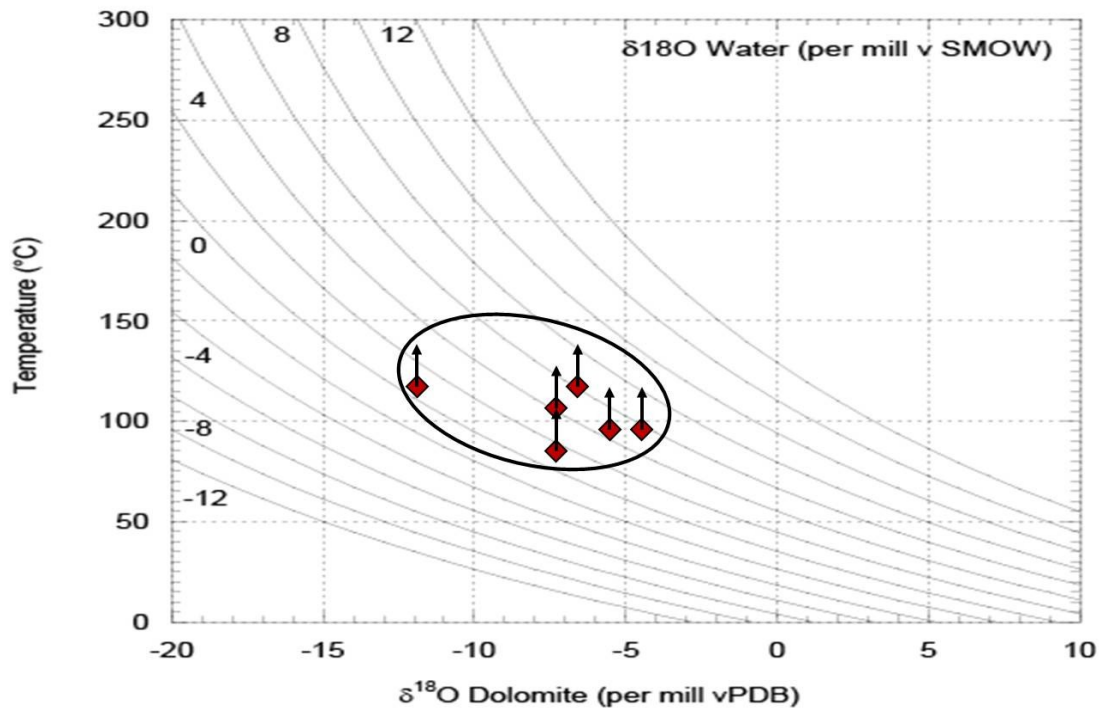


Figure 65: Plot of precipitation temperature versus  $\delta^{18}\text{O}$  values of the void-filling dolomite (Dol2). The  $\delta^{18}\text{O}$  composition of the fluid in equilibrium with dolomite as function of the temperature was calculated using the fractionation equation of Land (1983). The  $\delta^{18}\text{O}$  values of single dolomite sample were plotted against the mode values of Th for the same sample. Arrows above the dots indicate the maximum possible pressure correction for each sample.

Two possible sources for the dolomitizing fluids of the *Calcari con selce* Formation can be envisaged:

- 1) Fluids could relate to pore-waters squeezed out from the surrounding Triassic and Cretaceous fine-clastic formations (*Monte Facito* and *Flysch Galestrino*, respectively). In this case, however, because of the prolonged water-rock interaction in the subsurface, more radiogenic and more saline fluids would be expected compared to the low salinity and only slightly radiogenic fluids inferred from the present study data. Nevertheless, there is also the possibility that these low salinity fluids could derived from dilution of saline pore waters with fresh waters delivered during the smectite-illite transformation at depth (Kastner *et al.*, 1991; Fitts and Brown, 1999). This latter process is common in accretionary

wedges and generally occur at a depth range of 3.5-7 km and at elevated temperature of about 120-165°C (Dählmann and de Lange, 2003). Both conditions (i.e. maximum burial of about 4 km and temperature peak of 130-160°C) occurred during the Lagonegro Units deformation (Corrado *et al.*, 2005). Water released during smectite to illite conversion is typically characterized by positive  $\delta^{18}\text{O}$  signatures (Boles and Franks, 1979; Vrolijk *et al.*, 1988; Taylor, 1990; Dählmann and de Lange, 2003). Thus, the positive signature inferred for the dolomitizing fluids is in agreement with this clay transformation.

A similar case of hot ( $T_h = 130\text{-}180^\circ\text{C}$ ) and low saline ( $T_{m_i} < -2.5^\circ\text{C}$ ) fluids displaying high  $\delta^{18}\text{O}_{\text{SMOW}}$  signatures (6 to 14 ‰) was found in Cretaceous shallow-water limestones from the Panormide platform exposed in north-central Sicily. These fluids were interpreted to migrate during fold and thrust belt development in Middle Miocene, and their low salinity and relatively high  $\delta^{18}\text{O}_{\text{SMOW}}$  signatures were interpreted to be the result of clay dewatering reactions (Dewever *et al.*, 2010).

- 2) Another possible fluid source for the Lagonegro dolomites could be represented by marine formation waters expelled from the Miocene formations involved in the tectonic *mélange*. This latter is a horizon, up to several hundred meters thick, which separates the Lagonegro Units and the tectonically underlying Apulian Platform reservoir carbonates (Mazzoli *et al.*, 2001; Shiner *et al.*, 2004). It consists mainly of intensely deformed and overpressured deepwater mudstones and siltstones of Miocene to Lower Pliocene age, including blocks of material derived from the overlying allochthon (Mazzoli *et al.*, 2001; Butler *et al.*, 2004; Shiner *et al.*, 2004). It is significant that Sr isotope values reported for the studied dolomites are close to those of Miocene seawater (see Fig.61; McArthur and Howarth, 2004).

The low salinity of the dolomitizing fluids of the Lagonegro Units is an uncommon feature for burial dolomites. Anyway, it is noteworthy that the occurrence of low salinity fluids in the Lagonegro Units is consistent with the present-day occurrence of very low saline fluids (generally less saline than seawater) in the formation waters encountered at high depths in the wells of the Val d'Agri oil field (Paola Ronchi, personal communication).

As already proposed by Dewever (2008), the composition of the fluids expelled during “squeegee” fluid flow seems to be dependent on the main *décollement*. In the Albanides, there is evidence for expulsion of highly saline fluids (Vilasi *et al.*, 2009) and the main *décollement* consists of Triassic evaporites (Fig.66A). Likewise, in the central Apennines, data of Ronchi *et al.* (2010) point to the action of saline formation waters, which likely sourced from the evaporites of the *Burano Anhydrites* Formation (Fig.66B). On the contrary, the Southern Apennines and others fold and thrust belts of the Mediterranean area (Southern Alps and Sicily), whose *décollement* horizons are not evaporites but siliciclastics deposits (Fig.67), are characterized by low salinity fluids (Ronchi *et al.* 2010; Dewever *et al.*, 2010). In these cases the fluids could derive from



clays dewatering, even though a meteoric input can also contribute to reduce fluids salinity.

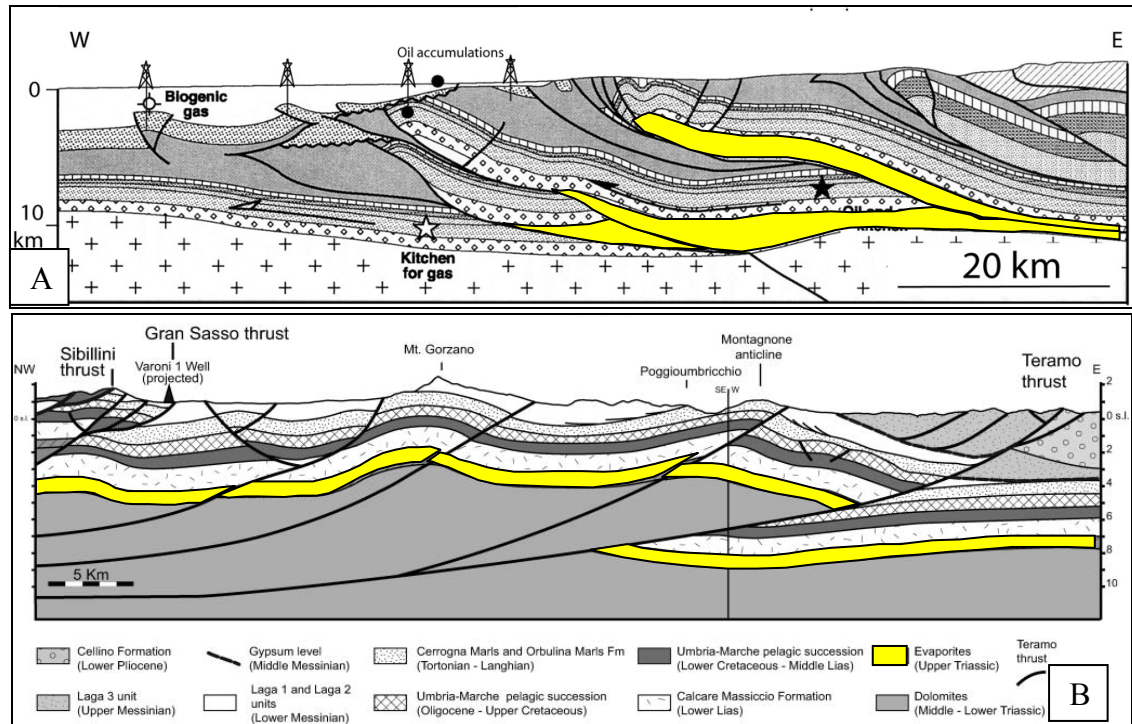


Figure 66: Simplified geological cross-sections through different fold and thrust belts of the Mediterranean area whose *décollements* consist of evaporitic deposits (evidenced in yellow). A) Albanides (modified after Roure *et al.*, 2004). B) Central Apennines (modified after Bigi *et al.*, 2011).

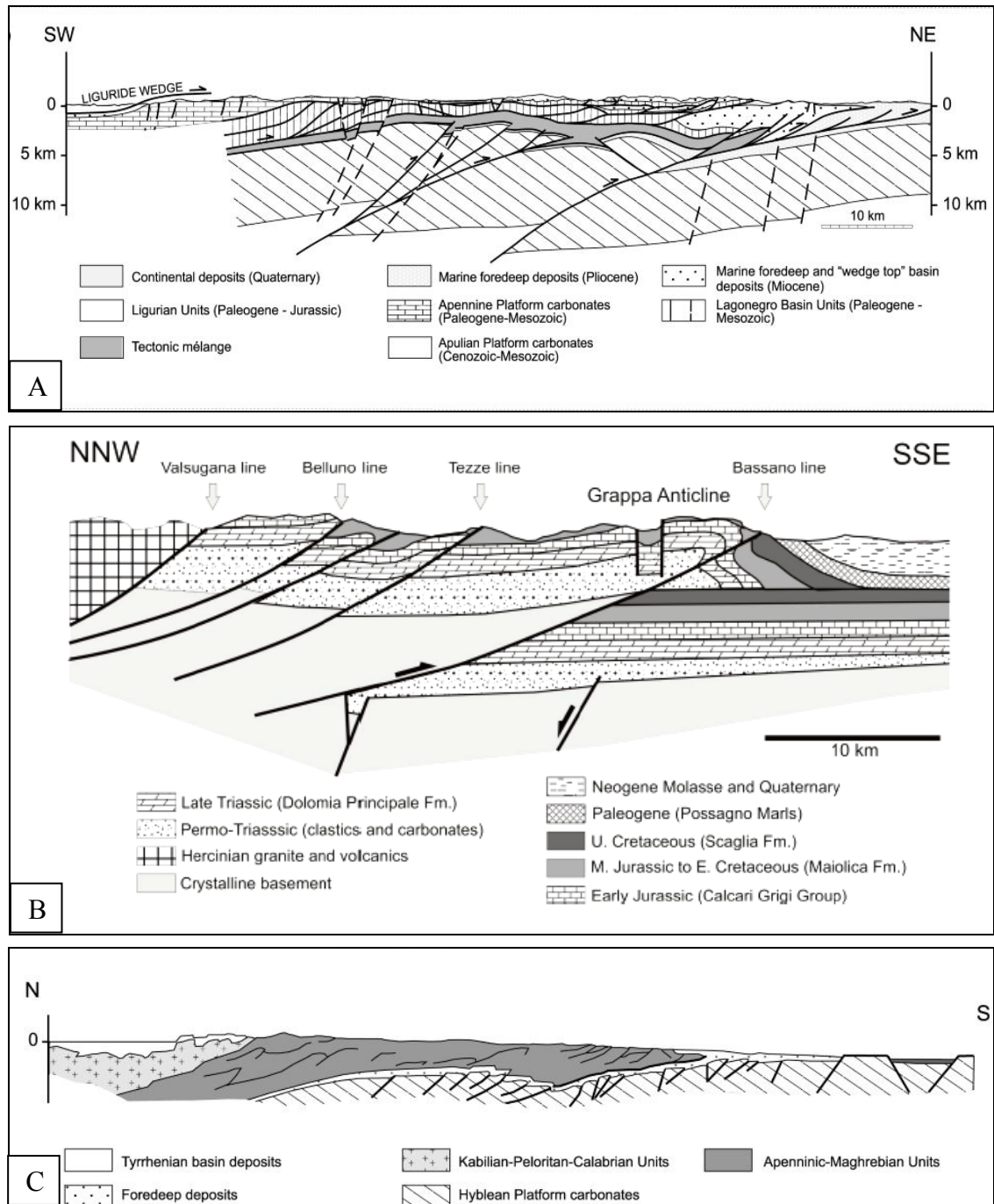


Figure 67: Simplified geological cross-sections through different fold and thrust belts of the Mediterranean area whose *décollements* consist of siliciclastics deposits. A) Southern Apennines (from Mazzoli *et al.*, 2006). B) Southern Alps (from Ronchi *et al.*, 2012). C) Sicily (from Lentini *et al.*, 2000)

## Conclusions and perspectives

This thesis illustrates the results of a regional study on dolomitization phenomena affecting the Triassic pelagic carbonates of the Lagonegro Units from the Southern Apennines fold and thrust belt. The aim of this study was to define extent, timing and fluids origin of the Lagonegro dolomite bodies, and in particular to define the relationships of the fluid flow and the structural history of the tectonic belt. The work methodology included field survey and petrographic, geochemical and fluid inclusions analyses, performed both on surface and on subsurface (cuttings from oil wells) samples. The main results can be summarized as follows:

- The Lagonegro Basin, during its evolution, was affected by two massive dolomitization events, which generated two dolomite types displaying different petrographic and geochemical features. A fine crystalline and fabric preservative dolomite crops out in the northern area (Molise, Campagna and San Fele-Mount Pierno), whereas a coarse crystalline and fabric destructive dolomite, showing zebra-like and hydrofracturing structures is present in the southern area (from Pignola to high Val d'Agri).
- Dolomite documented in the northern area is an early dolomite, possibly related to a large reflux of marine or marine-derived fluids from platform margins towards the proximal basin, and therefore, controlled by the Norian arid climate. A Kohout convection of cold seawater heated thanks to a geothermal anomaly, could also be invoked to explain this dolomite.
- The southern area was affected, during Neogene time, by a late burial dolomitization, which was the result of a large scale “squeegee” fluid flow during Southern Apennines fold and thrust belt formation. The geochemistry of saddle dolomite samples indicates an origin by warm fluids (105-125 °C). Integration with available thermal data into the regional deformation history, by assuming a fluid in thermal equilibrium with the host rocks, suggests that the fluid flow took place after maximum burial, in early stages of exhumation, between 5 and 4 Ma and under 3-4 km of burial.
- The dolomitizing fluids of the late burial dolomite of southern area had salinities in the range of slightly modified to normal marine seawater (1.9-6.4 eq. wt % NaCl with a mean of 3.7). It is suggested that dolomitization was accomplished by squeezing out of formation waters, diluted with fresh waters delivered during the smectite-illite transformation at depth, from the surrounding clastic formations, or from Miocene marine pore-waters from the deeper *mélange* units.
- The comparison between different fold and thrust belts of the Mediterranean area (Southern Alps, Central Apennines, Southern Apennines, Sicily and Albanides) pointed out that the composition of the fluids expelled during fold and thrust belts deformation probably depends on the main *décollement*. Highly saline fluids derive

from evaporitic *décollement* horizons, while low saline fluids came from siliciclastic deposits. This latter is the case of the Southern Apennines.

The origin of the dolomitizing fluids in the Lagonegro Units remains speculative. To better constrain their origin, different integrative studies could be carried out:

- 1) Temperatures, pressures and compositions (TPX) of dolomitizing fluids, obtained in this study, could be compared to TPX of fluids related to the first compressional phase of Southern Apennines deformation history. Veins and other diagenetic products, which could be coeval with this tectonic phase, could be studied to better picture the fluids evolution scenario (i.e. the hypothesized evolution from basinal brines towards less saline fluids).
- 2) Crush-leach analysis could be performed on samples carrying one generation of FIs, both in dolomites and in mineral phases related to the first phase of compression. The abundance of cations in the inclusions can help in discriminating between basinal, marine or meteoric fluids.
- 3) As the second compression and corresponding fluid pulse causing dolomitization must have caused some others diagenetic products (for example mineral veins) in the close siliciclastics formations, the origin of these products could be studied and easier correlated with the deformation episode of interest. Indeed the siliciclastics could have better recorded the deformation of the second compressional phase of the Southern Apennines deformation history.
- 4) A mass balance calculation on siliciclastics material above and below the *Calcaree Selce* Formation could be accomplished in order to calculate the amount of fluids which can be expelled from them, also by taking into consideration the water which can be liberated at depth from the smectite-illite transformation.

The fluid flow event that triggered the dolomitization of the Lagonegro pelagic carbonates was a major phenomenon affecting the Southern Apennines fold and thrust belt, and it could be expected that the dolomite bodies which are reported in the Apulian subsurface (Murgia *et al.*, 2004) might have the same origin of Lagonegro dolomites from the southern area. The Apulian Platform carbonates constituted the foreland of the Apenninic chain; they are now buried below the nappe stack and host the major oil fields of continental Europe.

The diagenetic data from the present study could provide input data for a future structural and fluid flow modeling in the Southern Apennines fold and thrust belt, thus giving some clues for exploration in this complex petroleum system.

# References

- Adams J.E. and Rhodes M.L. (1960) Dolomitization by seepage reflux. *AAPG Bulletin*, **44**, 1912-1920.
- Aldega L., Cello G., Corrado S., Cuadros J., Di Leo P., Giampaolo C., Invernizzi C., Martino C., Mazzoli S., Schiattarella M., Zattin M., Zuffa G. (2003) Tectono-sedimentary evolution of the Southern Apennines (Italy): thermal constraints and modelling. *Atti Ticinensi di Scienze della Terra - ser. spec.*, **9**, 135-140.
- Aldega L., Corrado S., Di Leo P., Giampaolo C., Invernizzi C., Martino C., Mazzoli S., Schiattarella M. and Zattin M. (2005) The Southern Apennines case history: thermal constraints and reconstruction of tectonic and sedimentary burials. *Atti Ticinensi di Scienze della Terra*, **10**, 45-53.
- Alderman A.R. and Skinner H.C. (1957) Dolomite sedimentation in the southeast of South Australia. *American Journal of Science*, **255**, 561-567.
- Amthor J.E., Mountjoy E.W. and Machel H.G. (1993) Subsurface dolomites in Upper Devonian Leduc Formation buildups, central part of Rimbey-Meadowbrook reef trend, Alberta, Canada. *Bulletin of Canadian Petroleum Geology*, **41**, 164-185.
- Anderson R. K. and Arthur M. A. (1983) Stable isotopes of oxygen and carbon and their application to sedimentologic and paleoenvironmental problems. In: Arthur, M. A., Anderson, T.F., Kaplan, I.R., Veizer, J., Land, S. (Eds.), *Stable isotopes in sedimentary geology*. SEPM short course, **10**, 1-151.
- Arne D.C. and Kissin S.A. (1989) The significance of "diagenetic crystallization rhythmites" at the Nanisivik Pb-Zn-Ag deposit, Baffin Island, Canada. *Mineralium Deposita*, **24**, 230-232.
- Bakker R.J. (2003) Package FLUIDS 1. Computer programs for analysis of fluid inclusion data and for modelling bulk fluid properties. *Chemical Geology*, **194**, 3-23.
- Bakker R.J. (2009) Package FLUIDS. Part 3: correlations between equation of state, thermodynamics and fluid inclusions. *Geofluids*, **9**, 3-23.
- Bakker R.J. and Diamond L.W. (2006) Estimation of volume fractions of liquid and vapor phases in fluid inclusions, and definition of inclusion shapes. *American Mineralogist*, **91**, 635-657.
- Balog A., Read L.F. and Haas J. (1999) Climate-controlled early dolomite, late Triassic cyclic platform carbonates, Hungary. *Journal of Sedimentary Research*, **69**, 267-282.
- Banner J.L. (1995) Application of the trace elements and isotope geochemistry of strontium to studies of carbonate diagenesis. *Sedimentology*, **42**, 805-824.
- Barnaby R.J. and Read J.F. (1992) Dolomitization of a carbonate platform during late burial: Lower to Middle Cambrian Shady Dolomite, Virginia Appalachians. *Journal of Sedimentary Petrology*, **62**, 1023-1043.
- Beales F.W. and Hardy J.L. (1980) Criteria for the recognition of diverse dolomite types with an emphasis on studies on host rocks for Mississippi Valley-Type ore deposits. *Soc. Econ. Petrol. Min. Spec. Publ.*, **28**, 197-213.
- Behrens E.W. and Land, L.S. (1972) Subtidal Holocene dolomite, Baffin Bay, Texas. *Journal of Sedimentary Petrology*, **42**, 155-166.
- Bertello F., Fantoni R., Franciosi R., Gatti V., Ghielmi M. and Pugliese A. (2010) From thrust-and-fold belt to foreland: hydrocarbon occurrences in Italy. In: Vining B.A., Pickering S.C.



- (Eds.) *Petroleum geology: from Mature Basin to New Frontiers*. Proceedings of the 7<sup>th</sup> petroleum geology conference, 113–112.
- Bertinelli A. (2003) Il Bacino Lagonegrese-Molisano nel contesto della Tetide occidentale durante il Triassico Superiore-Giurassico. Tesi di Dottorato in Scienze della Terra, Università degli Studi di Perugia, 219 pp.
- Bertinelli A., Ciarapica G. and Passeri L. (2002) The Late Triassic cherty dolostones of Mt. Marrone (Mainarde range) as a part of the Molise Basin. *Bollettino della Società Geologica Italiana*, Spec. Vol., **1** (2), 481–487.
- Bigi S., Casero P. and Ciotoli G. S. (2011) Seismic interpretation of the Laga basin; constraints on the structural setting and kinematics of the Central Apennines, *Journal of the Geological Society*, London, **168**, 179–190.
- Bodnar R.J. (1993) Revised equation and table for determining the freezing point depression of H<sub>2</sub>O-NaCl solutions. *Geochimica et Cosmochimica Acta*, **57**, 683–684.
- Bodnar R.J. and Vityk M.O. (1994) Interpretation of microthermometric data for H<sub>2</sub>O-NaCl fluid inclusions. In: De Vivo B. and Frezzotti M.L. (Eds.), *Fluid inclusions in minerals: methods and applications*, Virginia Tech, Potignano-Siena, 117–130.
- Bodzioch A. (2003) Calcite pseudomorphs after anhydrite from the Muschelkalk (Middle Triassic) of the Holy Cross Mountains (Poland). *Geologos*, **6**, 169–180.
- Bogacz K., Dzulynski S., Hasrancyk C. and Sobczynsky P. (1973) Sphalerite ores reflecting the pattern of primary stratification in the Triassic of the Cracow–Silesian region. *Annales Société Géologique de Pologne*, **43**, 285–300.
- Boles J. R. and Franks S. G. (1979) Clay Diagenesis in Wilcox sandstones of Southwest Texas - Implications of smectite diagenesis on sandstone cementation. *Journal of Sedimentary Petrology*, **49**(1), 55–70.
- Bonardi G., D'Argenio B. and Perrone V. (1988) Carta Geologica dell'Appennino meridionale. *Memorie della Società Geologica Italiana*, **41**, attached map.
- Boni M., Parente G., Bechstädt T., De Vivo B. and Iannace A. (2000) Hydrothermal dolomites in SW Sardinia (Italy): evidence for a widespread late-Variscan fluid flow event. *Sedimentary Geology*, **131**, 181–200.
- Bradbury H. J. and Woodwell G. R. (1987) Ancient fluid flow within foreland terrains. In: Goff, J. C. and Williams, B. P. J. (Eds.), *Fluid flow in sedimentary basins and aquifers*. Geologic society of London Special Publication, **34**, 87–102.
- Brand U. and Veizer J. (1980) Chemical diagenesis of a multi-component carbonate system. I. Trace elements. *Journal of Sedimentary Petrology*, **50**, 1219–1236.
- Buser S. (1986) Explanatory book, Sheet Tolmin and Videm (Udine) L33-64, L33-63. Basic geological map of SFRJ 1:100.000. *Zvezni Geol. Zavod*, Beograd, 1–103.
- Butler G.P. and Burns S.J. (1969) Modern evaporite deposition and geochemistry of co-existing brines, the Sabkha, Trucial Coast, Arabian Gulf. *Journal of Sedimentary Petrology*, **39**(1), 70–89.
- Butler R.W.H., Mazzoli S., Corrado S. *et al.* (2004) Applying thickskinned tectonic models to the Apennine thrust belt of Italy; limitations and implications. In: McClay K.R. *et al.* (Eds.) *Thrust Tectonics and Hydrocarbon Systems*. AAPG Memoirs, **82**, 647–667.
- Carballo J.D., Land L.S. and Miser D.E. (1987) Holocene dolomitization of supratidal sediments by active tidal pumping, Sugarloaf Key, Florida. *Journal of Sedimentary Petrology*, **57**, 153–165.

- Carbone S., Catalano S., Lazzari S., Lentini F., Monaco C. (1991) Presentazione della carta geologica del Bacino del Fiume Agri (Basilicata). *Memorie della Società Geologica Italiana*, **47**, 129-143.
- Carpenter A.B. (1978) Origin and chemical evolution of brines in sedimentary basins. In: Johnson K.S. and Russell J.R., *13<sup>th</sup> Industrial Minerals Forum* (Eds.), Okla, Geol. Surv. Circ., **79**, 60-70.
- Casero P., Roure F., Muller C., Moretti I., Sage L. and Vially R. (1988) Evoluzione geodinamica neogenica dell'Appennino meridionale. In: *L'Appennino Campano-Lucano nel quadro geologico dell'Italia meridionale*. 748° Congresso della Società Geologica Italiana, Sorrento, 59-66.
- Catalano R. and D'Argenio B. (1982) Guida alla geologia della Sicilia Occidentale. Società geologica italiana, guide geologia regionale, 189 p.
- Cello G. and Mazzoli S. (1998) Apennine tectonics in southern Italy: A review, *Journal of Geodynamics*, **27**(2), 191-211.
- Cello G., Guerra I., Tortorici L., Turco E., and Scarpa R. (1982) Geometry of the neotectonic stress field in southern Italy: geological and seismological evidence. *Journal of Structural Geology*, **4**, 385-393.
- Cervato C. (1990) Hydrothermal dolomitization of Jurassic-Cretaceous limestones in the southern Alps (Italy): Relation to tectonics and volcanism. *Geology*, **18**(5), 458-461.
- Choquette P.W. and James N.P. (1990) Limestones – the burial diagenetic environment. In: McIlleath I.A. and Morrow D.W. (Eds.), *Diagenesis. Geoscience Canada Reprint Series 4*, Ottawa, 75-111.
- Ciarapica G. and Passeri L. (1998) Evoluzione paleogeografica degli Appennini. *Atti Ticinensi di Scienze della Terra*, **40**, 233-290.
- Ciarapica G. and Passeri L. (2002) The palaeogeographic duplicity of the Apennines. *Bollettino della Società Geologica Italiana*, Vol. Spec., **1**, 67-75.
- Ciarapica G., Cirilli S., Panzanelli Fratoni R., Passeri L. and Zaninetti L. (1990) The Monte Facito Formation (Southern Apennines). *Bollettino della Società Geologica Italiana*, **109**(1), 135-142.
- Ciarcia S., Vitale S., Di Staso A., Iannace A., Mazzoli S. and Torre M. (2009) Stratigraphy and tectonics of an Internal Unit of the Southern Apennines: implications for the geodynamic evolution of the peri-Tyrrhenian mountain belt. *Terra Nova*, **21**, 88-96.
- Cinque A., Patacca E., Scandone P., and Tozzi M. (1993) Quaternary kinematic evolution of the Southern Apennines, relationships between surface geological features and deep lithospheric structures. *Annali di Geofisica*, **36**, 249-260.
- Coniglio M., Sherlock R., Williams-Jones A.E., Middleton K. and Frape S.K. (1994) Burial and hydrothermal diagenesis of Ordovician carbonates from the Michigan Basin, Ontario, Canada. *Spec. Publ. Int. Assoc. Sedimentol.*, **21**, 231-254.
- Corrado S., Invernizzi C. and Mazzoli S. (2002) Tectonic burial and exhumation in a foreland fold and thrust belt: The Monte Alpi case history (Southern Apennines, Italy), *Geodinamica Acta*, **15**(3) 159-177.
- Corrado S., Aldega L., Di Leo P., Giampaolo C., Invernizzi C., Mazzoli S., and Zattin M. (2005) Thermal maturity of the axial zone of the southern Apennines fold-and-thrust belt (Italy) from multiple organic and inorganic indicators. *Terra Nova*, **17**, 56-65.
- D'Argenio B., Pescatore T., and Scandone, P. (1975) Structural pattern of the Campania–Lucania Apennines. *Quaderni Ricerca di Scienze*, **90**, 313-327.

- Dahlmann A. and de Lange G. J. (2003) Fluid-sediment interactions at Eastern Mediterranean mud volcanoes: a stable isotope study from ODP Leg 160. *Earth and Planetary Science Letters*, **212**(3-4), 377-391.
- Davies G.R. and Smith L.B.J. (2006) Structurally controlled hydrothermal dolomite reservoir facies: An overview. *AAPG Bulletin*, **90** (11), 1641-1690.
- Deffeyes K.S., Lucia F.J., Weyl P.K. (1965) Dolomitization of recent and Plio-Pleistocene sediments by marine evaporate waters on Bonaire, Netherlands Antilles. In: Pray L.C., Murray R.C. (Eds.), *Dolomitization and Limestone Diagenesis*. Spec. Publ.-SEPM, **13**, 71-88.
- Deweever B. (2008) Diagenesis and fluid flow in the Sicilian fold-and-thrust belt. PhD Thesis, KU-Leuven, 184 p.
- Deweever B., Berwouts I., Swennen R., Breesch L., Ellam R.M. (2010) Fluid flow reconstruction in karstified Panormide platform limestones (norther-central Sicily): implications for hydrocarbon prospectivity in the Sicilian fold and thrust belt. *Marine and Petroleum Geology*, **27**, 939-958.
- Dickson J.A.D. (1966) Carbonate identification and genesis as revealed by staining. *Journal of Sedimentary Petrology*, **36**(2), 491-505.
- Diehl S.F., Hofstra A.H., Koenig A.E., Emsbo P., Christiansen W. and Johnson C. (2010) Hydrothermal Zebra Dolomite in the Great Basin, Nevada - Attributes and Relation to Paleozoic Stratigraphy, Tectonics, and Ore Deposits. *Geosphere*, **6** (5), 663-690.
- Drivet E. and Mountjoy E.W. (1997) Dolomitization of the Leduc Formation (Upper Devonian), southern Rimbey-Medowbrook reef trends, Alberta. *Journal of Sedimentary Research*, **67**, 411-423.
- Ebers M.L. and Kopp O.C. (1979) Cathodoluminescent microstratigraphy in gangue dolomite, the Mascot-Jefferson City District, Tennessee. *Economic Geology*, **74**, 908-918.
- Finetti I. (1982) Structure, stratigraphy and evolution of central Mediterranean. *Bollettino di Geofisica Teorica e Applicata*, **24**, 247-315.
- Fisher W.L. and Rodda P.U. (1969) Edwards Formation (Lower Cretaceous), Texas: dolomitization in a carbonate platform system. *AAPG Bulletin*, **53**, 55-72.
- Fitts T.G. and Brown K.M. (1999) Stress-induced smectite dehydration: ramifications for patterns of freshening and fluid expulsion in the N. Barbados accretionary wedge. *Earth and Planetary Science Letters*, **172**, 179-197.
- Folk R.J. and Land L.S. (1975) Mg/Ca ratio and salinity, two controls over crystallisation of dolomite. *AAPG Bulletin*, **59**, 60-68.
- Fontboté L. (1993) Self-organization fabrics in carbonate hosted ore deposits: the example of diagenetic crystallization rhythmites (DCR's). In: Fenoll Hach-Ali P., Torres-Ruiz J. and Gervilla F. (Eds.), *Current research in geology applied to ore deposits*, Granada, 2<sup>nd</sup> biennial SGA Meeting, 11-14.
- Fontboté L. and Amstutz G.C. (1983) Facies and sequence analysis of diagenetic crystallization rhythmites in strata-bound Pb-Zn (Ba-F) deposits in the Triassic of central and southern Europe. In: Schneider, H.J. (Eds.) *Mineral deposits of the Alps and of the Alpine epoch in Europe*. Springer, Berlin Heidelberg New York, 347- 358.
- Fontboté L. and Gorzawski H. (1990) Genesis of the mississippi valley-type Zn-Pb deposit of San Vicente, central Peru; geologic and isotopic (Sr, O, C, S, Pb) evidence. *Economic Geology*, **85**(7), 1402-1437.

- Friedman I. and O'Neil J.R. (1977) Compilation of stable isotope fractionation factors of geochemical interest. In: Fleischer M. (Eds.) *Data of Geochemistry*, US Geological Survey Professional Paper, **440**, 1-12.
- Frisia S. (1994) Mechanisms of complete dolomitization in a carbonate shelf: comparison between the Norian Dolomia Principale (Italy) and the Holocene of Abu Dhabi Sabkha. In: Purser B., Tucker M. and Zenger D., (Eds.), *Dolomites*, IAS Spec. Publ., **21**, 55–74.
- Fu Q., Qing H. and Bergman K.M. (2006) Early dolomitization and recrystallization of carbonate in an evaporite basin: the Middle Devonian Ratner laminite in southern Saskatchewan, Canada. *Journal of the Geological Society*, **163**, 937-948.
- Gale L. (2010) Microfacies analysis of the Upper Triassic (Norian) “Baca Dolomite”: early evolution of the western Slovenian Basin (eastern Southern Alps, western Slovenia). *Geologica Carpathica*, **61**, 293–308.
- Garven G. (1985) The role of regional fluid flow in the genesis of the Pine Point deposit, Western Canada sedimentary basin. *Economic Geology*, **80**, 307-324.
- Garven G. and Freeze R. (1984) Theoretical analysis of the role of groundwater flow in the genesis of stratabound ore deposits. *American Journal of Science*, **284**, 1085-1174.
- Gasparrini M., Bechstädt T., Boni M. (2006) Massive hydrothermal dolomite in the southwestern Cantabrian Zone (Spain) and its relation to the late Variscan evolution. *Marine and Petroleum Geology*, **23**, 543-568.
- Ghisetti F., Kirschner D.L., Vezzani L. and Agosta F. (2001). Stable isotope evidence for contrasting paleofluid circulation in thrust faults and normal faults of the central Apennines, Italy. *Journal of Geophysical Research-Solid Earth*, **106**(B5), 8811-8825.
- Given R.K. and Wilkinson B.H. (1985) Kinetic control of morphology composition and mineralogy of abiotic sedimentary carbonates. *Journal of Sedimentary Petrology*, **55**, 109-119.
- Goldstein R.H. and Reynolds T.J. (1994) *Systematics of fluid inclusions in diagenetic minerals*. SEPM Short Course, **31**, (Eds.), Tulsa, Oklahoma.
- Gregg J.M. and Sibley D.F. (1984) Epigenetic dolomitization and the origin of xenotopic dolomite texture. *Journal of Sedimentary Petrology*, **54**, 908–931.
- Haas J. and Demény A. (2002) Early dolomitization of Late Triassic platform carbonates in the Transdanubian Range (Hungary). *Sedimentary Geology*, **151**, 225–242.
- Hanshaw B.B., Back W. and Dieke R.G. (1971) A geochemical hypothesis for dolomitization by groundwater. *Economic Geology*, **66**, 710-724.
- Hardie L.A. (1987) Dolomitization: a critical view of some current views. *Journal of Sedimentary Petrology*, **57**, 166-183.
- Hardie L.A. (1990) The roles of rifting and hydrothermal CaCl<sub>2</sub> brines in the origin of potash evaporates: an hypothesis. *American Journal of Science*, **290**, 43–106.
- Heijlen W., Muchez P. and Banks D.A. (2001) Origin and evolution of high-salinity, Zn-Pb mineralising fluids in the Variscides of Belgium. *Mineralium Deposita*, **36**, 165-176.
- Heijlen W., Muchez P. and Banks D.A. (2003) Carbonate-hosted Zn-Pb deposits in Upper Silesia, Poland: Origin and evolution of mineralizing fluids and constraints on genetic models. *Economic Geology and the Bulletin of the Society of Economic Geologists*, **98**, 911-932.
- Hitzman M.W., Allan J.R. and Beaty D.W. (1998) Regional dolomitization of the Waulsortian limestone in southeastern Ireland: evidence of large scale fluid flow driven by the Hercynian orogeny. *Geology*, **26** (6), 547–550.

- Hurley N.F. and Budros R. (1990) Albion-Scipio and Stoney Point fields, U.S.A., Michigan Basin. In: Beaumont E.A., Foster N.H. (Eds.) *Stratigraphic Traps I: AAPG Treatise of Petroleum Geology, Atlas of Oil and Gas Fields*, Tulsa, 1–37.
- Iannace A. and Frisia S. (1994) Changing dolomitization styles from Norian to Rhaetian in the southern Tethys realm. In: Purser B., Tucker M. and Zenger D., (Eds.), *Dolomites*, IAS Spec. Publ., **21**, 75-89. Blackwell Scientific Publications, Cambridge.
- Iannace A., Gasparrini M., Gabellone T. and Mazzoli S. (in press) Late dolomitization in basinal limestones of the southern Apennines fold and thrust belt (Italy), *Oil & Gas Science and Technology - Revue d'IFP Energies Nouvelles*.
- Illing L.V. (1959) Deposition and diagenesis of some Upper Palaeozoic carbonate sediments in western Canada, Fifth World Petroleum Congress, New York, 23-52.
- Jones G.D., Whitaker F.F., Smart P.L., and Sanford W.E. (2004) Numerical analysis of seawater circulation in carbonate platforms: II. The dynamic interaction between geothermal and brine reflux circulation. *American Journal of Science*, **304**, 250-284.
- Kastner M., Elderfield H. and Martin J. B. (1991) Fluids in convergent margins - What do we know about their composition, origin, role in diagenesis and importance for oceanic chemical fluxes. *Philosophical Transactions of the Royal Society of London Series a-Mathematical Physical and Engineering Sciences*, **335**(1638), 243-259.
- Kelts K.R. and McKenzie J.A. (1982) Diagenetic dolomite formation in Quaternary anoxic diatomaceous muds of Deep Sea Drilling Project Leg 64, Gulf of California. *Initial Rep. Deep Sea Drill. Proj.*, **64**(2), 553–569.
- Kendal A.C. (2001) Late diagenetic calcitization of anhydrite from the Mississippian of Saskatchewan, western Canada. *Sedimentology*, **48**, 29-55.
- Kohout F.A., Henry H.R. and Banks J.E. (1977) Hydrogeology related to geothermal conditions of the Floridan Plateau. In: Smith K.L. and Griffin, G.M. (Eds.) *The Geothermal Nature of the Floridan Plateau*. Florida Department of Natural Resources Bureau, Geology Special Publications, **21**, 1-34.
- Korte C., Kozur H.W. and Veizer J. (2005)  $\delta^{13}\text{C}$  and  $\delta^{18}\text{O}$  values of Triassic brachiopods and carbonate rocks as proxies for coeval seawater and palaeotemperature. *Palaeogeography, Palaeoclimatology, Palaeoecology*, **226**, 287–306.
- Kretz R. (1982) A model for the distribution of trace elements between calcite and dolomite. *Geochimica et Cosmochimica Acta*, **46**, 1979-1981.
- Krumgalz B.S., Pogorelsky R. and Pitzer K.S. (1996) Volumetric properties of single aqueous electrolytes from zero to saturation concentrations at 298,15 K represented by Pitzer's Ion-Interaction Equation. *Journal of Physical Chemistry Reference Data*, **25**, 663-689.
- Land L.S. (1980) The isotopic and trace element geochemistry of dolomite: The state of the art. *SEPM Special Publication*, **28**, 87-110.
- Land L.S. (1983) The application of stable isotopes to studies of the origin of dolomite and to problems of diagenesis of clastic sediments. In: Arthur M.A., Anderson T.F., Kaplan I.R., Veizer J., Land L.S. (Eds.), *Stable Isotopes in Sedimentary Geology*, Society of Sedimentary Geology Short Course, **10**, 4.1- 4.22.
- Land L.S. (1985) The origin of massive dolomite. *Journal of Geological Education*, **33**, 112–125.
- Lasemi Z., Boardman M.R. and Sandberg P.A. (1989) Cement origin of supratidal dolomite, Andros Island, Bahamas. *Journal of Sedimentary Research*, **59**(2), 249-257.
- Lentini F., Catalano S., Carbone S. (2000) Carta geologica della provincia di Messina. Servizio Geologico, S.EL.CA., Provincia Regionale di Messina, Assessorato Territorio, scale 1:50.000, 3 sheets.



- Long J.V.P. and Angrell S.O. (1965) The cathodoluminescence of minerals in thin section. *Mineralogical Magazine*, **34**, 318-326.
- Lopez-Horgue M.A., Iriarte E., Schroder S., Fernandez-Mendiola P.A., Caline B., Corneyllie H., Fremont J., Sudrie M., Zerti S. (2010) Structurally controlled hydrothermal dolomites in Albian carbonates of the Ason Valley, Basque Cantabrian Basin, Northern Spain. *Marine and Petroleum Geology*, **27** (5), 1069-1092.
- Lugli S., Torres-Ruiz J., Garuti G. and Olmedo F. (2000) Petrography and geochemistry of the Eugui magnesite deposit (Western Pyrenees, Spain): evidence for the development of a peculiar zebra banding by dolomite replacement. *Economic Geology*, **95**, 1775-1791.
- Machel H.G. (1988) Fluid flow direction during dolomite formation as deduced from trace-element trends. In: Shukla V. and Baker P.A. (Eds.), *Sedimentology and geochemistry of dolostones*. SEPM Spec. Publ., **43**, 115-125.
- Machel H.G. (2004) Concepts and models of dolomitization: a critical reappraisal. In: Braithwaite C.J.R., Rizzi G. and Darke G (Eds.), *The Geometry and Petrogenesis of Dolomite Hydrocarbon Reservoirs*. Geological Society, London, Special Publications, **235**, 7-63.
- Machel H.G. and Cavell EA. (1999) Low-flux, tectonically-induced squeegee fluid flow ("hot flash") into the Rocky Mountain Foreland Basin. *Bulletin of Canadian Petroleum Geology*, **47**, 510-533.
- Machel H.G. and Lonnee J. (2002) Hydrothermal dolomite – A product of poor definition and imagination. *Sedimentary Geology*, **152**, 163-171.
- Machel H.G. and Mountjoy E.W. (1986) Chemistry and environments of dolomitization – a reappraisal. *Earth Science Reviews*, **23**, 175-222.
- Machel H.G. and Mountjoy E.W. (1987) General constraints on extensive pervasive dolomitization and their application to the Devonian carbonates of western Canada. *Bulletin of Canadian Petroleum Geology*, **35**, 143-158.
- Machel H.G., Mason R.A., Mariano A.N. and Mucci A. (1991) Causes and emission of luminescence in calcite and dolomite. In: Barker C.E. and Kopp O.C. (Eds.), *Luminescence microscopy and spectroscopy: qualitative and quantitative applications*. SEPM Short Course, **25**, 9-25.
- Machel H.G., Cavell P.A., Buschkuehle B.E. and Michael K. (2000) Tectonically induced fluid flow in Devonian carbonate aquifers of the Western Canada Sedimentary Basin. *Journal of Geochemical Exploration*, **69-70**, 213-217.
- Mackenzie F. T. and Morse J. W. (1992) Sedimentary Carbonates through Phanerozoic Time. *Geochimica et Cosmochimica Acta*, **56**(8), 3281-3295.
- Major R.P., Micheal Lloyd R. and Lucia J. (1992) Oxygen isotope composition of Holocene dolomite formed in a humid hypersaline setting. *Geology*, **20**(7), 586-588.
- Marsella E. (1988) I terreni lagonegresi tra San Fele e la Val d'Agri. Evoluzione tettonico-sedimentaria (Trias superiore-Giurassico). Tesi di Dottorato in Geologia del sedimentario. Consorzio delle Università di Napoli e Palermo, 159 p.
- Marsella E., Bally A.W., Cippitelli G., D'argenio B. and Pappone, G. (1995) Tectonic history of the Lagonegro domain and Southern Apennine thrust belt evolution, *Tectonophysics*, **252**, 307-330.
- Martín J.M., Torres-Ruiz J. and Fontboté L. (1987) Facies control of strata-bound ore deposits in carbonate rocks: the F-(Pb-Zn) deposits in the Alpine Triassic of the Alpujarrides, southern Spain. *Mineralium Deposita*, **22**, 216-226.

- Mastandrea A., Perri E., Russo F., Spadafora A. and Tucker M. (2006) Microbial primary dolomite from a Norian carbonate platform: northern Calabria, southern Italy, *Sedimentology*, **53**, 465-480.
- Mattes B.W. and Mountjoy E.W. (1980) Burial dolomitization of the Upper Devonian Miette buildup, Jasper National Park, Alberta. In: Zenger D.H., Dunham J.B. and Ethington R.L. (Eds.), *Concepts and models of dolomitization*. SEPM Spec. Publ., **28**, 259-297.
- Mazzoli S. and Di Bucci D. (2003) Critical displacement for normal fault nucleation from en-échelon vein arrays in limestones: A case study from the southern Apennines (Italy). *Journal of Structural Geology*, **25**(7), 1011-1020.
- Mazzoli S. and Helman M. (1994) Neogene patterns of relative plate motion for Africa–Europe: some implications for recent central Mediterranean tectonics. *Geologische Rundschau*, **83**, 464-468.
- Mazzoli S., Barkham S., Cello G., Gambini R., Mattioni L., Shiner P. and Tondi E. (2001) Reconstruction of continental margin architecture deformed by the contraction of the Lagonegro basin, Southern Apennines, Italy. *Journal of the Geological Society, London*, **158**(2), 309-320.
- Mazzoli S., Invernizzi C., Marchegiani L., Mattioni L. and Cello G. (2004) Brittle-ductile shear zone evolution and fault initiation in limestones, Monte Cugnone (Lucania), Southern Apennines, Italy. *Geological Society, London, Special Publications*, **224**, 353-373.
- Mazzoli S., Aldega L., Corrado S., Invernizzi C. and Zattin M. (2006) Pliocene-Quaternary thrusting, syn-orogenic extension and tectonic exhumation in the southern Apennines (Italy): insights from the Monte Alpi area. In: *Styles of Continental Contraction*, Geological Society of America, Special paper, **414**, 55-77.
- Mazzoli S., D’Errico M., Adelga L., Corrado S., Invernizzi C., Shiner P. and Zattin M. (2008) Tectonic burial and “young” (<10 Ma) exhumation in the southern Apennines fold-and-thrust belt (Italy). *Geology*, **36**(3), 243-246.
- Mazzullo S.J. (2000) Organogenic dolomitization in peritidal to deep-sea sediments. *Journal of Sedimentary Research*, **70**(1), 10-23.
- McArthur J.M. and Howarth R.J. (2004) Strontium isotope Stratigraphy. In: Gradstein F.M., Ogg J.G., Smith A.G. (Eds.), *A Geological Time Scale 2004*, Cambridge University Press.
- McIntyre W.L. (1963) Trace element partition coefficients – a review of theory and applications to geology. *Geochimica et Cosmochimica Acta*, **27**, 1209-1264.
- Mckenzie J.A. (1981) Holocene dolomitization of calcium carbonate sediments from the coastal sabkhas of Abu Dhabi, U.A.E.: A stable isotope study. *Journal of Geology*, **89**, 185-198.
- Mckenzie J.A. and Vasconcelos C. (2009) Dolomite Mountains and the origin of the dolomite rock of which they mainly consist: historical developments and new perspectives. *Sedimentology*, **56**, 205-219.
- Merino E., Canals A. and Fletcher R.C. (2006) Genesis of self-organized zebra textures in burial dolomites: Displacive veins, induced stress, and dolomitization. *Geologica Acta*, **4**(3), 383-393.
- Miconnet P. (1988) Evolution Mésozoïque du secteur de Lagonegro. *Memorie della Società Geologica Italiana*, **41**, 321-330.
- Mitchell S.W. and Horton R.A. (1995) Dolomitization of modern tidal flat, tidal creek, and lacustrine sediments, Bahamas. *Geological Society of America Special Papers*, **300**, 201-221.

- Montañez I.P. (1994) Late diagenetic dolomitization of Lower Ordovician, Upper Knox Carbonates: a record of the hydrodynamic evolution of the southern Appalachian Basin. *AAPG Bulletin*, **78**(8), 1210-1239.
- Morrow D.W. (1982) Diagenesis 2. Dolomite - Part2: Dolomitization models and ancient dolostones. *Geoscience Canada*, **9**, 95-107.
- Morrow D.W. (1998) Regional subsurface dolomitization: models and constraints. *Geoscience Canada*, **25**(2), 57-70.
- Morse J.M. and Mackenzie F.T. (1990) Carbonates as sedimentary rocks in subsurfaces process, in *Geochemistry of sedimentary carbonates*, (Eds.), Elsevier, Amsterdam.
- Mostardini F. and Merlini S. (1986) Appennino centro-meridionale: sezioni geologiche e proposta di modello strutturale. *Memorie della Società Geologica Italiana*, **35**, 177-202.
- Mresah M.H. (1998) The massive dolomitization of platform and basinal sequences: proposed models from the Paleocene, Northeast Sirte Basin, Libya. *Sedimentary Geology*, **116**, 199-226.
- Mucci A. and Morse J.W. (1983) The incorporation of  $Mg^{2+}$  and  $Sr^{2+}$  into calcite overgrowths: Influences of growth rate and solution composition. *Geochimica et Cosmochimica Acta*, **47**, 217-233.
- Murgia M.V., Ronchi P. and Ceriani A. (2004) Dolomitization processes and their relationships with the evolution of an orogenic belt (Central Apennines and peri-adriatic foreland, Italy), In: Swennen R., Roure F. and Granath J.W. (Eds.), *Deformation, Fluid Flow, and Reservoir Appraisal in Foreland Fold and Thrust Belts*, AAPG Hedberg Series, 1 Tulsa, Oklahoma, USA, 277-294.
- Nader F.H., Swennen R. and Ellam R. (2004) Reflux stratabound dolostone and hydrothermal volcanism-associated dolostone: a two stage dolomitization model (Jurassic, Lebanon). *Sedimentology*, **51**, 339-360.
- Nielsen P., Swennen R., and Keppens E. (1994) Multiple-step recrystallization within massive ancient dolomite units: an example from the Dinantian of Belgium. *Sedimentology*, **41**, 567-584.
- Nielsen P., Swennen R., Muchez P. and Keppens E. (1998) Origin of Dinantian zebra-dolomites south of the Brabant-Wales Massif, Belgium. *Sedimentology*, **45**, 727-743.
- Ogniben L. (1969) Schema introduttivo alla geologia del confine calabro-lucano. *Memorie della Società Geologica Italiana*, **8**, 453-763.
- Ogorelec B., Dolenc T., Pezdic J. (1999) Isotope composition of O and C in Mesozoic carbonate rocks of Slovenia - effect of facies and diagenesis. *Geologija*, **42**, 171-205.
- Oliver J. (1986) Fluids expelled tectonically from orogenic belts: their role in hydrocarbon migration and other geologic phenomena. *Geology*, **14**, 99-102.
- Passeri L., Bertinelli A. and Ciarapica G. (2005) Paleogeographic meaning of the Late Triassic – Early Jurassic Lagonegro units. *Bollettino della Società Geologica Italiana*, **124**, 231-245.
- Patacca E. (2007) Stratigraphic constraints on the CROP-04 seismic line interpretation San Fele1, Monte Foil and San Gregorio Magno1 wells (Southern Apennines, Italy). *Bollettino della Società Geologica Italiana*, Spec. Issue, **7**, 185-293.
- Patacca E. and Scandone P. (2003) Paleogeographic restoration of the Lagonegro basin. New constraints from subsurface data - Workshop: Late Triassic-early Jurassic events in the framework of the Pangea break-up, Capri.

- Patacca E. and Scandone P. (2004) A geological transect across the Southern Apennines along the seismic line CROP 04. 32<sup>nd</sup> International Geological Congress, Field Trip Guide Book, **1** (20), 24 pp.
- Pescatore T. and Tramutoli M. (1980) I rapporti tra i depositi del bacino di Lagonegro e del bacino irpino nella media valle del Basento (Lucania). *Rend. Acc. Sci. Fis. Mater. Soc. Naz. Sci. Lett. Art. Napoli*, **47**, 19-41.
- Pescatore T., Renda P., Schiattarella M. and Tramutoli M. (1999) Stratigraphic and structural relationships between Meso-Cenozoic Lagonegro basin and coeval carbonate platforms in southern Apennines, Italy. *Tectonophysics*, **315**, 269-286.
- Phillips O.M. (1991) Flow and Reactions in Permeable Rocks. Cambridge University Press, Cambridge, 285 p.
- Pieri M. (1966) Tentativo di ricostruzione paleogeografico-strutturale dell'Italia centro-meridionale. *Geologia Romana*, **5**, 407-424.
- Pierson B.J. (1981) The control of cathodoluminescence in dolomite by iron and manganese. *Sedimentology*, **28**, 601-610.
- Qing H. and Mountjoy E.W. (1992) Large-scale fluid flow in the Middle Devonian Presqu'île barrier, Western Canada Sedimentary Basin. *Geology*, **20**, 903-906.
- Qing H. and Mountjoy E.W. (1994) Formation of coarsely crystalline, hydrothermal dolomite reservoirs in the Presqu'île Barrier, Western Canada Sedimentary Basin. *AAPG Bulletin*, **78**(1), 55-77.
- Radke B.M. and Mathis R.L. (1980) On the formation and occurrence of saddle dolomite. *Journal of Sedimentary Petrology*, **50**, 1149-1168.
- Ronchi P., Di Giulio A., Ceriani A. and Scotti P. (2010) Contrasting fluid events giving rise to apparently similar diagenetic products; late-stage dolomite cements from the Southern Alps and central Apennines, Italy. *Geological Society, London, Special Publications*, **329**, 397-413.
- Ronchi P., Masetti D., Tassan S. and Camocino D. (2012) Hydrothermal dolomitization in platform and basin carbonate successions during thrusting: A hydrocarbon reservoir analogue (Mesozoic of Venetian Southern Alps, Italy). *Marine and Petroleum Geology*, **29**, 68-89.
- Rosenbaum J. and Sheppard S.M. (1986) An isotopic study of siderites, dolomites and ankerites at high temperatures. *Geochimica et Cosmochimica Acta*, **50**, 1147-1150.
- Roure F., Nazaj S., Muska K., Fili I., Cadet J.P. and Bonneau M. (2004.) Kinematic evolution and petroleum systems: an appraisal of the Outer Albanides. In: McKlay (Eds.), *Thrust Tectonics and Hydrocarbon Systems, AAPG Memoirs*, **82** (24), 474-493.
- Roure F., Swennen R., Schneider F., Faure J. L., Ferket H., Guilhaumou N., Osadetz K., Robion P. and Vandeginste V. (2005) Incidence of tectonics and natural fluid migration on reservoir evolution in foreland fold and thrust belts. *Oil & Gas Science and Technology, Revue de l'IFP*, **60**, 67-106.
- Saller A.H. (1984) Petrologic and geochemical constraints on the origin of subsurface dolomite, Enewetak Atoll; an example of dolomitization by normal seawater. *Geology*, **12**(4), 217-220.
- Samson I.M., Anderson A.J. and Marshall D.D. (2003) Fluid inclusions. Analysis and interpretation. *Mineralogical Association of Canada Short Course Series* (Eds.), **32**, 374 p.

- Sanford W.E., Whitaker F.A., Smart P.L. and Jones G. (1998) Numerical analysis of seawater circulation in carbonate platforms: I. Geothermal convection. *American Journal of Science*, **298**, 801-828.
- Scandone P. (1967) Studi di geologia lucana: la serie calcareo-silico-marnosa e i suoi rapporti con l'Appennino calcareo. *Bollettino Società dei Naturalisti in Napoli*, **76**, 1-175.
- Scandone P. (1972) Studi di geologia lucana: carta dei terreni della serie calcareo-silico-marnosa e note illustrative. *Bollettino Società dei Naturalisti in Napoli*, **81**, 225-300.
- Scandone P. (1975) The preorogenic history of the Lagonegro Basin (Southern Apennines). In: Squyres C. (Eds.), *Geology of Italy*. The Earth Sciences Society of the Libyan Arab Republic, Tripoli, 305-315.
- Sengör A.M.C., Yilmaz Y. and Sungurlu O. (1984) Tectonics of the Mediterranean Cimmerides: nature and evolution of the western termination of Palaeo-Tethys. In: Dixon J.E. and Robertson A.H.F. (Eds.), *The Geological Evolution of the Eastern Mediterranean*. Geological Society, London Special Publications, **17**, 77-112.
- Sgrosso I. (1988) Nuovi elementi per un più articolato modello paleogeografico nell'Appennino centro meridionale. *Memorie della Società Geologica Italiana*, **41**, 225-242.
- Shiner P., Beccacini A. and Mazzoli S. (2004) Thin-skinned versus thick-skinned structural models for Apulian carbonate reservoirs: Constraints from the Val D'Agri Fields. *Marine and Petroleum Geology*, **21**, 805-827.
- Sibley D.F. and Gregg J.M. (1987) Classification of dolomite rock textures. *Journal of Sedimentary Petrology*, **54** (3), 908-931.
- Simms M. (1984) Dolomitization by ground water-flow systems in carbonate platforms. *Trans. Gulf Coast Ass. Geol. Soc.*, **34**, 411-420.
- Sommer S.E. (1972) Cathodoluminescence of carbonates, 1. Characterization of cathodoluminescence from carbonate solid solutions. *Chemical Geology*, **9**, 257-273.
- Stampfli G.M., Mosar J., Marquer D., Marchant R., Baudin T. and Borel G.D. (1998) Subduction and obduction processes in the Swiss Alps. *Tectonophysics*, **296**, 159-204.
- Stampfli G.M., Vavassis I., De Bono A., Rosselet F., Matti B. and Bellini M. (2003) Remnants of the Palaeotethys oceanic suture-zone in the western Tethyan area. *Bollettino della Società Geologica Italiana*, Vol. Spec., **2**, 1-23.
- Sun S. Q. (1994) A reappraisal of dolomite abundance and occurrence in the Phanerozoic. *Journal of Sedimentary Research Section a-Sedimentary Petrology and Processes*, **64**(2), 396-404.
- Swennen R., Viaene W., Jacobs L. and Van Orsmael J. (1981) Occurrence of calcite pseudomorphs after gypsum in the Lower Carboniferous of the Vesder region (Belgium). *Bulletin de la Société Belge de Géologie*, **90**, 231-247.
- Swennen R., Ferket H., Benchilla L., Roure F. and Ellam R. (2003a) Fluid flow and diagenesis in carbonate dominated foreland fold and thrust belts: petrographic inferences from field studies of late diagenetic fabrics from Albania, Belgium, Canada, Mexico and Pakistan. *Journal of Geochemical Exploration*, **78-79**, 481-485.
- Swennen R., Vandeginste V. and Ellam R. (2003b) Genesis of zebra dolomites (Cathedral Formation: Canadian Cordillera Fold and Thrust Belt, British Columbia). *Journal of Geochemical Exploration*, **78-79**, 571-577.
- Swennen R., Roure F. and Granath J. (2004) *Deformation history, fluid flow reconstruction and reservoir appraisal in foreland fold and thrust belts*. (Eds.), American association of petroleum geology - Hedberg Memoir 1.



- Taylor T.R. (1990) The Influence of calcite dissolution on reservoir porosity in Miocene sandstones, Picaroon Field, Offshore Texas Gulf-Coast. *Journal of Sedimentary Petrology*, **60**(3), 322-334.
- Taylor T.R. and Sibley D.F. (1986) Petrographic and geochemical characteristics of dolomite in the Trenton Formation, Ordovician, Michigan Basin. *Sedimentology*, **33**, 61–86.
- Tompkins L.A., Murray J.R. and Groves D.I. (1994) Evaporites: in situ source for rhythmically banded ore in the Cadjebut Mississippi Valley-Type Zn-Pb deposit, Western Australia. *Economic Geology*, **89**, 467-492.
- Tucker M.E. and Wright V.P. (1990) Carbonate sedimentology. Blackwell Scientific, Oxford, 482 p.
- Vahrenkamp V.C. and Swart P.K. (1994) Late Cenozoic dolomites of the Bahamas: metastable analogues for the genesis of ancient platform dolomites. In: Purser B., Tucker M. and Zenger D., (Eds.), *Dolomites*, IAS Spec. Publ., **21**, 133–153. Blackwell Scientific Publications, Cambridge.
- Vandeginste V., Swennen R., Gleeson S.A., Ellam R.M., Osadetz K. and Roure F. (2005) Zebra dolomitization as a result of focused fluid flow in the Rocky Mountains Fold and Thrust Belt, Canada. *Sedimentology*, **52**, 1067-1095.
- Vasconcelos C. and Mckenzie J.A. (1997) Microbial mediation of modern dolomite precipitation and diagenesis under anoxic conditions (Lagoa Vermelha, Rio de Janeiro, Brazil). *Journal of Sedimentary research*, **67**(3), 378-390.
- Vasconcelos C., McKenzie J., Warthmann R. and Bernasconi S.M. (2005) Calibration of the  $\delta^{18}\text{O}$  paleothermometer for dolomite precipitated in microbial cultures and natural environments. *Geology*, **33**(4), 317-320.
- Veizer J. (1983) Chemical diagenesis of carbonates: theory and application of trace element technique. In: Arthur M.A., Anderson T.F., Kaplan I.R., Veizer J. and Land L.S. (Eds.), *Stable isotopes in sedimentary geology*. SEPM Short Course, **10**, 3.1-3.100.
- Veizer J., Ala D., Azmy K., Bruckschen P., Buhl D., Bruhn F., Carden G.A.F., Diener A., Ebner S., Godderis Y., Jasper T., Korte C., Pawellek F., Podlaha O.G., Strauss H. (1999)  $^{87}\text{Sr}/^{86}\text{Sr}$ ,  $\delta^{13}\text{C}$  and  $\delta^{18}\text{O}$  evolution of Phanerozoic seawater. *Chemical Geology*, **161**, 59-88.
- Vilasi N., Malandain J., Barrier L., Callot J.P., Amrouch K., Guilhaumou N., Lacombe O., Muskha K., Roure F. and Swennen R. (2009) From outcrop and petrographic studies to basin-scale fluid flow modelling: the use of the Albanian natural laboratory for carbonate reservoir characterisation. *Tectonophysics*, **474**, 367-392.
- Von der Borch C.C. and Lock D. (1979) Geological significance of Coorong dolomites. *Sedimentology*, **23**, 587-591.
- Vrolijk P., Myers G. and Moore J. C. (1988) Warm fluid migration along tectonic melanges in the Kodiak Accretionary complex, Alaska. *Journal of Geophysical research*, **93**(B9), 10313-10324.
- Walker T.R. (1962) Reversible nature of chert-carbonate replacement in sedimentary rocks. *Geological Society of America Bulletin*, **73**, 237-242.
- Wallace M.W., Both R.A., Ruano S.M., Hach-Ali P.F. and Lees T. (1994) Zebra textures from carbonate-hosted sulfide deposits: Sheet cavity networks produced by fracture and solution enlargement. *Economic Geology*, **89**, 1183–1191.
- Warren J.K. (1990) Sedimentology and mineralogy of dolomitic Coorong lakes, South Australia. *Journal of Sedimentary Petrology*, **60**(6), 843-858.

- Warren, J.K. (1991): Sulfate dominated sea-marginal and platform evaporative settings. In: Melvin J.L. (Eds.), *Evaporites, Petroleum and Mineral Resources*. Dev. Sedimentol., Elsevier, Amsterdam, **50**, 477-533.
- Warren J. (2000) Dolomite: occurrence, evolution and economically important association. *Earth Science Reviews*, **52**, 1-81.
- Whitaker F.F., Smart P.L., Vahrenkamp V.C., Nicholson H. and Wogelius R.A. (1994) Dolomitization by near-normal seawater? Field evidence from the Bahamas. In: Purser B., Tucker M. and Zenger D., (Eds.), *Dolomites*, IAS Spec. Publ., **21**, 111–132. Blackwell Scientific Publications, Cambridge.
- Wilson E.N., Lawrence A.H. and Phillips O.M. (1990) Dolomitization front geometry, fluid flow patterns, and the origin of massive dolomite: the Triassic Latemar buildup, northern Italy. *American Journal of Science*, **290**, 741-796.
- Zenger D.H. (1972) Dolomitization and uniformitarianism. *Journal of Geological Education*, **20**, 107-124.

# Appendix

## Appendix 1: Structural data

Veins				
Locality	Lithology	Filling	Dip direction	Angle of dip
Pignola	Dolostone	Dolomite	282	87
Pignola	Dolostone	Dolomite	288	88
Pignola	Dolostone	Dolomite	122	84
Pignola	Dolostone	Dolomite	50	80
Pignola	Dolostone	Dolomite	290	88
Pignola	Dolostone	Dolomite	284	86
Pignola	Dolostone	Dolomite	62	79
Pignola	Dolostone	Dolomite	202	84
Pignola	Dolostone	Dolomite	286	67
Pignola	Dolostone	Dolomite	294	58
Pignola	Dolostone	Dolomite	292	84
Pignola	Limestone	Dolomite	220	82
Pignola	Limestone	Dolomite	236	85
Pignola	Limestone	Dolomite	64	86
Pignola	Limestone	Dolomite	242	88
Pignola	Limestone	Dolomite	58	84
Pignola	Limestone	Dolomite	66	82
Pignola	Limestone	Calcite	290	88
Pignola	Limestone	Calcite	260	87
Pignola	Limestone	Calcite	112	83
Pignola	Limestone	Dolomite	274	85
Pignola	Limestone	Dolomite	260	88
Pignola	Limestone	Dolomite	262	83
Pignola	Limestone	Dolomite	52	78
Pignola	Limestone	Dolomite	58	71
Pignola	Limestone	Dolomite	38	80
Pignola	Limestone	Dolomite	34	85
Pignola	Limestone	Calcite	31	66
Pignola	Limestone	Dolomite	42	78
Pignola	Limestone	Calcite	114	66
Pignola	Limestone	Calcite	214	60
Pignola	Limestone	Calcite	78	82
Pignola	Limestone	Calcite	62	83
Pignola	Limestone	Calcite	90	64
Pignola	Limestone	Calcite	70	65
Pignola	Limestone	Calcite	87	64
Pignola	Limestone	Calcite	268	90
Pignola	Limestone	Calcite	258	82
Pignola	Limestone	Calcite	262	90
Pignola	Limestone	Calcite	261	86
Pignola	Limestone	Calcite	95	68
Pignola	Limestone	Calcite	95	68
Pignola	Limestone	Calcite	290	70
Pignola	Limestone	Calcite	182	71
Pignola	Limestone	Calcite	124	69
Pignola	Limestone	Calcite	98	62
Pignola	Limestone	Calcite	97	58

Veins				
Locality	Lithology	Filling	Dip direction	Angle of dip
Pignola	Limestone	Calcite	110	63
Pignola	Dolostone	Dolomite	258	81
Pignola	Dolostone	Dolomite	220	70
Pignola	Dolostone	Dolomite	234	80
Pignola	Dolostone	Dolomite	235	65
Pignola	Dolostone	Dolomite	252	79
Pignola	Dolostone	Dolomite	237	88
Pignola	Dolostone	Dolomite	271	80
Pignola	Dolostone	Dolomite	249	80
Pignola	Dolostone	Dolomite	241	80
Pignola	Dolostone	Dolomite	235	61
Pignola	Dolostone	Dolomite	121	62
Pignola	Dolostone	Dolomite	222	81
Pignola	Limestone	Calcite	132	64
Pignola	Limestone	Calcite	121	67
Pignola	Limestone	Calcite	42	74
Pignola	Limestone	Calcite	116	70
Pignola	Limestone	Calcite	168	82
Pignola	Limestone	Calcite	98	72
Pignola	Limestone	Calcite	22	84
Pignola	Limestone	Calcite	102	71
Pignola	Limestone	Calcite	60	82
Pignola	Dolostone	Dolomite	118	67
Pignola	Dolostone	Dolomite	82	74
Pignola	Dolostone	Dolomite	137	72
Pignola	Dolostone	Dolomite	60	73
Pignola	Dolostone	Dolomite	30	89
Pignola	Dolostone	Dolomite	92	70
Pignola	Dolostone	Dolomite	104	70
Pignola	Dolostone	Dolomite	98	74
Pignola	Dolostone	Dolomite	68	79
Pignola	Dolostone	Dolomite	58	82
Pignola	Dolostone	Dolomite	52	84
Pignola	Dolostone	Dolomite	48	82
Pignola	Dolostone	Dolomite	212	80
Pignola	Dolostone	Dolomite	214	76
Pignola	Dolostone	Dolomite	18	85
Pignola	Dolostone	Dolomite	208	75
Pignola	Dolostone	Dolomite	214	83
Pignola	Dolostone	Dolomite	216	86
Pignola	Dolostone	Dolomite	53	82
Pignola	Dolostone	Dolomite	218	88
Pignola	Dolostone	Dolomite	220	86
Pignola	Dolostone	Dolomite	152	68
Pignola	Dolostone	Dolomite	218	76
Pignola	Dolostone	Dolomite	172	56
Pignola	Dolostone	Dolomite	272	78

Veins				
Locality	Lithology	Filling	Dip direction	Angle of dip
Pignola	Dolostone	Dolomite	276	76
Pignola	Dolostone	Dolomite	278	77
Pignola	Dolostone	Dolomite	88	72
Pignola	Limestone	Calcite	122	72
Pignola	Limestone	Calcite	118	85
Pignola	Limestone	Calcite	126	80
Pignola	Limestone	Calcite	128	81
Pignola	Limestone	Dolomite	90	73
Pignola	Limestone	Calcite	122	74
Pignola	Limestone	Dolomite	136	75
Pignola	Limestone	Dolomite	136	81
Pignola	Limestone	Calcite	128	78
Pignola	Limestone	Calcite	131	84
Pignola	Limestone	Calcite	168	80
Pignola	Limestone	Calcite	166	78
Pignola	Limestone	Calcite	164	77
Pignola	Limestone	Calcite	167	82
Pignola	Limestone	Calcite	88	82
Pignola	Limestone	Calcite	92	86
Pignola	Limestone	Calcite	152	88
Pignola	Limestone	Calcite	94	88
Pignola	Limestone	Calcite	138	75
Pignola	Limestone	Calcite	146	82
Pignola	Limestone	Calcite	148	87
Pignola	Limestone	Calcite	242	88
Pignola	Limestone	Calcite	132	83
Pignola	Limestone	Calcite	128	75
Pignola	Limestone	Calcite	58	85
Pignola	Limestone	Calcite	66	78
Pignola	Dolostone	Dolomite	66	71
Pignola	Dolostone	Dolomite	78	87
Pignola	Dolostone	Dolomite	74	78
Pignola	Dolostone	Dolomite	72	73
Pignola	Dolostone	Dolomite	84	71
Pignola	Dolostone	Dolomite	73	76
Pignola	Dolostone	Dolomite	68	78
Pignola	Dolostone	Dolomite	67	76
Pignola	Dolostone	Dolomite	316	84
Pignola	Dolostone	Dolomite	136	88
Pignola	Dolostone	Dolomite	138	86
Pignola	Dolostone	Dolomite	56	86
Pignola	Dolostone	Dolomite	320	75
Pignola	Dolostone	Dolomite	250	86
Pignola	Dolostone	Dolomite	68	82
Pignola	Limestone	Dolomite	252	81
Pignola	Limestone	Dolomite	86	84
Pignola	Limestone	Dolomite	76	78



Veins				
Locality	Lithology	Filling	Dip direction	Angle of dip
Pignola	Limestone	Dolomite	18	64
Pignola	Limestone	Dolomite	102	87
Pignola	Limestone	Dolomite	82	88
Pignola	Limestone	Dolomite	266	82
Pignola	Limestone	Dolomite	268	87
Pignola	Limestone	Dolomite	84	78
Pignola	Limestone	Dolomite	74	76
Pignola	Limestone	Dolomite	68	82
Pignola	Limestone	Dolomite	296	85
Pignola	Limestone	Dolomite	107	74
Pignola	Limestone	Dolomite	102	85
Pignola	Limestone	Dolomite	90	76
Pignola	Limestone	Dolomite	294	82
Pignola	Limestone	Calcite	121	68
Pignola	Limestone	Calcite	138	69
Pignola	Limestone	Calcite	118	70
Pignola	Limestone	Calcite	133	78
Pignola	Limestone	Dolomite	263	85
Pignola	Limestone	Dolomite	257	86
Pignola	Limestone	Dolomite	278	82
Pignola	Limestone	Calcite	106	78
Pignola	Limestone	Calcite	103	66
Pignola	Limestone	Calcite	92	66
Pignola	Limestone	Calcite	99	67
Pignola	Limestone	Dolomite	81	82
Pignola	Limestone	Calcite	303	63
Pignola	Limestone	Calcite	304	77
Pignola	Limestone	Calcite	288	84
Pignola	Limestone	Calcite	281	79
Pignola	Limestone	Calcite	257	80
Pignola	Limestone	Calcite	281	83
Madonna del Sasso	Dolostone	Dolomite	100	69
Madonna del Sasso	Dolostone	Dolomite	90	66
Madonna del Sasso	Dolostone	Dolomite	83	74
Madonna del Sasso	Dolostone	Dolomite	93	63
Madonna del Sasso	Dolostone	Dolomite	88	60
Madonna del Sasso	Dolostone	Dolomite	88	60
Madonna del Sasso	Dolostone	Dolomite	94	62
Madonna del Sasso	Dolostone	Dolomite	92	61
Madonna del Sasso	Dolostone	Dolomite	102	57
Madonna del Sasso	Dolostone	Dolomite	90	58
Madonna del Sasso	Dolostone	Dolomite	67	68
Madonna del Sasso	Dolostone	Dolomite	70	60
Madonna del Sasso	Dolostone	Dolomite	72	43
Madonna del Sasso	Dolostone	Dolomite	77	40
Madonna del Sasso	Dolostone	Dolomite	78	51
Madonna del Sasso	Dolostone	Dolomite	78	64

Veins				
Locality	Lithology	Filling	Dip direction	Angle of dip
Madonna del Sasso	Dolostone	Dolomite	88	62
Madonna del Sasso	Dolostone	Dolomite	77	64
Madonna del Sasso	Dolostone	Dolomite	81	65
Madonna del Sasso	Dolostone	Dolomite	83	59
Madonna del Sasso	Dolostone	Dolomite	90	60
Madonna del Sasso	Limestone	Dolomite	60	72
Madonna del Sasso	Limestone	Dolomite	62	71
Madonna del Sasso	Limestone	Dolomite	82	73
Madonna del Sasso	Limestone	Dolomite	87	71
Madonna del Sasso	Limestone	Dolomite	256	79
Madonna del Sasso	Limestone	Dolomite	58	69
Madonna del Sasso	Limestone	Dolomite	58	70
Madonna del Sasso	Limestone	Dolomite	303	87
Madonna del Sasso	Limestone	Calcite	218	88
Madonna del Sasso	Limestone	Dolomite	66	75
Madonna del Sasso	Limestone	Dolomite	260	87
Madonna del Sasso	Limestone	Dolomite	78	72
Madonna del Sasso	Limestone	Dolomite	92	71
Madonna del Sasso	Limestone	Dolomite	254	86
Madonna del Sasso	Limestone	Dolomite	54	75
Madonna del Sasso	Limestone	Dolomite	58	72
Madonna del Sasso	Limestone	Calcite	118	83
Madonna del Sasso	Limestone	Calcite	114	77
Madonna del Sasso	Limestone	Calcite	112	76
Madonna del Sasso	Limestone	Calcite	52	76
Madonna del Sasso	Limestone	Calcite	54	73
Madonna del Sasso	Limestone	Calcite	46	75
Madonna del Sasso	Limestone	Calcite	234	89
Madonna del Sasso	Limestone	Calcite	44	78
Madonna del Sasso	Limestone	Calcite	116	81
Madonna del Sasso	Limestone	Calcite	302	85
Madonna del Sasso	Limestone	Calcite	308	82
Madonna del Sasso	Limestone	Calcite	102	79
Madonna del Sasso	Limestone	Calcite	62	71
Madonna del Sasso	Limestone	Calcite	242	88
Madonna del Sasso	Limestone	Calcite	64	84
Madonna del Sasso	Limestone	Calcite	304	77
Madonna del Sasso	Limestone	Calcite	100	44
Madonna del Sasso	Limestone	Calcite	92	41
Madonna del Sasso	Limestone	Calcite	98	45
Madonna del Sasso	Limestone	Calcite	94	43
Madonna del Sasso	Limestone	Calcite	83	49
Madonna del Sasso	Limestone	Calcite	336	87
Madonna del Sasso	Dolostone	Dolomite	78	67
Madonna del Sasso	Dolostone	Dolomite	78	65
Madonna del Sasso	Dolostone	Dolomite	250	86
Madonna del Sasso	Dolostone	Dolomite	70	75

Veins				
Locality	Lithology	Filling	Dip direction	Angle of dip
Madonna del Sasso	Dolostone	Dolomite	232	88
Madonna del Sasso	Dolostone	Dolomite	242	87
Madonna del Sasso	Dolostone	Dolomite	112	71
Madonna del Sasso	Dolostone	Dolomite	70	72
Madonna del Sasso	Dolostone	Dolomite	248	87
Madonna del Sasso	Dolostone	Dolomite	124	82
Madonna del Sasso	Dolostone	Dolomite	69	84
Madonna del Sasso	Dolostone	Dolomite	76	71
Sasso di Castalda	Limestone	Calcite	42	75
Sasso di Castalda	Limestone	Calcite	44	81
Sasso di Castalda	Limestone	Calcite	112	88
Sasso di Castalda	Limestone	Calcite	302	81
Sasso di Castalda	Limestone	Calcite	40	76
Sasso di Castalda	Limestone	Calcite	252	67
Sasso di Castalda	Limestone	Calcite	272	81
Sasso di Castalda	Limestone	Calcite	62	86
Sasso di Castalda	Limestone	Calcite	58	78
Sasso di Castalda	Limestone	Calcite	259	76
Sasso di Castalda	Limestone	Calcite	248	82
Sasso di Castalda	Limestone	Calcite	36	82
Sasso di Castalda	Limestone	Calcite	87	87
Sasso di Castalda	Limestone	Calcite	146	83
Sasso di Castalda	Limestone	Calcite	78	81
Sasso di Castalda	Limestone	Calcite	94	83
Sasso di Castalda	Limestone	Calcite	108	79
Sasso di Castalda	Limestone	Calcite	120	86
Sasso di Castalda	Limestone	Calcite	108	81
Sasso di Castalda	Limestone	Calcite	32	74
Sasso di Castalda	Limestone	Calcite	15	69
Sasso di Castalda	Limestone	Calcite	110	86
Sasso di Castalda	Limestone	Calcite	348	78
Sasso di Castalda	Limestone	Calcite	144	84
Sasso di Castalda	Limestone	Calcite	114	83
Sasso di Castalda	Limestone	Calcite	146	78
Sasso di Castalda	Limestone	Calcite	348	77
Sasso di Castalda	Limestone	Calcite	10	79
Sasso di Castalda	Limestone	Calcite	88	84
Sasso di Castalda	Limestone	Calcite	106	81
Sasso di Castalda	Limestone	Calcite	102	83
Sasso di Castalda	Limestone	Calcite	320	84
Sasso di Castalda	Limestone	Calcite	122	87

Bedding planes			
Locality	Lithology	Dip direction	Angle of dip
Pignola	Dolostone	332	34
Pignola	Dolostone	318	35
Pignola	Limestone	325	28
Pignola	Limestone	316	36
Pignola	Limestone	309	30
Pignola	Limestone	338	28
Pignola	Limestone	316	32
Pignola	Limestone	340	29
Pignola	Dolostone	345	31
Pignola	Dolostone	338	28
Pignola	Dolostone	328	35
Pignola	Dolostone	334	31
Pignola	Dolostone	340	31
Pignola	Dolostone	342	30
Pignola	Limestone	334	27
Pignola	Limestone	338	34
Pignola	Dolostone	338	34
Madonna del Sasso	Dolostone	242	32
Madonna del Sasso	Limestone	266	42
Madonna del Sasso	Limestone	282	15
Madonna del Sasso	Limestone	274	12
Sasso di Castalda	Limestone	224	11
Sasso di Castalda	Limestone	268	4
Sasso di Castalda	Limestone	297	25
Sasso di Castalda	Limestone	258	12
Sasso di Castalda	Limestone	354	4
Sasso di Castalda	Limestone	6	5
Sasso di Castalda	Limestone	8	9

Cleavage planes			
Locality	Lithology	Dip direction	Angle of dip
Pignola	Limestone	116	75
Pignola	Dolostone	58	77
Pignola	Limestone	98	70
Pignola	Limestone	108	75
Pignola	Limestone	100	75
Pignola	Limestone	98	72
Pignola	Limestone	104	76
Pignola	Limestone	106	75
Pignola	Limestone	96	78
Pignola	Dolostone	60	75
Pignola	Dolostone	58	77
Pignola	Limestone	108	85
Pignola	Dolostone	78	80
Pignola	Dolostone	84	79
Madonna del Sasso	Limestone	132	84
Madonna del Sasso	Limestone	128	84
Madonna del Sasso	Limestone	142	78
Madonna del Sasso	Limestone	124	88
Madonna del Sasso	Limestone	128	87
Madonna del Sasso	Limestone	130	81
Madonna del Sasso	Limestone	128	86
Madonna del Sasso	Limestone	130	85



## Appendix 2: Results of geochemical analyses

### **Legend for the table of geochemical results**

**M** = matrix

**C** = cement

**Dol1** = replacement dolomite

**Dol2** = void-filling dolomite

Sample	Locality	Phase	$\delta^{18}\text{O}_{\text{PDB}}$ [‰]	$\delta^{13}\text{C}_{\text{PDB}}$ [‰]	$^{87}\text{Sr}/^{86}\text{Sr}$	Ca (%)	Mg (%)	Sr (ppm)	Fe (ppm)	Mn (ppm)	Ba (ppm)
TG 1A	Campagna	M	-0,89	2,62	-	-	-	-	-	-	-
TG 1B	Campagna	C	-1,40	2,74	-	-	-	-	-	-	-
TG 2	Campagna	M	-0,70	2,88	0,707661	-	-	-	-	-	-
TG 3	Campagna	M	-0,02	3,58	0,708038	21,63	12,80	69	198	92	-
TG 4	Fiumarella d'Anzi	M	-5,24	2,62	-	-	-	-	-	-	-
TG 9	Campagna	M	0,58	3,01	-	21,50	12,61	78	473	70	-
TG 10 A	Fiumarella d'Anzi	Dol1	-3,97	2,69	-	-	-	-	-	-	-
TG 10 B	Fiumarella d'Anzi	Dol2	-6,38	2,27	-	-	-	-	-	-	-
TG 11	Mt. Pierno	M	0,02	3,35	-	22,67	10,78	97	954	156	-
TG 12	Mt. Pierno	M	0,29	3,25	-	23,64	11,20	96	226	154	-
TG 13	Mt. Pierno	M	0,11	3,19	-	-	-	-	-	-	-
TG 14	Mt. Pierno	M	0,08	3,45	-	23,21	11,50	101	214	176	-
TG 15	Mt. Pierno	M	0,12	3,54	-	23,20	11,33	95	440	129	-
TG 16	Mt. Pierno	M	0,24	3,10	-	-	-	-	-	-	-
TG 17	Mt. Pierno	M	-1,57	2,88	-	-	-	-	-	-	-
TG 18	Mt. Pierno	M	-2,01	2,97	-	-	-	-	-	-	-
TG 19	Mt. Pierno	M	-0,31	3,18	-	-	-	-	-	-	-
TG 20	Mt. Pierno	M	-1,32	3,23	-	23,17	11,66	88	108	89	-
TG 21	Mt. Pierno	M	-0,85	3,23	-	-	-	-	-	-	-
TG 22	San Fele	M	-2,53	2,73	-	23,40	11,20	82	463	192	-
TG 25 A	Cava Pignola	Dol1	-4,52	2,47	-	-	-	-	-	-	-
TG 25 B	Cava Pignola	Dol2	-5,54	2,64	-	-	-	-	-	-	-
TG 26	Cava Pignola	Dol1	-4,19	2,67	-	-	-	-	-	-	-
TG 28 A	Strada La Sellata-Rifreddo	Dol1	-4,31	2,24	-	21,64	12,59	42	736	279	-
TG 28 B	Strada La Sellata-Rifreddo	Dol2	-6,18	2,23	-	21,64	12,58	66	917	268	-
TG 29	Strada La Sellata-Rifreddo	Dol1	-4,42	2,26	-	-	-	-	-	-	-
TG 30	Strada La Sellata-Rifreddo	Dol1	-7,45	2,40	-	-	-	-	-	-	-
TG 31	Strada La Sellata-Rifreddo	Dol1	-4,79	2,20	-	20,32	10,34	81	1116	250	-

Sample	Locality	Phase	$\delta^{18}\text{O}_{\text{PDB}}$ [‰]	$\delta^{13}\text{C}_{\text{PDB}}$ [‰]	$^{87}\text{Sr}/^{86}\text{Sr}$	Ca (%)	Mg (%)	Sr (ppm)	Fe (ppm)	Mn (ppm)	Ba (ppm)
TG 32 A	Strada La Sellata-Rifreddo	Dol1	-4,64	2,23	-	21,00	10,43	99	1739	276	-
TG 32B	Strada La Sellata-Rifreddo	Dol2	-4,91	2,37	-	21,87	11,73	92	802	243	-
TG 33	Strada La Sellata-Rifreddo	Dol1	-8,32	2,30	-	-	-	-	-	-	-
TG 34	Strada La Sellata-Rifreddo	Dol1	-3,97	2,30	-	-	-	-	-	-	-
TG 35 A	Strada La Sellata-Rifreddo	Dol1	-5,03	2,35	-	-	-	-	-	-	-
TG 35B	Strada La Sellata-Rifreddo	Dol2	-9,09	2,21	-	-	-	-	-	-	-
TG 36	Fiumarella d'Anzi	Dol1	-5,50	2,49	-	-	-	-	-	-	-
TG 37 A	Fiumarella d'Anzi	Dol1	-5,48	2,54	-	21,27	12,23	44	653	325	-
TG 37B	Fiumarella d'Anzi	Dol2	-6,13	2,32	-	21,70	12,75	50	546	292	-
TG 38	Fiumarella d'Anzi	Dol1	-5,00	2,62	-	-	-	-	-	-	-
TG 39 A	Fiumarella d'Anzi	Dol1	-4,53	2,51	-	20,68	11,92	36	1034	269	-
TG 39B	Fiumarella d'Anzi	Dol2	-5,57	2,34	-	21,94	12,57	111	2286	283	-
TG 40 A	Fiumarella d'Anzi	Dol1	-5,11	2,51	-	-	-	-	-	-	-
TG 40B	Fiumarella d'Anzi	Dol2	-5,50	2,43	-	-	-	-	-	-	-
TG 41	Fiumarella d'Anzi	Dol1	-4,36	2,72	-	-	-	-	-	-	-
TG 42	Fiumarella d'Anzi	Dol1	-5,08	2,58	-	20,44	11,36	56	1617	334	-
TG 43	Fiumarella d'Anzi	Dol1	-4,35	2,57	-	-	-	-	-	-	-
TG 45 A	Strada Pergola-Marsico nuovo	Dol1	-4,88	2,34	-	20,65	12,08	45	431	161	2,20
TG 45 B	Strada Pergola-Marsico nuovo	Dol2	-6,86	2,42	-	20,88	12,44	52	611	153	0,25
TG 47	Strada Pergola-Marsico nuovo	Dol1	-4,94	2,56	-	21,01	12,34	52	129	184	0,58
TG 48 A	Manca di Vespe	Dol1	-5,12	2,58	-	20,97	12,15	55	550	283	1,60
TG 48 B	Manca di Vespe	Dol2	-7,53	2,52	-	21,32	12,40	79	1043	187	0,57
TG 58 A	Santuario di Monteforte	Dol1	-9,50	2,90	-	21,09	12,28	58	577	219	1,52
TG 58 B	Santuario di Monteforte	Dol2	-6,33	2,40	-	21,74	12,12	92	477	173	0,63
TG 60 A	Madonna del Sasso	Dol1	-9,49	2,42	0,708595	20,98	12,36	33	202	230	1,00
TG 60 B	Madonna del Sasso	Dol2	-4,52	2,49	-	22,49	11,66	136	378	214	0,82
TG 61 A	Madonna del Sasso	Dol1	-4,47	2,48	-	20,81	12,21	51	432	238	1,40
TG 61 B	Madonna del Sasso	Dol2	-7,33	2,33	-	21,31	12,44	89	1120	247	0,51
TG 65	San Fele	M	-1,28	3,16	-	22,38	11,33	205	2949	234	3,84
TG 70	Fosso di Fossacupa	Dol1	-3,79	2,43	-	21,18	12,60	41	208	203	0,62

Sample	Locality	Phase	$\delta^{18}\text{O}_{\text{PDB}}$ [‰]	$\delta^{13}\text{C}_{\text{PDB}}$ [‰]	$^{87}\text{Sr}/^{86}\text{Sr}$	Ca (%)	Mg (%)	Sr (ppm)	Fe (ppm)	Mn (ppm)	Ba (ppm)
TG 73	Madonna del Sasso	Dol1	-8,60	2,36	-	21,03	12,58	57	479	214	0,54
TG 78	Santuario di Monteforte	Dol1	-5,35	2,82	-	20,87	12,24	38	700	153	0,51
TG 81 A	Vietri di Potenza	Dol1	-6,97	2,58	-	20,87	12,34	52	187	206	0,67
TG 81 B	Vietri di Potenza	Dol2	-11,82	2,59	-	21,04	12,45	41	331	208	0,52
TG 83	Tito-Satriano	Dol1	-2,95	2,86	-	21,32	12,64	49	34	143	0,45
TG 84 A	Tito-Satriano	Dol1	-4,75	2,53	-	20,97	12,38	42	147	218	0,64
TG 84 B	Tito-Satriano	Dol2	-6,44	2,51	-	21,12	12,69	45	136	214	0,05
TG 89 A	Monte Arioso	Dol1	-4,03	2,44	-	21,03	12,54	43	295	224	1,00
TG 89 B	Monte Arioso	Dol2	-4,56	2,47	-	21,07	12,71	52	254	227	0,29
TG 103 B	Mt. Tigliano	Dol2	-5,61	2,29	-	21,52	12,01	76	494	245	0,93
TG 104 A	Mt. Tigliano	Dol1	-9,44	2,42	0,707908	21,15	12,19	38	312	219	1,27
TG 104 B	Mt. Tigliano	Dol2	-6,99	2,43	-	21,37	11,83	73	355	195	3,04
TG 105	Monte Marrone	M	0,72	3,60	-	20,89	12,37	76	161	51	1,34
TG 106	Monte Marrone	M	0,28	3,29	-	22,11	11,29	130	156	52	1,54
TG 107	Monte Marrone	M	1,04	3,10	-	21,17	12,41	72	59	26	0,48
AC 460	Acerno well	M	0,14	2,75	-	-	-	-	-	-	-
AC 360	Acerno well	M	-4,25	2,16	-	6,91	2,84	454	11940	484	122
AC 390	Acerno well	M	-0,99	2,75	-	10,00	5,61	409	10610	313	99
AC 430	Acerno well	M	0,61	2,82	-	20,81	12,07	109	344	113	22
AC 440	Acerno well	M	-0,34	2,87	-	18,93	10,78	171	2463	161	27
AC 3418	Acerno well	M	-0,78	3,04	-	21,09	12,09	87	604	61	142
AC 3439	Acerno well	M	0,47	3,82	-	21,10	12,27	92	333	31	195
AC 3850	Acerno well	C	-	-	-	21,03	12,30	95	530	31	142
AC 3445	Acerno well	M	0,23	3,91	-	21,48	12,50	64	193	50	252
AC 3886	Acerno well	M	-0,70	2,37	-	21,24	12,30	63	225	50	176
GA 2220	Mt. Gargaruso well	M	-3,22	2,17	-	-	-	-	-	-	-
GA 2370	Mt. Gargaruso well	M	-2,81	2,75	-	-	-	-	-	-	-
GA 2480	Mt. Gargaruso well	M	-3,64	2,54	-	-	-	-	-	-	-
GA 2490	Mt. Gargaruso well	M	-4,19	2,39	0,708274	19,84	11,05	60	1110	241	46
GA 4105	Mt. Gargaruso well	M	-5,43	2,68	-	-	-	-	-	-	-

Sample	Locality	Phase	$\delta^{18}\text{O}_{\text{PDB}}$ [‰]	$\delta^{13}\text{C}_{\text{PDB}}$ [‰]	$^{87}\text{Sr}/^{86}\text{Sr}$	Ca (%)	Mg (%)	Sr (ppm)	Fe (ppm)	Mn (ppm)	Ba (ppm)
GA 4110	Mt. Garganuso well	M	-5,44	2,72	-	-	-	-	-	-	-
GA 4145	Mt. Garganuso well	M	-6,95	2,62	0,707831	21,05	12,20	66	135	178	50
GA 4155	Mt. Garganuso well	M	-5,72	2,70	-	-	-	-	-	-	-
FO 335	Mt. Foi well	M	-3,62	1,65	-	20,83	4,92	97	5129	554	11
FO 565	Mt. Foi well	M	-3,18	2,67	-	21,16	12,23	50	265	198	0,97
FO 670	Mt. Foi well	M	-6,86	2,57	-	18,54	10,93	52	950	202	2,27
FO 930	Mt. Foi well	M	-4,86	1,93	-	10,15	5,63	31	3413	313	7,10
FO 1065	Mt. Foi well	M	-5,88	2,70	-	-	-	-	-	-	-
FO 2480	Mt. Foi well	M	-6,96	2,76	-	-	-	-	-	-	-
FO 2515	Mt. Foi well	M	-4,76	2,62	-	20,93	12,33	42	222	269	2,15
FO 2565	Mt. Foi well	M	-4,75	2,69	-	20,19	11,86	37	184	226	1,18
FO 3120	Mt. Foi well	M	-4,48	2,67	-	15,99	9,28	37	86	157	4,50
FO 3220	Mt. Foi well	C	-6,04	2,34	-	22,26	12,17	82	228	191	7,16
FO 3315	Mt. Foi well	M	-6,54	2,55	-	21,01	12,26	63	422	195	2,48
FO 3385	Mt. Foi well	M	-4,45	2,76	-	12,71	6,98	43	1085	184	4,81
FO 3400	Mt. Foi well	M	-4,44	2,70	-	21,18	11,09	91	1968	272	5,82



## Appendix 3: Results of fluid inclusions microthermometry

### Legend for microthermometry tables

**FIA** = Fluid Inclusion Assemblage

**FI** = Fluid Inclusion

**Incl.** = Inclusion

**Aq** = Aqueous

**P-Sec** = Pseudo-secondary

**Sec** = Secondary

**O** = Oblate

**I** = Irregular

**E** = Elongated

**R** = Roundish

**C** = Cubic

**Rec** = Rectangular

**CR** = Crystallographically controlled

**FI** = Flat

**Tr** = Triangular

**A-FI** = total area of the inclusion

**A-Bub** = area of the gas bubble

**F** = degree of fill

**Th** = homogenization temperature. **L** = Leakage; it indicates that the inclusion underwent leakage.

**Th'** = second measurement of Th

**Tn<sub>g</sub>** = temperature of nucleation of the gas bubble after homogenisation. **n.g.** = no gas bubble; it indicates the metastability of the gas bubble nucleation after homogenisation: the bubble does not appear after cooling the inclusion down to room temperature.

**Tn<sub>i</sub>** = temperature at which ice nucleate during cooling runs, causing abrupt contraction or disappearance of the gas bubble.

**Tm<sub>i</sub>** = melting temperature of ice.

**Tm<sub>i(MET)</sub>** = melting temperature of ice, showing metastable behavior, i.e. the melting occurs abruptly and above the real melting temperature.

826 (calcite): Pignola																			
N°				Room temperature						Heating runs					Cooling runs				Salinity
Chip	FIA	FI	System	Type	Occurrence	Shape	A-FI	A-Bub	F	Th	±	Th'	±	Tn <sub>g</sub>	Tn <sub>i</sub>	±	Tm <sub>(MED)</sub>	±	eq. wt % NaCl
1	1	1	Aq		Patchy	I/FI				69	1			34	-35		3,5	0,2	
1	2	2	Aq		Patchy	CR	3065	149	0,95	>180									
1	3	3	Aq		Patchy	E				79	1								
1	4	4	Aq		Patchy	CR	2344	119	0,95	138	3	138	1	111	-44	-2,3	0,2		3,9
1	4	5	Aq		Patchy	O				>200									
1	5	6	Aq		Crystal border	Rec				105	2					-5,7	0,2		8,8
1	5	7	Aq		Crystal border	Rec				147	1			115					
1	5	8	Aq		Crystal border	E				157	1					-1,7	0,2		2,9
1	5	9	Aq		Crystal border	O				76	2			n.g.					
1	5	10	Aq		Crystal border	I				121	1					-5,3	0,2		8,3
1	5	11	Aq		Crystal border	O/I				105	1					-6	0,2		9,2
2	6	12	Aq		Indeterminate	CR	1207	108	0,91	111	1				-41		0,5	0,1	
2	7	13	Aq		Indeterminate	I				93	1						-2,4	0,1	
2	7	14	Aq		Indeterminate	I				89	1						-0,6	0,1	
2	7	15	Aq		Indeterminate	Tr				129	1			96	-49				
2	8	16	Aq		Indeterminate	E									-44		-2,1	0,1	
2	9	17	Aq		Indeterminate	C				77	1								
3	10	18	Aq		Indeterminate	I				127	1	127	1	112	-46				
3	10	19	Aq		Indeterminate	I				86	2	87	1	66		-3,9	0,1		6,3
3	10	20	Aq		Indeterminate	Tr				159	1				-46	-3,5	0,2		5,7
3	10	21	Aq		Indeterminate	CR				81	1			29			-2,5	0,1	
3	10	22	Aq		Indeterminate	CR				82	1			19	-48		3,6	0,2	
3	10	23	Aq		Indeterminate	CR				90	1			44			-3	0,1	
3	11	24	Aq		Indeterminate	O/I				69	1				-46				
3	11	25	Aq		Indeterminate	R									-3,9	0,1			6,3
3	12	26	Aq		Indeterminate	Tr				85	1			23	-49		-4,5	0,5	
3	12	27	Aq		Indeterminate	O				113	1			89			-2,8	0,2	

826 (calcite): Pignola																			
N°				Room temperature						Heating runs					Cooling runs				Salinity
Chip	FIA	FI	System	Type	Occurrence	Shape	A-FI	A-Bub	F	Th	±	Th'	±	Tn <sub>g</sub>	Tn <sub>i</sub>	±	Tm <sub>(MED)</sub>	±	eq. wt % NaCl
3	13	28	Aq		Indeterminate	I				107	1	107	1		-50				
3	13	29	Aq		Indeterminate	CR				101	1			68		-5,5	0,2		8,5
3	13	30	Aq		Indeterminate	E				111	1			86			-5,5	0,2	
3	13	31	Aq		Indeterminate	Rec				>180									
3	13	32	Aq		Indeterminate	Rec				85							-4,8	0,2	
4	14	33	Aq		Indeterminate	CR				135	1			93	-43	-1,3	0,2		2,2
4	14	34	Aq		Indeterminate	CR				149	1						-0,8	0,2	
4	15	35	Aq		Indeterminate	I				123	1	121	1	103	-41		1	0,1	
4	15	36	Aq		Indeterminate	O				105	1			n.g.			5	0,5	
4	16	37	Aq		Indeterminate	I				96	1			35	-50		-4,8	0,3	
4	16	38	Aq		Indeterminate	CR	3255	195	0,94	134	1					-2,4	0,2		4,0
4	16	39	Aq		Indeterminate	Rec				98	1			n.g.					
4	16	40	Aq		Indeterminate	CR				112	1			n.g.					
4	17	41	Aq		Indeterminate	CR				109	1			n.g.			-3	0,2	
4	17	42	Aq		Indeterminate	I				69	1			n.g.			-1,2	0,2	
4	17	43	Aq		Indeterminate	CR				77	1			n.g.			-1,6	0,1	
5	18	44	Aq		Indeterminate	I				119	1			92	-44	-3,4	0,2		5,6
5	18	45	Aq		Indeterminate	CR				97	1						-3,1	0,1	
5	18	46	Aq		Indeterminate	Tr				161	1								
5	19	47	Aq		Indeterminate	E/I				101	1			65	-48		met		
5	19	48	Aq		Indeterminate	E				73	1			n.g.					
5	19	49	Aq		Indeterminate	Rec				91	1			n.g.			-1,5	0,1	
5	19	50	Aq		Indeterminate	CR				111	1			92	-48				
5	19	51	Aq		Indeterminate	Tr				147	1			116					
5	20	52	Aq		Indeterminate	CR				145	1				-47	-1,5	0,2		2,6
5	20	53	Aq		Indeterminate	Tr				137	1				-49	-4,5	0,2		7,2
5	20	54	Aq		Indeterminate	E				97	1						met		

TG104 (dolomite): Mount Tigliano																			
N°		Room temperature					Heating runs					Cooling runs					Salinity		
Chip	FIA	FI	System	Type	Occurrence	Shape	A-FI	A-Bub	F	Th	±	Th'	±	Tn <sub>g</sub>	Tn <sub>i</sub>	Tm <sub>i</sub>	±	Tm <sub>i(MET)</sub>	±
2	1	1	Aq		Crystal core	I	9456	212	0,98	65	1			46	-45			-22	1
2	2	2	Aq		Growth zone	CR	1608	101	0,94	91	2			44	-42			0,7	0,1
2	2	3	Aq		Growth zone	CR				74	1			n.g.					
2	2	4	Aq		Growth zone	I				105	0,5				-42	-1,1	0,1		1,9
2	2	5	Aq		Growth zone	CR				93	0,5			n.g.					
2	2	6	Aq		Growth zone	CR				118	0,3								
2	3	7	Aq		Crystal border	CR	3179	76	0,98	104	2			128					
2	3	8	Aq		Crystal border	I/E				103	1			100	-44	-3,2	2		5,3
2	3	9	Aq		Crystal border	E/Rec				109	1			96	-45	-3,2	2		5,3
2	3	10	Aq		Crystal border	O				126	1			96					
2	3	11	Aq		Crystal border	CR				>200									
2	3	12	Aq		Crystal border	O/E				122	1			88					
2	3	13	Aq		Crystal border	I				>200									
2	3	14	Aq		Crystal border	Rec				71	1			74	-45		-1,4	0,1	
5	4	15	Aq		Crystal border	I				71	1			59	-44				
5	4	16	Aq		Crystal border	CR				65	1			55					
5	4	17	Aq		Crystal border	CR				95	3				-36			0	0,1
5	5	18	Aq		Crystal border	CR	5979	353	0,94	99	1			87	-44				
5	5	19	Aq		Crystal border	CR				103	1			88	-44			-2,8	0,1
5	5	20	Aq		Crystal border	Rec				76	1			n.g.					
5	6	21	Aq		Isolated	Rec				115	1			n.g.					
7	7	22	Aq		Growth zone	I				>160					-42			-0,1	0,1
7	7	23	Aq		Growth zone	Tr												-0,2	0,1
7	7	24	Aq		Growth zone	Tr/I												-0,3	0,2
7	7	25	Aq		Growth zone	Rec												0,3	0,1
7	8	26	Aq		Growth zone	Rec				95	1							-0,4	0,1
7	8	27	Aq		Growth zone	CR/E				135	1			80			met		
7	8	28	Aq		Growth zone	I/E				147	1			104	-42	-1,7	0,1		2,9
7	8	29	Aq		Growth zone	E				155	1			45				-19	2
7	8	30	Aq		Growth zone	O				156	0,5			101				-1,1	0,1

TG104 (dolomite): Mount Tigliano																			
N°		Room temperature						Heating runs					Cooling runs				Salinity		
Chip	FIA	FI	System	Type	Occurrence	Shape	A-FI	A-Bub	F	Th	±	Th'	±	Tn <sub>g</sub>	Tn <sub>i</sub>	Tm <sub>i</sub>	±	Tm <sub>i(MET)</sub>	±
7	8	31	Aq		Growth zone	Tr				88	2			41	-42			-0,4	0,1
1	9	32	Aq		Crystal core	Rec				>200									
1	9	33	Aq		Crystal core	Rec				>200									
1	9	34	Aq		Crystal core	Tr				>200									
1	9	35	Aq		Crystal core	Tr/I				>200									
1	10	36	Aq		Growth zone	CR				175	1			146	-46			-2,8	0,1
1	10	37	Aq		Growth zone	I/E				109	1			n.g.					
1	10	38	Aq		Growth zone	E				103	2			n.g.					
1	11	39	Aq		Growth zone	I/E				103	1			61					
1	11	40	Aq		Growth zone	I/E				147	1								
1	11	41	Aq		Growth zone	I/Rec				>200									
1	12	42	Aq		Growth zone	I/E				118	1			98	-44			-2,2	0,1
1	12	43	Aq		Growth zone	Rec/I				96	1			66	-44			-0,6	0,1
1	12	44	Aq		Growth zone	E/I				80	2								
8	13	45	Aq		Growth zone	I/CR	9358	421	0,96	L					-43	-1,9	0,2		3,2
8	13	46	Aq		Growth zone	I/Rec				91	1			79	-42			-1	0,2
8	13	47	Aq		Growth zone	E				117	1								
8	13	48	Aq		Growth zone	E				87	1								
3	14	49	Aq		Crystal border	I	8351	756	0,91	107	2								
3	14	50	Aq		Crystal border	I				107	1			64	-44	-1,1	0,2		1,9
3	14	51	Aq		Crystal border	O/I				153	1								
3	14	52	Aq		Crystal border	Tr				105	1								
3	14	53	Aq		Crystal border	E/I				111	1								
3	14	54	Aq		Crystal border	CR				131	1			n.g.					
3	14	55	Aq		Crystal border	CR				165	1			103					
3	14	56	Aq		Crystal border	Rec/I				127	1								
3	14	57	Aq		Crystal border	CR				105	1							1	0,1
3	14	58	Aq		Crystal border	CR	4976	120	0,98	97	1			60	-41			1,1	0,1
3	14	59	Aq		Crystal border	E				83	1								
3	14	60	Aq		Crystal border	CR												1	0,1



TG61 (dolomite): Madonna del Sasso																			
N°			Room temperature						Heating runs					Cooling runs				Salinity	
Chip	FIA	FI	System	Type	Occurrence	Shape	A-FI	A-Bub	F	Th	±	Th'	±	Tn <sub>g</sub>	Tn <sub>i</sub>	Tm <sub>i</sub>	±	Tm <sub>i(MET)</sub>	±
3	1	1	Aq		Crystal border	I	1509	105	0,93	80	0,5			66					
3	1	2	Aq		Crystal border	Rec				68	2			55	-44			-2	
3	1	3	Aq		Crystal border	R/I				68	2			40	-44			-2	
3	1	4	Aq		Crystal border	I/E				54	1			35		-1,1	0,1		1,9
3	1	5	Aq		Crystal border	Rec/E				67	2			63	-44			-2	
3	2	7	Aq		Crystal border	Rec/I	2338	140	0,94	98	0,5				-44			-1,1	
3	2	8	Aq		Crystal border	Rec				141	0,5			88					
3	2	9	Aq		Crystal border	I				88	2								
2	3	10	Aq		Growth zone	I				70	1			16				>25	
2	3	11	Aq		Growth zone	I				<70								-1	0,5
2	3	12	Aq		Growth zone	I/O				70	1			49				0	0,5
2	4	13	Aq		Growth zone	Tr				74	1								
2	4	14	Aq		Growth zone	CR				83	2								
2	4	15	Aq		Growth zone	Tr/I				102	1								
2	4	16	Aq		Growth zone	CR				>160									
2	5	17	Aq		Growth zone	E/Rec				75	2								
2	5	18	Aq		Growth zone	I				75	2								
2	6	19	Aq		Growth zone	O				150	1				-44			-2,7	0,1
2	6	20	Aq		Growth zone	Tr/I				86	1				-42			-1,2	0,1
2	6	21	Aq		Growth zone	Rec				88	1			23				-1,5	0,5
2	6	22	Aq		Growth zone	E				81	2							-1,1	0,1
2	6	23	Aq		Growth zone	Rec				86	1							-0,9	0,1
1	7	24	Aq		Growth zone	Rec	1347	68	0,95	L					-45			-4,1	0,2
1	7	25	Aq		Growth zone	Rec/E												-2	0,1
1	7	26	Aq		Growth zone	Rec/E												-1,4	0,1
1	7	27	Aq		Growth zone	I/E				143	1							-4,4	0,2
5	8	28	Aq		Growth zone	CR	11897	335	0,97						-41				
5	8	29	Aq		Growth zone	I				L								-1	0,5

TG61 (dolomite): Madonna del Sasso																				
N°		Room temperature					Heating runs					Cooling runs				Salinity				
Chip	FIA	FI	System	Type	Occurrence	Shape	A-FI	A-Bub	F	Th	±	Th'	±	Tn <sub>g</sub>	Tn <sub>i</sub>	Tm <sub>i</sub>	±	Tm <sub>(MET)</sub>	±	eq. wt % NaCl
5	8	30	Aq		Growth zone	I				101	1									
5	8	31	Aq		Growth zone	E				167	0,1							-0,6	0,1	
5	8	32	Aq		Growth zone	Tr				166	1							-1,2	0,1	
5	8	33	Aq		Growth zone	Rec				104	1				-52	-1,1	0,1			1,9
5	9	34	Aq		Crystal border	CR	1674	156	0,91	128	0,5									
5	9	35	Aq		Crystal border	O				87	1									
5	9	36	Aq		Crystal border	I				90	0,5									
5	9	37	Aq		Crystal border	CR				114	0,5									
5	10	38	Aq		Crystal border	CR	5393	154	0,97	85	1			74,5				-0,5	0,5	
5	10	39	Aq		Crystal border	R				94	1			53				-0,5	0,5	
5	10	40	Aq		Crystal border	E				102	1			51	-43			-0,5	0,5	
13	11	41	Aq		Crystal border	Rec				L					-43			-10	2	
13	11	42	Aq		Crystal border	CR				L								-11	1	
13	11	43	Aq		Crystal border	I	3756	478	0,87	>185								-1	1	
13	11	44	Aq		Crystal border	CR				94	0,5				-43			-0,7	0,1	
13	11	45	Aq		Crystal border	Rec				97	1				-43			-0,9	0,1	
13	11	46	Aq		Crystal border	E				>185										
13	12	47	Aq		Crystal core	I				75	1									
13	12	48	Aq		Crystal core	CR				98	1			n.g.						
13	12	49	Aq		Crystal core	Tr				115	1			55	-43			2,9	0,1	
13	12	50	Aq		Crystal core	Rec				125	1									
14	13	51	Aq		Crystal core	Rec				59	1			36	-38					
14	13	52	Aq		Crystal core	CR	3363	114	0,97	67	1			48	-44	-1,3	0,1			2,2
14	13	53	Aq		Crystal core	CR				95	1							-1,5	0,4	
14	13	54	Aq		Crystal core	CR/Rec				105	0,5				-43			-1,5	0,4	
14	13	55	Aq		Crystal core	CR				70	1			24						
14	14	56	Aq		Crystal core	Rec				88	2									
14	14	57	Aq		Crystal core	I				119	1									
14	14	58	Aq		Crystal core	I/E				>200										
14	14	59	Aq		Crystal core	I/E				>201										

## TG89 (dolomite): Mount Arioso

TG89 (dolomite): Mount Arioso																						
N°			Room temperature								Heating runs					Cooling runs				Salinity		
			Chip	FIA	FI	System	Type	Occurrence	Shape	A-FI	A-Bub	F	Th	±	Th'	±	Tn <sub>g</sub>	Tn <sub>i</sub>	Tm <sub>i</sub>	±	Tm <sub>i(MET)</sub>	±
3	1	3	1	Aq		Growth zone	CR/E				78	2			62		-1,5	0,5			2,6	
3	1	3	1	Aq		Growth zone	E				87	1			10							
3	2	3	2	Aq		Growth zone	R/I				101	1			n.g.	-44			-1,7	0,1		
3	3	3	3	Aq		Growth zone	Rec				99	1			71	-42			-0,4	0,2		
3	3	3	3	Aq		Growth zone	O				127	1			71	-43			-2	0,1		
3	3	3	3	Aq		Growth zone	CR				121	1							-0,4	0,1		
3	4	3	4	Aq		Crystal core	I				93	1			24	-46			-0,2	0,1		
3	4	3	4	Aq		Crystal core	CR				>200											
3	4	3	4	Aq		Crystal core	R/I				>200											
4	5	4	5	Aq		Isolated	Rec				110	5				-44			-1	0,1		
4	6	4	6	Aq		Growth zone	CR/I				128	2				-42			0,4	0,1		
4	6	4	6	Aq		Growth zone	E									-42			0,4	0,2		
4	7	4	7	Aq		Isolated	CR				92	2			n.g.							
9	8	9	8	Aq		Crystal core	E				98,5	0,5			32	-46			-2,4	0,1		
9	8	9	8	Aq		Crystal core	Tr												-3,2	0,1		
9	8	9	8	Aq		Crystal core	E				95	1			40				-1,5	0,2		
9	8	9	8	Aq		Crystal core	E				87	1										
9	8	9	8	Aq		Crystal core	E				115	1										
9	9	9	9	Aq		Crystal core	CR	2286	142	0,94	113	1			n.g.							
9	10	9	10	Aq		Crystal core	CR				>180											
9	11	9	11	Aq		Growth zone	I	8497	192	0,98	95	1			80							
9	11	9	11	Aq		Growth zone	I				>180											
9	11	9	11	Aq		Growth zone	Rec/E	2953	144	0,95	>180											
1	12	1	12	Aq		Isolated	I	3253	122	0,96	>180											
1	13	1	13	Aq		Indeterminate	CR				>200											
1	13	1	13	Aq		Indeterminate	CR				>200											
5	14	5	14	Aq		Crystal border	CR/Rec	3476	257	0,93	95	1			80	-46	-3,2	0,1			5,3	

TG89 (dolomite): Mount Arioso																				
N°		Room temperature							Heating runs					Cooling runs				Salinity		
Chip	FIA	FI	System	Type	Occurrence	Shape	A-FI	A-Bub	F	Th	±	Th'	±	Tn <sub>g</sub>	Tn <sub>i</sub>	Tm <sub>i</sub>	±	Tm <sub>i(MED)</sub>	±	eq. wt % NaCl
5	14	28	Aq		Crystal border	I				79	1			59				-2	0,5	
5	14	29	Aq		Crystal border	CR				89	1									
5	14	30	Aq		Crystal border	CR				101	1			83	-46					
5	15	31	Aq		Crystal border	Tr				155	1			n.g.						
5	15	32	Aq		Crystal border	Rec				101	1			56				-0,3	0,1	
5	16	33	Aq	P-sec	Trail in a border	E/I				117	1				-38			-2,6	0,1	
5	16	34	Aq	P-sec	Trail in a border	R				105	1							-1,5	0,1	
5	16	35	Aq	P-sec	Trail in a border	E				75	3							-0,8	0,2	
5	17	36	Aq		Crystal border	CR	1908	49	0,97	99	1			34	-45			-2,8	0,2	
5	17	37	Aq		Crystal border	CR				80	5	86	1	67	-41			-0,1	0,1	
5	17	38	Aq		Crystal border	CR				86	2							-0,8	0,1	
5	17	39	Aq		Crystal border	O				86	2							-1,3	0,1	
5	17	40	Aq		Crystal border	CR				89	1			n.g.						
5	17	41	Aq		Crystal border	CR				103	1									
8	18	42	Aq		Crystal core	Rec				>170										
8	18	43	Aq		Crystal core	CR				93	1									
8	19	44	Aq		Crystal core	CR				>180										

TG40 (dolomite): Fiumarella d'Anzi																				
N°			Room temperature							Heating runs				Cooling runs				Salinity		
Chip	FIA	FI	System	Type	Occurrence	Shape	A-Fl	A-Bub	F	Th	±	Th'	±	Tn <sub>g</sub>	Tn <sub>i</sub>	Tm <sub>i</sub>	±	Tm <sub>i(MED)</sub>	±	eq. wt % NaCl
1	1	1	Aq		Growth zone	Rec				98	2			76	-43			-11	1	
1	1	2	Aq		Growth zone	Rec				70	3	111	1	77				-1,7	0,1	
1	1	3	Aq		Growth zone	CR				75	1							-1,8	0,1	
1	1	4	Aq		Growth zone	CR/I				92	2									
1	1	5	Aq		Growth zone	CR/I												-0,8	0,1	
1	1	6	Aq		Growth zone	Tr				67	1									
1	1	7	Aq		Growth zone	O				123	1				-44			-2,4	0,1	
1	1	8	Aq		Growth zone	R				90	2							-0,9	0,1	
1	1	9	Aq		Growth zone	CR												-1,8	0,1	
1	1	10	Aq		Growth zone	Rec	1946	143	0,93						-44			-2,3	0,1	
1	1	11	Aq		Growth zone	CR	1840	129	0,93	117	1							-2,3	0,1	
7	2	12	Aq		Patchy	CR	2340	156	0,93	103	1									
7	2	13	Aq		Patchy	CR				>160										
7	3	14	Aq		Patchy	I				>170										
7	4	15	Aq		Patchy	E									-42			0,1	0,1	
7	5	16	Aq		Patchy	O									-44			-1,2	0,1	
7	5	17	Aq		Patchy	Tr/I									-44			-1,2	0,1	
7	5	18	Aq		Patchy	Tr/I				149	1									
10	6	19	Aq		Crystal core	CR									-46			-2	0,1	
10	6	20	Aq		Crystal core	O/I												-1,1	0,1	
10	6	21	Aq		Crystal core	E/I									-46			-1,9	0,2	
10	7	22	Aq		Patchy	R/I				109	1				-33			-0,5	0,2	
10	8	23	Aq		Patchy	CR				103	1				-42	-1,8	0,2			3,1
10	8	24	Aq		Patchy	I				75	1			n.g.						
10	9	25	Aq		Patchy	O				113	1				-43			-1,8	0,1	
10	9	26	Aq		Patchy	E/I				115	5							-1,7	0,1	
10	9	27	Aq		Patchy	E/I												-0,4	0,1	
10	9	28	Aq		Patchy	E/I												-2	0,2	
10	9	29	Aq		Patchy	E/I												-0,4	0,1	
10	9	30	Aq		Patchy	R				93	1									
11	10	31	Aq		Patchy	CR				79	1									



TG40 (dolomite): Fiumarella d'Anzi																				
N°			Room temperature						Heating runs				Cooling runs				Salinity			
Chip	FIA	FI	System	Type	Occurrence	Shape	A-FI	A-Bub	F	Th	±	Th'	±	Tn <sub>g</sub>	Tn <sub>i</sub>	Tm <sub>i</sub>	±	Tm <sub>i(MED)</sub>	±	eq. wt % NaCl
11	10	32	Aq		Patchy	CR				93	1				-43			-0,2	0,1	
11	10	33	Aq		Patchy	E				93	1			86						
6	11	34	Aq		Crystal border	Rec				99	1			38	-45			-1,9	0,1	
6	11	35	Aq		Crystal border	CR				75	1							-0,9	0,1	
6	11	36	Aq		Crystal border	CR				95	1				-44			-1,4	0,1	
6	11	37	Aq		Crystal border	E/I				83	1									
6	11	38	Aq		Crystal border	E/I				71	1							-0,9	0,1	
6	11	39	Aq		Crystal border	E				71	1							-0,9	0,1	
6	11	40	Aq		Crystal border	CR				75	1							1,2	0,2	
6	12	41	Aq		Crystal border	E				133	1			112	-41			0,3	0,1	
6	12	42	Aq		Crystal border	Rec				73	1			44	-45			-0,9	0,1	
9	13	43	Aq		Patchy	CR	1036	86	0,92	141	1	141	1	115	-40			0	0,1	
9	13	44	Aq		Patchy	Tr				93	1									
9	14	45	Aq		Patchy	E				113	1			64	-42			-1	0,1	
9	14	46	Aq		Patchy	E				95	1							0,1	0,1	
9	14	47	Aq		Patchy	Rec				160	1	160	1	143						
9	15	48	Aq		Patchy	CR				<55								0,5	0,2	
9	15	49	Aq		Patchy	Rec				120	1				-48					
9	15	50	Aq		Patchy	Rec				100	1							-2,2	0,1	
8	16	51	Aq		Patchy	CR				119	1			108	-42			-0,2	0,1	
12	17	52	Aq		Patchy	I				101	1			93	-42			0,4	0,1	
12	17	53	Aq		Patchy	I				101	2				-41					
12	17	54	Aq		Patchy	C				107	1			95						
13	18	55	Aq		Patchy	I				115	1				-42					
13	18	56	Aq		Patchy	Cr				105	1									
13	19	57	Aq		Patchy	CR				91	1			58	-42			-0,6	0,1	
13	19	58	Aq		Patchy	CR				101	1									
13	19	59	Aq		Patchy	E				105	1									
13	19	60	Aq		Patchy	I				117	1									
13	20	61	Aq		Patchy	CR				135	1			127		-2,6	0,1	-2,8	0,2	4,3
13	20	62	Aq		Patchy	E				133	1				-42					

## TG81 (dolomite): Vietri di Potenza

N°			Room temperature							Heating runs					Cooling runs				Salinity
Chip	FIA	FI	System	Type	Occurrence	Shape	A-FI	A-Bub	F	Th	±	Th'	±	Tn <sub>i</sub>	Tm <sub>i</sub>	±	Tm <sub>(MET)</sub>	±	eq. wt % NaCl
3	1	1	Aq		Growth zone	CR				89	1			-45			-1,6	0,2	
3	1	2	Aq		Growth zone	Rec				105	1						1,7	0,1	
3	1	3	Aq		Growth zone	CR				95	1								
3	1	4	Aq		Growth zone	C				115	1	115	1				1,8	0,2	
3	1	5	Aq		Growth zone	R				119	1			n.g.					
3	1	6	Aq		Growth zone	CR				101	1						0,8	0,1	
3	1	7	Aq		Growth zone	CR				103	1								
3	1	8	Aq		Growth zone	CR				113	1						0,8	0,1	
3	1	9	Aq		Growth zone	E				109	1						1,6	0,2	
3	1	10	Aq		Growth zone	E/I				105	1								
3	2	11	Aq		Growth zone	Rec				115	1			-42			-2	0,2	
3	2	12	Aq		Growth zone	CR				143	1	90	5	68	-43		-2	0,2	
3	2	13	Aq		Growth zone	E				115	1								
3	2	14	Aq		Growth zone	Rec				143	1			n.g.					
1	3	15	Aq		Growth zone	Rec				103	1						0,5	0,1	
1	3	16	Aq		Growth zone	C				>180									
1	4	17	Aq		Growth zone	E				115	1			-42			3,5	0,1	
1	5	18	Aq		Growth zone	C	862	147	0,83	>180									
1	6	19	Aq		Along a trail	FI											-2,5	0,1	
1	7	20	Aq		Growth zone	CR				148	1	149	1	117	-1,9	0,2			3,2
1	7	21	Aq		Growth zone	R/I				146	1	147	1	99	-2,6	0,2			4,3
1	8	22	Aq		Growth zone	Rec				151	1	151	1	-45			-3	0,1	
1	8	23	Aq		Growth zone	CR				173	1	173	1				-3	0,2	
1	8	24	Aq		Growth zone	E				143	2	145	1				1,5	0,5	
2	9	25	Aq		Indetermined	O	1311	116	0,91	107	1						2,4	0,1	
2	9	26	Aq		Indetermined	CR				103	1	119	1				0,2	0,1	
2	9	27	Aq		Indetermined	I				119	1						0,4	0,1	

## TG81 (dolomite): Vietri di Potenza

TG81 (dolomite): Vietri di Potenza																				
N°			Room temperature							Heating runs					Cooling runs				Salinity	
Chip	FIA	FI	System	Type	Occurrence	Shape	A-FI	A-Bub	F	Th	±	Th'	±	Tn <sub>g</sub>	Tn <sub>i</sub>	Tm <sub>i</sub>	±	Tm <sub>i(MET)</sub>	±	eq. wt % NaCl
2	9	28	Aq		Indetermined	Rec				121	1	121	1					1,1	0,2	
2	9	29	Aq		Indetermined	I				119	1									
2	9	30	Aq		Indetermined	E/I				121	1									
6	10	31	Aq		Crystal Core	CR				87	3			n.g.						
6	10	32	Aq		Crystal Core	E/CR				111	1									
6	11	33	Aq		Crystal Core	CR				131	1					-2,7	0,2			4,5
6	12	34	Aq		Crystal Core	Rec				145	1	145	1	82		-2,5	0,1			4,2
9	13	35	Aq	Sec	Along a trail	CR				>180										

## TG84 (dolomite): Tito-Satriano

TG84 (dolomite): Tito-Satriano																				
N°			Room temperature							Heating runs					Cooling runs				Salinity	
Chip	FIA	FI	System	Type	Occurrence	Shape	A-FI	A-Bub	F	Th	±	Th'	±	Tn <sub>g</sub>	Tn <sub>i</sub>	Tm <sub>i</sub>	±	Tm <sub>i(MET)</sub>	±	eq. wt % NaCl
13	1	1	Aq		Crystal border	Rec				113	1			67	-45	-2,9	0,1			4,8
13	1	2	Aq		Crystal border	E				79	1							-0,9	0,1	
13	1	3	Aq		Crystal border	CR				117	1							0,8	0,1	
13	1	4	Aq		Crystal border	E				109	1							-1,4	0,2	
13	1	5	Aq		Crystal border	CR				89	1									
13	1	6	Aq		Crystal border	CR				111	1			34						
13	1	7	Aq		Crystal border	CR	894	77	0,91	151	1	151	1	106	-41	-1,2	0,1			2,1
13	1	8	Aq		Crystal border	CR				121	1							1,4	0,1	
13	2	9	Aq		Crystal border	O/I									-44			-0,9	0,1	
13	2	10	Aq		Crystal border	Rec				87	1							0,3	0,1	
13	3	11	Aq		Crystal border	CR/I	1404	112	0,92	115	1			n.g.						
13	3	12	Aq		Crystal border	CR				113	1							0,5	0,2	

## TG84 (dolomite): Tito-Satriano

TG84 (dolomite): Tito-Satriano																				
N°		Room temperature								Heating runs				Cooling runs				Salinity		
Chip	FIA	FI	System	Type	Occurrence	Shape	A-FI	A-Bub	F	Th	±	Th'	±	Tn <sub>g</sub>	Tn <sub>i</sub>	Tm <sub>i</sub>	±	Tm <sub>i(MED)</sub>	±	eq. wt % NaCl
7	4	13	Aq		Crystal border	I				73	1	95	1		-45			-1	0,1	
7	4	14	Aq		Crystal border	C/I				74	1							-1	0,1	
7	5	15	Aq		Crystal core	E/CR	1785	169	0,91	97	1							-1,1	0,1	
7	6	16	Aq		Crystal core	I				119	1				-44					
7	7	17	Aq		Crystal core	Tr/I				97	1							-0,3	0,2	
7	8	18	Aq	P-sec	Trail in a border	CR				163	1					-2,6	0,2			4,3
7	9	19	Aq	P-sec	Trail in a border	Rec				89	1			39				-2,4	0,1	
11	10	20	Aq		Crystal core	CR				>170										
11	11	21	Aq		Crystal border	CR				159	1	159	1		-44	-2,8	0,1			4,6
11	11	22	Aq		Crystal border	E				155	1	155	1	102				-2,8	0,2	
8	12	23	Aq		Crystal border	I										-2,9	0,2			4,8
8	13	24	Aq		Crystal core	CR				117	1			59				1,9	0,1	
8	13	25	Aq		Crystal core	FI				103	1			52				1,6	0,1	
8	13	26	Aq		Crystal core	E				115	1			n.g.						
8	14	27	Aq		Crystal core	CR/Rec				129	1				-42			3,8	0,2	
6	15	28	Aq		Crystal border	CR				>180										
6	16	29	Aq		Crystal core	E/I				>140										
6	17	30	Aq	P-sec	Trail in a border	I									-45			-2,1	0,1	
6	17	31	Aq	P-sec	Trail in a border	CR				112	1				-46			-2,5	0,1	
6	17	32	Aq	P-sec	Trail in a border	R/I				130	1							-3	0,2	
4	18	33	Aq		Crystal border	E/CR				163	1	163	1	97	-45	-2,6	0,1			4,3
4	19	34	Aq		Crystal border	Rec				99	1			65				-1,1	0,1	
4	20	35	Aq		Crystal border	Rec				135	1			34	-43			25	1	
4	20	36	Aq	P-sec	Trail in a border	O				79	1							-2,4	0,2	
4	21	37	Aq		Crystal border	CR				131	1				-42			-1,9	0,1	
4	21	38	Aq		Crystal border	CR				197	1			148						

TG58 (dolomite): Monteforte																				
N°			Room temperature						Heating runs						Cooling runs				Salinity	
Chip	FIA	FI	System	Type	Occurrence	Shape	A-FI	A-Bub	F	Th	±	Th'	±	Tn <sub>g</sub>	Tn <sub>i</sub>	±	Tm <sub>i(MET)</sub>	±	eq. wt % NaCl	
8	1	1	Aq		Isolated	CR				>200										
8	2	2	Aq		Growth zone	CR/I				139	1			126	-42	-2	0,2			3,4
8	2	3	Aq		Growth zone	CR				>200						-1,5	0,5			2,6
8	3	4	Aq		Growth zone	Tr				109	1			52	-43		8,6	0,1		
8	3	5	Aq		Growth zone	E/I				129	1									
8	3	6	Aq		Growth zone	CR				>200										
8	4	7	Aq		Isolated	Rec	2490	161	0,94	>200										
8.2	5	8	Aq		Isolated	CR/I				>200										
8.2	6	9	Aq		Isolated	CR				106	2									
8.2	7	10	Aq		Isolated	R	1375	128	0,91	151	1			99	-42	-1,5	0,5	2,2	0,1	
1	8	11	Aq		Isolated	I/CR	3208	139	0,96	>200										2,6
1	9	12	Aq		Indeterminate	O				>200										
1	9	13	Aq		Indeterminate	I				>200										
9		14	Aq		Isolated	CR				75	2									
9		15	Aq		Isolated	CR				>180										
9		16	Aq		Isolated	Tr/I				>180										
7		17	Aq		Isolated	CR				>200										
2		18	Aq		Indeterminate	E				95	5									
2		19	Aq		Indeterminate	R				160	5			140		-2	0,5			3,4
2		20	Aq		Isolated	CR				>200										
2.2		21	Aq		Growth zone	I				>200										

GA2490 (dolomite): Mount Gargaruso well																				
N°		Room temperature							Heating runs				Cooling runs				Salinity			
Chip	F/A	FI	System	Type	Occurrence	Shape	A-FI	A-Bub	F	Th	±	Th'	±	Tn <sub>g</sub>	Tn <sub>i</sub>	Tm <sub>i</sub>	±	Tm <sub>i(MET)</sub>	±	eq. wt % NaCl
6	1	1	Aq		Crystal core	C				98	1				-44					
6	1	2	Aq		Crystal core	Rec				124	1									
6	1	3	Aq		Crystal core	FI				154	1							-2,5	0,2	
6	1	4	Aq		Crystal core	FI				>180										
6	1	5	Aq		Crystal core	CR				105	1	107	1		-44			-2,2	0,1	
6	1	6	Aq		Crystal core	CR				125	1	114	1							
6	1	7	Aq		Crystal core					142	2									
6	1	8	Aq		Crystal core					85	5							-0,5	0,2	
6	2	9	Aq		Crystal core	CR/I				171	1	171	1	153	-46					
6	2	10	Aq		Crystal core	CR				179	1	181	1							
6	2	11	Aq		Crystal core	Rec				173	1			148						
6	2	12	Aq		Crystal core	Rec				177	1	177	1	148						
6	2	13	Aq		Crystal core	CR				>180		185	1							
7	3	14	Aq		Trail	E/I				>180										
7	3	15	Aq		Trail	E/I				>180										
3	4	16	Aq	P-sec	Crystal border	Rec/I				111	1				-44			-2,5	0,2	
3	5	17	Aq		Crystal border	O				97	1			47						
3	6	18	Aq		Crystal border	Rec				111	1			44	-45			-0,2	0,1	
4	7	19	Aq		Crystal border	R/I				128	2	125	1	102	-47	-4	0,2			6,4
4	8	20	Aq		Crystal border	CR				165	1							-0,6	0,1	
4	9	21	Aq		Crystal border	CR				133	1				-38			-1,2	0,1	
4	10	22	Aq		Crystal border	CR				173	1				-46	-2,6	0,2			4,3
4	11	23	Aq		Crystal core	CR				149	1				-42			2,2	0,1	
4	11	24	Aq		Crystal core	CR										-2,2	0,2			3,7
4	11	25	Aq		Crystal core	CR				117	1									
4	11	26	Aq		Crystal core	E				97	1									
4	11	27	Aq		Crystal core	Tr				145	1									



GA4105 (dolomite): Mount Gargaruso well																			
N°				Room temperature						Heating runs					Cooling runs				Salinity
Chip	FIA	FI	System	Type	Occurrence	Shape	A-FI	A-Bub	F	Th	±	Th'	±	Tn <sub>g</sub>	Tn <sub>i</sub>	±	Tm <sub>i(MET)</sub>	±	eq. wt % NaCl
5	1	1	Aq		Incl. Free zone	Tr				>180									
5	2	2	Aq		Incl. Free zone	E				>180									
5	3	3	Aq		Along a trail	O				>170									
8	4	4	Aq		Growth zone	E				>180									
8	4	5	Aq		Growth zone	O				110	2			n.g.					
8	4	6	Aq		Growth zone	E/I	3085	159		>180									
9	5	7	Aq		Crystal core	E				>180									
9	6	8	Aq		Vein in the matrix	Tr				>180									
9	6	9	Aq		Vein in the matrix	Tr				>180									
9	6	10	Aq		Vein in the matrix	Tr				>180									
3	7	11	Aq		Indeterminate	O				>170									
3	8	12	Aq		Indeterminate	I				>180									
3	9	13	Aq		Indeterminate	I				>180									
10	10	14	Aq		Along a trail	R				>200									
10	11	15	Aq		Incl. Free zone	CR				>180									
10	11	16	Aq		Incl. Free zone	O/R				132	2								
10	12	17	Aq		Along a trail	E/I				>180									
12	13	18	Aq		Crystal core	CR				160	5			n.g.					
12	13	19	Aq		Crystal core	E				125	5			140					

GA4145 (dolomite): Mount Gargaruso well																				
N°		Room temperature							Heating runs				Cooling runs				Salinity			
Chip	F/A	FI	System	Type	Occurrence	Shape	A-FI	A-Bub	F	Th	±	Th'	±	Tn <sub>g</sub>	Tn <sub>i</sub>	Tm <sub>i</sub>	±	Tm <sub>i(MET)</sub>	±	eq. wt % NaCl
7	1	1	Aq		Crystal core	Tr				>180										
7	1	2	Aq		Crystal core	Rec				>180										
7	1	3	Aq		Crystal core	Tr				>180										
7	1	4	Aq		Crystal core	CR				61				110						
7	1	5	Aq		Crystal core	CR				>180										
7	1	6	Aq		Crystal core	CR				>180										
7	1	7	Aq		Crystal core	Rec				>180										
7	1	8	Aq		Crystal core	Tr				>180										
7	1	9	Aq		Crystal core	CR				>180										
7	1	10	Aq		Crystal core	C				>180										
7	1	11	Aq		Crystal core	E				>180										
7	1	12	Aq		Crystal core	Rec				>180										
7	2	13	Aq		Crystal core	R/I				141	1	141	1	58	-45			1,9	0,1	
7	2	14	Aq		Crystal core	Rec				145	1	145	1	136		-3,7	0,1			6,0
7	2	15	Aq		Crystal core	E				143	1									
8	3	16	Aq		Growth zone	O/I	1647	158		>180										
8	3	17	Aq		Growth zone	R				>180										
8	3	18	Aq		Growth zone	Rec				>180										
8	3	19	Aq		Growth zone	C				175	5									
8	4	20	Aq	P-sec	Along a trail	E				>180										
8	4	21	Aq	P-sec	Along a trail	C				>180										
8	4	22	Aq	P-sec	Along a trail	Rec				175	5							-1,9	0,1	
8	4	23	Aq	P-sec	Along a trail	CR				175	5				-40	-1,7	0,1			2,9
8	5	24	Aq		Growth zone	CR				155	1			n.g.						
8	5	25	Aq		Growth zone	CR				137	1			n.g.						
8	5	26	Aq		Growth zone	CR				153	1			n.g.						
9	6	27	Aq		Growth zone	E				>180										